

University of Nevada, Reno

**Catalytic Conversion of Lignocellulosic
Biomass to Carboxylic Acids and Derivatives**

A dissertation submitted in partial fulfillment of the
Requirements for the degree of Doctor of Philosophy in
Chemical Engineering

By

Lisha Yang

Dr. Hongfei Lin/ Dissertation Advisor

August 2015



THE GRADUATE SCHOOL

We recommend that the dissertation
prepared under our supervision by

LISHA YANG

Entitled

**Catalytic Conversion of Lignocellulosic Biomass to Carboxylic Acids and
Derivatives**

be accepted in partial fulfillment of the
requirements for the degree of

DOCTOR OF PHILOSOPHY

Hongfei Lin, Advisor

Charles J. Coronella, Committee Member

Victor R. Vasquez, Committee Member

John C. Cushman, Committee Member

Brian J. Frost, Graduate School Representative

David W. Zeh, Ph. D., Dean, Graduate School

August, 2015

Catalytic Conversion of Lignocellulosic Biomass to Carboxylic Acids and Derivatives

Abstract

The transition from today's fossil fuel based economy to a sustainable economy that is grounded in renewable biomass is driven by concern of climate change and anticipation of dwindling fossil fuel resources. Biofuel is a central theme of the sustainable transition due to the large market demand in the transportation sector. However, transformation of biomass into high value added chemicals is advantageous to secure optimal use of the biomass resources from economical and ecological perspectives. Therefore, it is important for a modern biorefinery to integrate fuel and chemical production from biomass derived platform chemicals. The aim of this dissertation is to design and develop a novel and environmentally benign process to produce carboxylic acids and their derivatives, which are the building blocks for biofuels and biobased chemicals, from various lignocellulosic biomass types using recyclable heterogeneous catalysts in water and/or alcohol solutions. In this process, wet lignocellulosic biomass is pre-treated by low-temperature partial oxidation that selectively converts lignin to carboxylic acids or phenolics in aqueous-phase solutions. The remaining structured hemicellulose and cellulose are catalytically converted to lactic acid or its esters which can be further upgraded to liquid hydrocarbon fuels or value added chemicals.

Although a variety of lignocellulosic biomass can be used as feedstocks in designed conversion processes, the arid-land adapted, highly water-use efficient CAM (crassulacean acid metabolism) species, (e.g., *Agave tequilana* and *Opuntia ficus-indica*)

which are unique biomass species compared to other C₃ and C₄ plants, are especially promising. In Chapter 2, *Agave* and *Opuntia* were characterized by a series of standard biomass analytical procedures wherein both species were found to contain high water contents which would be potentially useful for aqueous phase processing of biomass, as well as low lignin and high para-crystalline cellulose contents, making them more amenable to deconstruction. In Chapter 3, a lignin model compound, guaiacol, was selectively oxidized with H₂O₂ as the oxidant and titanium silicate (TS-1) catalyst at low temperatures. The value-added dicarboxylic acid, maleic acid, was obtained in this TS-1/H₂O₂ catalytic aqueous-phase partial oxidation reaction system. In Chapter 4, hemicellulosic biomass, xylan, and xylose can be converted to lactic acid using ZrO₂ catalyst in pH-neutral hydrothermal solutions. The yields of lactic acid, up to 25% and 18%, were produced from xylose and xylan, respectively. The Lewis acid property of ZrO₂ was demonstrated to effectively facilitate the retro-aldol condensation of xylose, which is the initial step of the conversion of xylose to lactic acid. In Chapter 5, the mesoporous Zr-SBA-15 materials with increased Lewis acidity compared to ZrO₂ were synthesized in order to increase the yields of lactic acid esters. Alkyl lactates were produced from sugars and cellulose with this catalyst in relevant alcohols in a one-pot reaction. The yields of methyl lactate at up to 41 % and 44% were produced from pentose and hexose, respectively, with methanol solvent, while the yield of up to 31% ethyl lactate was directly produced from cellulose in ethanol-water solutions with the Zr-SBA-15 catalyst. Lastly, in Chapter 6, the conclusion remarks and future research directions are given.

Acknowledgements

First, I would like to express heartfelt gratitude to my advisor, Dr. Hongfei Lin, primarily for his guidance throughout my PhD studies, and also for his patience, encouragement and support. It would have been impossible for me to complete this work without his enduring mentoring. I have learned a great deal during these three years about creating new ideas, designing experiments, and solving scientific and engineering problems, which have equipped me to be an independent researcher. I believe that all of the knowledge and research skills that Dr. Lin has imparted to me will help me to reach my future career goal.

Further, sincere appreciation is extended to my committee members: Dr. Charles Coronella, Dr. Victor Vasquez, Dr. John Cushman, and Dr. Brian Frost, all of whom gave so graciously of their valuable time and insightful comments and suggestions. Especially, I am indebted to Dr. John Cushman for his generous financial support of me during my difficult time, as well as his consistent technical support on the analysis of drought-tolerant biomass feedstocks.

Much thanks to Dr. Stephen Spain and Dr. Glenn Miller for their valuable input and advice on various analytical skills (e.g., HPLC, GC/MS, NMR, LC/MS and GC-FID). Additionally, I cannot thank enough Dr. Dhanesh Chandra, Dr. Mojtaba Ahmadiantehrani, Dr. Wenming Chian, Dr. Alan Fuchs, Dr. Vaidyanathan Subramanian, and Dr. Sage Hiibel, for their help over the last three years.

I owe a particularly large degree of thanks to my fellow graduate students and friends: Ji Su, Xiaokun Yang, Mi Lu, Jason Strull, Ying Liu, Jesse Mayer, Joan Lynam, Toufiq Reeza, and John Grant, every one of them sacrificing much in the way of assistance and support. I would not have succeeded in either my research or coursework without their enthusiasm and motivation in seeing me through to this end.

I have also had the pleasure of working with a great group of intelligent undergraduate students: Emily Truong, Sarah Carl, Justin Donat, Reed Liu, and Elli Tian. Each had their own unique set of influences on me, thus providing constructive inspiration at various times over the past three years.

Special thanks to my genuine American friends - David and Kris Lahti; both have provided much in the way of personal encouragement, and emotional as well as moral support.

My parents deserve credit for all my achievements. My deepest sense of personal gratitude is reserved for them alone as their unconditional love and sponsorship have carried me spiritually throughout life. I am also grateful to my brother and his entire family for their boundless love and encouragement.

Lastly, I want to thank the U.S. National Science Foundation for the financial support.

Table of Contents

Abstract.....	i
Acknowledgements	iii
Table of Contents	v
Figures.....	vii
Tables	xv
Chapter 1 Introduction	1
1.1 Requirement and challenge for renewable energy resources	1
1.2 Lignocellulosic biomass	2
1.3 Drought-tolerant bioenergy crops in marginal environment.....	5
1.4 Routes for the biofuel products from biomass conversion.....	6
1.5 Carbohydrates to carboxylic acids	9
1.5.1 Lactic acid	9
1.5.2 Other carboxylic acids.....	15
1.6 Lignin to phenolic acids.....	20
1.7 Dissertation Structure.....	23
Chapter 2 Biomass characterization of <i>Agave</i> and <i>Opuntia</i> as potential biofuel feedstocks	34
2.1 Introduction	34
2.2 Materials and methods	38
2.2.1 Plant cultivation	38
2.2.2 Materials.....	38
2.2.3 Sample preparation.....	39
2.2.4 Elemental analysis.....	40
2.2.5 Extractive, ash, protein, and dry bagasse analysis.....	40
2.2.6 Juice Analysis.....	40
2.2.7 Higher heating value analysis.....	41
2.2.8: Holocellulose fractionation	42
2.2.9 Solid state NMR analysis	42
2.3 Results and discussion	42
2.3.1 Elemental analysis.....	42
2.3.2 Compositional analysis	43
2.3.3 Higher heating value analysis of dry bagasse.....	51
2.3.4 Cellulose characterization	52
2.4 Conclusions	54
2.5 References	55
Chapter 3 Selective oxidation of lignin model compounds to maleic acid over TS-1 catalyst	62
3.1 Introduction	62
3.2 Materials and methods	65
3.2.1 Catalyst preparation and characterization	65
3.2.2 Aqueous-phase oxidation	65
3.2.3 Product analysis	66
3.3 Results and discussion	67
3.4 Conclusions	81
3.5 References	82

Chapter 4 Catalytic conversion of hemicellulose to lactic acid with zirconia catalyst in pH neutral aqueous phase media.....	88
4.1 Introduction	88
4.2 Materials and methods	90
4.2.1 Materials.....	90
4.2.2 Catalytic reactions	90
4.2.3 Product analysis	92
4.2.4 Catalyst characterisation	94
4.3 Results and discussion	94
4.3.1 Conversion of xylose to lactic acid	94
4.3.2 Direct conversion of xylan to lactic acid	112
4.4 Conclusions	116
4.5 References	117
Chapter 5: Catalytic conversion of holocellulose (cellulose and hemicellulose) into lactic acid derivatives via mesoporous Zr-SBA-15	121
5.1: Introduction	121
5.2: Materials and methods	126
5.2.1: Materials.....	126
5.2.2: Catalyst preparation	127
5.2.3: Catalyst characterization	128
5.2.4: Catalytic reactions	129
5.2.5: Product analysis	130
5.3: Results and discussion	131
5.3.1: Mechanistic insights into the production of methyl lactate by catalytic conversion of carbohydrates on mesoporous Zr-SBA-15	131
5.3.2: Directly catalytic conversion of cellulose into ethyl lactate via Zr-SBA-15	153
5.4: Conclusions	170
5.5: References	171
Chapter 6 Conclusions and recommendation for future research.....	180
6.1 Conclusions	180
6.2 Recommendations for Future Work.....	182
6.3 References	184

Figures

Figure 1.1 Chemical components of lignocellulosic biomass	4
Figure 1.2 C ₃ and C ₄ carbon fixation reactions in CAM photosynthetic plants. In these plants, C ₃ carbon fixation utilizing RuBisCo occurs during the day, while C ₄ carbon fixation occurs utilizing PEPC at night	6
Figure 1.3 Routes for the conversion of biomass into liquid fuels. Red arrows refer to thermal routes, green arrows refer to biological routes, and blue arrows refer to catalytic routes	8
Figure 1.4 Lactic acid as a platform intermediate for the chemical and fuels	10
Figure 1.5 Conversion of D-glucose into lactic acid over base catalysts	11
Figure 1.6 Proposed reaction pathway for the conversion of fructose to methyl lactate. The reaction formally comprises a retro aldol fragmentation of fructose and isomerization-esterification of the trioses	15
Figure 1.7 Levulinic acid as a platform intermediate for chemicals and fuels	17
Figure 1.8 Reaction pathway of (a) converting a cellobiose unit in cellulose to glucose and gluconic acid by superoxide radical anions. (b) converting gluconic acid to levulinic acid by a Hofer–Moest-type decarboxylation reaction followed by consecutive dehydration/rehydration reactions	18
Figure 1.9 Product yields from the conversion of different sacchariferous reactants using HPM as the catalyst	20
Figure 1.10 The possible structure of lignin (A) and three common lignin monomers (B). B1, H-lignin (p-coumaryl alcohol); B2, G-lignin (coniferyl alcohol); B3, S-lignin (sinapyl alcohol)	21
Figure 1.11 Oxidation reaction pathway of different model compounds of lignin	22
Figure 1.12 Integrated biorefining process for lignocellulosic biomass	25
Figure 2.1 Scheme of the processing steps for the compositional analysis of <i>Agave tequilana</i> and <i>Opuntia ficus-indica</i> samples	44

Figure 2.2 ESI/MS spectra of <i>Agave tequilana</i> (upper panel) and <i>Opuntia ficus-indica</i> (lower panel) juice.....	46
Figure 2.3 GC/MS spectra of <i>Agave tequilana</i> (red trace) and <i>Opuntia ficus-indica</i> (black trace) juices.....	46
Figure 2.4 Spectral fitting for the C-4 region of CP/MAS ^{13}C NMR spectra of isolated cellulose of <i>Agave tequilana</i> (a) and <i>Opuntia ficus-indica</i> (b).	54
Figure 3.1 Schematic diagram of the aqueous-phase oxidation reactor system. Eight leak-proof 30 ml narrow-mouth perfluoroalkoxy (PFA) vials (Thermo Scientific) were placed in the bottle holder which was rotated at 90 RPM along the horizontal axis driven by an external motor. The reaction temperature was controlled by a preheated oven.....	66
Figure 3.2 Scanning electronic microscope image of as-synthesized TS-1 catalyst.....	69
Figure 3.3 Guaiacol conversions at different pH values with and without the TS-1 catalyst. TS-1 enhanced the guaiacol conversion in a wide range of pH values ($1.0 < \text{pH} < 13.3$).....	71
Figure 3.4 Electrospray ionization mass spectra (ESI-MS) of the aqueous-phase products of guaiacol oxidation.....	72
Figure 3.5 HPLC spectra of the aqueous-phase products of guaiacoloxidation.....	72
Figure 3.6 The GC/MS total ion chromatogram of the aqueous-phase products of guaiacol oxidation.....	73
Figure 3.7 Influence of the TS-1 catalyst on (a) maleic acid concentration; and (b) conversion of guaiacol. Inset is the photo of aqueous-phase product at different guaiacol oxidation reaction periods (0-12 h) with the presence of the TS-1 catalyst. The color gradually changed from colorless to dark brown as the reaction time increased. Other reaction conditions are: Guaiacol=0.1 g (0.8 mmol), H_2O_2 (35 wt %) = 0.5 g (5.1 mmol), TS-1 Catalyst=0.1 g, H_2O = 10 g, reaction temperature = 80 °C, initial pH = 13.3.....	75

Figure 3.8 A, XRD pattern of different TS-1 catalyst; B, pH value in different reaction time. Trap agent is BMPO. The concentration of H ₂ O ₂ in reaction solution and amount of TS-1 catalyst is same with real reaction. And before EPR spectra collection, there is a 10 min activate process in reaction temperature (80 °C).....	76
Figure 3. 9 HPLC spectra of aqueous-phase products of guaiacol and catechol oxidation. The main acid product of catechol oxidation reaction is malic acid, while maleic acid is the major product of guaiacol oxidation, implying that guaiacol and catechol oxidation have different reaction pathways even under the identical reaction conditions. We propose that the benzene ring of guaiacol could be opened directly without proceeding hydrolysis first.....	77
Figure 3.10 The proposed reaction pathway of selective oxidation of guaiacol in TS-1/H ₂ O ₂ system.....	78
Figure 3.11 Raman spectra of TS-1 sample in contact with a H ₂ O ₂ /H ₂ O solution. 1) the Raman spectra of pure TS-1; 2) TS-1 in contact with a H ₂ O ₂ /H ₂ O solution (pH=7), 3) TS-1 in contact with a H ₂ O ₂ /H ₂ O solution (pH=13.5).....	79
Figure 3.12 A, XRD pattern of different TS-1 catalyst; B, pH value in different reaction time. TS-1A stand for the fresh TS-1, TS-1B stand for the spent TS-1 catalyst after the reaction (initial pH value is 13.3, reaction temperature is 80 °C, and reaction time is 24 h), TS-1C stand for the TS-1 sample was treated with NaOH solution (pH value is 13.3) at 80 °C for 24 h.....	81
Figure 4.1 Temperature effect on the yields aqueous-phase products of xylose conversion with the ZrO ₂ catalyst in pH neutral aqueous solution. The inset figure shows the temperature effect on the solid residue yields and the TOC yields in the same reaction.....	96
Figure 4.2 Effect of O ₂ partial pressure on the yields of the aqueous-phase products by the conversion of xylose with the ZrO ₂ catalyst in pH neutral aqueous solutions.....	97
Figure 4.3 Effect of catalyst loading on the yields of the aqueous-phase products by the conversion of xylose with the ZrO ₂ catalyst in pH neutral aqueous solutions	97

Figure 4.4 ESI-MS spectra of aqueous-phase products using xylose as the biomass feedstock.	
Effect of O ₂ partial pressure.....	98
Figure 4.5 Comparison of ¹³ C NMR spectra: (a) Pure lactic acid; (b) Aqueous-phase products with xylose as the feedstock. Reaction conditions: 200 °C, 40 min, 5 % O ₂ , 0.8 g ZrO ₂ , 1 g xylose, 20 g water, and 2.4 MPa N ₂ +O ₂ ; (c) Aqueous-phase products with xylose as the feedstock. Reaction conditions: 200 °C, 40 min, 0% O ₂ , and 0.8 g ZrO ₂ , 1 g xylose, 20 g water, and 2.4 MPa N ₂	99
Figure 4.6 GC/MS spectra of aqueous-phase products with xylose as the feedstock.....	100
Figure 4.7 Proposed reaction mechanism of xylose retro-aldol condensation with the ZrO ₂ catalyst. Xylose is converted to glyceraldehyde and glycolaldehyde via the C-C bond cleavage.....	104
Figure 4.8 Proposed reaction mechanism for conversion of xylose to lactic acid and other intermediate and final products in subcritical water with the bi-functional ZrO ₂ catalyst.....	105
Figure 4.9 Proposed reaction mechanism of converting pyruvaldehyde to lactic acid via intramolecular Cannizzaro with the ZrO ₂ catalyst. Lewis acids (Zr ⁴⁺) activates the carbonyl function groups of the pyruvaldehyde, following the nucleophilic attack by the electron donor (OH-), then the intramolecular rearrangement with a shift of the hydride, and finally the protonation to form the hydroxyl group at the C2 position.....	105
Figure 4.10 GC/MS spectra of aqueous-phase products with glycolaldehyde dimer as the feedstock.....	107
Figure 4.11 Temperature-programmed desorption profile of CO on ZrO ₂ and MgO.....	109
Figure 4.12 Temperature-programmed desorption profile of CO ₂ on ZrO ₂ and MgO.....	110
Figure 4.13 Effect of re-use of the ZrO ₂ catalyst on the yields of lactic acid and furfural by the conversion of xylose in pH neutral aqueous solutions. The spent catalyst was not regenerated.....	111

Figure 4.14 Comparison of the ATR-FTIR spectra of the fresh and spent ZrO ₂ catalysts. The spent catalyst was used once and was not regenerated.....	112
Figure 4.15 Effect of temperature on the yields of aqueous-phase products from the xylan conversion with the ZrO ₂ catalyst in pH neutral aqueous solution.....	114
Figure 4.16 Effect of catalyst loading on the yields of aqueous-phase products from the xylan conversion with the ZrO ₂ catalyst in pH neutral aqueous solution. Reaction conditions: 200 °C, 90 min, 2.4 MPa N ₂ , 5 wt% xylan loading.....	116
Figure 5.1 Comparison of different catalysts towards the xylose conversion in methanol solution	132
Figure 5.2 Temperature-programmed desorption of ammonia (NH ₃ -TPD) for Zr-SBA-15 materials with different Si/Zr molar ratios. All materials were synthesized at the hydrothermal temperature of 100°C.....	134
Figure 5.3 Comparison of different Zr ion loading on SBA-15 catalysts towards the xylose conversion in methanol solutions.....	134
Figure 5.4 Small-angle X-ray scattering patterns of Zr-SBA-15 materials.....	135
Figure 5.5 High-resolution transmission electron microscopy (HRTEM) image of Zr-SBA-15: (a) Si/Zr=20; (b) Si/Zr=10.....	135
Figure 5.6 Effect of temperature on the yields liquids-phase products of xylose conversion with the Zr-SBA-15 catalyst in methanol.....	137
Figure 5.7 Effect of reaction time on the yields liquids-phase products of xylose conversion with the Zr-SBA-15 catalyst in methanol.....	137
Figure 5.8 Effect of catalyst loading on the yields of liquids-phase products of xylose conversion with the Zr- SBA-15 catalyst in methanol.....	138

Figure 5.9 Nitrogen adsorption–desorption isotherms of Zr-SBA-15 materials; inset is the pore size distribution determined by NLDFT model for adsorption branch for N ₂ on silica at 77K (cylindrical pore model).....	139
Figure 5.10 Effect of re-use of the Zr-SBA-15 catalyst on the major products by the conversion of xylose in methanol. The spent catalyst was not regenerated.....	141
Figure 5.11 High-resolution transmission electron microscopy (HRTEM) image of Zr-SBA-15: a, fresh sample; b, after five times used.....	142
Figure 5.12 GC/MS spectra of methyl lactate stability test in methanol solvent with Zr-SBA-15 catalyst.....	142
Figure 5.13 Proposed reaction mechanism for conversion of xylose to methyl lactate and other intermediate and final products in methanol solvent with Zr-SBA-15 catalyst.....	144
Figure 5.14 Temperature-programmed desorption of ammonia (NH ₃ -TPD) for Zr-SBA-15 materials.....	145
Figure 5.15 FTIR spectra of adsorbed pyridine on Zr-SBA-15.....	145
Figure 5.16 GC/MS spectra of products from glycoaldehyde conversion in methanol solvent with Zr-SBA-15 as catalyst.....	149
Figure 5.17 GC/MS spectra of products from glycolaldehyde dimethyl acetal conversion in methanol solvent with Zr-SBA-15 as catalyst.....	149
Figure 5.18 GC/MS spectra of products from furfural conversion in methanol solvent with Zr-SBA-15 as catalyst.....	150
Figure 5.19 GC/MS spectra of the products from the conversion of glucose, fructose and sucrose in methanol solvent with the Zr-SBA-15 catalyst.....	152
Figure 5.20 GC/MS spectra of the products from the conversion of cellulose, cellobiose and starch in methanol solvent with the Zr-SBA-15 catalyst.....	153

Figure 5.21 Solvent effect on the yields liquids-phase products of cellulose conversion with the Zr-SBA-15 catalyst	158
Figure 5.22 Effects of temperature and reaction time on the yields of the products from the conversion of cellulose with the Zr-SBA-15 catalyst in ethanol-water mixture solution (95 wt% ethanol and 5 wt% water).	160
Figure 5.23 Different feedstocks conversion at different reaction temperatures with the Zr-SBA-15 catalyst. (a) Glucose conversion; (b) fructose conversion; (c) cellulose conversion; (d) solid residue (S.R.) after the conversion of the different feedstocks	161
Figure 5.24 Effect of catalyst loading on the yields of the products from the conversion of cellulose with the Zr- SBA-15 catalyst in ethanol-water mixture solution (95 wt% ethanol and 5 wt% water).	162
Figure 5.25 Proposed reaction mechanism for the conversion of cellulose to ethyl lactate in ethanol solvent with the Zr-SBA-15 catalyst	163
Figure 5.26 Re-use of the spent Zr-SBA-15 catalyst for the conversion of cellulose in ethanol-water solvent. The spent catalyst was not regenerated	165
Figure 5.27 Comparison of the ATR-FTIR spectra of the fresh, spent and calcination Zr-SBA-15 catalysts. The spent catalyst was used once and was not regenerated. The regenerated Zr-SBA-15 was used five times and then regenerated by calcination	165
Figure 5.28 Effect of re-use of the Zr-SBA-15 catalyst on the yields of the main products from the conversion of cellulose in the ethanol-water mixture solvent containing 5 wt% water. The spent catalyst was regenerated by the calcination in air at 550 °C for 5 h	166
Figure 5.29 High-resolution transmission electron microscopy (HRTEM) images of Zr-SBA-15: (a) fresh sample; (b) spent sample after three time use and regenerated in flowing air at 550 °C for 6 h	166

Figure 5.30 GC spectra of the gas-phase products from the ethanol-water solvent stability test	168
Figure 5.31 GC/MS spectra of the liquid-phase products from the ethanol-water solvent stability test	168
Figure 5.32 Solvent effects on the yield of ADA from the cellulose conversion with the Zr-SBA-15 catalyst	169
Figure 5.33 GC/MS spectra of the liquid-phase products from the conversion of glycolaldehyde dimer in the ethanol-water mixture solvent (95 wt% ethanol and 5 w% water) with the Zr-SBA-15 catalyst	169

Tables

Table 2.1 Elemental analysis and higher heating values of <i>Agave tequilana</i> and <i>Opuntia ficus-indica</i>	43
Table 2.2 Mass fraction distribution of fresh <i>Agave tequilana</i> and <i>Opuntia ficus-indica</i> samples (%, wet biomass basis).....	47
Table 2.3 pH and Composition of sample juices.....	47
Table 2.4 Composition of <i>Agave</i> leaf and <i>Opuntia</i> cladode bagasse reported in literature and the present study-mass fraction of dry material (%).....	49
Table 2.5 Inorganic Elements of <i>Opuntia ficus-indica</i> ash before and after extractive with EDS test.....	51
Table 2.6 Inorganic Elements of <i>Agave tequilana</i> ash before and after extractive with EDS test.....	51
Table 2.7 Assignments of signals in the C ₄ region of CP/MAS ¹³ C NMR spectra obtained from isolated cellulose of <i>Agave tequilana</i> and <i>Opuntia ficus-indica</i>	53
Table 3.1 The results of oxidation of guaiacol with H ₂ O ₂ with and without the TS-1 catalyst.....	68
Table 3.2 The comparison of the effect of the different solid catalysts on the catalytic oxidation of guaiacol with H ₂ O ₂	70
Table 4.1 Comparison of different catalysts and pH values towards the xylose conversion in aqueous solutions.....	102
Table 4.2 The yields of main products using furfural as the feedstock with and without the ZrO ₂ catalyst at different temperatures.....	102
Table 4.3 Comparison of different biomass derived molecules as the probe reactants which are also possible key intermediates during the catalytic conversion of xylose to lactic acid with the ZrO ₂ catalyst.....	108

Table 4.4 Experimental results of the Box-Behnken design using xylan as the feedstock. All runs operated under an initial pressure of 2.4 MPa N ₂	115
Table 4.5 Effect of acetyl group in the different probe additives, ethyl acetate or acetic acid, on the catalytic conversion of xylose with the ZrO ₂ catalyst.....	116
Table 5.1 Surface and Bulk Properties of Zr-SBA-15 silicates.....	140
Table 5.2 Comparison of different pore sizes effect of Zr-SBA-15 during the catalytic conversion of xylose to methyl lactate in methanol solvent	140
Table 5.3 Comparison of different feedstocks' conversion with Zr-SBA-15 as catalyst in methanol solvent.....	148
Table 5.4 The comparison of the main products yields of cellulose conversion with and without catalysts in different solvents.....	154
Table 5.5 Critical conditions of the ethanol-water solutions at different ethanol to water ratio	157

Chapter 1 Introduction

1.1 Requirement and challenge for renewable energy resources

With the depletion of fossil fuels and related petrochemicals, the need for renewable energy resources is expected to increase in the future. Additionally, with the worldwide concern over the excessive emission of greenhouse gases, additional pressures will be placed upon environmental resources. These new sources of energy include solar energy, wind, geothermal, hydropower, and biofuels. Among these alternatives, biomass is a renewable class of materials of growing interest among researchers aiming to achieve global sustainability. The application of biomass in the current energy system will necessarily need the development of new technologies for the large-scale production of biofuels and chemicals [1,2]. One of desirable routes for the biorefining is to selectively convert lignocellulosic biomass into value-added chemicals or into platform compounds, which can be easily converted to versatile chemicals or fuels in subsequent step [3,4]. Catalytic conversion of biomass can lead to multiple products, and the challenge is to direct the reaction pathways to the desired products. The US Department of Energy recently issued a report which listed 12 chemical building blocks considered as potential building blocks for the future. Organic acids (e.g., succinic, lactic, levulinic acid, etc.) are among the wide-spread “platform-molecules”, which may be further converted into possibly derivable high-value-added chemicals. The transition from a fossil chemical industry to a renewable chemical industry will likewise depend upon our ability to focus research and development efforts on the most promising alternatives.

1.2 Lignocellulosic biomass

Conversion of biomass to renewable fuels and value-added chemicals has attracted significant attention in the past [5–7]. Biomass generally refers to a variety of organisms produced by biological photosynthesis such as plants, animals and their wastes, including some domestic garbage and organic wastewater [8]. The biomass organisms are the carrier of biomass energy, converting solar energy into chemical energy through the photosynthesis of green plants. The process of biomass generation is as follows:



Biomass energy originally results from photosynthesis by using readily available atmospheric CO₂, water, and sunlight. Therefore, biomass is a sustainable and green feedstock for the production of fuels and fine chemicals. Also, recovering chemical resources from biomass waste can be used to control the circulation of carbon in the biosphere. Nearly 3% of the total energy consumption in the US was supplied by biomass in 2003 and biomass is the single largest renewable energy resource, recently surpassing hydropower [8]. A relatively significant amount of biomass (about 6 to 9 million dry tons) is also currently used in the production of a variety of industrial and consumer bioproducts that can directly displace petroleum-based feedstocks [9]. Similarly, the EU received 66.1% of its renewable energy from biomass, which thus surpassed the total combined contribution from hydropower, wind power, geothermal energy, and solar power [10]. In addition to energy, the production of materials from biomass such as biocrude, hydrogen, glucose, lactic acid, acetic acid, amino acids, is also essential [11–13].

Lignocellulose refers to plant dry matter (biomass), so called lignocellulosic biomass. It is the most abundantly available raw material on the Earth for the production of biofuels [14]. Lignocellulosic biomass can be broadly classified into virgin biomass, waste biomass, and energy crops. Virgin biomass includes all naturally occurring terrestrial plants such as trees, shrubs, and grasses. Waste biomass is produced as a low-value byproduct of various industrial sectors such as agricultural (e.g., corn stover, sugarcane bagasse, straw, etc.), forestry (e.g., saw mill and paper mill discards). Energy crops are crops with high yields of lignocellulosic biomass produced to serve as a raw material for the production of second generation biofuel examples include switch grass (*Panicum virgatum*) and Elephant grass. The main components of lignocellulosic biomass resources include carbohydrate polymers (e.g., cellulose, hemicellulose), and an aromatic polymer (e.g., lignin) (Figure 1.1). These carbohydrate polymers contain different sugar monomers (six and five carbon sugars) and they are tightly bound to lignin. Cellulose is the most common organic compound on earth. About 33% of all plant matter is cellulose (the cellulose content of cotton is 90% and that of wood is 40-50%) [15]. Cellulose is a linear homo-polysaccharide of D-glucose (C6 sugar) units linked through β -(1,4) glycosidic linkages. Hemicellulose is any of several hetero-polymers (matrix polysaccharides), such as arabinoxylans, present along with cellulose in almost all plant cell walls with a random, amorphous structure [16]. Xylose, the main building block of xylan, comprises about 25% of the dry weight biomass of some plant species such as hardwoods and agricultural residues [17]. While cellulose is crystalline, strong and resistant to hydrolysis, hemicellulose has a random, amorphous structure with little strength [18]. Hemicellulose is easily hydrolyzed by dilute acid or base as well as myriad

hemicellulase enzymes. Lignin is an irregular, heterogeneous and 3D polymer consisting of phenylpropane units, which can account for up to 40% of dry biomass by weight [19]. The concept of a biorefinery that integrates biomass conversion processes to produce fuels, power, heat, and value-added chemicals demands efficient utilization of all three components. However, most of the biomass conversion research is focused on utilizing of cellulose and hemicelluloses; while lignin remains relatively underutilized to its potential. The lignocellulosics-to-ethanol process makes use of the cellulose and hemicelluloses, leaving lignin as waste. Additionally, pulp and paper industry also generate huge amounts of lignin; however, lignin is only being utilized as a low-value fuel to provide heat and power despite the fact that lignin accounts for up to 40% of the energy value of biomass [20–22]. Nevertheless, the chemical structure of lignin suggests that it has significant potential as a source for the sustainable production of fuels and high-value chemicals if it could be broken into smaller molecular units [23].

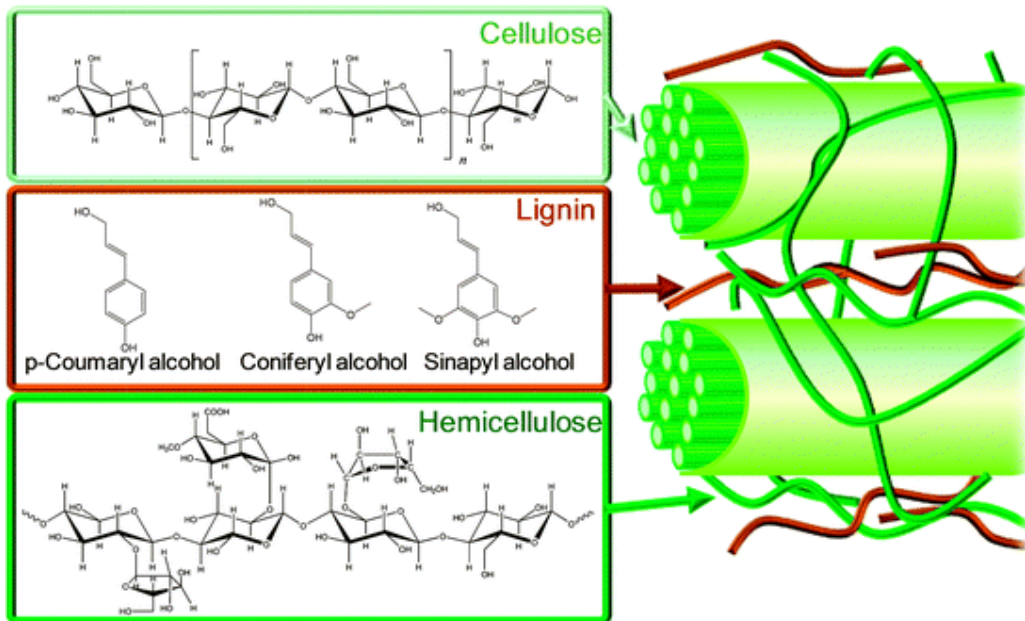


Figure 1.1 Chemical components of lignocellulosic biomass [24].

1.3 Drought-tolerant bioenergy crops in marginal environment

Most biomass feedstock used for the first-generation biofuels production is competing with foods production [4]. The development of drought-tolerant species on semi-arid and arid marginal lands where food crops cannot be cultivated, can avoid the competition of arable lands for food production [25]. Crassulacean acid metabolism (CAM) plants (Figure 1.2), possessing the remarkable quality of being able to take up and store water within a short time, which can thrive in the harsh conditions present in arid and semi-arid region [26], have stepped into our sight. There are three basic mechanisms involving in the assimilation of CO₂ from the atmosphere by plants: C3 photosynthesis, C4 photosynthesis and Crassulacean Acid Metabolism (CAM) [27]. During the night, a plant employing CAM has its stomata open, CO₂ is acquired and incorporated into the carboxyl group of an organic acid (normally malic acid) that are stored in vacuoles. During the day, the stomata are closed (thus preventing water loss), and the accumulated organic acid is decarboxylated to produce CO₂ that is consumed by the reactions of the photosynthetic carbon reduction cycle. The participation of malic acid as an intermediate of CO₂ fixation has been extensively studied in relation to stomatal aperture and water use efficiency [28,29]. Besides malate, the nocturnal accumulation of citrate may also provide some particular benefits to CAM plants under stressful conditions [30]. Anyway, there is no doubt about the important ecological significance of organic acid metabolism in CAM plants, allowing them to survive in arid regions, such as deserts and rocky outcrops [27,31].

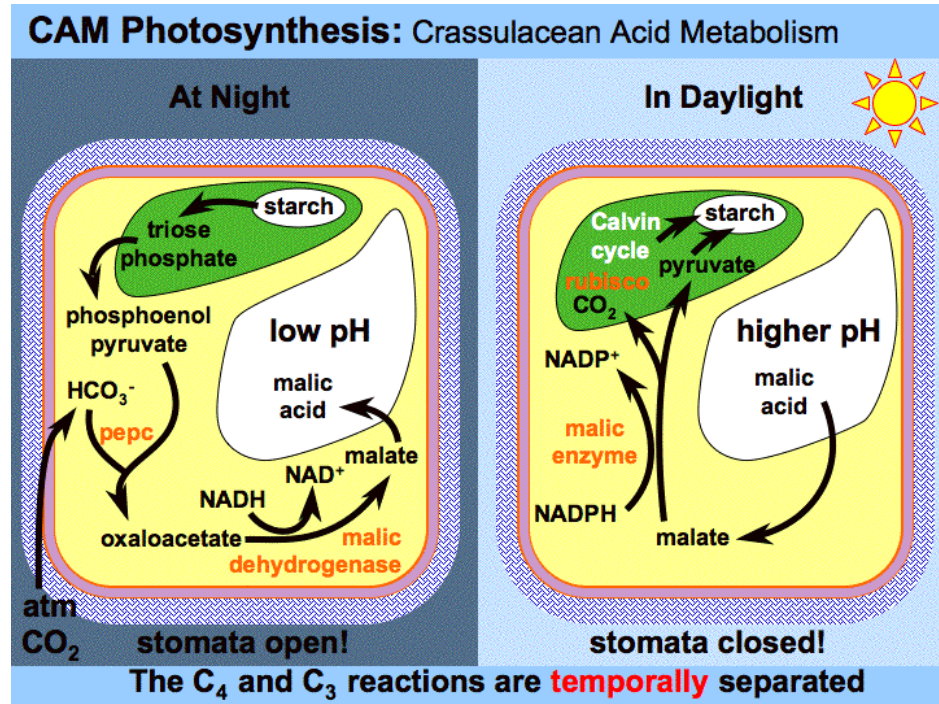


Figure 1.2 C₃ and C₄ carbon fixation reactions in CAM photosynthetic plants. In these plants, C₃ carbon fixation utilizing RuBisCo occurs during the day, while C₄ carbon fixation occurs utilizing PEPC at night [32].

1.4 Routes for the biofuel products from biomass conversion

Current technologies for converting lignocellulose to liquid hydrocarbon transportation fuels involve three major routes: gasification, pyrolysis, and hydrothermal processes (Figure 1.3). By means of these primary routes, lignocellulose is converted into gaseous and liquid fractions that are subsequently upgraded to liquid hydrocarbon fuels. Gasification converts solid biomass to syngas, the mixture of carbon monoxide, carbon dioxide and hydrogen [33], which can be regarded as a precursor of liquid hydrocarbon fuels and can be further upgraded to liquid fuels through Fischer–Tropsch reactions. This pathway is suitable for any kind of biomass, but the very high energy requirement is a disadvantage. Pyrolysis allows transformation of lignocellulosic biomass into a liquid fraction known as bio-oil that can be subsequently upgraded to hydrocarbon fuels by a

variety of catalytic processes. The third route involves pretreatment–hydrolysis steps to yield aqueous solutions of C₅ and C₆ sugars derived from lignocellulose. While gasification and pyrolysis are pure thermal routes in which lignocellulose is decomposed with temperature under a controlled atmosphere, aqueous-phase processing, in contrast, involves a series of catalytic reactions to selectively convert sugars, and important platform chemicals derived from them, into targeted liquid hydrocarbon fuels with molecular weights and structures appropriate for gasoline, diesel, and jet fuel applications.

Adding catalysts in the hydrothermal process has been demonstrated to enhance the substrate decomposition rate and to increase the reaction selectivity towards specific products [34–36]. The addition of an acid catalyst may lead to an increase of dehydration reactions and thus to the formation of hydroxymethylfufural, 5-HMF, and its derivative product, levulinic acid, in higher concentrations of the acid-catalyzed reaction scheme. The acid-catalyzed reaction mechanism is seen in control reactions through the increased acidity as a result of higher ionic content in high temperature water as a result of dissociation of water at elevated temperatures of water to H₃O⁺ and OH⁻ [37]. At these elevated temperatures, high-temperature water has a catalytic effect, which is able to acid catalyze the formation of levulinic acid from fructose. This effect of higher ionic content in water is necessary for understanding catalytic effect, as certain catalysts are able to inhibit the acid catalytic effects by suppressing the ionic product in water, and they are thus able to produce different products through different reaction mechanisms.

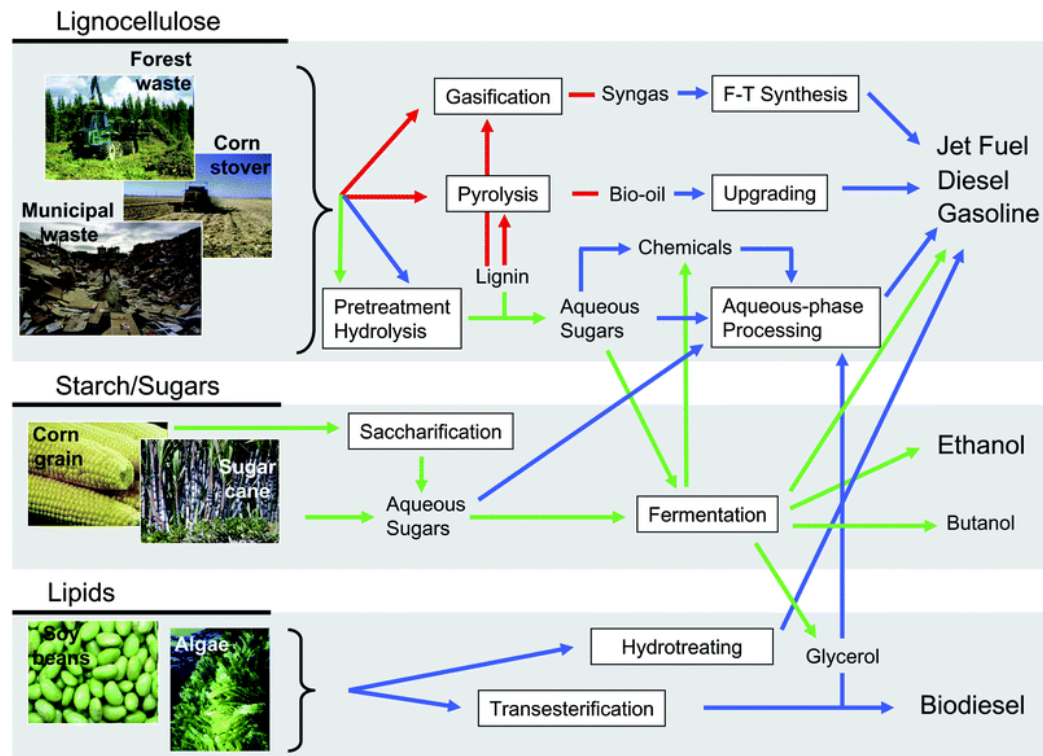


Figure 1.3 Routes for the conversion of biomass into liquid fuels. Red arrows refer to thermal routes, green arrows refer to biological routes, and blue arrows refer to catalytic routes [38].

In contrast, base catalysis favors the retro-aldol condensation reactions and results in the formation of lactic acid [39]. The use of base catalysts was shown to minimize levulinic acid production through inhibiting the acid catalysed reaction mechanism in high temperature water. Lactic acid is produced through the base-catalyzed reaction of pyruvaldehyde formed from the retro-aldol condensation of fructose. Lactic acid has also been produced through utilizing heterogeneous Lewis-acid catalysts, such as tungstated zirconia and aluminium [40].

The products generated from catalytic process can include oligosaccharides, sugars, sugar alcohols, aldehydes, ketones, and carboxylic acids [41–43]. Carboxylic acids represent an important class of renewable chemicals derived from biomass. The US Department of Energy released a list of 30 basic molecules that can be derived from

carbohydrate biomass to guide the emerging research in production of biobased chemicals [44]. Bozell et al. has updated this list recently based on criteria used in evaluating biobased product opportunities [45]. In both lists, carbohydrate-derived organic acids (e.g., lactic, succinic, and levulinic acid) are among the “platform-molecules”, which can be further converted into high-value-added chemicals.

1.5 Carbohydrates to carboxylic acids

There are two types of carbohydrates, C5 and C6 sugars, which account for 65-85% of lignocellulosic biomass in two forms of biopolymers, cellulose, and hemicellulose. Hydrolysis of carbohydrate biomass followed by sugar degradation can produce organic acids by an acid-catalyzed hydrolysis reaction [46].

1.5.1 Lactic acid

Lactic acid (2-hydroxy-propanoic acid) has both a hydroxyl group and a carboxylic acid group and can be used as a precursor to produce a wide range of chemicals. Thus, it is one of important biomass-derived organic acids. Lactic acid has recently been receiving much attention as a building block to synthesize other commodity chemicals with a growing market (Figure 1.4). It is applied in the food and pharmaceutical industries as mild acid flavor, pH-regulator, and preservative. An emerging product is poly (lactic acid), PLA, used in manufacturing biodegradable plastics [47]. However, lactic acid supply is insufficient for future demands and an expended role for lactic acid in the future will depend on lowing its manufacture costs [39].

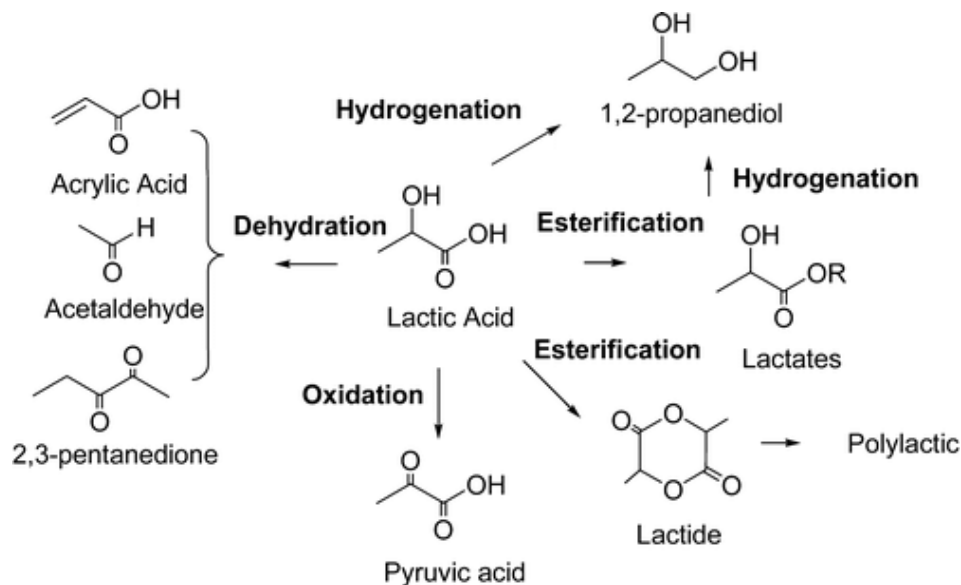


Figure 1.4 Lactic acid as a platform intermediate for the chemical and fuels [13].

There has been a steady increase in production of lactic acid since the early 1990's all over the world. The mainstream production process of lactic acid is the fermentation of glucose from starch hydrolysis by using genetically-modified enzymes [48–51]. However, the fermentation process cannot directly utilize non-food cellulosic biomass. Chemical processes that convert saccharides into lactic acids or lactates were investigated in hot water with alkali or metal salts [47]. These chemical processes are simpler and more flexible than fermentation processes, which help to increase the lactic acid supply. However, these chemical processes use a high concentration of alkaline, operate at high reaction temperatures, and generate a large amount of by-products, all of which are undesirable.

Alkaline hydrothermal conversion of lignocellulosic biomass into lactic acid has been discussed by many researchers. Yan *et al.* showed that both NaOH and Ca(OH)₂ can promote the formation of lactic acid in a hydrothermal reaction of glucose [52]. Lactic acid was obtained at a yield of 27% at 300 °C for 1 min with addition of NaOH. They

also investigated the hydrothermal conversion of other carbohydrates including cellulose and starch to lactic acid using NaOH and Ca(OH)₂ catalysts. Lactic acid was obtained from cellulose and starch in almost the same yield as that obtained from glucose under the same reaction conditions of 300°C and 0.32 M Ca(OH)₂, but in the case of cellulose, a slightly longer reaction time of 1.5 min was required [11]. Ma *et al.* investigated alkaline hydrothermal experiments of glucose, fructose, and xylose in a batch reactor with the temperature range of 250 to 350 °C to examine the production of lactic acid [53]. Result showed that the formation of lactic acid could be strongly affected by the concentration of alkaline catalysts such as NaOH, KOH, and Ca(OH)₂. The yield of lactic acid from glucose, fructose, and xylose followed the sequence of fructose > glucose > xylose with NaOH as alkaline catalyst. A high lactic acid yield of 42.7% was obtained from fructose. Figure 1.5 shows the reaction mechanism of alkaline degradation of glucose into lactic acid including a reverse aldol condensation from C6 to C3 chemicals.

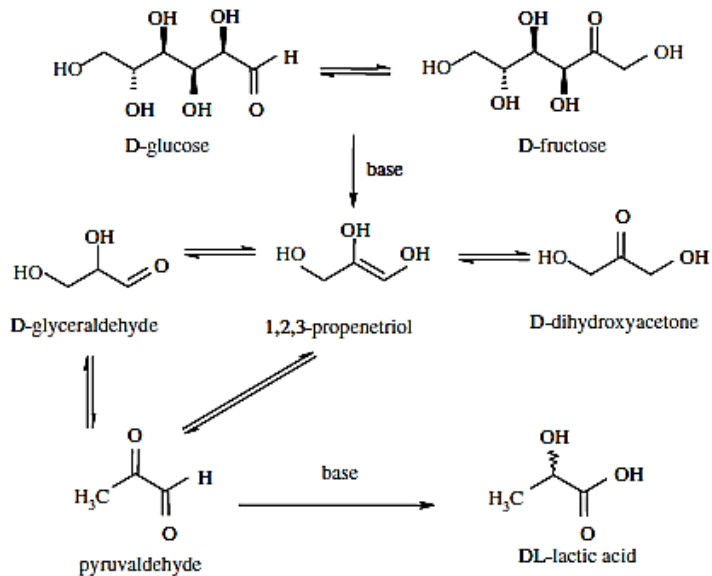


Figure 1.5 Conversion of D-glucose into lactic acid over base catalysts [39].

The use of inorganic salts as catalysts for the conversion of various sugars to lactic acid in aqueous solutions has been reported. Rasrendra *et al.* investigated the use of inorganic salts as catalysts for the reactions of D-glucose in aqueous solutions and found that Al^{3+} and Cr^{2+} salts gave the highest conversion of D-glucose [54]. The type of inorganic salt greatly affected the chemo-selectivity. The major liquid product for the Al-salts is lactic acid with the hypothesis that the intermediate trioses like glyceraldehyde and dihydroxyacetone may be converted in high yields to lactic acid when using Al-salts. Bicker *et al.* found that by adding small quantities of metal ions such as Co^{2+} , Ni^{2+} , Cu^{2+} and Zn^{2+} in subcritical water, the lactic acid yield was increased up to 42% starting from sucrose and 86% starting from dihydroxyacetone at 300 °C and 25 MPa. Zn^{2+} gave the best results with regard to the lactic acid yield [47]. Kong *et al.* [55] reported the influence of metal ions (Zn^{2+} , Ni^{2+} , Co^{2+} , and Cr^{3+}) on biomass decomposition in subcritical water ($T = 300$ °C). In comparison with a non-catalytic process, the lactic acid yield from glucose was 9.5 wt% for 400 ppm Co(II) catalyst at 300 °C and 2 min. Besides metal salts, Zhang *et al.* [56] investigated the effect of Zn, Ni, and activated carbon on the yield of lactic acid from cellulose under alkaline hydrothermal conditions. The results showed that the lactic acid yield can be improved greatly by adding Zn, Ni, and activated carbon. The highest lactic acid yield was 42% under this condition, which was much higher than only using NaOH (15%). Li *et al.* [57] also reported that the CuO can be reduced completely to Cu with cellulose as a reductant under alkaline hydrothermal condition.

The catalytic production of lactic acid from biomass-derived sugars over solid base catalysts was an effective process with low impact to the environment. Onda *et al.* [39]

studied the activated hydrotalcites for the reaction of converting glucose to lactic acid in a flow reactor at 323 K in water media. In this study, the number of accessible Brønsted-base sites of hydrotalcite ($Mg/Al = 2$) is correlated to the calcination temperature, which had profound effects on the amount of Brønsted-base sites. The lactate yield was 20.3 C% at 8 h of time-on-stream over the hydrotalcite catalyst calcined at 723 K. They also found that under the same conditions, MgO and $\gamma\text{-Al}_2\text{O}_3$ catalysts showed little and almost no catalytic activity for the reaction, respectively. In contrast, Liu *et al.* demonstrated that MgO was an active solid base catalyst for the production of methyl lactate from glucose in methanol. The yield of methyl lactate reached 29% under optimal reaction conditions [58]. In another interesting study, a series of Al-Zr mixed oxides with different molar ratios were examined with glucose reaction in hot compressed water at 180 °C [59]. Al_2O_3 and ZrO_2 are well known for their acid–base bifunctional property and stability. In their work, mixed oxides showed better catalytic activity to lactic acid compared to single oxide, Al–3Zr and 3Al–Zr showed high selectivity to lactic acid, ~33%. Both moderate and strong base sites on the metal oxides are helpful for the formation of lactic acid.

Onda *et al.* also investigated the catalytic conversion of monosaccharides, such as D-glucose, D-fructose, D-mannose, D-galactose, and D-xylose, into lactic acid and aldonic acid in an alkaline media using supported noble metal catalysts under flowing air [60]. This one-pot reaction improved the carbon efficiency for the D-glucose conversion and decreased the by-products. It succeeded in yielding about 45 C-% of lactic acid and about 45 C-% of gluconic acid from D-glucose in a one-pot reaction using Pt/C catalysts in NaOH aqueous solution at 353 K under flowing air. The reaction of xylose, an aldopentose, resulted in about 20 C-% and 27 C-% yields of C5 aldonic acid and lactic

acid, respectively. Thus, D-Glucose, D-fructose, and D-mannose were favorable for alkaline degradations into lactic acid as compared to D-galactose and D-xylose, which suggested that the favorability might be due to alternative actual geometry of the third and fourth asymmetric carbons in monosaccharides.

Solid Lewis acids such as tungstated zirconia (ZrW) and tungstated alumina (AlW) has exhibited a remarkable promoting effect on the cellulose depolymerisation with 27 mol% and 18.5 mol% lactic acid yield being achieved on AlW and ZrW, respectively [40]. Moreover, tungsten based Lewis acids exhibited a good stability and recyclability. The efficiency of the solid Lewis acids ZrW and AlW to produce lactic acid directly from crystalline cellulose was explained by a positive synergy between water autoprotolysis responsible of the cellulose depolymerization into soluble intermediates, which are further converted on the solid Lewis catalyst surface. The catalytic conversion of mono- and di- saccharides for the direct formation of methyl lactate using Lewis acidic zeotypes, such as Sn-Beta, was investigated by Taarning and coworkers (Figure 1.6) [61]. In this process, resembling the alkaline degradation of sugars, sucrose, glucose, and fructose dissolved in methanol were converted into methyl lactate in yields up to 68% at 160 °C. However, in contrast to the traditional alkaline degradation, a stoichiometric amount of base is not consumed in acid-catalyzed conversion of mono- and disaccharides. Nonetheless, the reaction pathway in the acid-catalyzed conversion is greatly sensitive to the kind of acid used: Brønsted acids catalyzed monosaccharide dehydration reactions primarily result in HMF and its decomposition products while Lewis acidic zeotype catalysts lead to retro-aldol reaction of the monosaccharides and subsequent transformation to hydroxycarboxylic acid derivatives. It is critical to diminish the

catalytic effect of Brønsted acids to achieve a high selectivity in the Lewis acid catalyzed process, for example, esters rather than carboxylic acids were formed by using methanol as solvent.

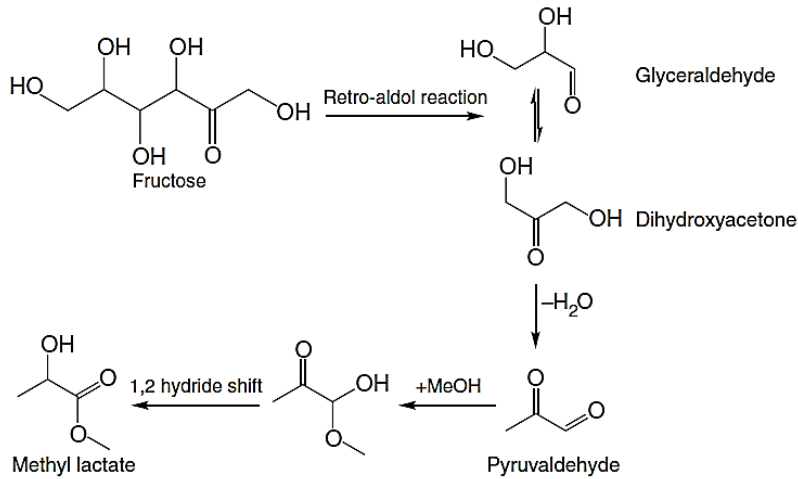


Figure 1.6 Proposed reaction pathway for the conversion of fructose to methyl lactate. The reaction formally comprises a retro aldol fragmentation of fructose and isomerization-esterification of the trioses [61].

1.5.2 Other carboxylic acids

Cellulose can be transformed to many value-added platform chemicals as mentioned above. Whereas the conversion of biomass to fuel must undergo a costly hydrogenation process, it is important to make conversion from renewable hydrogen provider. Formic acid can form hydrogen reversibly in the present of a metal catalyst. In order to satisfy this need, the conversion of cellulose to formic acid turns out to be significant since cellulose is the most abundant and non-edible biomass. There are two processes for cellulose to formic acid conversion. First, cellulose will be hydrolyzed to glucose. Then, glucose will be oxidized to formic acid. Li *et al.* [62] reported a catalytic air oxidation method with $H_5PV_2Mo_{10}O_{40}$ as catalyst. This heteropolyacid can be used as a

bifunctional catalyst in the conversion of cellulose to formic acid with a yield of 35%. And the yield of formic acid from glucose is up to 52%. Jin *et al.* reported a higher yield of formic acid up to 75% when using H₂O₂ as oxidant at a mild temperature of 25 °C in the presence of base [11,63].

Levulinic acid, also known as 4-oxopentanoic acid or γ -ketovaleric acid, is a short-chain fatty acid having a ketone carbonyl group and an acidic carboxylic group. Although levulinic acid has been known for almost 150 years [64], its current status is still an expensive specialty chemical available in limited quantities. However, levulinic acid is a versatile platform chemical with numerous potential uses, which can be used as a textile dye, antifreeze, animal feed, coating material, solvent, food flavoring agent, pharmaceutical compounds, and hydrocarbon fuels (Figure 1.7) [36,64–70]. Biomass feedstocks have been used to synthesize levulinic acid and the most widely used approach is the controlled dehydrative treatment of carbohydrates with acid catalyst. Many sugar materials such as glucose, sucrose, fructose, and cellulosic biomass materials including wood, starch, cane sugar, grain sorghum, and agricultural wastes have been used to produce levulinic acid [38,61,64–84].

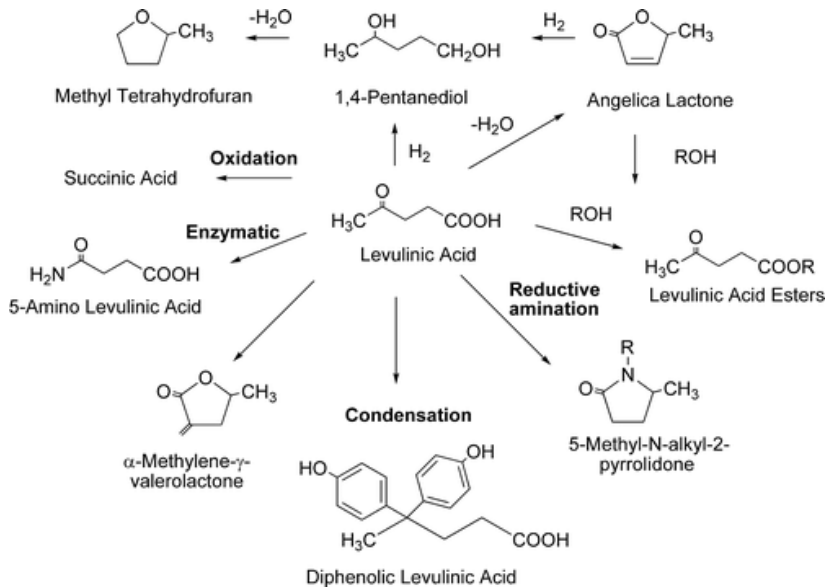


Figure 1.7 Levulinic acid as a platform intermediate for chemicals and fuel [13].

Our group recently presents an alternative pathway, aqueous phase partial oxidation (APPO), to produce levulinic acid directly from cellulose with lean air and water over inexpensive solid metal oxide catalysts [91]. The maximum obtainable yield of levulinic acid in the APPO process is ~60 mol%, comparable to yields of levulinic acid which have been achieved via acid hydrolysis. Our findings reveal that redox properties of the APPO catalyst play a key role and that superoxide radical anions are the possible active oxidant species in aqueous media, which distinguish APPO from acid hydrolysis. As shown in Figure 1.8, hydrogen at the C1 position is abstracted by a superoxide radical, and then molecular oxygen is inserted into the C1 position and formed a new organic radical. The organic radical is combined with a proton to form hydroperoxy radical and leaves the carbonyl bond on the C1 carbon. The carbonyl bond is hydrated and the glycosidic bond connecting the two sugar units is cleaved. And the 3,4,5-trihydroxy-6-hydroxymethyl-tetrahydro-pyran-2-one is further hydrated to form gluconic acid, which is deoxygenated through an initial Hofer–Moest-type decarboxylation followed by a series of consecutive

dehydration/rehydration reactions to form levulinic acid. The APPO process has the inherent merits of environmental friendliness, low humin formation, and ease of separation of catalyst, and thus it has the potential to replace the current acid hydrolysis process for commercial production of levulinic acid.

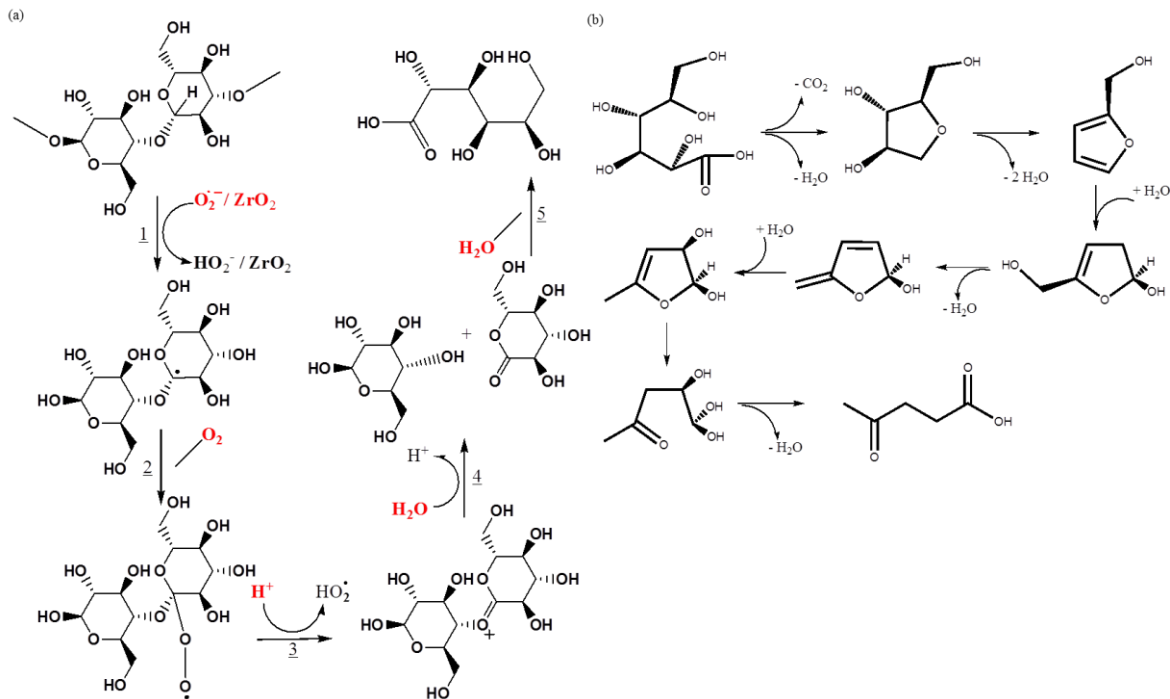


Figure 1.8 Reaction pathway of (a) converting a cellobiose unit in cellulose to glucose and gluconic acid by superoxide radical anions. (b) converting gluconic acid to levulinic acid by a Hofer–Moest-type decarboxylation reaction followed by consecutive dehydration/rehydration reactions [91].

Glycolic acid is a significant bulk fine chemical, which is consumed greatly in the US annually. It has wide use in the leather, oil and gas, and textile industries. It can be used for adhesives and is a component in many personal care products. Glycolic acid is also the monomer to synthesize a variety of polyglycolic acid (PGA) based polymers, including thermoplastic resins and biodegradable polymers for use in sutures. Glycolic acid is commercially manufactured by reacting chloroacetic acid with sodium hydroxide.

Reacting formaldehyde with carbon monoxide in the presence of an acid catalyst, such as HF, also produces glycolic acid. It can be made using glycolonitrile in an enzymatic process [92,93]. Due to the extremely hazardous nature of reactants involved in these routes, other ways to produce glycolic acid have been investigated.

Recently, Zhang *et al.* [94] directly converted various cellulosic biomass to glycolic acid with heteromolybdic acids, which act as multifunctional catalysts in a water medium, and oxygen atmosphere. Four types of Keggin-type HPAs, including $H_3PW_{12}O_{40}$ (HPW), $H_3PMo_{12}O_{40}$ (HPM), $H_4SiW_{12}O_{40}$ (HSW), and $H_4SiMo_{12}O_{40}$ (HSM), were used as catalysts for the conversion of α -cellulose powder. The best result was achieved by $H_3PMo_{12}O_{40}$ with the production of glycolic acid of 49%. Also, $H_3PMo_{12}O_{40}$ is even capable of converting raw cellulosic materials, such as bagasse and hay, to glycolic acid with yields of ~30%. The strong Brönsted acidity of $H_3PMo_{12}O_{40}$ facilitates the hydrolysis of cellulose; whereas the moderate oxidative activity allows selective oxidation of the aldehyde groups in the fragmentation products. Successive retro- aldol reactions dominate the fragmentation of monosaccharides generated from cellulose hydrolysis, resulting in high selectivity of glycolic acid. The author proposed a reaction pathway for the conversion of cellulose to glycolic acid and formic acid, as shown in Figure 1.9.

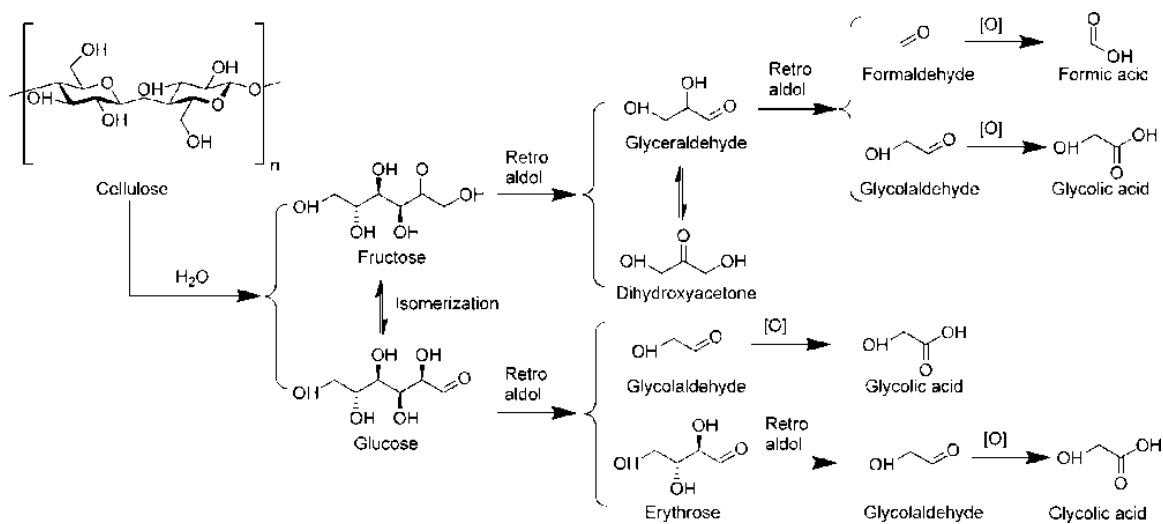


Figure 1.9 Product yields from the conversion of different sacchariferous reactants using HPM as the catalyst [94].

1.6 Lignin to phenolic acids

Lignin is generally defined as polymeric natural products arising from three primary monomers: p-coumaryl alcohol (B1), coniferyl alcohol(B2) and sinapyl alcohol(B3), as shown in Figure 1.10 [95,96]. The enzyme-initiated polymerization results in bonds of exceptional stability: biphenyl carbon–carbon linkages between aromatic carbons (5-5’), alkyl–aryl carbon–carbon linkages between an aliphatic and aromatic carbon (β -1), and hydrolysis-resistant ether linkages. The only linkage that is relatively weak and hydrolysable is the α -aryl ether bond (β -O-4).

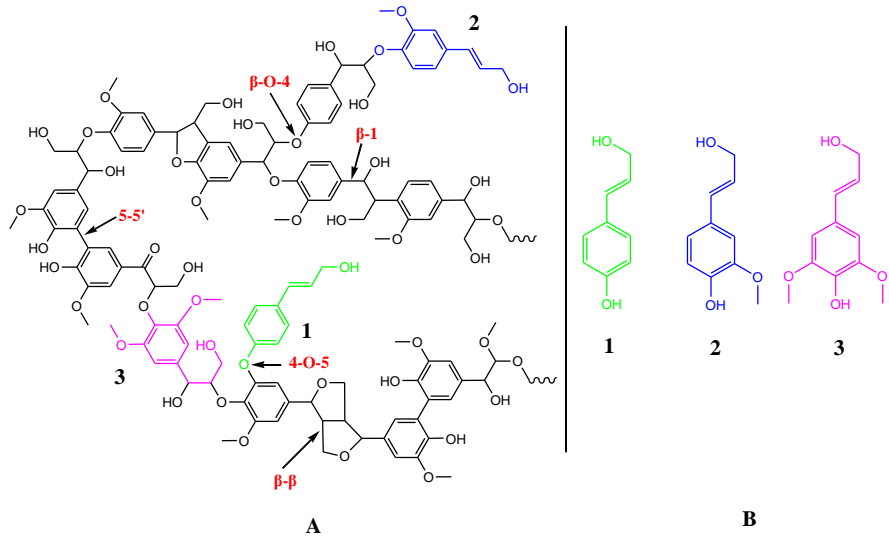


Figure 1.10 The possible structure of lignin (A) and three common lignin monomers (B). B1, H-lignin (*p*-coumaryl alcohol); B2, G-lignin (coniferyl alcohol); B3, S-lignin (sinapyl alcohol).

The utilization of lignin in the chemical industry has largely been limited because of the complicated chemical structure and persistent property of lignin [22]. Generally, there are two kinds of products for lignin conversion, chemical and fuel. Catalytic oxidation has the potential to selectively convert lignin into various useful chemicals and this methodology has rapidly progressed in the past several years. Figure 1.11 shows the oxidation reaction of different model compounds of lignin. Based up on the different structure of the lignin precursors, the oxidation reaction pathways can be divided into three categories: 1) *p*-coumaryl alcohol resembling lignin model compounds to 4-hydrobenzaldehyde [96–98] and then 4-hydrobenzoic acid [99]; 2) coniferyl alcohol resembling lignin model compounds to vanillin [100] and vanillic acid [101]; 3) sinapyl alcohol resembling lignin model compounds to syringaldehyde and syringic acid.

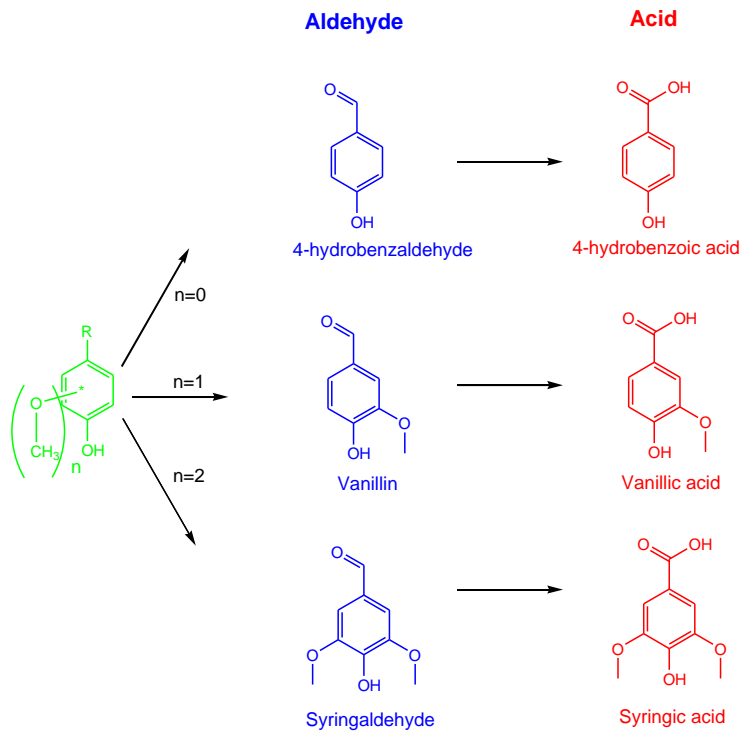


Figure 1.11 Oxidation reaction pathways of different model compounds of lignin.

Partenheimer used a cobalt/manganese/zirconium/bromide (Co/Mn/Zr/Br) catalyst to oxidize five different lignin model compounds (4-hydroxy-benzaldehyde, 3-methoxy-4-acetoxy-benzaldehyde, 4-methoxy-toluene, 3-methoxy-4-hydroxy-toluene, 3-methoxy-4-acetoxy-toluene) in acetic acid solution by air. Eighteen products were identified via gas chromatography/mass spectrometry (GC/MS). The most valuable products from lignin were 4-hydroxybenzaldehyde, 4-hydroxybenzoic acid, 4-hydroxy-3-methoxybenzaldehyde (vanillin), 4-hydroxy-3-methoxybenzoic acid (vanillic acid), 4-hydroxy-3,5-dimethoxybenzaldehyde (syringaldehyde), and 4-hydroxy-3,5-dimethoxybenzoic acid (syringic acid). By the use of model compounds they demonstrated that i) the presence of the phenolic functionality on an aromatic ring inhibits the rate of reaction, but that the alkyl group on the ring still oxidizes to the carboxylic acid; ii) the masking of phenol by acetylation occurs at a reasonable rate in

acetic acid; iii) the alkyl group of the masked phenol very readily oxidizes; iv) an acetic anhydride/acetic acid mixture is a good oxidation solvent; and v) a two-step acetylation/oxidation to the carboxylic acid was feasible [99].

Crestini *et al.* had reported a convenient and efficient application of heterogeneous methyl-rhenium trioxide (MTO) systems for the selective oxidation of lignin model compounds and lignin [101]. H₂O₂ was used as the oxidant. They found that the immobilized MTO catalysts were able to extensively oxidize both phenolic and non-phenolic, monomeric, and dimeric, lignin model compounds with H₂O₂. The diphenylmethane model reactant was found to be extensively oxidized. Immobilized MTO catalytic systems are potential candidates for the development of alternative chlorine-free and thus environmentally sustainable delignification processes.

Yokoyama *et al.* investigated the effect of lignin-biopolymer structure on the mechanism of its oxidative depolymerization by polyoxometalates (POMs) by reacting an equilibrated POM ensemble with a series of ring-substituted benzyl alcohols. Their results indicated that the reaction proceeds via successive oxidations of the benzylic carbon atom and aromatic-ring cleavage was not observed [102].

Furthermore, various catalysts such as base metals, noble metals, perovskite-type oxide catalysts, and metal organic frameworks, *etc*, either heterogeneous or homogeneous, can be used to improve the efficiency of oxidation lignin and lignin-derived compounds.

1.7 Dissertation Structure

The overall goal of this dissertation was to develop a catalytic reaction process to convert lignocellulosic biomass to desired carboxylic acids by utilizing heterogeneous catalysts. Due to the complicated chemical structure and persistent property of lignin, it is

only being utilized as a low value fuel to provide heat and power despite the fact that lignin can account for up to 30% of the energy value of biomass. Also, the requirement of integrated processing and the effective utilization of both hemicellulose and cellulose, consisting primarily of C5 and C6 sugars, respectively, are important challenges for technically viable and economic conversion of lignocellulosic biomass into chemicals and fuels. While the simultaneous processing of all carbohydrates, such as in gasification or pyrolysis, offers the potential for simplicity of operation, the fractionation of lignin, hemicellulose, and cellulose allows the processing of each fraction to be tailored to take advantage of the different chemical and physical properties of these fractions. This fractionation also offers increased flexibility of operation. Thus, two classes of processing strategies have been explored in this work ([Figure 1.12](#)): 1) the lignin is converted into phenolic aldehydes or acids such as maleic acid at low temperature using TS-1 catalyst with H₂O₂ as green oxidant in aqueous phase; 2) the hemicellulose and cellulose fractions could be either processed together or separated, and processed individually to carboxylic acid by solid Lewis acid catalysts (ZrO₂ and Zr-SBA-15) in aqueous phase or in related alcohol solvent to obtain lactic acid and relative lactic acid esters. The carbohydrate derived carboxylic acids or derivatives can be further upgraded into value polymers or paraffinic hydrocarbons through polymerization, hydrogenation, dehydration, and oligomerization. The lignin derived phenolic compounds can be converted into aromatic hydrocarbons by hydrodeoxygenation.

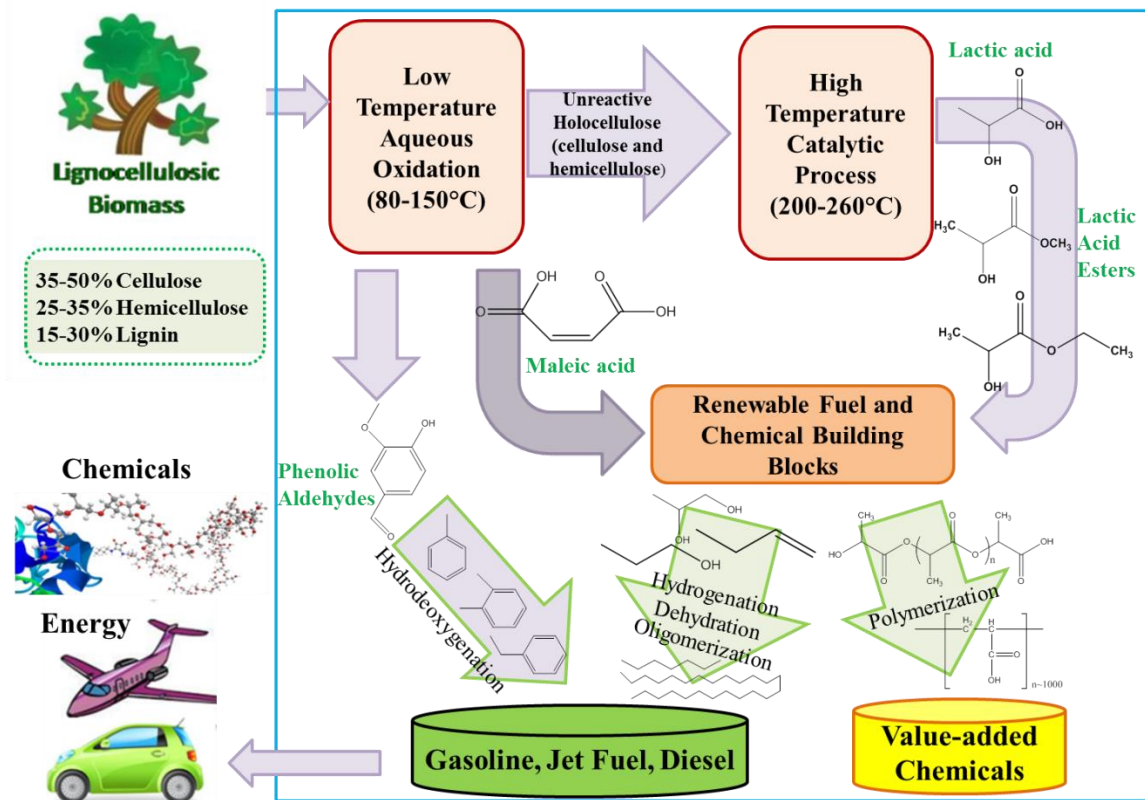


Figure 1.12 Integrated biorefining process for lignocellulosic biomass.

The following chapters investigate different catalysts and optimize the reaction process through chemical analysis and materials characterization, catalytic effect, and reaction conditions for lignocellulosic biomass conversion. First, chapter two characterizes the biomass composition of drought-tolerant plants, *Agave tequilana* and *Opuntia ficus-indica*. In chapter three, the feasibility of low-temperature selective oxidation of lignin model compound, guaiacol to value-added dicarboxylic acid, maleic acid, was investigated in a titanium silicalite/hydrogen peroxide (TS-1/H₂O₂) reaction system. Chapter four investigated the catalytic properties of the ZrO₂ catalyst and it was found that the acid-base function was superior towards the lactic acid synthesis from hemicellulose. Chapter five developed the mesoporous Zr-silicates catalysts, which were

synthesized with tunable structures and pore sizes showing excellent catalytic performance for the conversion of carbohydrates to lactic acid derivatives. The final chapter gives a brief synopsis and summary of the work and includes possible future directions.

1.8 References

1. Farrell, A.E., Plevin, R.J., Turner, B.T., et al. (2006) Ethanol can contribute to energy and environmental goals. *Science* **311**, 506–508.
2. Dodds, D.R., and Gross, R.A. (2007) Chemicals from biomass better computing with photons. *Science* **318** (7), 1250.
3. Chhedra, J.N., Huber, G.W., and Dumesic, J. a (2007) Liquid-phase catalytic processing of biomass-derived oxygenated hydrocarbons to fuels and chemicals. *Angew. Chem. Int. Ed. Engl.* **46** (38), 7164–7183.
4. Ragauskas, A.J., Williams, C.K., Davison, B.H., et al. (2006) The path forward for biofuels and biomaterials. *Science* **311** (5760), 484–489.
5. Casanova, O., Iborra, S., and Corma, A. (2009) Biomass into chemicals: aerobic oxidation of 5-hydroxymethyl-2-furfural into 2,5-furandicarboxylic acid with gold nanoparticle catalysts. *ChemSusChem* **2** (12), 1138–1144.
6. Serrano-Ruiz, J.C., and Dumesic, J.A. (2011) Catalytic routes for the conversion of biomass into liquid hydrocarbon transportation fuels. *Energy Environ. Sci.* **4** (1), 83–99.
7. Gounder, R. (2014) Hydrophobic microporous and mesoporous oxides as Bronsted and Lewis acid catalyst for biomass conversion in liquid water. *Catal. Sci. Technol.* **4**, 2877–2886.
8. U.S. Department of Energy (2005) “Biomass as feedstock for a bioenergy ans bioproducts industry: the technical feasibility of a billion-ton annual suply.”
9. U.S. Department of Energy (2004) “The Bioproducts Industry : Today and Tomorrow” **(March 2004)**.
10. European union (2007) “Rrnewable energy road map,” 1–4.
11. Yan, X. (2010) “Hydrothermal conversion of carbohydrate biomass to lactic acid” **56** (**10**), 2727–2733.
12. Mosier, N., Wyman, C., Dale, B., et al. (2005) Features of promising technologies for pretreatment of lignocellulosic biomass.Bioresource technol. **96**(**6**) (6), 673–686.

13. Corma, A., Iborra, S., and Velty, A. (2007) Chemical routes for the transformation of biomass into chemicals. *Chem. Rev.* **107** (6), 2411–2502.
14. Phitsawan, P., Sakka, K., and Ratanakhanokchai, K. (2013) Improvement of lignocellulosic biomass in planta: A review of feedstocks, biomass recalcitrance, and strategic manipulation of ideal plants designed for ethanol production and processability. *Biomass and Bioenergy* **58**, 390–405.
15. “Cellulose.” [Online]. Available: <http://en.wikipedia.org/wiki/Cellulose>.
17. Ladisch, M.R., Lin, K.W., Voloch, M., and Tsao, G.T. (1983) Process considerations in the enzymatic hydrolysis of biomass. *Enzyme Microb. Technol.* **5** (2), 82–102.
18. Kobayashi, H., Ohta, H., and Fukuoka, A. (2012) Conversion of lignocellulose into renewable chemicals by heterogeneous catalysis. *Catal. Sci. Technol.* **2** (5), 869–883.
19. Zhou, C.-H., Xia, X., Lin, C.-X., et al. (2011) Catalytic conversion of lignocellulosic biomass to fine chemicals and fuels. *Chem. Soc. Rev.* **40** (11), 5588–5617.
20. Yun Yu, Xia Lou, H.W. (2008) Some recent advances in hydrolysis of biomass in hot-compressed water and its comparisons with other hydrolysis methods. *Energy & Fuels* **22** (1), 46–60.
21. Sales, F., Maranhão, L., and Abreu, C. (2007) Experimental evaluation and continuous catalytic process for fine aldehyde production from lignin. *Chem. Eng. Sci.* **62**, 5386–5391.
22. Collinson, S.R., and Thielemans, W. (2010) The catalytic oxidation of biomass to new materials focusing on starch, cellulose and lignin. *Coord. Chem. Rev.* **254** (15-16), 1854–1870.
23. Ragauskas, A.J., Beckham, G.T., Biddy, M.J., et al. (2014) Lignin valorization: improving lignin processing in the biorefinery. *Science* **344** (6185), 1246843.
24. Alonso, D.M., Wettsteinab, S.G., Dumesic, J.A. (2012) Bimetallic catalysts for upgrading of biomass to fuels and chemicals, *Chemical Society Reviews* **24**, 8075-8098.
25. Cushman, J.C., Davis, S.C., Yang, X., and Borland, A.M. (2015) Development and use of bioenergy feedstocks for semi-arid and arid lands. *J. Exp. Bot.*, 1–17.
26. Borland, A.M., Griffiths, H., Hartwell, J., and Smith, J.A.C. (2009) Exploiting the potential of plants with crassulacean acid metabolism for bioenergy production on marginal lands. *J. Exp. Bot.* **60** (10), 2879–2896.

27. López-Bucio, J., Nieto-Jacobo, M.F., Ramírez-Rodríguez, V., and Herrera-Estrella, L. (2000) Organic acid metabolism in plants: from adaptive physiology to transgenic varieties for cultivation in extreme soils. *Plant Sci.* **160** (1), 1–13.
28. Buser-Suter, C., Wiemken, A., and Matile, P. (1982) A malic acid permease in isolated vacuoles of a crassulacean acid metabolism plant. *Plant Physiol.* **69** (2), 456–459.
29. Nimmo, H.G. (2000) The regulation of phosphoenolpyruvate carboxylase in CAM plants. *Trends Plant Sci.* **5** (2), 75–80.
30. Freschi, L., Rodrigues, M.A., Tiné M.A.S., and Mercier, H. (2010) Correlation between citric acid and nitrate metabolisms during CAM cycle in the atmospheric bromeliad *Tillandsia pohliana*. *J. Plant Physiol.* **167** (18), 1577–1583.
31. De Andrade, L.R.M., Ikeda, M., do Amaral, L.I.V., and Ishizuka, J. (2011) Organic acid metabolism and root excretion of malate in wheat cultivars under aluminium stress. *Plant Physiol. Biochem.* **49** (1), 55–60.
32. “One Evidence That Plants Are Smarter Than You Think.” availbe online: <https://staff.blog.ui.ac.id/ratna/2012/10/>.
33. Demirbas, A. (2001) Biomass resource facilities and biomass conversion processing for fuels and chemicals. *Energy Convers. Manag.* **42**, 1357–1378.
34. Asghari, F.S., and Yoshida, H. (2006) Acid-Catalyzed Production of 5-hydroxymethyl furfural from D -fructose in subcritical water. *Ind. Eng. Chem. Res.* **45** (7), 2163–2173.
35. Besson, M., and Descorme, C. (2010) Supported noble metal catalysts in the catalytic wet air oxidation of industrial wastewaters and sewage sludges. *Environ. ...* (May 2012), 37–41.
36. Braden, D.J., Henao, C.A., Heltzel, J., et al. (2011) Production of liquid hydrocarbon fuels by catalytic conversion of biomass-derived levulinic acid. *Green Chem.* **13** (7), 1755–1765.
37. Akiya, N., and Savage, P.E. (2002) Roles of water for chemical reactions in high-temperature water. *Chem. Rev.* **102** (8), 2725–2750.
38. Serrano-Ruiz, J.C., and Dumesic, J.A. (2011) Catalytic routes for the conversion of biomass into liquid hydrocarbon transportation fuels. *Energy Environ. Sci.* **4** (1), 83–89.
39. Onda, A., Ochi, T., Kajiyoshi, K., and Yanagisawa, K. (2008) Lactic acid production from glucose over activated hydrotalcites as solid base catalysts in water. *Catal. Commun.* **9** (6), 1050–1053.

40. Chambon, F., Rataboul, F., Pinel, C., et al. (2011) Cellulose hydrothermal conversion promoted by heterogeneous Brønsted and Lewis acids: Remarkable efficiency of solid Lewis acids to produce lactic acid. *Appl. Catal. B Environ.* **105** (1-2), 171–181.
41. Zheng, Y., Pan, Z., and Zhang, R. (2009) Overview of biomass pretreatment for cellulosic ethanol production. *Int J Agric Biol Eng* **2(3)** (3), 51–68.
42. Kobayashi, H., Komanoya, T., Guha, S.K., et al. (2011) Conversion of cellulose into renewable chemicals by supported metal catalysis. *Appl. Catal. A Gen.* **409-410**, 13–20.
43. Yin, S., and Tan, Z. (2012) Hydrothermal liquefaction of cellulose to bio-oil under acidic, neutral and alkaline conditions. *Appl. Energy* **92**, 234–239.
44. Werpy, T., and Petersen, G. (2004) “U.S. Department of Energy, Top value added chemicals from biomass volume I - results of screening for potential candidates from sugars and synthesis gas.”
45. Bozell, J.J., and Petersen, G.R. (2010) Technology development for the production of biobased products from biorefinery carbohydrates—the US Department of Energy’s “Top 10” revisited. *Green Chem.* **12(4)** (4), 539–728.
46. Mosier, N.S., Ladisch, C.M., and Ladisch, M.R. (2002) Characterization of acid catalytic domains for cellulose hydrolysis and glucose degradation. *Biotechnol. Bioeng.* **79** (6), 610–618.
47. Bicker, M., Endres, S., Ott, L., and Vogel, H. (2005) Catalytical conversion of carbohydrates in subcritical water: A new chemical process for lactic acid production. *J. Mol. Catal. A Chem.* **239** (1-2), 151–157.
48. Lunt, J. (1998) Large-scale production, properties and commercial applications of polylactic acid polymers. *Polym. Degrad. Stab.* **59** (1-3), 145–152.
49. Fan, Y., Zhou, C., and Zhu, X. (2009) Selective catalysis of lactic acid to produce commodity chemicals. *Catal. Rev.* **51** (3), 293–324.
50. John, R.P., Nampoothiri, K.M., and Pandey, A. (2007) Fermentative production of lactic acid from biomass: an overview on process developments and future perspectives. *Appl. Microbiol. Biotechnol.* **74** (3), 524–34.
51. Maas, R.H.W., Bakker, R.R., Eggink, G., and Weusthuis, R.A. (2006) Lactic acid production from xylose by the fungus Rhizopus oryzae. *Appl. Microbiol. Biotechnol.* **72** (5), 861–868.
52. Yan, X., Jin, F., Tohji, K., et al. (2010) Hydrothermal conversion of carbohydrate biomass to lactic acid. *AICHE J.* **56** (10), 2727–2733.

53. Ma, C., Jin, F., Cao, J., and Wu, B. (2010) Hydrothermal conversion of carbohydrates into lactic acid with alkaline catalysts. *2010 4th Int. Conf. Bioinforma. Biomed. Eng.*, 1–4.
54. Rasrendra, C.B., Makertihartha, I.G.B.N., Adisasmito, S., and Heeres, H.J. (2010) Green Chemicals from d-glucose: Systematic studies on catalytic effects of inorganic salts on the chemo-selectivity and yield in aqueous solutions. *Top. Catal.* **53**, 1241–1247.
55. Kong, L., Li, G., Wang, H., et al. (2008) Hydrothermal catalytic conversion of biomass for lactic acid production. *J. Chem. Technol. Biotechnol.* **388**, 383–388.
56. Zhang, S., Jin, F., Hu, J., and Huo, Z. (2011) Improvement of lactic acid production from cellulose with the addition of Zn/Ni/C under alkaline hydrothermal conditions. *Bioresour. Technol.* **102** (2), 1998–2003.
57. Li, Q., Yao, G., Zeng, X., et al. (2012) Facile and green production of Cu from CuO using cellulose under hydrothermal conditions. *Ind. Eng. Chem. Res.* **51** (7), 3129–3136.
58. Liu, Z., Li, W., Pan, C., et al. (2011) Conversion of biomass-derived carbohydrates to methyl lactate using solid base catalysts. *Catal. Commun.* **15** (1), 82–87.
59. Zeng, W., Cheng, D., Chen, F., and Zhan, X. (2009) Catalytic conversion of glucose on Al–Zr mixed oxides in hot compressed water. *Catal. Letters* **133** (1-2), 221–226.
60. Onda, A., Ochi, T., Kajiyoshi, K., and Yanagisawa, K. (2008) A new chemical process for catalytic conversion of d-glucose into lactic acid and gluconic acid. *Appl. Catal. A Gen.* **343** (1-2), 49–54.
61. Holm, M.S., Saravanamurugan, S., and Taarning, E. (2010) Conversion of sugars to lactic acid derivatives using heterogeneous zeotype catalysts. *Science* **328** (5978), 602–605.
62. Li J., Ding D.J., Deng L., Guo Q.X., Fu Y. (2012) Catalytic air oxidation of biomass-derived carbohydrates to formic acid. *ChemSusChem* **5**(7), 1313-1318.
63. Jin, F., Yun, J., Li, G., et al. (2008) Hydrothermal conversion of carbohydrate biomass into formic acid at mild temperatures. *Green Chem.* **10** (6), 612-615.
64. Leonard, R.H. (1956) Levulinic acid as a basic chemical raw material. *Ind. Eng. Chem.* **48** (8), 1330–1341.
65. Bond, J.Q., Alonso, D.M., Wang, D., et al. (2010) Integrated catalytic conversion of γ -valerolactone to liquid alkenes for transportation fuels. *Science* **327**, 1110–1114.
66. Case, P. a., van Heiningen, A.R.P., and Wheeler, M.C. (2012) Liquid hydrocarbon fuels from cellulosic feedstocks via thermal deoxygenation of levulinic acid and formic acid salt mixtures. *Green Chem.* **14** (1), 85-89.

67. Lange, J.P., Price, R., Ayoub, P.M., et al. (2010) Valeric biofuels: a platform of cellulosic transportation fuels. *Angew. Chem. Int. Ed. Engl.* **49** (26), 4479–4483.
68. Serrano-Ruiz, J.C., Luque, R., and Sepúlveda-Escribano, A. (2011) Transformations of biomass-derived platform molecules: from high added-value chemicals to fuels via aqueous-phase processing. *Chem. Soc. Rev.* **40** (11), 5266–5281.
69. Palkovits, R. (2010) Pentenoic acid pathways for cellulosic biofuels. *Angew. Chem. Int. Ed. Engl.* **49** (26), 4336–4338.
70. Bozell, J.J., Moens, L., Elliott, D.C., et al. (2000) Production of levulinic acid and use as a platform chemical for derived products. *Resour. Conserv. Recycl.* **28**, 227–239.
71. Patent 1997 US5608105 Production of levulinic acid from carbohydrate-containing materials.pdf.
72. Hegner, J., Pereira, K.C., DeBoef, B., and Lucht, B.L. (2010) Conversion of cellulose to glucose and levulinic acid via solid-supported acid catalysis. *Tetrahedron Lett.* **51** (17), 2356–2358.
73. Cha, J.Y., and Hanna, M.A. (2002) Levulinic acid production based on extrusion and pressurized batch reaction. *Ind. Crops Prod.* **16** (2), 109–118.
74. Assary, R.S., Redfern, P.C., Hammond, J.R., et al. (2010) Computational studies of the thermochemistry for conversion of glucose to levulinic acid. *J. Phys. Chem. B* **114** (27), 9002–9009.
75. Rackemann, D.W., and Doherty, W.O.S. (2011) The conversion of lignocellulosics to levulinic acid. *Biofuels, Bioprod. Biorefining* **5**, 198–214.
76. Tominaga, K., Mori, A., Fukushima, Y., et al. (2011) Mixed-acid systems for the catalytic synthesis of methyl levulinate from cellulose. *Green Chem.* **13** (4), 810–812.
77. Peng, L., Lin, L., Zhang, J., et al. (2010) Catalytic conversion of cellulose to levulinic acid by metal chlorides. *Molecules* **15** (8), 5258–5272.
78. Girisuta, B., Janssen, L.P.B.M., and Heeres, H.J. (2007) Kinetic study on the acid-catalyzed hydrolysis of cellulose to levulinic acid. *Ind. Eng. Chem. Res.* **46** (6), 1696–1708.
79. Zhang, J., and Weitz, E. (2012) An in situ NMR study of the mechanism for the catalytic conversion of fructose to 5-hydroxymethylfurfural and then to levulinic acid using ¹³C labeled D-fructose. *ACS Catal.* **2**, 1211–1218.
80. Horvat, J., Klaic, B., Metelko, B., and Sunjic, V. (1985) Mechanism of levulinic acid formation. *Tetrahedron Lett.* **26** (17), 2111–2114.

81. Peng, L., Lin, L., Li, H., and Yang, Q. (2011) Conversion of carbohydrates biomass into levulinic esters using heterogeneous catalysts. *Appl. Energy* **88** (12), 4590–4596.
82. Van de Vyver, S., Thomas, J., Geboers, J., et al. (2011) Catalytic production of levulinic acid from cellulose and other biomass-derived carbohydrates with sulfonated hyperbranched poly(arylene oxindole)s. *Energy Environ. Sci.* **4** (9), 3601–3610.
83. Cabiac, A., Guillon, E., Chambon, F., et al. (2011) Cellulose reactivity and glycosidic bond cleavage in aqueous phase by catalytic and non catalytic transformations. *Appl. Catal. A Gen.* **402** (1-2), 1–10.
84. Takeuchi, Y., Jin, F., Tohji, K., and Enomoto, H. (2007) Acid catalytic hydrothermal conversion of carbohydrate biomass into useful substances. *J. Mater. Sci.* **43** (7), 2472–2475.
85. Geboers, J.A., Van de Vyver, S., Ooms, R., et al. (2011) Chemocatalytic conversion of cellulose: opportunities, advances and pitfalls. *Catal. Sci. Technol.* **1** (5), 714–726.
86. Jow, J., Rorrer, G.L., Hawley, M.C., and Lamport, D.T.A. (1987) Dehydration of d-fructose to levulinic acid over LZY zeolite catalyst. *Biomass* **14** (3), 185–194.
87. Bozell, J.J. (2010) Connecting biomass and petroleum processing with a chemical bridge. *Science* **329** (5991), 522–523.
88. Lai, D., Deng, L., Guo, Q., and Fu, Y. (2011) Hydrolysis of biomass by magnetic solid acid. *Energy Environ. Sci.* **4** (9), 3552–3557.
89. Yu, Y., and Wu, H. (2011) Kinetics and Mechanism of Glucose Decomposition in hot-compressed water: effect of initial glucose concentration. *Ind. Eng. Chem. Res.* **50** (18), 10500–10508.
90. Verendel, J., Church, T., and Andersson, P. (2011) Catalytic one-pot production of small organics from polysaccharides. *Synthesis (Stuttg.)* **2011** (11), 1649–1677.
91. Lin, H., Strull, J., Liu, Y., et al. (2012) High yield production of levulinic acid by catalytic partial oxidation of cellulose in aqueous media. *Energy Environ. Sci.* **5** (12), 9773–9777.
92. Ben-Bassat, A., Walls, A.M., Plummer, M.A., et al. (2008) Optimization of biocatalyst specific activity for glycolic acid production. *Adv. Synth. Catal.* **350** (11-12), 1761–1769.
93. Wu, S., Fogiel, A.J., Petrillo, K.L., et al. (2008) Protein engineering of nitrilase for chemoenzymatic production of glycolic acid. *Biotechnol. Bioeng.* **99** (3), 717–720.
94. Zhang, J., Liu, X., Sun, M., et al. (2012) Direct Conversion of cellulose to glycolic acid with a phosphomolybdic acid catalyst in a water medium. *ACS Catal.* **2** (8), 1698–1702.

95. Calvo-Flores, F.G., and Dobado, J. a (2010) Lignin as renewable raw material. *ChemSusChem* **3** (11), 1227–1235.
96. Dorrestijn, E., Laarhoven, L.J.J., Arends, I.W.C.E., and Mulder, P. (2000) The occurrence and reactivity of phenoxylinkages in lignin and low rank coal. *J. Anal. Appl. Pyrolysis* **54** (1-2), 153–192.
97. Canevali, C., Orlandi, M., Pardi, L., et al. (2002) Oxidative degradation of monomeric and dimeric phenylpropanoids: reactivity and mechanistic investigation. *J. Chem. Soc. Dalt. Trans.* (15), 3007–3014.
98. Fabbri, C., Aurisicchio, C., and Lanzalunga, O. (2008) Iron porphyrins-catalysed oxidation of α -alkyl substituted mono and dimethoxylated benzyl alcohols. *Cent. Eur. J. Chem.* **6** (2), 145–153.
99. Partenheimer, W. (2009) The Aerobic Oxidative cleavage of lignin to produce hydroxyaromatic benzaldehydes and carboxylic acids via metal/bromide catalysts in acetic acid/water mixtures. *Adv. Synth. Catal.* **351** (3), 456–466.
100. Li, J., Gellerstedt, G., and Toven, K. (2009) Steam explosion lignins; their extraction, structure and potential as feedstock for biodiesel and chemicals. *Bioresour. Technol.* **100** (9), 2556–2561.
101. Crestini, C., Caponi, M.C., Argyropoulos, D.S., and Saladino, R. (2006) Immobilized methyltrioxo rhenium (MTO)/H₂O₂ systems for the oxidation of lignin and lignin model compounds. *Bioorg. Med. Chem.* **14** (15), 5292–5302.
102. Yokoyama, T., Chang, H.-M., Reiner, R.S., et al. (2004) Polyoxometalate oxidation of non-phenolic lignin subunits in water: Effect of substrate structure on reaction kinetics. *Holzforschung* **58** (2), 116–121.

Chapter 2 Biomass characterization of *Agave* and *Opuntia* as potential biofuel feedstocks

Sustainable production of lignocellulosic biofuels requires a sufficient supply of biomass feedstocks. *Agave* and *Opuntia* represent highly water-use efficient bioenergy crops that are suitable for expanding feedstock production into semi-arid marginal lands. These feedstocks have garnered interest as dedicated biofuel feedstocks because of their high water- and fertilizer- use efficiency and not competing with major food crops or conventional biofuel feedstocks. To better understand the potential of these feedstocks, the biomass composition of *Agave tequilana* and *Opuntia ficus-indica* was analyzed. Previous extraction procedures and analytical methods have led to variable estimates of the chemical compositions of the biomass of these species. Therefore, National Renewable Energy Laboratory (NREL) standard methods were used in the present study.

2.1 Introduction

With the gradual depletion of fossil fuels, the demand for renewable biomass-based carbon resources to use for lignocellulosic biofuels is expected to increase in the future [1,2]. However, most biomass feedstocks currently used for biofuels production compete with the use of those feedstocks for food [3,4]. Competition for arable land for growing biofuel feedstocks and food can be avoided, in part, by the development of drought-tolerant biomass feedstocks that can be grown in an environmentally responsible manner on semi-arid, marginal, degraded, or abandoned agricultural lands where food crops are typically not cultivated, with an estimated mean productivity of $4.3 \text{ Mg ha}^{-1} \text{ y}^{-1}$ [4–6].

Furthermore water availability is the major factor that constrains the cultivation of bioenergy crops [7]. One potential opportunity for the production of biomass feedstocks on water-limited areas is to use various cultivated crassulacean acid metabolism (CAM) species from the genera *Agave* (Agavaceae) and *Opuntia* (Cactaceae, “prickly pear cactus”), which have growth characteristics that allow these species to thrive in semi-arid regions [8].

CAM plants are typically highly tolerant of high temperatures, UV-B radiation, and drought conditions by virtue of their ability to rapidly take up and store water in above-ground succulent tissues, while tolerating large losses in water mass fraction [8,9]. The high water-use efficiency of CAM species, typically 3- to 10-fold higher than that of C₃ or C₄ species, results in crop water demands that average only 16% to 28% of those of C₃ and C₄ crops, respectively, while maintaining comparable above-ground biomass productivities [8,10]. For example, average annual productivity values for various *Agave* species can range from <1–34 Mg ha⁻¹ y⁻¹ under ambient precipitation conditions [4,11–13]. Under cultivated conditions with supplemental irrigation, average annual dry-weight productivities can reach as high as 38–42 Mg ha⁻¹ y⁻¹ [10,14–16]. Under rain-fed conditions, average annual productivity for *Opuntia* species are about 15 Mg ha⁻¹ year⁻¹ or more [17]. However, under well-irrigated conditions, average annual dry matter productivities in the range of 40–50 Mg ha⁻¹ year⁻¹ have been reported [10,14–16,18]. Such biomass production rates are comparable with those of other bioenergy feedstocks such as maize, sugarcane, switchgrass, and poplar [4,8,12].

Although native to the Americas, *Agave* species have been introduced worldwide for commercial production in many countries including Australia, Brazil, Tanzania, Kenya,

Madagascar, Mexico, China, and across the Caribbean and Mediterranean regions [11,12].

Although more information is needed from field trials to model the biomass production associated with the water-wise feedstocks [19,20], productivity estimates from immediately available land suggest that an additional 6.1 hm³ of lignocellulosic ethanol production could be produced with minimal impacts on the environment [11]. Similarly, *Opuntia* originates from the Americas with its center of diversity in Mexico [21], but it has been introduced worldwide with major production occurring in Algeria (and other northern African nations), Brazil, Chile, Mexico, and Italy [22,23]. *Opuntia* species are cultivated primarily for commercial fodder and forage in semi-arid regions worldwide [24,25]. However, tender, young cladodes and fruits from *Opuntia* species are consumed by humans, primarily in Mexico, the southwestern US, and Italy [26–28]. The young cladodes and fruits are also dried and sold as dietary supplements [29,30], in cosmetic formulations [29], and for medicinal use [31–33]. The fruits can be consumed as fresh or made into a variety of jams, jellies, sauces, marmalades, candies, syrups, juices, liquor, and as a natural sweetener due to the high sugar mass fraction (>50%) of the fruit syrup [34].

Due to their high mass fraction of water-soluble sugars, many different *Agave* species are currently used for production of alcoholic beverages, such as tequila (*Agave tequilana*) mescal or pulque (*Agave mapisaga*, *A. salmiana*, *A. Americana*, *A. fourcroydes*, and others), aquaamiel (honey water), nectar or syrup sweeteners. Some of these species are also used for fiber production (e.g., *Agave sisalana*, *A. fourcroydes*) [7,8,11,12,35–37]. *Agave* bagasse as a raw material can be used for animal feed, fiberboard production, and other by-products [26,38]. Following extraction of sugars for fermentation to produce

mezcal, the bagasse and waste fiber from *Agave salmiana* can be used as a renewable energy source for combustion [39]. The cladodes of *Opuntia* cactus are also a potential biomass feedstock for bioethanol production [40]. *Agave* would be comparable to or superior to other ethanol feedstocks, such as maize, switchgrass, and sugarcane, for bioethanol production in terms of life cycle energy and greenhouse gas (GHG) balances [19], while being far more water-use efficient than these crops [41].

The efficient conversion of lignocellulosic biomass into renewable biofuels and value-added chemical compounds is limited by the recalcitrance of plant cell wall material to degradation [42]. Deconstructive pretreatments of raw lignocellulosic biomass account for a majority of the costs associated with lignocellulosic biofuel production [3]. In order to optimize such pretreatments, the composition of lignocellulosic biomass feedstocks must be known. Among plant cell wall biopolymers, lignin is the major cause of recalcitrance to hydrolysis [43,44]; thus, reducing lignin mass fraction or altering its structure are important goals for overcoming this recalcitrance and improving saccharification [45]. For most woody feedstock species, the lignin mass fraction is approximately 9–30% [13,45], whereas for *Agave* and *Opuntia*, the lignin mass fraction are estimated to be lower, in the range of 5–16% depending on the species and technical approaches used [12,13,44,46–48]. However, the readily fermentable, water-soluble carbohydrate (WSC) fraction of *Agave* leaves was comparable to that of conventional lignocellulosic feedstocks, such as sugarcane bagasse and corn stover [38,49]. *Opuntia* stems exhibit similar percentages (3–7% fresh mass fractions) of such carbohydrates [33]. Depending on the study, the compositions of *Agave* and *Opuntia* feedstocks can vary considerably. Such variation might arise from the diverse species, plant or leaf age,

growth conditions, and the analytical methods used. In order to obtain more reliable information about the composition and chemical structures of *Agave tequilana* and *Opuntia ficus-indica*, standardized National Renewable Energy Laboratory (NREL) analytical methods were used to determine the ash, protein, extractives, lignin, hemicellulose, and cellulose mass fraction, as well as the chemical structures of isolated cellulose, of sampled materials. Such information is critical for the optimization of strategies for conversion of these feedstocks to renewable biofuels.

2.2 Materials and methods

2.2.1 Plant cultivation

Opuntia ficus-indica ((L.) Mill.) and *Agave tequilana* (Weber var. *azul*) were grown at the Nevada Agricultural Experiment Station Valley Road Greenhouse Complex in Reno, NV. *Opuntia* and *Agave* were planted in eight-liter and nineteen-liter pots, respectively, containing Metromix® 200 soilless mix (Sun Gro Horticulture, Bellevue, WA, USA). Plants were maintained under standard greenhouse conditions with natural light at approx. 1100-1500 $\mu\text{mol m}^{-2} \text{s}^{-1}$ and temperature at 28-32 °C day/17-18 °C night. Watering was performed twice a week along with monthly fertilization (Miracle Gro®, Scott's MiracleGro Inc., Marysville, OH, US) and insecticide treatments (Marathon® 1% Granular, OHP, Mainland, PA, US).

2.2.2 Materials

Mature, fresh *Opuntia ficus-indica* (approximately 1 year old) cladodes and *Agave tequilana* (approximately 2 years old) leaves were harvested between 9 and 10 AM from plants maintained in the greenhouse, were snap-frozen and stored in liquid nitrogen, and

were transported to the laboratory where they were stored at -80 °C until processing. For chemical analysis and derivatization, the following reagents and products were purchased from Sigma-Aldrich (St. Louis, MO): D-(+)-xylose (99%), xylan from beechwood (90%), glucose (European Pharmacopoeia (EP) Reference Standard), galactose (United States Pharmacopeia (USP) Reference Standard), mannose (United States Pharmacopeia (USP) Reference Standard), D-arabinose ($\geq 99.0\%$), Bis (trimethylsilyl) trifluoroacetamide (BSTFA) + trimethylchlorosilane (TMCS) (99:1), anhydrous pyridine (99.8%), sulfuric acid (ACS reagent 98%), hydrochloric acid (~36.5–38.0%), ethanol (>99.5%), sodium chlorite (80%), hexane (95%), glacial acetic acid (>99.7%), formic Acid ($\geq 95\%$) phenol (Tris-buffered, pH = 8.0), and dense SDS buffer (30% sucrose, 2% SDS, 0.1 mol L⁻¹ Tris-HCl, pH 8.0, 5% 2-mercaptoethanol).

2.2.3 Sample preparation

Figure 1 depicts the flowchart of the major steps used to prepare the samples for analysis. The leaves were first cut into strips, then juice was expelled from the material by placing it in a metal pipe and forcing a tight-fitting metal cylinder through the pipe using a 4350 Carver hydraulic press (Carver Inc., Wabash, IN). The juice was stored in 50 cm³ polypropylene centrifuge tubes at 4 °C until further analysis. The unwashed bagasse solids were freeze-dried, then milled into particles with an average size of 300 µm in diameter. The water mass fraction and the amount of total solids remaining after 105 °C drying of the biomass sample were determined by the standard National Renewable Energy Laboratory (NREL) laboratory analytical procedure [50]. All the

analytical data reported were the mean values of three biological replicates (\pm standard deviation from the mean).

2.2.4 Elemental analysis

Elemental analysis was performed using the dried, ground samples by Galbraith Laboratories, Inc. (Knoxville, TN). Carbon, hydrogen, and oxygen mass fractions were determined using the Perkin Elmer 2400 Series II CHNS/O Analyzer. Sulfur determination was performed using a LECO SC-432DR Sulfur Analyzer and determination of Cl^- anions was performed by suppressed ion chromatography. Energy-dispersive X-ray spectroscopy (EDS) analysis was performed using a Hitachi S-4700 II Scanning Electron Microscope (Hitachi High Technologies America, Inc., Schaumburg, IL).

2.2.5 Extractive, ash, protein, and dry bagasse analysis

The ash mass fraction of the samples from each plant species was measured using the standard NREL analytical procedures for biomass analysis [51]. Each of the samples were extracted with water and ethanol, respectively, for the determination of extractives [52]. The crude protein mass fraction was estimated using a universal phenol-based protein extraction method [53]. Structural carbohydrates and acid insoluble lignin mass fraction for the extractive-free bagasse from *Agave tequilana* and *Opuntia ficus-indica* were determined using the standard NREL laboratory analytical procedures [54].

2.2.6 Juice Analysis

The juices were analyzed using a Shimadzu high performance liquid chromatograph (HPLC) (Model LC-10; Shimadzu Scientific Instruments, Columbia, MD) equipped with

a UV-VIS Detector (Shimadzu SPD 10-AV), a Refractive Index Detector (Shimadzu RID-10A), and a Bio-Rad Aminex HPX-87P column (Bio-Rad Laboratories, Inc., Hercules, CA) using DI water as the mobile phase, at a flow rate of $0.6 \text{ cm}^3 \text{ min}^{-1}$ and a column temperature of $80 \text{ }^\circ\text{C}$. For electrospray ionization mass spectrometry (ESI/MS) measurements, the juice samples were analyzed using a Waters e2695 separation module (Waters Corporation, Milford, MA) operated in the negative mode. Free sugar analysis was performed according to the NREL method [55]. The derivatization of the polar components in the juice was performed for qualitative gas chromatography-mass spectrometry (GC-MS) analysis to identify unknown components. The samples were analyzed on an Agilent 6890 series gas chromatograph-mass spectrometer (GC-MS) equipped with an Agilent DB5-MS column ($30 \text{ m} \times 0.25 \text{ mm ID}, 0.25 \mu\text{m}$ film thickness) and an Agilent 5973 Mass Selective Detector (Agilent Technologies, Inc., Santa Clara, CA). The column temperature was maintained at $80 \text{ }^\circ\text{C}$ for 5 min then ramped at 10 K min^{-1} to $260 \text{ }^\circ\text{C}$ and held at $260 \text{ }^\circ\text{C}$ for 2 minutes. Additionally, the concentrations of total soluble solids (TSS) in sample juices were determined by pipetting 10 cm^3 of juice that had been passed through a $0.45 \mu\text{m}$ filter into pre-dried and pre-weighed aluminum weighing dishes, and drying at $100 \text{ }^\circ\text{C}$ for 24 h in an oven until a constant weight was reached.

2.2.7 Higher heating value analysis

The higher heating values (HHV) of *Opuntia ficus-indica* and *Agave tequilana* based on dry bagasse was measured by combusting the samples in an adiabatic oxygen bomb

calorimeter (Model 6200 Isoperibol Calorimeter, Parr Instrument Company, Moline, IL) according to the ASTM D5865 method.

2.2.8: Holocellulose fractionation

The holocellulose (cellulose + hemicellulose) samples were conducted according to a modified method in the literature [56].

2.2.9 Solid state NMR analysis

Cellulose was isolated by refluxing a holocellulose sample (1.0 g dry weight) in the 2.5 mol dm⁻³ HCl (100.00 cm³) solution according to the method of Hallac *et al.* [56]. The CP/MAS ¹³C NMR analysis of the cellulose samples was performed using 2-channel 400 MHz Tecmag Discovery instrument (Tecmag Inc., Houston, TX). A NMR Service GmbH MAS H-X broadband probe was used. The samples were packed in a 4 mm ZrO₂ rotor. The MAS rate was 9 kHz. Acquisition was performed with a proton decoupling pulse sequence using a 6 microsecond carbon 90° pulse. A 10-second delay between pulses was used. After acquisition, the C-4 region of each spectrum was fitted and the quantification of the different cellulose forms was calculated based on the time dependence of the fitted signal intensities [57].

2.3 Results and discussion

2.3.1 Elemental analysis

The relative elemental percentages of *A. tequilana* and *O. ficus-indica* were determined based on the oven-dried samples. Elemental mass fractions were similar for both *A. tequilana* and *O. ficus-indica* (Table 2.1). However, *A. tequilana* displayed a

slightly higher C mass fraction than did the sample from *O. ficus-indica*. These values are similar to the C, H, O mass fractions of herbaceous and woody biomass feedstocks, which typically have elemental compositions of 45–50% C, 6–7% H, 40–46% O, and trace amounts of several metal ions [58,59]. Notably, sulfur (S) and chlorine (Cl) mass fractions were higher in *O. ficus-indica* than in *A. tequilana*, which might be a consideration for air pollution impacts. Additionally, such elemental mass fraction data are important information prior to developing procedures for processing biomass into biofuels, because elemental mass fractions might affect subsequent processes. Sulfur (S) and chlorine (Cl), for example, can both cause catalyst poisoning and reactor corrosion [60].

Table 2.1 Elemental analysis and higher heating values of *Agave tequilana* and *Opuntia ficus-indica*.

Sample	Dried and ground ^a / atomic mass fractions (%)					Higher heating values (MJ kg ⁻¹) ^b
	C%	H%	O%	S%	Cl%	
<i>Agave tequilana</i>	42.8 ±1.1	5.9 ±0.2	39.9 ±1.4	0.19 ±0.007	0.09 ±0.001	17.50 ±0.09
<i>Opuntia ficus-indica</i>	35.1 ±1.1	4.4 ±0.3	41.3 ±0.5	0.33 ±0.006	0.81 ±0.09	16.95 ±0.04

^a Data reported are the mean values of three replicates ± standard deviation from the mean.

^b Heating values reported are the mean values of three replicates based on water/ethanol extracted bagasse ± standard deviation from the mean.

2.3.2 Compositional analysis

A detailed compositional analysis of the leaves of *Agave tequilana* and the modified stems (cladodes) of *Opuntia ficus-indica* was performed according to the processing scheme outlined in Figure 2.1. The mass fraction distributions of the components in the samples are summarized in Table 2.2. *A. tequilana* contained a 4-fold higher mass fraction of dry bagasse (10.7%) than did *O. ficus-indica* (2.6%). In contrast, *O. ficus-indica* contained a slightly higher juice mass fraction (97.4%) compared with *A.*

tequilana (89.3%), likely reflecting the higher water content of *O. ficus-indica*. However, *A. tequilana* displayed a higher total soluble solid fraction (11.9%) in the juice and higher total dry matter (15.1%) compared with *O. ficus-indica*. These values are similar to those previously reported for *A. tequilana* leaves by Li *et al.* [48] and account for the suitability of this species for fermentation to alcoholic beverages and high ethanol conversion efficiency [11].

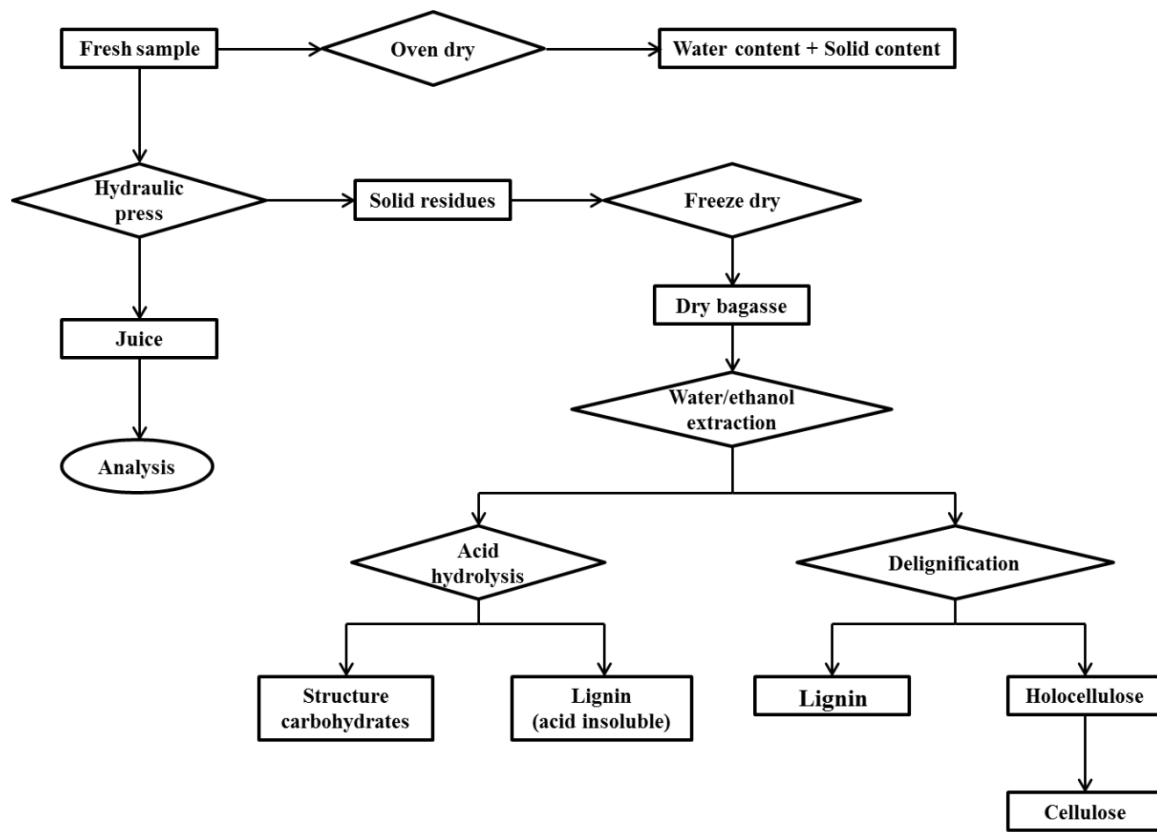


Figure 2.1 Scheme of the processing steps for the compositional analysis of *Agave tequilana* and *Opuntia ficus-indica* samples.

The electrospray ionization mass spectrometry (ESI-MS) was used to identify the major constituents of the juice. The sugars and other water-soluble organic compounds in the samples appear in the total ion chromatogram between m/z 40 and 200 (Figure 2.2). The identification of these compounds was validated by GC/MS analysis (Figure 2.3). In

A. tequilana, the major soluble monosaccharides were glucose and fructose ([Table 2.3](#)), which is consistent with earlier observations [\[48\]](#). The water-soluble monosaccharide mass fraction of *O. ficus-indica* was much lower than that of *A. tequilana*, indicating that to be useful as a biofuel feedstock, additional physiochemical pretreatments or microbial digestion of this material would be needed to improve its conversion efficiency. The juice from both species displayed weakly acidic pH values ([Table 2.3](#)) consistent with the performance of crassulacean acid metabolism (CAM) and the associated nocturnal carbon fixation into malate, which is stored in the vacuole as malic acid [\[8\]](#). As shown in [Table 2.3](#), both *A. tequilana* and *O. ficus-indica* have relatively high malic acid when compared with other species. A relatively high citric acid was also found in *A. tequilana* and *O. ficus-indica* juice. In CAM plants, accumulation and storage of these organic acids occur at night as the products of primary CO₂ uptake and fixation when the leaf-to-air vapor pressure difference is lower than that during the day, which improves the water-use efficiency of these plants [\[61\]](#). The stored malic acid is decarboxylated and used as a substrate for daytime photosynthesis *via* the Calvin-Benson cycle to generate starch or other storage glucans behind closed stomata.

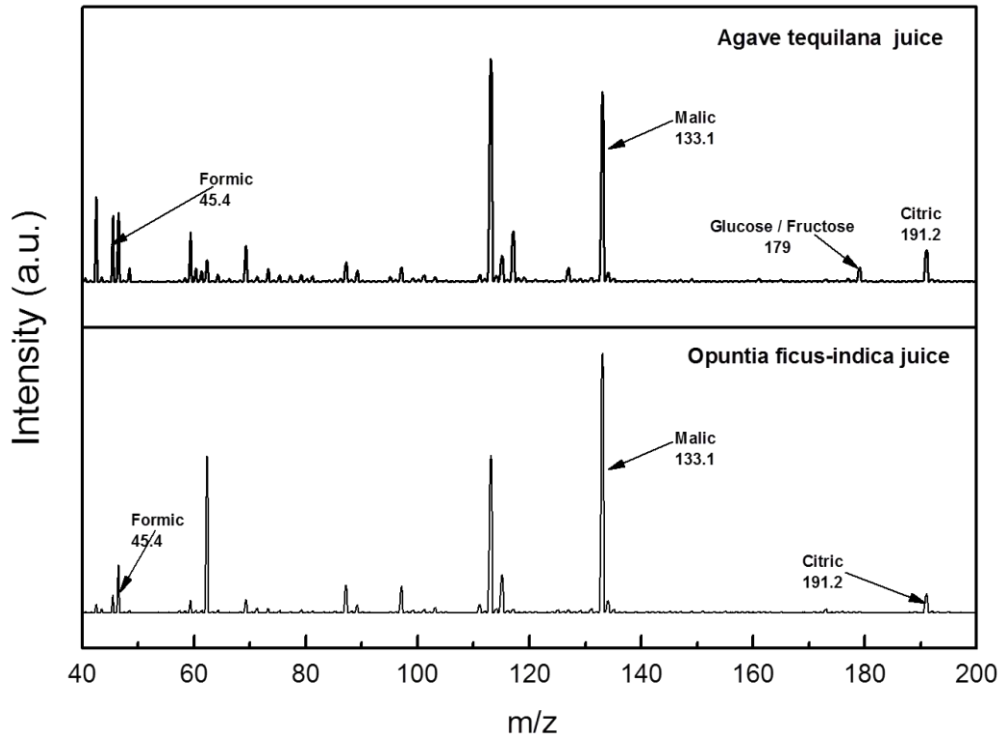


Figure 2.2 ESI/MS spectra of *Agave tequilana* (upper panel) and *Opuntia ficus-indica* (lower panel) juice.

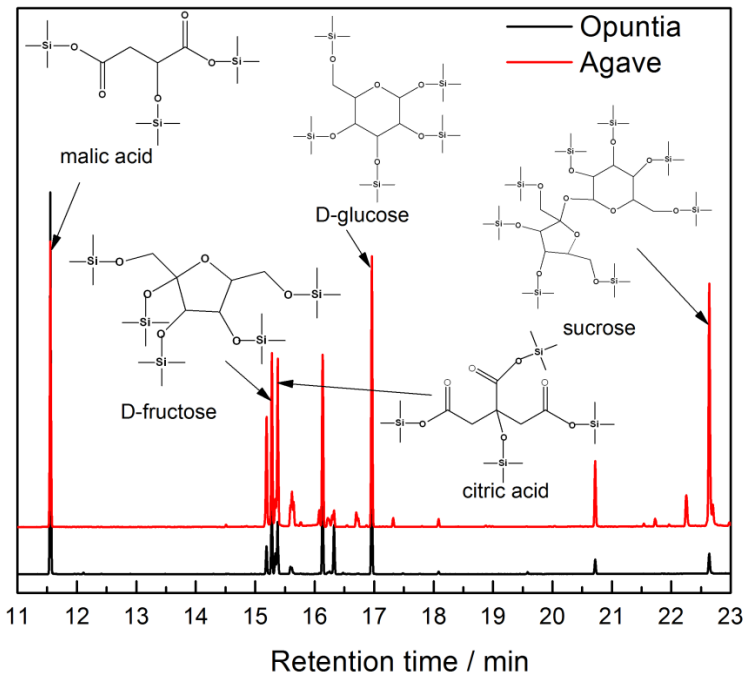


Figure 2.3 GC/MS spectra of *Agave tequilana* (red trace) and *Opuntia ficus-indica* (black trace) juices.

Table 2.2 Mass fraction distribution of fresh *Agave tequilana* and *Opuntia ficus-indica* samples (% wet biomass basis).

Sample ^a	Dry bagasse	Juice	TSS ^b in Juice	Water	Total solids
Agave tequilana	10.7 ±0.7	89.3 ±0.7	11.9 ±2.8	84.9 ±0.6	15.1 ±0.6
Opuntia ficus-indica	2.6 ±0.2	97.4 ±0.2	3.8 ±0.3	93.9 ±0.4	6.1 ±0.4

^a Data reported are the mean values of six replicates ± standard deviation from the mean.

^b TSS: total soluble solids

Table 2.3 pH and Composition of sample juices (g dm⁻³).

Samples ^a	pH	Malic	Citric	Formic	Glucose	Galactose	Fructose
Agave Tequilana	4.74 ±0.002	35.3 ±0.3	9.5 ±0.1	39.0 ±0.2	18.1 ±0.1	0.7 ±0.2	16.8 ±0.3
Opuntia ficus-indica	4.17 ±0.001	10.9 ±0.7	3.9 ±0.1	/	1.0 ±0.01	0.1 ±0.005	1.6 ±0.01

^a Data reported are the mean values of three replicates ± standard deviation from the mean.

The solid, freeze-dried residue (bagasse) remaining after hydraulic extraction of the juice was milled and mixed thoroughly to ensure representative samples before being subjected to further mass balance analysis following sequential water and ethanol extractions, acid hydrolysis, and delignification (Figure 2.1). The previous reports of the compositions of *A. tequilana* and *O. ficus-indica* varied widely due to different plants or leaf ages, growth conditions, and the analytical methods used [12]. Thus in our study, a comprehensive compositional analysis of the residual dry matters was performed (Table 2.4). *A. tequilana* showed a 4-fold higher mass fraction of dry bagasse than *O. ficus-indica* (Table 2.2). The mass fractions of combined water and ethanol extractives of the dried material were higher than published reports for both *A. tequilana* leaves and *O. ficus-indica* cladodes, whereas the structural carbohydrate mass fractions were similar for *A. tequilana* leaves [48], but more variable for *O. ficus-indica* cladodes [40,62] (Table 2.4). The amount of extractives shown in Table 5.4 was calculated by subtracting the amount of soluble ash.

The lignin mass fraction of *A. tequilana* leaves (13.8%) was similar to that of *O. ficus-indica* cladodes (12.3%) (Table 2.4). The lignin mass fraction of *A. tequilana* leaves was *on par* with values reported previously by Iñiguez-Covarrubias *et al.* and Li *et al.* [26,48]. Likewise, the lignin mass fraction of *O. ficus-indica* cladodes was similar to the value reported by Mciteka [63], lower than the value of the field-grown plants reported by Ginestra *et al.* [62], yet higher than that reported by Kuloyo [40]. Overall, the lignin mass fractions in *A. tequilana* and *O. ficus-indica* dry bagasses were generally comparable to the values reported for herbaceous feedstocks (9–18%; e.g., *Miscanthus*, switchgrass, and corn stover) and substantially lower than those for woody feedstocks (21–32%; e.g., poplar, eucalyptus, and pine) [45]. Feedstocks with reduced lignin mass fractions might display reduced recalcitrance during pulp and paper production and lignocellulosic biofuel production [45]. Structural carbohydrate mass fractions were found to be 43.8% and 36.6% for dry *A. tequilana* leaves and *O. ficus-indica* cladodes, respectively.

In order to evaluate the mass fractions of cellulose and hemicellulose, which comprise the principal structural carbohydrates in the dry matter, holocellulose (cellulose + hemicellulose) was first separated from lignin. The cellulose mass fraction of *A. tequilana* (26.0%) was twice than that of *O. ficus-indica* (13.1%), whereas the hemicellulose mass fractions were 22.8% and 18.5%, respectively (Table 2.4). The lower holocellulose mass fraction of *O. ficus-indica* can likely be explained in part by the higher ash and protein mass fractions of this species. The high water mass fractions of *A. tequilana* (84.9%) and *O. ficus-indica* (93.9%) (Table 2.2) suggest that these feedstocks might be suitable for our recently reported catalytic aqueous phase process for direct

conversion of cellulose and hemicellulose into levulinic acid and lactic acid, respectively [64,65]. This process converts lignocellulosic biomass into organic acids using water as an environmentally benign reaction media, with heterogeneous catalysts such as ZrO₂. The high endogenous water mass fractions of these species would reduce water consumption during the lignocellulosic processing steps. Aside from the production of biofuels, the production of high-value chemical precursors, such as levulinic and lactic acids, which can be used as bio-based chemical intermediates in the production of other useful compounds [66,67], indicates that these arid-land feedstocks might serve as useful biomass sources for a variety of biosynthetic reactions.

Table 2.4 Composition of *Agave* leaf and *Opuntia* cladode bagasse reported in literature and the present study-mass fraction of dry material (%).

Species	Extractives	Structure Carbohydrate	Lignin	Cellulose	Hemi-cellulose	Ash	Protein
<i>Agave tequilana</i> (Li et al., 2012) [48]	21.8	41.7	11.9	n/a	n/a	6.4	5.6
<i>Agave tequilana</i> (Iñiguez-Covarrubias et al., 2001) [26]	14	n/a	15.9	64.8	5.1	1.0	n/a
<i>Agave tequilana^a</i> (present study)	29.0 ±1.2	43.8 ±1.3	13.8 ±1.3	26.0 ±1.2	22.8 ±1.2	6.0 ±0.1	2.4 ±0.1
<i>Opuntia ficus-indica^b</i> (Mciteka, 2008) [63]	n/a	n/a	11.8	6.8	9.1	22.5	5.5
<i>Opuntia ficus-indica^c</i> (Ginestra et al., 2009) [62]	17.7	26	16	n/a	n/a	n/a	6.42
<i>Opuntia ficus-indica</i> (Kuloyo, 2012) [40]	24.3	42	7.9	13.5	n/a	16.8	7.5
<i>Opuntia ficus-indica^a</i> (present study)	25 ±0.9	36.3 ±1.1	12.3 ±1.1	13.1 ±0.7	18.5 ±0.7	23.7 ±0.1	7.4 ±0.3

^aData reported are the mean values of three replicates ± standard deviation from the mean. ^bMean of six different varieties. ^cMean of three different varieties.

O. ficus-indica had a 3.9-fold higher ash mass fraction (23.7%) than *A. tequilana* (6.0%) (Table 2.4), due primarily to the accumulation of inorganic ions and salts, such as

Ca^{2+} -oxalate crystals [68]. The ash mass fraction of *A. tequilana* and *O. ficus-indica* was relatively high compared to that of woody biomass feedstocks, which are in the 1–3% range [59]. However, these ash values are similar to those for herbaceous feedstocks, such as *Miscanthus*, reed canary grass, wheat or rice straw, or hay, which can range from 2% to 21% [58,59]. EDS analysis demonstrated that pre-extraction ash was comprised mainly of the monovalent cations potassium (K^+) and sodium (Na^+), and the divalent cations calcium (Ca^{2+}) and magnesium (Mg^{2+}) in the following order of relative abundance in both species ($\text{Ca}^{2+} \gg \text{K}^+ > \text{Mg}^{2+} > \text{Na}^+$) (Table 2.5 and 2.6). Notably, *A. tequilana* had more than 6-fold higher Na^+ mass fraction than *O. ficus-indica*. However, after water and ethanol extraction, most of the K^+ , Na^+ , sulfur (S), and phosphorus (P) were removed, whereas only Ca^{2+} , Mg^{2+} , and manganese (Mn^{2+} or Mn^{3+}) were retained (Table 2.5 and 2.6). The high quantitative estimation of ash mass fraction and their relative alkalization potential from alkali chloride deposits is a critical concern because ash can potentially cause corrosion and slagging problems during bioprocessing [69]. However, for subsequent bioprocessing of *A. tequilana* and *O. ficus-indica* into a biofuel, these inorganic elements represent a waste stream that could be recycled and reused as fertilizers.

The protein mass fraction of *A. tequilana* (2.4%) was 3-fold lower than that of *O. ficus-indica* (7.4%) (Table 2.4) and was lower than the value previously reported [48]. For *O. ficus-indica*, the protein mass fraction estimate was similar to the value reported by Kuloyo [40] and higher than values reported earlier [62,63]. The removal of proteins might be necessary to avoid possible deactivation of catalysts during the biofuel production, which, however, would likely increase processing costs.

Table 2.5 Inorganic Elements of *Opuntia ficus-indica* ash before and after extractive with EDS test.

Ash before extractive			Ash after extractive		
Element	Weight%	Atomic%	Element	Weight%	Atomic%
Na	1.32	2.07	Mg	20.06	29.38
Mg	12.41	18.39	Ca	78.32	69.57
Ca	45.06	40.50	Mn	1.62	1.05
Mn	0.82	0.54	Totals	100.00	
Cl	0.67	0.68			
P	3.33	3.87			
S	2.09	2.35			
K	34.30	31.60			
Totals	100.00				

Table 2.6 Inorganic Elements of *Agave tequilana* ash before and after extractive with EDS test.

Ash before extractive			Ash after extractive		
Element	Weight%	Atomic%	Element	Weight%	Atomic%
Na	8.99	13.57	Mg	14.29	21.43
Mg	11.23	16.04	Ca	85.71	78.57
Ca	57.32	49.64	Totals	100.00	
P	2.94	3.29			
S	0.68	0.74			
K	18.85	16.73			
Totals	100.00				

2.3.3 Higher heating value analysis of dry bagasse

The higher heating values (HHVs) of the dry bagasse constituents were measured to assess total energy values. *A. tequilana* leaves and *O. ficus-indica* cladodes had the HHVs of 17.50 MJ kg⁻¹ and 16.95 MJ kg⁻¹, respectively (Table 2.1). These values were lower than those typical for most softwood or hardwood species, which tend to be close to 20 MJ kg⁻¹ [70]. The heating value of a plant biomass increases with higher lignin and extractive mass fractions [71]. Thus, the lower heating values observed here were consistent with the relatively low lignin mass fractions measured for both species.

2.3.4 Cellulose characterization

One of the major barriers to biofuels production from lignocellulosic feedstocks is the recalcitrance of crystalline cellulose to hydrolysis [72]. Thus, pretreatment of lignocellulosic feedstocks is often required to alter the biomass structure in order to make the cellulose more accessible [73]. One of the primary goals of pretreating biomass is to reduce its recalcitrance by degrading the crystalline structure of cellulose. In order to investigate the relative amounts of various crystalline cellulose allomorphs and fibril surface characteristics, CP/MAS ^{13}C NMR analysis was performed on isolated cellulose from *A. tequilana* and *O. ficus-indica*. This analysis was performed by fitting one Gaussian and three Lorentzian line curves to the C₄ signals at δ 75 - 100 ppm [74], resulting in a 7-peak non-linear line-fit spectrum of the cellulose C₄ region (Figure 2.4). The signal assignments for cellulose I _{α} , I _{β} , and *para*-crystalline cellulose domains are summarized in Table 2.7. Additionally, the non-crystalline cellulose C₄ region signals at around δ 80–95 ppm, which is associated with accessible and inaccessible cellulose fibril surfaces, was simultaneously fitted to three Gaussian line-curves. Celluloses I _{α} and I _{β} are two natural forms of highly ordered crystalline cellulose (Type I) that are believed to be the most difficult to deconstruct [75]. In contrast, *para*-crystalline cellulose, which has a disordered crystalline structure, is described as a cellulose allomorph with features intermediate to those of crystalline and amorphous cellulose in both chain order and mobility [76]. *Para*-crystalline cellulose is much more readily hydrolyzed than crystalline cellulose [77]. Based on the CP/MAS ^{13}C NMR analysis (Table 2.6), *A. tequilana* displayed 50.8% *para*-crystalline cellulose mass fraction. This value is much higher than those found in woody biomass, such as loblolly pine (24.8%) and poplar (31.1%) [72,78],

and switchgrass (32.7%) [79]. Additionally, ordered crystalline celluloses in *A. tequilana* were relatively low in mass fractions, with I_{α} of 7.6% and I_{β} of 3.3%. The mass fraction of amorphous cellulose in the total cellulose of *A. tequilana* was 36.2%. For *O. ficus-indica*, the mass fraction of *para*-crystalline cellulose was 27.2%, lower than that in *A. tequilana*. The I_{β} of *O. ficus-indica* is a little higher at 16.6%; however, the amorphous cellulose mass fraction was as high as 55.9%. The resultant compositional analysis indicates that cellulose from *A. tequilana* and *O. ficus-indica* is likely to be far less recalcitrant to deconstruction than cellulose derived from herbaceous or woody biomass feedstocks. However, further investigation of the physiochemical pretreatments and enzymatic hydrolysis of these feedstocks is needed to determine the optimal conditions for deconstructing them prior to saccharification or other biofuel conversion processes.

Table 2.7 Assignments of signals in the C₄ region of CP/MAS ¹³C NMR spectra obtained from isolated cellulose of *Agave tequilana* and *Opuntia ficus-indica*.

Assignment	Chemical shift (ppm)	FWHH ^a (ppm)	Intensity ^a	FWHH ^b (ppm)	Intensity ^b	Line type
Cellulose I _α	96.8	5.25	7.6%	2.16E+144	0.0%	Lorentzian
Cellulose I _{α+β}	96.3	2.73	2.2%	0.87	0.3%	Lorentzian
Cellulose I _β	91.7	2.14	3.3%	4.35	16.6%	Lorentzian
Para-crystalline cellulose	94.1	4.90	50.8%	4.59	27.2%	Gaussian
Accessible fibril surface	83.5	3.89	6.2%	15.83	49.2%	Gaussian
Inaccessible fibril surface	84.6	12.17	23.2%	0.20	0.0%	Gaussian
Accessible fibril surface	81.6	5.47	6.8%	4.01	6.7%	Gaussian

^a Full width at half-height; ^a *Agave tequilana*; ^b *Opuntia ficus-indica*

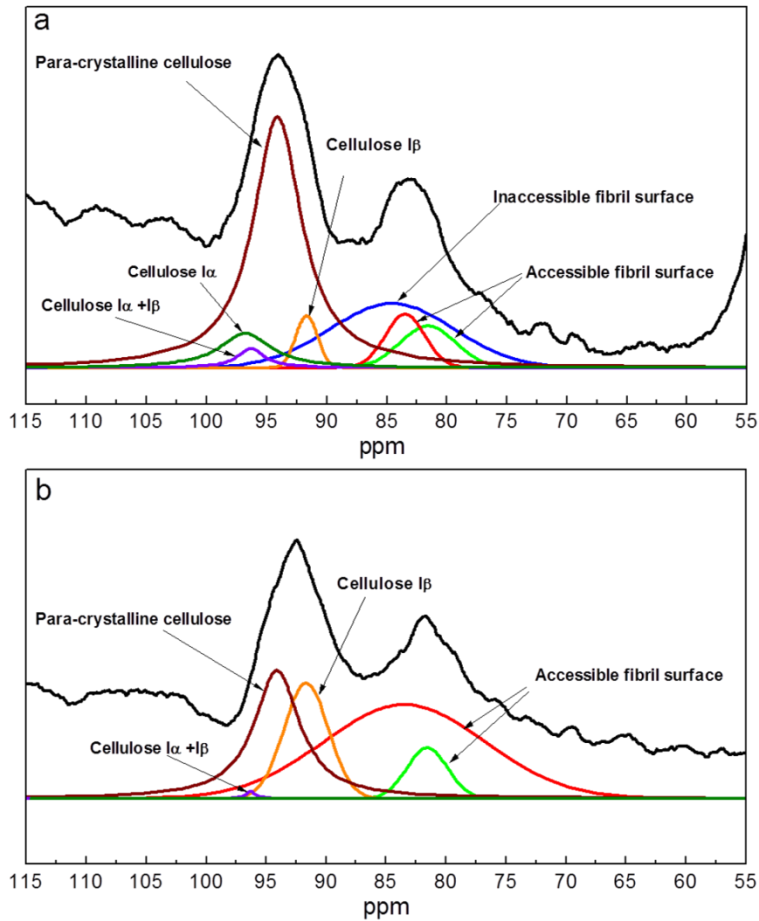


Figure 2.4 Spectral fitting for the C-4 region of CP/MAS ^{13}C NMR spectra of isolated cellulose of *Agave tequilana* (a) and *Opuntia ficus-indica* (b).

2.4 Conclusions

The arid-land adapted, highly water-use efficient CAM species *A. tequilana* and *O. ficus-indica*, which are unique biomass species compared to other C₃ and C₄ plants, were characterized by series of standard biomass analytical procedures. Both *Agave* and *Opuntia* contained a high amount of water at 84.9% and 93.9%, respectively. In addition, carboxylic acids and simple sugars were found to be the major constituents of freshly expelled juice. *A. tequilana* and *O. ficus-indica* dry bagasses possessed structural carbohydrate mass fractions of 43.8% and 36.3%, respectively, with low relative lignin

mass fractions of 13.1% and 12.3%, respectively. The higher heating values observed here for both species were lower than those for woody biomass due to the relatively low lignin mass fractions. Moreover, the amorphous and para-crystalline cellulose fractions accounted for over 80% of the total cellulose in both species. The low lignin mass fraction and low cellulose crystallinity indicated that bagasse from both *Agave* and *Opuntia* might be more readily deconstructed into fermentable sugars than biomass from traditional herbaceous or woody feedstocks. Although, the relatively high protein and ash mass fractions of these feedstocks present chemical engineering challenges to effect optimal strategies for their handling and processing into biofuels, their high water mass fractions might make them especially attractive for aqueous phase processes.

2.5 References

1. National Research Council (2011) “Renewable fuel standard: potential economic and environmental effects of U.S. biofuel policy.”
2. Aosaar, J., Varik, M., and Uri, V. Biomass production potential of grey alder (*Alnus incana* (L.) Moench.) in Scandinavia and Eastern Europe: A review. *Biomass Bioenerg* 2012 Oct; **45**, 11–26.
3. Ragauskas, A.J., Williams, C.K., Davison, B.H., et al. (2006) The path forward for biofuels and biomaterials. *Science* **311**(5760), 484–489.
4. Somerville, C., Youngs, H., Taylor, C., et al. (2010) Feedstocks for lignocellulosic biofuels. *Science* **329**(5993), 790–792.
5. Campbell, J.E., Lobell, D.B., Genova, R.C., and Field, C.B. (2008) The global potential of bioenergy on abandoned agriculture lands. *Environ. Sci. Technol.* **42**(15), 5791–5794.
6. Owen, N.A., and Griffiths, H. (2013) Marginal land bioethanol yield potential of four crassulacean acid metabolism candidates (*Agave fourcroydes* , *Agave salmiana* , *Agave tequilana* and *Opuntia ficus-indica*) in Australia. *GCB Bioenergy* **6**(6), 687–703.
7. Dauber, J., Brown, C., Fernando, A.L., et al. Bioenergy from “surplus” land: environmental and socio-economic implications. *BioRisk* 2012 Oct;7, 5–50.

8. Borland, A.M., Griffiths, H., Hartwell, J., and Smith, J.A.C. (2009) Exploiting the potential of plants with crassulacean acid metabolism for bioenergy production on marginal lands. *J. Exp. Bot.* **60**(10), 2879–2896.
9. Martínez-Torres, J., Barahona-Pérez, F., Lappe-Oliveras, P., et al. (2011) Ethanol production from two varieties of henequen (*Agave fourcroydes* Lem). *GCB Bioenergy* **3**(1), 37–42.
10. Nobel, P.S. (1991) Achievable productivities of certain CAM plants: basis for high values compared with C3 and C4 plants. *New Phytol* **119**(2), 183–205.
11. Yan, X., Tan, D.K.Y., Inderwildi, O.R., et al. (2011) Life cycle energy and greenhouse gas analysis for agave-derived bioethanol. *Energy Environ. Sci.* **4**(9), 3110–3121.
12. Davis, S.C., Dohleman, F.G., and Long, S.P. (2011) The global potential for Agave as a biofuel feedstock. *GCB Bioenergy* **3**(1), 68–78.
13. Escamilla-Treviño, L.L. (2012) Potential of plants from the genus agave as bioenergy crops. *BioEnergy Res.* **5**(1), 1–9.
14. Garcia-Moya, E., Romero-Manzanares, A., and Nobel, P.S. (2011) Highlights for Agave productivity. *GCB Bioenergy* **3**(1), 4–14.
15. Nobel, P.S., Garcia-moya, E., and Quero, E. (1992) High annual productivity of certain agaves and cacti under cultivation. *Plant. Cell Environ.* **15**(3), 329–335.
16. (1996) Nobel PS. High Productivity of Certain Agronomic CAM Species. In: Winter K, Smith JAC, editors. *Crassulacean acid metabolism: biochemistry, ecophysiology and evolution*, Springer-Verlag, Berlin, pp. 255–65.
17. Noble PS (1991) Environmental productivity indices and productivity for *Opuntia ficus-indica* under current and elevated atmospheric CO₂ levels. *Plant Cell Environ.* **14**(7), 637–646.
18. Garcia, V., Cort, D., and Nobel, P.S. (1991) Prediction and measurement of high annual productivity for *Opuntia ficus-indica*. *Agr Forest Meteorol.* **56**(3), 261–272.
19. Nair, S.S., Kang, S., Zhang, X., et al. (2012) Bioenergy crop models: descriptions, data requirements, and future challenges. *GCB Bioenergy* **4**(6), 620–633.
20. Holtum, J.A.M., Chambers, D., Morgan, T., and Tan, D.K.Y. (2011) Agave as a biofuel feedstock in Australia. *GCB Bioenergy* **3**(1), 58–67.
21. Chávez-Moreno, C.K., Tecante, A., and Casas, A. (2009) The Opuntia (Cactaceae) and Dactylopius (Hemiptera: Dactylopiidae) in Mexico: a historical perspective of use, interaction and distribution. *Biodivers. Conserv.* **18**(13), 3337–3355.

22. (2002) Inglese P, Basile F, Schirra M. Cactus pear fruit production. In: Nobel PS, editor. *Cacti : biology and uses*, University of California Press, Berkeley, CA, pp. 163–183.
23. Basile, F. Economic aspects of cactus pear production and market. *J Prof Assoc Cactus 2001 Apr; 5*, 31–46.
24. Russell, C.E., and Felker, P. (1987) The Prickly-pears (*Opuntia* spp ., Cactaceae): A source of human and animal food in semiarid regions. *Econ. Bot.* **41**(3), 433–445.
25. Nobel, P.S. (1988) *Environmental biology of agaves and cacti*, Cambridge University Press, New York.
26. Iñiguez-Covarrubias, G., Lange, S.E., and Rowell, R.M. (2001) Utilization of byproducts from the tequila industry: part 1: agave bagasse as a raw material for animal feeding and fiberboard production. *Bioresource technol.* **77**(1), 25–32.
27. Shedbalkar, U.U., Adki, V.S., Jadhav, J.P., and Bapat, V.A. (2010) Opuntia and other cacti: applications and biotechnological insights. *Tropical Plant Biol.* **3**(3), 136–150.
28. Hegwood, D.A. (1990) Human health discoveries with opuntia sp . (Prickly Pear). *HortScience* **25**(12), 1515–1516.
29. (2002) Sáenz -H, C, Corrales-Garcia J A-PG. Nopalitos, mucilage, fiber, and chohineal. In: Nobel PS, editor. *Cactus biology and uses*, University of California Press, Berkeley, CA, pp. 211–234.
30. Bensadón, S., Hervert-Hernández, D., Sáyago-Ayerdi, S.G., and Goñi, I. (2010) By-products of *Opuntia ficus-indica* as a source of antioxidant dietary fiber. *Plant food Hum. Nutr.* **65**(3), 210–216.
31. Feugang, J., Konarski, P., Zou, D., et al. Nutritional and medicinal use of cactus pear (*Opuntia* spp.) cladodes and fruits. *Front. Biosci. 2006 Sep; 11*, 2574–2589.
32. De Los Angeles Aguilera-Barreiro, M., Rivera-Marquez, J., Trujillo-Arriaga, H., et al. Intake of dehydrated nopal (*Opuntia ficus indica*) improves bone mineral density and calciuriain adult Mexican women. *Food Nutr. Res. 2013 May; 57*, 19106.
33. Stintzing, F.C., and Carle, R. (2005) Cactus stems (*Opuntia* spp.): a review on their chemistry, technology, and uses. *Mol. Nutr. Food Res.* **49**(2), 175–194.
34. Sáenz, C., Estévez, M., Sepúlveda, E., and Mecklenburg, P. (1998) Cactus pear fruit: a new source for a natural sweetner. *Plant food Hum. Nutr.* **52**(2), 141–149.
35. Valenzuela, A. (2011) A new agenda for blue agave landraces: food, energy and tequila. *GCB Bioenergy* **3**(1), 15–24.

36. Núñez, H.M., Rodríguez, L.F., and Khanna, M. (2011) Agave for tequila and biofuels: an economic assessment and potential opportunities. *GCB Bioenergy* **3**(1), 43–57.
37. Espinoza-Escalante, F.M., Pelayo-Ortíz, C., Navarro-Corona, J., et al. (2009) Anaerobic digestion of the vinasses from the fermentation of Agave tequilana weber to tequila: The effect of pH, temperature and hydraulic retention time on the production of hydrogen and methane. *Biomass Bioenerg* **33**(1), 14–20.
38. Iñiguez-Covarrubias, G., Díaz-Teres, R., Sanjuan-Dueñas, R., et al. (2001) Utilization of by-products from the tequila industry. Part 2: Potential value of Agave tequilana weber azul leaves. *Bioresource technol.* **77**(2), 101–108.
39. Chávez-Guerrero, L., and Hinojosa, M. (2010) Bagasse from the mezcal industry as an alternative renewable energy produced in arid lands. *Fuel* **89**(12), 4049–4052.
40. Kuloyo, O. (2012) “Ethanol production by yeast fermentation of and opuntia ficus-indica biomass hydrolysate.”
41. Davis, S.C., House, J.I., Diaz-Chavez, R.A., et al. (2011) How can land-use modelling tools inform bioenergy policies? *Interface Focus* **1**(2), 212–223.
42. DeMartini, J.D., Pattathil, S., Miller, J.S., et al. (2013) Investigating plant cell wall components that affect biomass recalcitrance in poplar and switchgrass. *Energy Environ. Sci.* **6**(3), 898–909.
43. Zeng, Y., Zhao, S., Yang, S., and Ding, S.Y. Lignin plays a negative role in the biochemical process for producing lignocellulosic biofuels. *Curr. Opin. biotech* 2014 Jun; **27**, 38–45.
44. Trajano, H.L., Engle, N.L., Foston, M., et al. (2013) The fate of lignin during hydrothermal pretreatment. *Biotechnol. Biofuels* **6**(1), 110–125.
45. Ragauskas, A.J., Beckham, G.T., Biddy, M.J., et al. (2014) Lignin valorization: improving lignin processing in the biorefinery. *Science* **344**(6185), 1246843.
46. Perez-Pimienta, J.A., Lopez-Ortega, M.G., Varanasi, P., et al. Comparison of the impact of ionic liquid pretreatment on recalcitrance of agave bagasse and switchgrass. *Bioresource technol* 2013 Jan; **127**, 18–24.
47. Vieira, M.C., and Heinze, T. (2002) Cellulose derivatives from cellulosic material isolated from Agave lechuguilla and fourcroydes. *Cellulose* **9**(2), 203–212.
48. Li, H., Foston, M.B., Kumar, R., et al. (2012) Chemical composition and characterization of cellulose for Agave as a fast-growing, drought-tolerant biofuels feedstock. *RSC Adv.* **2**(11), 4951–4958.

49. Mancilla-Margalli, N.A., and L ópez, M.G. (2006) Water-soluble carbohydrates and fructan structure patterns from Agave and Dasylirion species. *J. agr food Chem.* **54**(20), 7832–9.
50. Sluiter, A., Hames, B., Hyman, D., et al. “Determination of total solids in biomass and total dissolved solids in liquid process samples. Golden, Colorado: National Renewable Energy Laboratory; 2008,Mar,9p, Report No.TP-510-42621.” (March).
51. Sluiter, A., Hames, B., Ruiz, R., et al. “Determination of ash in biomass. Golden, Colorado: National Renewable Energy Laboratory; 2008,Jan,8p, Report No.TP-510-42622” (January).
52. Sluiter, A., Ruiz, R., Scarlata, C., et al. “Determination of extractives in biomass. Golden, Colorado: National Renewable Energy Laboratory; 2008,Jan,12p, Report No.TP-510-42619.” (January).
53. Wang, W., Vignani, R., Scali, M., and Cresti, M. (2006) A universal and rapid protocol for protein extraction from recalcitrant plant tissues for proteomic analysis. *Electrophoresis* **27**(13), 2782–2786.
54. Sluiter, A., Hames, B., Ruiz, R., et al. Determination of structural carbohydrates and lignin in biomass. Golden, Colorado: National Renewable Energy Laboratory; 2011,Jan,18p, Report No.TP-510-42618.
55. Sluiter, A., Hames, B., Ruiz, R., et al. “Determination of sugars , byproducts , and degradation products in liquid fraction process samples. Golden, Colorado: National Renewable Energy Laboratory; 2008,Jan,14p, Report No.TP-510-42623” (January).
56. Hallac, B.B., Sannigrahi, P., Pu, Y., et al. (2009) Biomass characterization of Buddleja davidii: a potential feedstock for biofuel production. *J. agr food Chem.* **57**(4), 1275–1281.
57. Larsson, P.T., Wickholm, K., and Iversen, T. (1997) A CP / MAS ^{13}C NMR investigation of molecular ordering in celluloses. *Carbohydr Res.* **302**(1-2), 19–25.
58. Stahl, R., Henrich, E., Gehrmann, H., et al. (2004) “Definition of a standard biomass”, *Renew. fuels Adv. powertrains*, 1–14.
59. Tumuluru, J.S., Sokhansanj, S., Wright, C.T., et al. (2011) “A review on biomass classification and composition , co-Firing issues and pretreatment methods”, *ASABE Meet.*
60. Christopher, L.P. (2013) Current state and development potential. In: Christopher LP, editor. *Integrated forest biorefineries : challenges and opportunities*, Royal Society of Chemistry, Cambridge, UK.

61. Borland, A.M., Hartwell, J., Weston, D.J., et al. (2014) Engineering crassulacean acid metabolism to improve water-use efficiency. *Trends Plant Sci.* **19**(5), 327–338.
62. Ginestra, G., Parker, M.L., Bennett, R.N., et al. (2009) Anatomical, chemical, and biochemical characterization of cladodes from prickly pear [Opuntia ficus-indica (L.) Mill.]. *J. agr food Chem.* **57**(21), 10323–10330.
63. Mciteka, H. (2008) “Fermentation charateristics and nutritional value of Opuntia ficus-indica var. fusicaulis cladode silage” (November).
64. Lin, H., Strull, J., Liu, Y., et al. (2012) High yield production of levulinic acid by catalytic partial oxidation of cellulose in aqueous media. *Energy Environ. Sci.* **5**(12), 9773–9777.
65. Yang, L., Su, J., Carl, S., et al. Catalytic conversion of hemicellulosic biomass to lactic acid in pH neutral aqueous phase media. *Appl. Catal. B Environ. 2015 Jan;* **162**, 149–157.
66. Weingarten, R., Conner, W.C., and Huber, G.W. (2012) Production of levulinic acid from cellulose by hydrothermal decomposition combined with aqueous phase dehydration with a solid acid catalyst. *Energy Environ. Sci.* **5**(6), 7559–7574.
67. Garde, A., Jonsson, G., Schmidt, A.S., and Ahring, B.K. (2002) Lactic acid production from wheat straw hemicellulose hydrolysate by *Lactobacillus pentosus* and *Lactobacillus brevis*. *Bioresource Technol.* **81**(3), 217–223.
68. Contreras-Padilla, M., Pérez-Torrero, E., Hernández-Urbiola, M.I., et al. (2011) Evaluation of oxalates and calcium in nopal pads (*Opuntia ficus-indica* var. redonda) at different maturity stages. *J. Food Compos. Anal.* **24**(1), 38–43.
69. Runge, T., Wipperfurth, P., and Zhang, C. (2013) Improving biomass combustion quality using a liquid hot water treatment. *Biofuels* **4**(1), 73–83.
70. White, R.H. (1986) Effect of lignin content and extractives on the higher heating value of wood. *Wood Fiber Sci* **19**(4), 446–452.
71. Günther, B., Gebauer, K., Barkowski, R., et al. (2012) Calorific value of selected wood species and wood products. *Eur. J. Wood Prod* **70**(5), 755–757.
72. Sannigrahi, P., Ragauskas, A.J., and Miller, S.J. (2008) Effects of two-stage dilute acid pretreatment on the structure and composition of lignin and cellulose in loblolly pine. *BioEnergy Res.* **1**(3), 205–214.
73. Mosier, N., Wyman, C., Dale, B., et al. (2005) Features of promising technologies for pretreatment of lignocellulosic biomass. *Bioresource technol.* **96**(6), 673–686.

74. Larsson, P.T., Hult, E., Wickholm, K., et al. (1999) CP/MAS ^{13}C -NMR spectroscopy applied to structure and interaction studies on cellulose I. *Solid State Nucl. Mag* **15**(1), 31–40.
75. Sun, Q., Foston, M., Sawada, D., et al. (2014) Comparison of changes in cellulose ultrastructure during different pretreatments of poplar. *Cellulose* **21**(4), 2419–2431.
76. Foston, M. Advances in solid-state NMR of cellulose. *Curr. Opin. biotech* 2014 Jun; **27**, 176–184.
77. Zheng, Y., Pan, Z., and Zhang, R. (2009) Overview of biomass pretreatment for cellulosic ethanol production. *Int J Agric Biol Eng* **2**(3), 51–68.
78. Sannigrahi, P., and Ragauskas, A.J. (2010) Poplar as a feedstock for biofuels : A review of compositional characteristics. *Biofuel Bioprod Bior* **4**(2), 209–226.
79. Samuel, R., Pu, Y., Foston, M., and Ragauskas, A.J. (2010) Solid-state NMR characterization of switchgrass cellulose after dilute acid pretreatment. *Biofuels* **1**(1), 85–90.
80. Bui, L., Luo, H., Gunther, W.R., and Román-Leshkov, Y. (2013) Domino reaction catalyzed by zeolites with Brønsted and Lewis acid sites for the production of γ -valerolactone from furfural. *Angew. Chemie Int. Ed.* **52** (31), 8022–8025.

Chapter 3 Selective oxidation of lignin model compounds to maleic acid over TS-1 catalyst

The utilization of lignin in the chemical industry has largely been limited because of the complicated chemical structure and persistent property of lignin. Catalytic oxidation has the potential to selectively convert lignin biomass into various useful chemicals and this methodology has rapidly progressed in the last several years. Lignins derived compounds (e.g. guaiacol) are common by-products of fast pyrolysis of lignocellulosic biomass. In this chapter, the feasibility of low-temperature selective oxidation of guaiacol to value-added dicarboxylic acids (e.g. maleic acid) was investigated in a titanium silicalite/hydrogen peroxide (TS-1/H₂O₂) reaction system. Under the oxidation reaction conditions (80 °C and pH=13.3), the molar yields of maleic acid from guaiacol were approximately 20-30%. The effects of catalyst loading, pH values, reaction time, and temperature on the yield of maleic acid were investigated. A possible TS-1 catalyzed aromatic ring opening reaction mechanism was proposed.

3.1 Introduction

In the biorefinery industry, fast pyrolysis is a thermochemical process that can produce up to 70 wt% bio-oils from raw biomass and is being deployed at pilot-scale [1–7]. However, due to high oxygen contents (35-40 wt%), low heating values, instability, corrosiveness, and immiscibility with gasoline and diesel, the bio-oil products cannot be used as liquid transportation fuels without substantial upgrading [8,9]. Hydrodeoxygenation (HDO) is extensively studied for upgrading pyrolysis oil [10–12].

However, the H₂ consumption for upgrading pyrolysis oil is a major hurdle of making HDO cost-effective. The unselective nature of HDO, unnecessary saturation of aromatic molecules, which account for ~30 wt% of the total pyrolysis oil, causes excess H₂ consumption, and therefore, makes HDO cost-prohibitive, considering the low profit margin of fuel products [13]. In contrast, selective oxidation of low-value lignin derived compounds into value-added commodity chemicals could improve the overall process economics of a biorefinery.

Guaiacol (2-methoxyphenol), one of the major lignin-derived bio-oil components, is widely used as the model feed for HDO upgrading [14–30]. However, the catalytic upgrading of guaiacol via oxidation methods is much less explored. Sasaki's group reported that the main products of hydrothermal oxidation of guaiacol in sub- and supercritical water were catechol, phenol, and o-cresol [31,32]. Suzuki *et al.* found that guaiacol was unselectively oxidized to low-molecular weight carboxylic acids like acetic acid and formic acid with molecular oxygen in aqueous media at 300 °C [33]. Although mechanistic studies of guaiacol oxidation are scarce in literature, knowledge learned from extensive studies of mineralization of phenol, a common water pollutant, by catalytic wet oxidation can be leveraged because phenol is a possible intermediate during guaiacol oxidation. The main intermediate products detected in phenol mineralization were ring compounds (e.g., hydroquinone, catechol, benzoquinones, *etc.*) and short chain carboxylic acids including maleic, malonic, succinic, fumaric, formic, acetic and oxalic acids. However, the yields of organic acids, especially C₄ diacids, were negligible [34–39].

Among the biomass-derived dicarboxylic acids, maleic acid is an important raw material used in the manufacture of phthalic-type alkyd and unsaturated polyester resins, surface coatings, lubricant additives, plasticizers, and copolymers [40]. Industrial processes of the production of maleic anhydride, a dehydrated form of maleic acid, use petroleum-based butane or benzene as the feedstock. Thus, oxidation of lignin derived by-products would be an appealing process to produce green maleic acid. The challenge, however, is how to cost-effectively accomplish a high yield of the desired carboxylic acid product.

Our group recently found that levulinic acid was generated in a high production yield by the aqueous-phase partial oxidation of cellulose over the ZrO_2 catalyst via a possible radical reaction pathway [41]. Herein, we expand our search for heterogeneous oxidation catalysts for the selective conversion of lignin-derived compounds. Titanium silicalite-1 (TS-1), a synthetic zeolite in which a small number of Ti atoms substitute tetrahedral Si atoms in a purely siliceous framework with the MFI structure [42], is an active and selective catalyst for a number of low-temperature oxidation reactions with aqueous hydrogen peroxide (H_2O_2) as the oxidant. The TS-1/ H_2O_2 reaction system has been one of the most actively studied green processes in the past decade [43–45]. In the present study, we demonstrate the feasibility of the selective oxidation of guaiacol to produce maleic acid with TS-1/ H_2O_2 under mild conditions. In addition, the oxidative ring-opening reaction mechanism is also tentatively discussed.

3.2 Materials and methods

3.2.1 Catalyst preparation and characterization

The TS-1 catalyst (Si/Ti ratio is 33) was synthesized using the modified method in literature [42]. Briefly, 50 g tetraethyl orthosilicate (TEOS) was added into 70 g aqueous solution of 20 wt% tetrapropylammonium hydroxide (TPAOH). To the resultant clear solution, a solution of 2.3 g titanium butoxide (Ti(OBu)_4) in isopropyl alcohol (15 g) was added and then 60 g water was added. The mixture was crystallized at 433K for 12 h under autogeneous pressure. The as-synthesized samples were calcined at 813 K for 5 h before use. All TS-1 precursors were bought from Sigma Aldrich (St. Louis, MO). Other catalytic materials including ZrO_2 , TiO_2 , Al_2O_3 , and H-ZSM-5 were purchased from Alfa Aesar (Ward Hill, Massachusetts). The surface morphology of catalysts was characterized by a Hitachi S-4700 scanning electron microscopy (SEM) (Chiyoda, Tokyo, Japan). Raman spectra were obtained on Renishaw InVia Raman Microscope System (Wotton-under-Edge, Gloucestershire, UK) with the excitation laser wavelength of 512 nm. EPR spectra were recorded at room temperature in air using a Bruker EMX Plus spectrometer (Billerica, MA) operated in the X band with 100-kHz field modulation with 10 mW microwave power, 100 kHz modulation frequency, 1G modulation amplitude, 30 dB receiver gain, 0.01 ms time constant, 100 G scan range, 35 s scan time, and 8 number of scan.

3.2.2 Aqueous-phase oxidation

The aqueous-phase oxidation reaction experiments were carried out in the leak-proof 30mL perfluoroalkoxy (PFA) vials (Thermo Scientific, Waltham, Massachusetts). In a typical experiment, 10 mL of aqueous solution of guaiacol (10 wt%), 0.5 ml H_2O_2

solution (35 wt%) and 0.1g solid catalyst were added into each PFA vial. Eight vials were fixed on the rotating vial holder and then placed in a preheated oven at the set temperature. The rotational speed was at 90 RPM to ensure a good mixing of catalysts in aqueous solutions. The schematic diagram of the reactor is shown in [Figure 3.1](#). After the reaction, the vials were quenched immediately in an ice water bath.

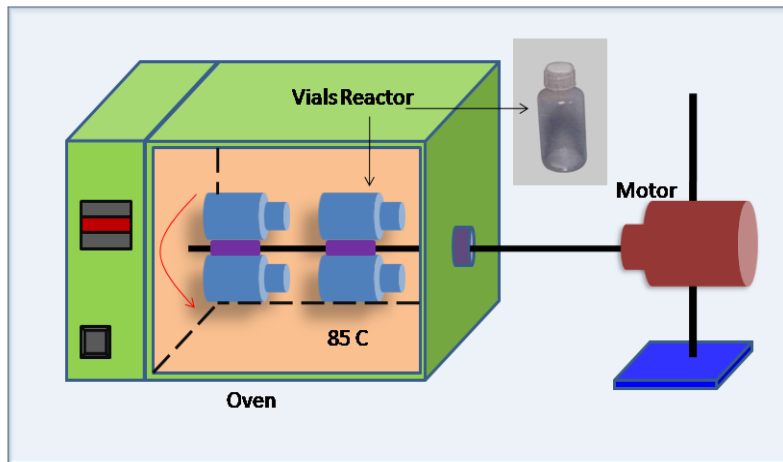


Figure 3.1 Schematic diagram of the aqueous-phase oxidation reactor system. Eight leak-proof 30 ml narrow-mouth perfluoroalkoxy (PFA) vials (Thermo Scientific) were placed in the bottle holder which was rotated at 90 RPM along the horizontal axis driven by an external motor. The reaction temperature was controlled by a preheated oven.

3.2.3 Product analysis

Aqueous samples collected from the oxidation experiments were diluted as needed and filtered through a 0.22 μm pore-size filter for analysis using total organic carbon (TOC) analyzer, high performance liquid chromatography (HPLC), electrospray ionization mass spectrometer (ESI-MS), and gas chromatography with mass spectrometer detector (GC/MS). TOC was measured by a Shimadzu (Kyoto, KYT) Total Organic Carbon Analyzer (model TOC-V). HPLC analysis was performed using a Shimadzu HPLC system equipped with a dual UV-VIS Detector (Shimadzu SPD 10-AV) at 208 and 290 nm and a Refractive Index Detector (Shimadzu RID-10A). For the analysis of organic

acids and reaction intermediates, the samples were separated in an Aminex 87-H column from Bio-Rad, with 5 mM H₂SO₄ as the mobile phase at 0.7 mL/min flow and a column temperature of 55 °C. All samples for ESI-MS analysis were diluted with a base solution containing 0.1 wt% triethylamine and the analysis was performed using a Waters Micromass ZQ quadrupole mass spectrometer (Milford, MA). GC/MS analysis was carried out using an Agilent (Santa Clara, CA) 6890 series equipped with a DB5-MS column (30 m x 0.25 mm ID, 0.25 µm film thickness) and an Agilent 5973 Mass Selective Detector. The derivitization of aqueous-phase samples by silylation was performed for GC/MS analysis. Briefly, 100 µL aqueous-phase product was lyophilized overnight in a deactivated 1.5 mL vial. To the dried solids, 150 µL of acetonitrile was added and mixed to allow the solids to dissolve, and then 50 µL of pyridine and 150 µL of BSFTA with TMCS (99:1) were added. The capped vial was placed in a sand bath maintained at 65 °C for 2 h to allow a complete silylation. After the silylation, the sample was cooled and 5 µL silylation mixture was diluted with 1.5 mL of hexane for GC/MS analysis.

3.3 Results and discussion

The scanning electron micrograph, shown in [Figure 3.2](#), displays that the as-synthesized TS-1 catalysts are porous spherical particles with an average size of ~100 nm. [Table 3.1](#) shows the guaiacol conversions, the total organic carbon (TOC) yields, and the molar yields of major aqueous-phase products by reacting guaiacol over the TS-1 catalyst at different reaction conditions. The pH, reaction temperature, and the H₂O₂ loading all affect the conversions of guaiacol and the yields of carboxylic acid products. The guaiacol oxidation could be carried out even at room temperature (25 °C). However,

increasing temperature until 80 °C enhanced the guaiacol conversions, the yields of maleic acid, and the H₂O₂ utilization efficiency. Moreover, increasing the loading amount of H₂O₂ (35 wt%) from 0.25 g to 1 g also enhanced the guaiacol conversion and the yield of maleic acid. Further increasing temperature and H₂O₂ loading led to the increase of guaiacol conversions, but to a decrease in maleic acid yields and H₂O₂ utilization efficiencies. Under the optimum reaction condition (80 °C, pH 13.3, and 1 g H₂O₂), the guaiacol is almost fully converted and the highest yield of maleic acid, 27.7%, were achieved.

Table 3.1 The results of oxidation of guaiacol with H₂O₂ with and without the TS-1 catalyst.

Catal.	Reaction conditions ^a				Con. %	TOC yield ^b %	TIC Yield ^c %	Molar yields of products % ^d				ROR ^e %	U _{H2O2} ^f %
	pH	Temp. °C	Time hour	H ₂ O ₂ g				Ma A	FuA	MA	OA		
none	12.3	80	24	0.5	39.6	88.5	5.0	6.6	0.1	0.3	3.4	26.3	6.5
TS-1	12.3	80	24	0.5	62.3	86.9	5.2	7.6	0.2	0.6	4.7	21.3	8.2
none	14.3	80	24	0.5	79.0	70.5	13.6	9.9	0.8	0.9	10.5	14.7	13.9
TS-1	14.3	80	24	0.5	88.0	70.6	15.8	13.7	1.3	1.7	12.4	20.1	18.2
none	13.3	80	24	0.5	63.2	80.2	9.2	8.9	0.6	1.2	6.5	17.0	10.7
TS-1	13.3	80	24	0.5	78.0	75.1	10.8	19.9	0.9	1.7	12.5	28.9	21.7
TS-1	13.3	85	24	0.5	88.6	70.2	11.6	16.9	0.6	0.6	13.6	20.0	17.8
TS-1	13.3	65	24	0.5	75.3	73.4	9.9	18.5	0.9	1.9	11.2	28.9	20.2
TS-1	13.3	50	24	0.5	66.9	79.9	10.3	17.7	0.6	0.9	10.5	28.7	18.5
TS-1	13.3	25	24	0.5	54.0	77.8	8.2	15.5	0.8	1.1	8.9	32.2	16.4
TS-1	13.3	80	24	0.25	47.0	84.9	7.6	7.2	0.1	0.3	6.2	16.0	17.6
TS-1	13.3	80	24	1	99.9	57.6	12.3	27.7	1.6	2.9	13.5	32.6	14.5
TS-1	13.3	80	24	2	99.9	58.8	13.9	21.9	1.3	2.3	12.2	25.6	6.9

CaT =Catechol, MaA=Maleic Acid, FuA = Fumaric Acid, MA = Malic Acid, AA = Acetic acid, OA = Oxalic Acid.

a. Reaction conditions: Guaiacol = 0.1 g, Catalyst=0.1 g, H₂O=10 g. The pH value of reaction solutions were adjusted by NaOH, H₂O₂ is 35 wt %. In order to make the most of H₂O₂ utilization, a reaction time 24 h is adopted.

b. TOC yield =Total organic carbon (TOC) of liquid after reaction/Total carbon (TC) of liquid before reaction.

c. TIC yield =Total inorganic carbon (TIC) of liquid after reaction/TC of liquid before reaction.

d. Molar yield = moles of product formed/ moles of guaiacol total converted in reaction.

e. ROR is Ring Opening Ratio, ROR= moles of converted guaiacol (ring opening) / moles of total converted guaiacol. The moles of guaiacol opened the benzene ring were estimated to be the total moles of all identified C₄ acid products.

f. U_{H2O2} = Utilization of H₂O₂to produce carboxylic acids. U_{H2O2} were estimated to be the total moles of all identified carboxylic acid products / moles of total H₂O₂.

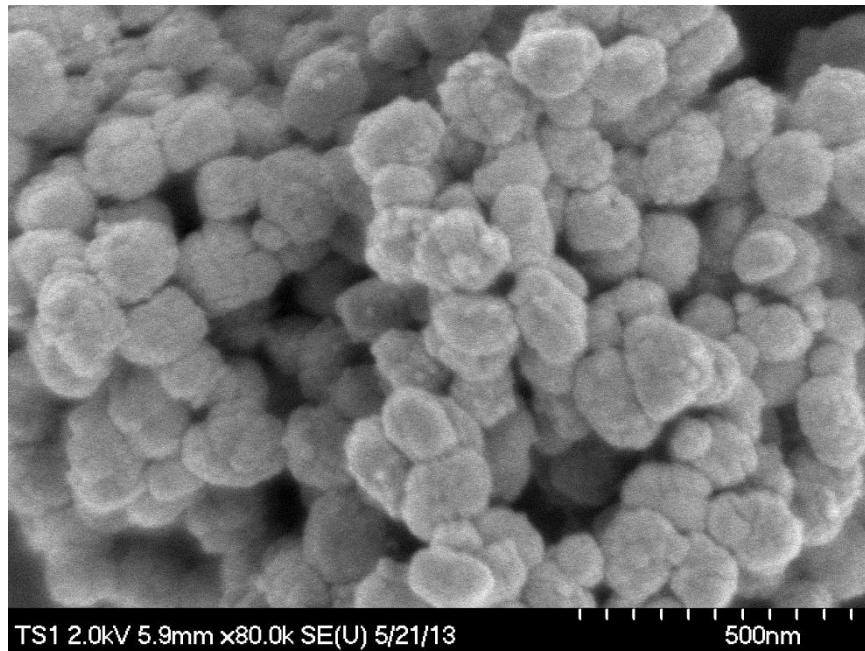


Figure 3.2 Scanning electronic microscope image of as-synthesized TS-1 catalyst.

Table 3.2 compares the different catalysts and shows that, when the reactant solutions were neutral (pH 6.8), all solid catalysts including TS-1, ZrO₂, TiO₂, Al₂O₃, and zeolite ZSM-5, enhanced conversions of guaiacol compared to those without a solid catalyst. Figure 3.3 shows that the conversions of guaiacol without a solid catalyst were only ~20% in the range of pH 1.0 to 10.0, while increasing pH led to the increase of guaiacol conversions, reaching ~80% at pH 14.3. On the other hand, the highest conversion of guaiacol, ~88%, was achieved with the presence of the TS-1 catalyst in a narrow range of pH (13.3 < pH < 14.3). The pH of the starting reactant solution also significantly affected the product distribution, indicating that both Brønsted base (OH⁻) and Brønsted acid (H⁺) exhibit the strong homogeneously catalytic effects. The TOC yields, which indicated the total organic carbon content in the aqueous-phase products, maintained at 80-90%. However, the TOC decreased slightly when the pH of the starting reactant solutions increased from 1.0 to 13.3. The total inorganic carbon (TIC) yields were less than 0.5%

in the acidic and neutral solutions, but were increased to ~5-15 % at pH 12.3 to 14.3. The increase of TIC was due to the formation of NaHCO₃ or Na₂CO₃ in the basic solutions by reacting CO₂ with excess NaOH. The high guaiacol conversions and TOC yields, as well as the low TIC yields, suggested that the carbon loss to CO₂ due to complete oxidation of guaiacol with aqueous H₂O₂ was low over the TS-1 catalyst. Such a selective oxidation was different from catalytic wet oxidation, in which CO₂ was the dominant product [46–55].

Table 3.2 The comparison of the effect of the different solid catalysts on the catalytic oxidation of guaiacol with H₂O₂. Reaction conditions: Guaiacol = 0.1 g, H₂O₂ (35 wt %) = 0.5 g, catalyst = 0.1 g, H₂O = 10 g, reaction temperature = 80 °C, reaction time = 24 h.

Catal.	pH ^a		Con v. %	TOC yield ^b %	TIC Yield ^c %	Molar yields of products % ^d					ROR ^e %
	Initial	Final				CaT	MaA	FuA	MA	OA	
none	7.0	6.3	19.9	99.6	0.1	0	0	0	0	0	0
TS-1	7.0	4.5	46.3	97.7	0.1	0.2	3.9	0.9	0.5	6.9	11.4
Al ₂ O ₃	6.8	6.3	34.8	97.1	0.4	0	0	0	0	0	0
ZSM-5	6.8	6.3	23.5	98.9	0.1	0.7	0	0	0	0	0

CaT = Catechol, MaA = Maleic Acid, FuA = Fumaric Acid, MA = Malic Acid, AA = Acetic acid, OA = Oxalic Acid.

a. The acidic solutions (pH value = 1.0) were adjusted by H₂SO₄; the alkaline solutions (pH value = 13.3) were adjusted by NaOH.

b. TOC yield = Total organic carbon (TOC) of liquid after reaction / Total carbon (TC) of liquid before reaction.

c. TIC yield = Total inorganic carbon (TIC) of liquid after reaction / TC of liquid before reaction.

d. Molar yield = moles of product formed / moles of guaiacol total converted in reaction.

e. ROR is Ring Opening Ratio, ROR = moles of converted guaiacol opening the benzene ring / moles of total converted guaiacol. The moles of guaiacol opened the benzene ring were estimated to be the total moles of all identified C₄ acid products.

The aqueous-phase products of guaiacol oxidation with TS-1/H₂O₂ were in three categories: 1) carboxylic acids such as maleic acid, fumaric acid, malic acid, acrylic acid, acetic acid, formic acid, and oxalic acid, which were the aromatic ring opening products detected by ESI-MS (Figure 3.4) and HPLC (Figure 3.5); 2) Aromatic compounds including catechol, o-benzoquinone, and 1,2,4-benzenetriol, which were the intermediate

products without breaking the benzene ring detected by GC/MS (Figure 3.6) and HPLC (Figure 3.5). Catechol was the hydrolysis product of guaiacol, while o-benzoquinone and 1,2,4-benzenetriol are the oxidation and hydroxylation products of catechol, respectively; and 3) Unidentified di-cyclic or tri-cyclic colored aromatic compounds or deep colored pigments which were observed from the color change of the aqueous products during the oxidation reaction. These colored compounds evolved complicated structures via the radical induced reaction pathway [56–58]. Brønsted base promoted the formation of carboxylic acids and combining TS-1 with the base catalyst created synergy that significantly increased the selectivity to maleic and oxalic acids.

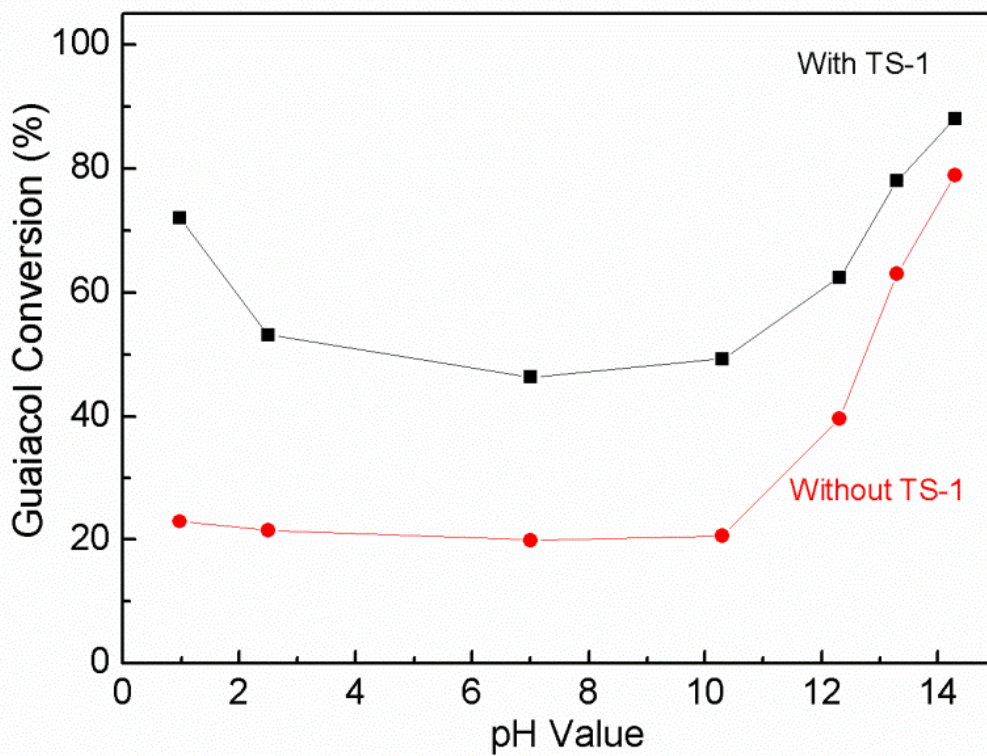


Figure 3.3 Guaiacol conversions at different initial pH values with and without the TS-1 catalyst. TS-1 enhanced the guaiacol conversion in a wide range of pH values ($1.0 < \text{pH} < 13.3$). Reaction conditions: Guaiacol = 0.1 g (0.8 mmol), H_2O_2 (35 wt %) = 0.5 g (5.1 mmol), Catalyst = 0.1 g, H_2O = 10 g, reaction temperature = 85 °C.

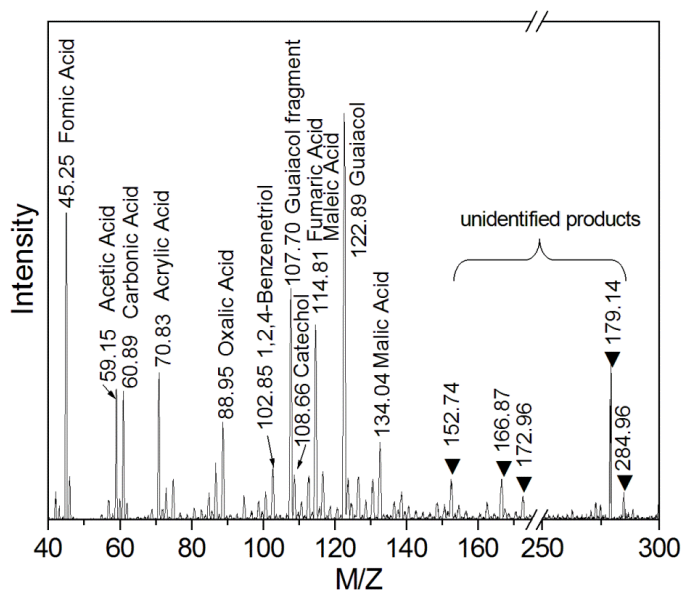


Figure 3.4 Electrospray ionization mass spectra (ESI-MS) of the aqueous-phase products of guaiacol oxidation. Reaction conditions: Guaiacol = 0.1 g (0.8 mmol), H_2O_2 (35 wt %) = 0.5 g (5.1 mmol), Catalyst = 0.1 g, H_2O = 10 g, reaction temperature = 85 °C, initial pH = 13.3. In this experiment, all samples were tested in a negative ion mode by ESI-MS. The source temperature and desolvation temperature were 130 °C and 250 °C, respectively. The pump flow was 10 $\mu L/min.$

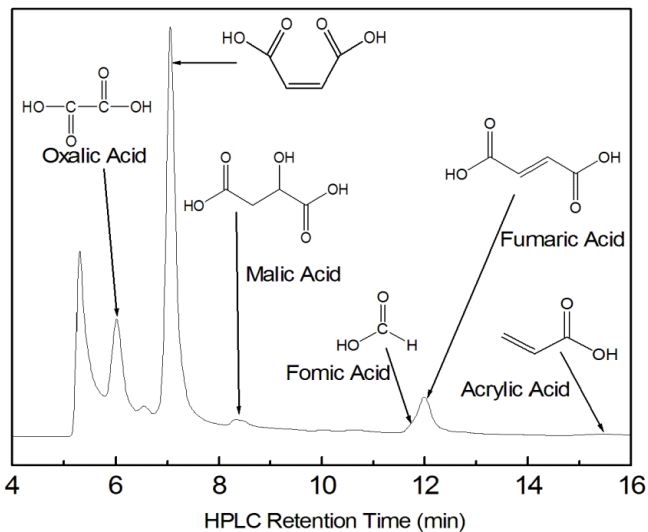


Figure 3.5 HPLC spectra of the aqueous-phase products of guaiacol oxidation. Reaction conditions: Guaiacol = 0.1 g (0.8 mmol), H_2O_2 (35 wt %) = 0.5 g (5.1 mmol), Catalyst = 0.1 g, H_2O = 10 g, reaction temperature = 85 °C, initial pH = 13.3. In this experiment, all samples were tested in a negative ion mode by ESI-MS. The source temperature and desolvation temperature were 130 °C and 250 °C, respectively. The pump flow was 10 $\mu L/min.$

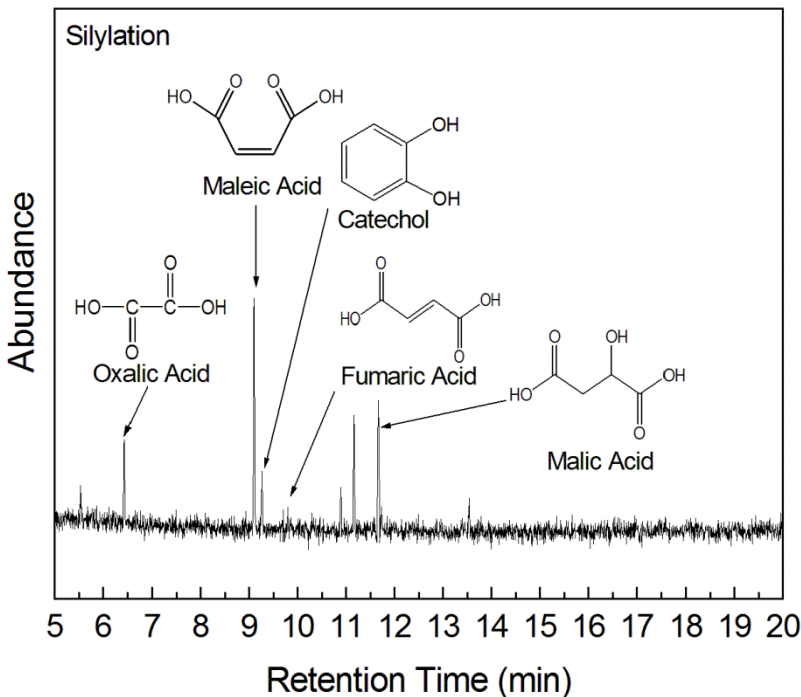


Figure 3.6 The GC/MS total ion chromatogram of the aqueous-phase products of guaiacol oxidation. Reaction conditions: Guaiacol = 0.1 g (0.8 mmol), H_2O_2 (35 wt %) = 0.5 g (5.1 mmol), Catalyst = 0.1 g, H_2O = 10 g, reaction temperature = 85 °C, initial pH = 13.3. In this experiment, all samples were tested in a negative ion mode by ESI-MS. The source temperature and desolvation temperature were 130 °C and 250 °C, respectively. The pump flow was 10 $\mu L/min$.

To further investigate the catalytic effect of the TS-1 catalyst, maleic acid concentrations and guaiacol conversion versus reaction times were compared with and without TS-1, as shown in Figure 3.7. Both the yields of maleic acid and the guaiacol conversions increased rapidly during the initial stage of reaction and reached a plateau after 6 h. However, with the TS-1 catalyst, the concentrations of maleic acid were significantly higher than those without the TS-1. After 6 h of reaction and starting from pH 13.3, the maleic acid concentrations were 1800 and 800 ppm with and without TS-1, respectively, as shown in Figure 3.7(a). In the initial period of reaction (within the first 6 h), the concentration of H_2O_2 was relatively high so that most of guaiacol were reacted in this period. As shown in Figure 3.7(b), ~75% of guaiacol was converted with the TS-1

catalyst whereas only ~50% of guaiacol was reacted without a solid catalyst after reacting for 6 h. Therefore TS-1 can activate the H₂O₂ to promote the ring opening reactions, which would be a key step for the production of maleic acid from guaiacol. Without the TS-1 catalyst, most of H₂O₂ probably were consumed in the oligomerization reactions or decompose data relative high temperature (80 °C). The inset photo in [Figure 3.7\(b\)](#) shows that at the beginning of oxidation, highly colored quinone intermediate compounds, such as p-benzoquinone (yellow) and o-benzoquinone (red), were generated at 30min and 3 h, respectively. The color comes from their quinoidal structure, which contains chromophore groups substituted in benzene rings. The color level monitored during oxidation gradually became darker with increasing reaction time, indicating that other intermediates might contribute. The inter-molecular interactions between quinones (yellow) and dihydroxylated rings (colorless) might form the highly colored quinhydrone species (purple to brown) [\[59\]](#), which might have been generated during the oxidation treatment.

The formation of colored aromatic compounds is an undesirable side reaction to the carboxylic acid production. Herein, we use the ring opening ratio (ROR) to define the efficiency of guaiacol ring opening over different catalysts. As shown in [Table 3.2](#), the ROR was zero without a catalyst. No ring-opening products were observed over the solid Lewis and Brønsted acid catalysts (Al₂O₃ and ZSM-5, respectively). However, the ROR over the TS-1 was 6.1% in the neutral solutions, indicating that the TS-1 catalyst catalyzed the ring opening reactions in the absence of base. Furthermore, the highest ROR, ~30%, was contributed by the synergistic effects of both homogeneous base catalysis (NaOH) and heterogeneous oxidation catalysis (TS-1/H₂O₂). The corresponding

selectivity to maleic acid reached ~70% among the carboxylic acids generated via ring opening under the optimized reaction conditions.

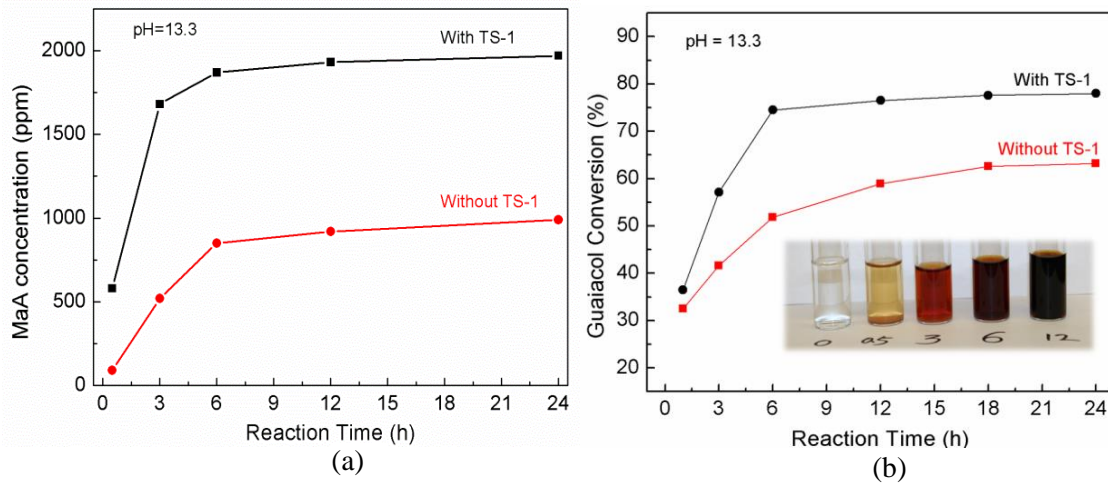


Figure 3.7 Influence of the TS-1 catalyst on (a) maleic acid concentration; and (b) conversion of guaiacol. Inset is the photo of aqueous-phase product at different guaiacol oxidation reaction periods (0–12 h) with the presence of the TS-1 catalyst. The color gradually changed from colorless to dark brown as the reaction time increased. Other reaction conditions are: Guaiacol=0.1 g (0.8 mmol), H_2O_2 (35 wt %)=0.5 g (5.1 mmol), TS-1 Catalyst=0.1 g, H_2O =10 g, reaction temperature = 80 °C, initial pH = 13.3.

Previous studies showed that the formation of carboxylic acids from catalytic wet oxidation of phenol passed through three steps: 1) hydroxylation of phenol with •OH radicals to dihydroxylated benzene such as hydroquinone or catechol; 2) the oxidation of hydroquinone or catechol to *para*- or *ortho*- benzoquinone; 3) the ring opening reaction of benzoquinone to form maleic and oxalic acids. So far, most of the studies supported that ring opening reactions were originated from an •OH radical oxidation mechanism [34–39]. As shown in Figure 3.8, we also found that •OH is the only radical in the TS-1/ H_2O_2 aqueous solutions based on the electron paramagnetic resonance (EPR) spectra under the simulated reaction conditions without adding guaiacol. The intensity of the EPR signals increased in the order of H_2O_2 in pH neutral solution < $H_2O_2/TS-1$ in pH neutral solution < $H_2O_2/TS-1$ in pH 13.3 alkaline solution. Obviously, the TS-1 catalyst

promoted the decomposition of H_2O_2 in aqueous solutions to produce hydroxyl radicals, especially in the alkaline solution. We thus tentatively relate the guaiacol conversion and the yield of ring opening products to the concentration of the $\cdot\text{OH}$ radical.

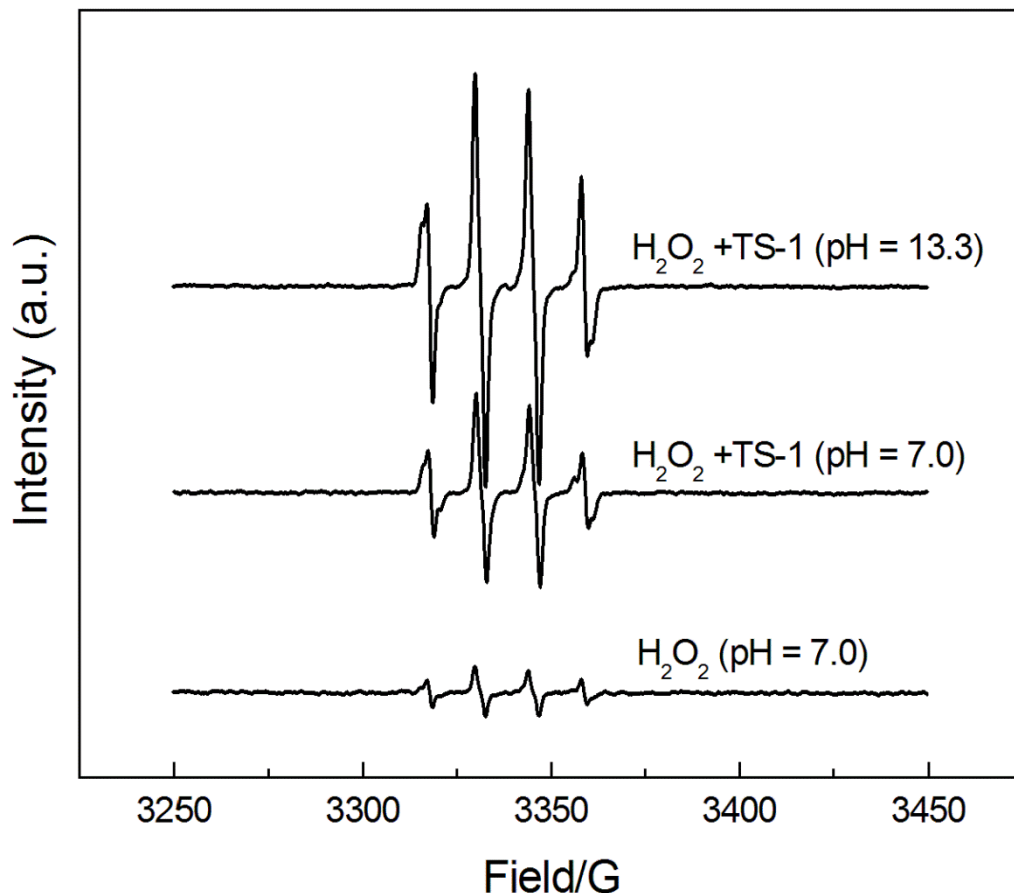


Figure 3.8 Comparison of the EPR spectra of hydroxyl radicals of H_2O_2 in pH neutral aqueous solution, $\text{H}_2\text{O}_2/\text{TS-1}$ in pH neutral aqueous solution, and $\text{H}_2\text{O}_2/\text{TS-1}$ in pH 13.3 aqueous solution. The spin trap agent is BMPO. The concentration of H_2O_2 and the amount of TS-1 are same as those in a typical guaiacol oxidation reaction. Before recording the EPR spectra, the samples were heated at 80 °C for 10min.

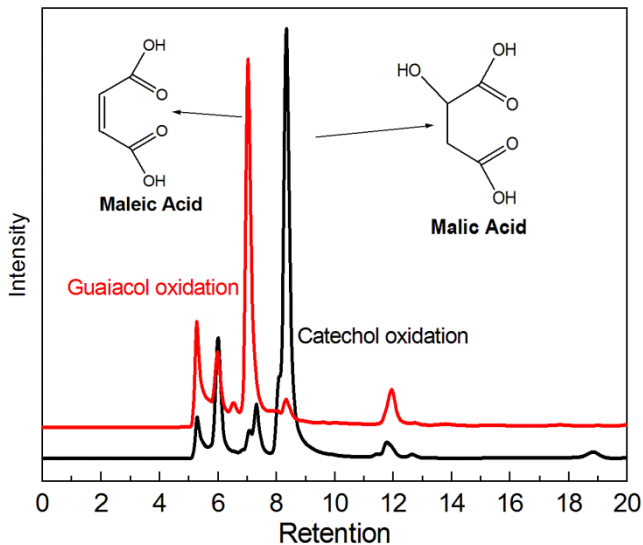


Figure 3.9 HPLC spectra of aqueous-phase products of guaiacol and catechol oxidation. The main product of catechol oxidation reaction is malic acid, while maleic acid is the major product of guaiacol oxidation, implying that guaiacol and catechol have different oxidation reaction pathways even under the identical reaction conditions. We propose that the benzene ring of guaiacol could be opened directly without proceeding hydrolysis first. (Guaiacol and catechol oxidation reaction conditions: Guaiacol or Catechol = 0.1 g, H_2O_2 (35 wt %) = 0.5 g (5.1 mmol), TS-1 catalyst = 0.1 g, H_2O = 10 g, reaction temperature = 85 °C, initial pH = 13.3).

For different biomass substrates, hydroxyl radicals may trigger the formation of various organic radicals, and thus lead to different reaction pathways and result in different final products. Interestingly, our results show that the main product of catechol oxidation is malic acid, whereas maleic acid is the dominant carboxylic acid product when guaiacol is the reactant substrate, as seen in Figure 3.9. The formation of different organic acid products suggests that catechol is not necessarily the key intermediate of guaiacol ring-opening oxidation in the TS-1/ H_2O_2 system. Therefore, we propose that there are three parallel reaction pathways of the conversion of guaiacol (Figure 10): 1) the demethylation of guaiacol to form catechol; 2) the oligomerization of guaiacol or its derivatives such as catechol and benzoquinone, which forms the complex macromolecular colored products following an unknown radical reaction pathway; and 3)

the oxidative ring-opening reaction to produce maleic acid and oxalic acid, followed by further reactions including hydration to malic acid, isomerization to fumaric acid, decarboxylation to acrylic acid, and oxidation to acetic acid, oxalic acid or formic acid. We hypothesize that the oxidative ring-opening reaction of guaiacol is induced by $\cdot\text{OH}$ radicals.

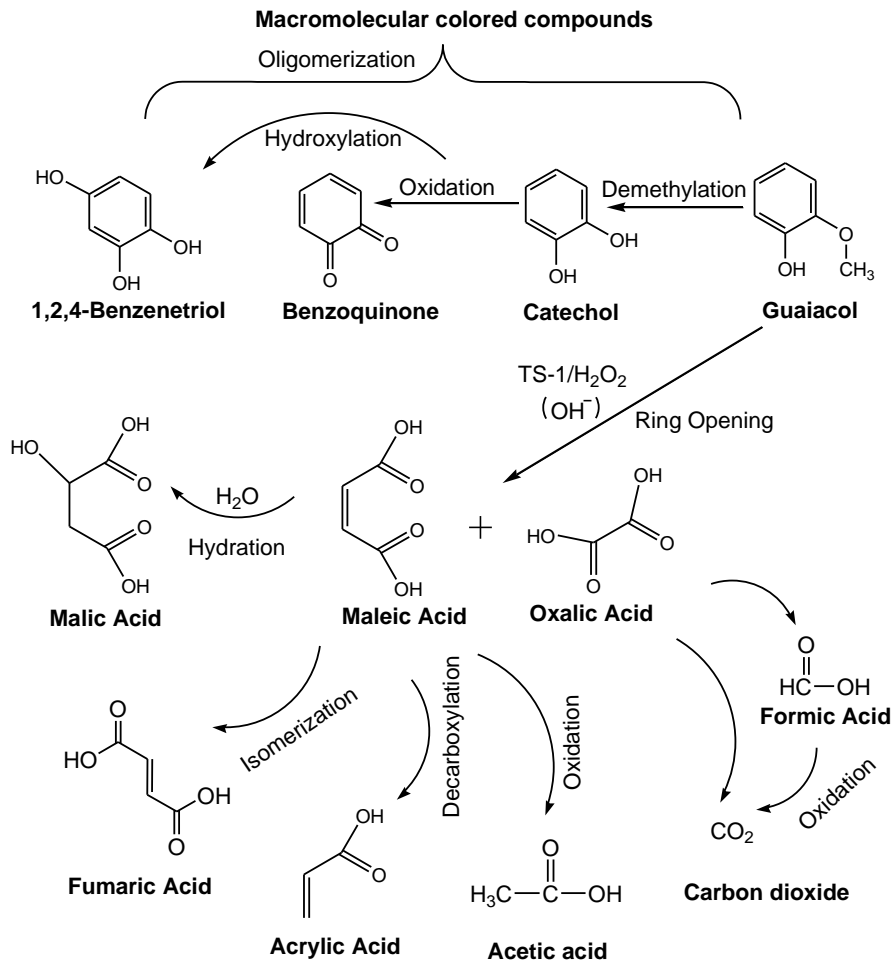


Figure 3.10 The proposed reaction pathway of selective oxidation of guaiacol in $\text{TS-1}/\text{H}_2\text{O}_2$ system.

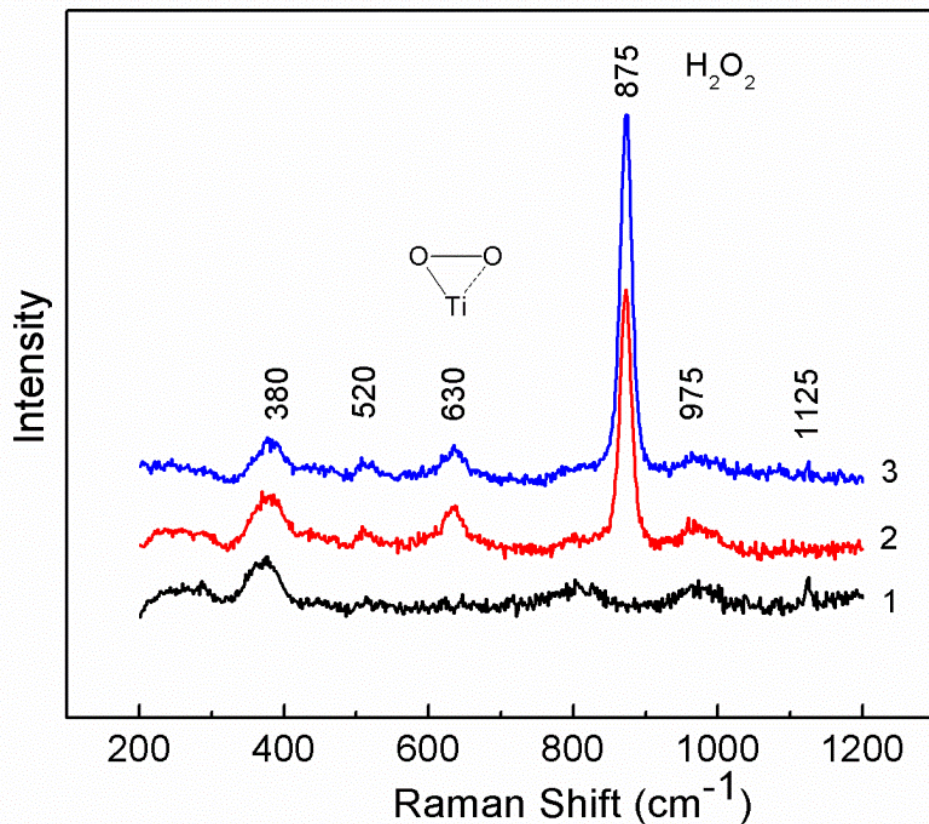


Figure 3.11 Raman spectrum of pure TS-1 and TS-1 samples in contact with a $\text{H}_2\text{O}_2/\text{H}_2\text{O}$ solution. 1) pure TS-1; 2) TS-1 in contact with a $\text{H}_2\text{O}_2/\text{H}_2\text{O}$ solution($\text{pH}=7$), 3) TS-1 in contact with a $\text{H}_2\text{O}_2/\text{H}_2\text{O}$ solution($\text{pH}=13.5$).

It is our great interest to understand how the radicals are formed on the TS-1 catalyst through the decomposition of H_2O_2 in an alkaline aqueous solution. According to previous studies, three reactive oxo-Ti species (η^1 and η^2 -Hydroperoxo-Ti, and Superoxotitanium) could be easily generated in the TS-1/ H_2O_2 system [60–64]. Upon contacting H_2O_2 , four types of superoxo-Ti radicals were generated on TS-1. They were different according to the EPR characterization: A-type: $g_z = 2.0260$; B-type: $g_z = 2.0235$; C-type: $g_z = 2.0220$; and D-type: $g_z = 2.031$. Both EPR and UV-Vis spectrometry techniques confirmed that these superoxo-Ti radicals were in equilibrium during the oxidation reaction and their concentration depended on temperature, pH and solvent [65–67]. In a

TS-1/H₂O₂/H₂O system, TS-1 could easily activate H₂O₂ to D-type superoxo-Ti radicals especially at high pH values [67]. As shown in Figure 11, the bands located at 380, 520, 975, and 1125 cm⁻¹ were the Raman features of the TS-1. After contact with a H₂O₂/H₂O solution, the bands at 975 and 1125cm⁻¹ disappeared and leading to the creation of two new peaks at 630 cm⁻¹ and 875cm⁻¹. The quenching of the bands at 975 and 1125cm⁻¹ implied that the reaction occurred within a framework of Ti on the TS-1 surface with H₂O₂. The strong Raman band at 875 cm⁻¹ stood for the (O-O) stretching mode of the physisorbed H₂O₂ on the TS-1 surface. The new band at 630 cm⁻¹ was assigned to the vibration mode of a side-on η^2 Ti-OO complex, which provided indirect evidence of superoxo-Ti radicals present within in the TS-1/H₂O₂/H₂O system. Therefore, we hypothesize that the D-type superoxo-Ti radicals are the active species for the generation of free •OH radicals.

Usually silicate materials are not stable in highly basic aqueous solutions. As shown in Figure 3.12, the peaks at 23.2°, 23.8° and 24.3° are characteristic XRD peaks of the MFI structure of TS-1. We compared the XRD pattern of the fresh TS-1 catalyst with that of the spent catalyst after it had reacted for 24 h at 80 °C with the initial pH value of 13.3, and found that both samples exhibited all three characteristic peaks with only slight difference in intensity. On the other hand, after treatment with NaOH solution (pH 13.3 but without adding guaiacol) at 80 °C for 24 h, the same TS-1 material was transformed from crystalline to amorphous, indicating that strong alkaline solvents could leach out silica, and therefore, eventually destroy the framework of TS-1. However, due to the neutralization of base with the carboxylic acid products, the pH value in the actual reaction media decreased quickly (Figure 3.12b). As the reaction proceeded, the pH

value decreased from 13.3 to 10.5 in 30min, and further decreased to 8.7 and 7.8, after 1 and 3 h, respectively. The catalytic effect of the TS-1 catalyst was obvious in the weakly basic solutions. Furthermore, the short-term stability of the TS-1 catalyst was validated in the alkaline H₂O₂ aqueous media due to the self-neutralization by the carboxylic acid products.

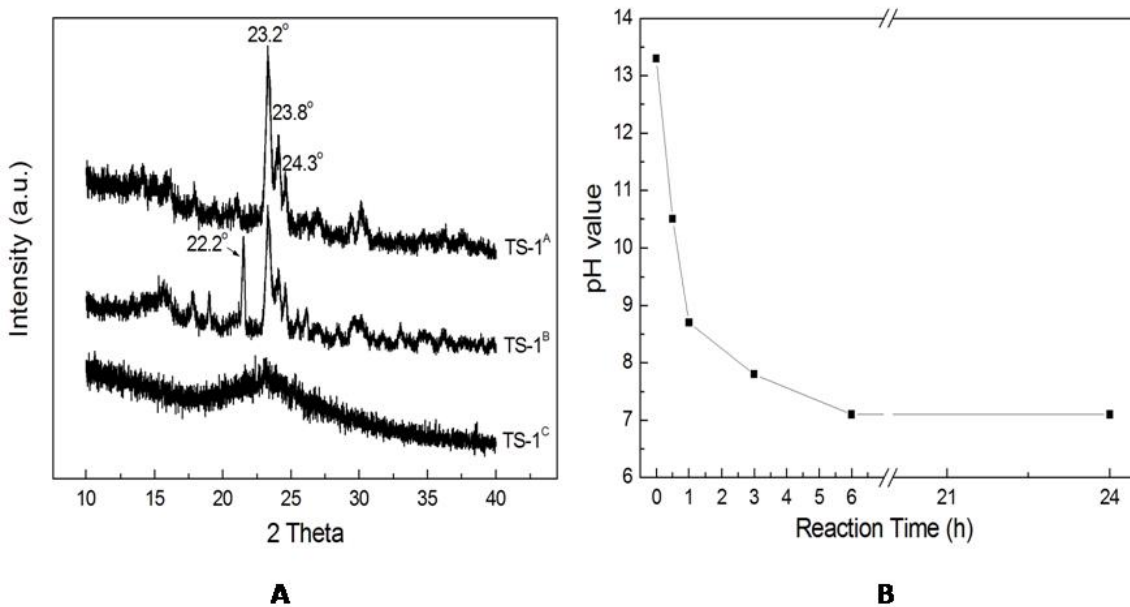


Figure 3.12 XRD patterns of different TS-1 catalysts (a) and pH value versus reaction time (b). TS-1^A stands for the fresh TS-1, TS-1^B stands for the spent TS-1 catalyst after the reaction (initial pH value is 13.3, reaction temperature is 80°C, and reaction time is 24 hour), TS-1^C stands for the TS-1 sample treated with NaOH solution (pH value is 13.3) at 80°C for 24 h.

3.4 Conclusions

In summary, we demonstrated a “green” alternative approach to produce maleic acid from selective oxidation of guaiacol at low temperatures with alkaline aqueous H₂O₂ over heterogeneous TS-1 catalysts. The yields of maleic acid were highly dependent up on the catalyst property, the temperature, the initial pH value, and the H₂O₂ loading amount. At 80 °C and the initial pH of 13.3, the maximum yield of maleic acid, ~28%, was achieved

from the guaiacol oxidation with the TS-1 catalyst. The synergistic effect of the Bronsted base and the TS-1 with H₂O₂ as the oxidant leads to the aromatic-ring opening reactions of guaiacol, a key step to selectively produce maleic acid. The proposed guaiacol oxidation reaction mechanism indicates that the oligomerization of guaiacol and its derivatives are undesired side reactions for the production of maleic acid. Further research will be carried out toward in-depth investigations of how to inhibit oligomerization in order to further enhance the yield of maleic acid.

3.5 References

1. Bridgwater, A.V., Meier, D., and Radlein, D. (1999) An overview of fast pyrolysis of biomass. *Org. Geochem.* **30** (12), 1479–1493.
2. Pattiya, A., Titiloye, J.O., and Bridgwater, a. V. (2010) Evaluation of catalytic pyrolysis of cassava rhizome by principal component analysis. *Fuel* **89** (1), 244–253.
3. Nowakowski, D.J., Bridgwater, a. V., Elliott, D.C., et al. (2010) Lignin fast pyrolysis: Results from an international collaboration. *J. Anal. Appl. Pyrolysis* **88** (1), 53–72.
4. Bridgwater, A. V, and Peacocke, G.V.C. (2000) Fast pyrolysis processes for biomass. *Renewable Sustain. Energy Rev.* **4**, 1–73.
5. Vispute, T.P., Zhang, H., Sanna, A., et al. (2010) Renewable chemical commodity feedstocks from integrated catalytic processing of pyrolysis oils. *Science* **330** (6008), 1222–7.
6. Carlson, T.R., Tompsett, G. a., Conner, W.C., and Huber, G.W. (2009) Aromatic production from catalytic fast pyrolysis of biomass-derived feedstocks. *Top. Catal.* **52** (3), 241–252.
7. Bridgwater, A.V. (2012) Review of fast pyrolysis of biomass and product upgrading. *Biomass and Bioenergy* **38**, 68–94.
8. Zhang, Q., Chang, J., Wang, T., and Xu, Y. (2007) Review of biomass pyrolysis oil properties and upgrading research. *Energy Convers. Manag.* **48** (1), 87–92.
9. De Miguel Mercader, F., Groeneveld, M.J., Kersten, S.R. a., et al. (2011) Hydrodeoxygenation of pyrolysis oil fractions: process understanding and quality assessment through co-processing in refinery units. *Energy Environ. Sci.* **4** (3), 985.

10. Crossley, S., Faria, J., Shen, M., and Resasco, D.E. (2010) Solid nanoparticles that catalyze biofuel upgrade reactions at the water/oil interface. *Science* **327** (5961), 68–72.
11. Zakzeski, J., Bruijnincx, P.C. a, Jongerius, A.L., and Weckhuysen, B.M. (2010) The catalytic valorization of lignin for the production of renewable chemicals. *Chem. Rev.* **110** (6), 3552–99.
12. Furimsky, E. (2000) Catalytic hydrodeoxygenation. *Appl. Catal. A Gen.* **199** (2), 147–190.
13. Zhao, C., Kou, Y., Lemonidou, A.A., et al. (2009) Highly selective catalytic conversion of phenolic bio-oil to alkanes. *Angew. Chemie* **121** (22), 4047–4050.
14. Gutierrez, a., Kaila, R.K., Honkela, M.L., et al. (2009) Hydrodeoxygenation of guaiacol on noble metal catalysts. *Catal. Today* **147** (3-4), 239–246.
15. Bykova, M.V., Ermakov, D.Y., Kaichev, V.V., et al. (2012) Ni-based sol–gel catalysts as promising systems for crude bio-oil upgrading: Guaiacol hydrodeoxygenation study. *Appl. Catal. B Environ.* **113-114**, 296–307.
16. Jongerius, A.L., Jastrzebski, R., Bruijnincx, P.C. a., and Weckhuysen, B.M. (2012) CoMo sulfide-catalyzed hydrodeoxygenation of lignin model compounds: An extended reaction network for the conversion of monomeric and dimeric substrates. *J. Catal.* **285** (1), 315–323.
17. Ruiz, P.E., Frederick, B.G., De Sisto, W.J., et al. (2012) Guaiacol hydrodeoxygenation on MoS₂ catalysts: Influence of activated carbon supports. *Catal. Commun.* **27**, 44–48.
18. Ghompson, I.T., Sepúlveda, C., Garcia, R., et al. (2012) Hydrodeoxygenation of guaiacol over carbon-supported molybdenum nitride catalysts: Effects of nitriding methods and support properties. *Appl. Catal. A Gen.* **439-440**, 111–124.
19. Zhang, X., Wang, T., Ma, L., et al. (2013) Characterization and catalytic properties of Ni and NiCu catalysts supported on ZrO₂–SiO₂ for guaiacol hydrodeoxygenation. *Catal. Commun.* **33**, 15–19.
20. Zhao, H.Y., Li, D., Bui, P., and Oyama, S.T. (2011) Hydrodeoxygenation of guaiacol as model compound for pyrolysis oil on transition metal phosphide hydroprocessing catalysts. *Appl. Catal. A Gen.* **391** (1-2), 305–310.
21. Bui, V.N., Laurenti, D., Delichère, P., and Geantet, C. (2011) Hydrodeoxygenation of guaiacol Part II: Support effect for CoMoS catalysts on HDO activity and selectivity. *Appl. Catal. B Environ.* **101** (3-4), 246–255.
22. Lee, C.R., Yoon, J.S., Suh, Y.-W., et al. (2012) Catalytic roles of metals and supports on hydrodeoxygenation of lignin monomer guaiacol. *Catal. Commun.* **17**, 54–58.

23. Wu, S.-K., Lai, P.-C., Lin, Y.-C., et al. (2013) Atmospheric hydrodeoxygenation of guaiacol over alumina-, zirconia-, and silica-supported nickel phosphide catalysts. *ACS Sustain. Chem. Eng.* **1** (3), 349–358.
24. Tyrone Ghompson, I., Sepúlveda, C., Garcia, R., et al. (2012) Comparison of alumina- and SBA-15-supported molybdenum nitride catalysts for hydrodeoxygenation of guaiacol. *Appl. Catal. A Gen.* **435-436**, 51–60.
25. Nimmanwudipong, T., Runnebaum, R.C., Block, D.E., and Gates, B.C. (2011) Catalytic conversion of guaiacol catalyzed by platinum supported on alumina: reaction network including hydrodeoxygenation reactions. *Energy & Fuels* **25** (8), 3417–3427.
26. Bui, V.N., Laurenti, D., Afanasiev, P., and Geantet, C. (2011) Hydrodeoxygenation of guaiacol with CoMo catalysts. Part I: Promoting effect of cobalt on HDO selectivity and activity. *Appl. Catal. B Environ.* **101** (3-4), 239–245.
27. Deutsch, K.L., and Shanks, B.H. (2012) Hydrodeoxygenation of lignin model compounds over a copper chromite catalyst. *Appl. Catal. A Gen.* **447-448**, 144–150.
28. Olcese, R., Bettahar, M.M., Malaman, B., et al. (2013) Gas-phase hydrodeoxygenation of guaiacol over iron-based catalysts. Effect of gases composition, iron load and supports (silica and activated carbon). *Appl. Catal. B Environ.* **129**, 528–538.
29. Olcese, R.N., Bettahar, M., Petitjean, D., et al. (2012) Gas-phase hydrodeoxygenation of guaiacol over Fe/SiO₂ catalyst. *Appl. Catal. B Environ.* **115-116**, 63–73.
30. Nimmanwudipong, T., Runnebaum, R.C., Block, D.E., and Gates, B.C. (2011) Catalytic reactions of guaiacol: reaction network and evidence of oxygen removal in reactions with hydrogen. *Catal. Letters* **141** (6), 779–783.
31. Sasaki, M., and Goto, M. (2011) Thermal decomposition of guaiacol in sub-and supercritical water and its kinetic analysis. *J. Mater. Cycles Waste Manag.* **13**, 68–79.
32. Kanetake, T., Sasaki, M., and Goto, M. (2007) Decomposition of a lignin model compound under hydrothermal conditions. *Chem. Eng. Technol.* **30** (8), 1113–1122.
33. Suzuki, H., Cao, J., Jin, F., et al. (2006) Wet oxidation of lignin model compounds and acetic acid production. *J. Mater. Sci.* **41** (5), 1591–1597.
34. Devlin, H.R., and Harris, I.J. (1984) Mechanism of the oxidation of aqueous phenol with dissolved oxygen. *Ind. Eng. Chem. Fundam.* **23**, 387–392.
35. Santos, a., Yustos, P., Quintanilla, a., et al. (2005) Study of the copper leaching in the wet oxidation of phenol with CuO-based catalysts: Causes and effects. *Appl. Catal. B Environ.* **61** (3-4), 323–333.

36. Santos, a., Yustos, P., Quintanilla, a., et al. (2004) Evolution of toxicity upon wet catalytic oxidation of phenol. *Environ. Sci. Technol.* **38** (1), 133–138.
37. Santos, A., Yustos, P., Quintanilla, A., et al. (2002) Route of the catalytic oxidation of phenol in aqueous phase. *Appl. Catal. B Environ.* **39**, 97–113.
38. Wu, Z., and Zhou, M. (2001) Partial degradation of phenol by advanced electrochemical oxidation process. *Environ. Sci. Technol.* **35** (13), 2698–2703.
39. Zazo, J. a., Casas, J. a., Molina, C.B., et al. (2007) Evolution of ecotoxicity upon Fenton's Oxidation of phenol in water. *Environ. Sci. Technol.* **41** (20), 7164–7170.
40. Felthouse, T.R., Burnett, J.C., Mitchell, S.F., and Mumney, M.J. (2005) “Maleic anhydride , maleic acid , and fumaric Acid”, *Van Nostrand's Encycl. Chem.*, 1–7.
41. Lin, H., Strull, J., Liu, Y., et al. (2012) High yield production of levulinic acid by catalytic partial oxidation of cellulose in aqueous media. *Energy Environ. Sci.* **5** (12), 9773.
42. Thangaraj, A., and Sivasanker, S. (1992) An improved method for TS-1 synthesis : 29Si NMR studies. *J. Chem. Soc. Chem. Commun.* (2), 123–124.
43. Blanco-Brieva, G., Capel-Sanchez, M.C., de Frutos, M.P., et al. (2008) New two-step process for propene oxide production (HPO) based on the direct synthesis of hydrogen peroxide. *Ind. Eng. Chem. Res.* **47** (21), 8011–8015.
44. Clerici, M.G. (2001) The role of the solvent in TS-1 chemistry: active or passive ? An early study revisited. *Top. Catal.* **15** (2-4), 257–263.
45. Klemm, E., Dietzsche, E., Schwarz, T., et al. (2008) Direct gas-phase epoxidation of propene with hydrogen peroxide on TS-1 zeolite in a microstructured reactor. *Ind. Eng. Chem. Res.* **47** (6), 2086–2090.
46. Beziat, J.-C., Besson, M., Gallezot, P., and Durecu, S. (1999) Catalytic wet air oxidation of carboxylic acids on TiO₂-supported ruthenium catalysts. *J. Catal.* **182**, 129–135.
47. Oliviero, L., Barbier, J., Duprez, D., et al. (2001) Wet air oxidation of aqueous solutions of maleic acid over Ru/CeO₂ catalysts. *Appl. Catal. B Environ.* **35**, 1–12.
48. Hamoudi, S., Larachi, F., and Sayari, a (1998) Wet oxidation of phenolic solutions over heterogeneous catalysts: Degradation profile and catalyst behavior. *J. Catal.* **177** (2), 247–258.
49. Akolekar, D.B., Bhargava, S.K., Shirgankar, I., and Prasad, J. (2002) Catalytic wet oxidation : an environmental solution for organic pollutant removal from paper and pulp industrial waste liquor. **236**, 255–262.

50. Gomes, H.T., Figueiredo, J.L., and Faria, J.L. (2000) Catalytic wet air oxidation of low molecular weight carboxylic acids using a carbon supported platinum catalyst. *Appl. Catal. B Environ.* **27**, 217–223.
51. Beziat, J., Gallezot, P., and Durecu, S. (1999) Catalytic wet air oxidation on a Ru/TiO₂ catalyst in a Trickle-Bed reactor. *Ind. Eng. Chem. Res.* **38**, 1310–1315.
52. Pintar, A., Besson, M., and Gallezot, P. (2001) Catalytic wet air oxidation of Kraft bleaching plant effluents in the presence of titania and zirconia supported ruthenium. *Appl. Catal. B Environ.* **30**, 123–139.
53. Imamura, S. (1999) Catalytic and noncatalytic wet oxidation. *Ind. Eng. Chem. Res.* **38** (5), 1743–1753.
54. Bhargava, S., Jani, H., Tardio, J., et al. (2007) Catalytic Wet oxidation of ferulic acid (A Model Lignin Compound) using heterogeneous copper catalysts. *Ind. Eng. Chem. Res.* **46**, 8652–8656.
55. Luck, F. (1999) Wet air oxidation: past , present and future. *Catal. Today* **53**, 81–91.
56. Doerge, D.R., Divi, R.L., and Churchwell, M.I. (1997) Identification of the colored guaiacol oxidation product produced by peroxidases. *Anal. Biochem.* **250** (1), 10–17.
57. Taurog, A., Dorris, M.L., and Guziec, F.S. (1992) An unexpected for peroxidase ' side reaction in the guaiacol assay. *Anal. Biochem.* **205** (9), 271–277.
58. Mijangos, F., Varona, F., and Villota, N. (2006) Changes in solution color during phenol oxidation by Fenton reagent. *Environ. Sci. Technol.* **40** (17), 5538–5543.
59. Regeimbal, J., Gleiter, S., Trumppower, B.L., et al. (2003) Disulfide bond formation involves a quinhydrone-type charge-transfer complex. *Proc. Natl. Acad. Sci. U. S. A.* **100** (24), 13779–13784.
60. Bonino, F., Damin, A., Ricchiardi, G., et al. (2004) Ti-peroxo species in the TS-1/H₂O₂/H₂O system. *J. Phys. Chem. B* **108**, 3573–3583.
61. Chaudhari, K., Srinivas, D., and Ratnasamy, P. (2001) Reactive oxygen species in titanosilicates TS-1 and TiMCM-41: an in situ EPR spectroscopic study. *J. Catal.* **203** (1), 25–32.
62. Shetti, V.N., Manikandan, P., Srinivas, D., and Ratnasamy, P. (2003) Reactive oxygen species in epoxidation reactions over titanosilicate molecular sieves. *J. Catal.* **216** (1-2), 461–467.

63. Srinivas, D., Manikandan, P., Laha, S.C., et al. (2003) Reactive oxo-titanium species in titanosilicate molecular sieves: EPR investigations and structure–activity correlations. *J. Catal.* **217**, 160–171.
64. Wang, L., Xiong, G., Su, J., et al. (2012) In situ UV Raman spectroscopic study on the reaction intermediates for propylene epoxidation on TS-1. *J. Phys. Chem. C* **116** (16), 9122–9131.
65. Gleeson, D., Sankar, G., Catlow, C.R.A., et al. (2000) The architecture of catalytically active centers in titanosilicate (TS-1) and related selective-oxidation catalysts. *Phys. Chem. Chem. Phys.* **2**, 4812–4817.
66. Zhao, Q., Bao, X., Wang, Y., et al. (2000) Studies on superoxide O₂– species on the interaction of TS-1 zeolite with H₂O₂. *J. Mol. Catal. A Chem.* **157** (1-2), 265–268.
67. Shetti, V.N., Srinivas, D., and Ratnasamy, P. (2004) Enhancement of chemoselectivity in epoxidation reactions over TS-1 catalysts by alkali and alkaline metal ions. *J. Mol. Catal. A Chem.* **210** (1-2), 171–178.

Chapter 4 Catalytic conversion of hemicellulose to lactic acid with zirconia catalyst in pH neutral aqueous phase media

Biomass-derived lactic acid is an important renewable chemical building block for synthesizing commodity chemicals, such as biodegradable plastics. After cellulose conversion with ZrO₂, this chapter reports that hemicellulosic biomass, xylan, and xylose, can be converted to lactic acid over the same ZrO₂ catalyst starting from pH neutral aqueous solutions. The effects of reaction conditions, including temperature, oxygen partial pressure, biomass loading, and catalyst loading, on the conversions of hemicellulosic biomass and the corresponding yields of lactic acid were investigated. Molar yields of lactic acid, up to 25% and 18% were produced from xylose and xylan, respectively, under the investigated reaction conditions with the ZrO₂ catalyst. The key intermediates such as glyceraldehyde, glycolaldehyde and pyruvaldehyde were used as reactants to probe the reaction mechanism. The role of the ZrO₂ catalyst in the retro-aldol condensation of xylose, as well as the catalyst stability, are discussed.

4.1 Introduction

Hemicellulose, along with cellulose and lignin, is presented in almost all plant cell walls of terrestrial biomass species, constituting approximately 20–35% of lignocellulosic biomass [1,2]. Hemicellulose is a mixture of heteropolymers (matrix polysaccharides), such as arabinoxylans, with a random, amorphous structure that can be readily hydrolyzed with dilute acids [3]. Xylose, a C5 sugar and the monomer of xylan, is one of the most abundant sugars found in nature [4]. Maize is composed of 13-25% xylan by dry

weight [5], while beech wood contains approximately 19% xylan [6]. However, xylan and xylose have not yet been fully utilized in industry. In the paper industry, a significant amount of xylose, from the hydrolysis of woody biomass, is mixed with lignin-derived compounds and burned to provide process heat [7]. Although xylose can be fermented to ethanol, commercial enzymes or yeasts are not yet fully available in the bio-ethanol industry. Thus, although the abundance and ease of isolation make xylose an ideal feedstock for the production of chemicals and fuels, cost-effective conversion processes are essential to fully explore its potential.

There are a few studies on the conversion of carbohydrates to lactic acid or lactates over heterogeneous catalysts. Chambon *et al.* found that lactic acid was produced directly from cellulose over heterogeneous Lewis acid catalysts, tungstated alumina and tungstated zirconia, with the carbon mole yields of 27% and 18.5%, respectively [8]. Holm *et al.* reported that the Lewis acidic zeotype materials, such as Sn-Beta, catalyzed the conversion of mono- and disaccharides to methyl lactate in methanol at 160 °C. With sucrose as the substrate, the methyl lactate yield reached a record high of 68%. However, changing the solvent from methanol to water led to the formation of much lower amounts of lactic acid (<30%) [9]. Solid base catalysts, including hydrotalcites [10] and magnesium oxide [11], and supported noble metal catalysts [12] were also used for catalysing the formation of lactic acid or methyl lactate from glucose; however, much lower yields than with Sn-Beta catalyst. However, there have been few studies on converting hemicellulose, such as xylose and xylan, to lactic acid with heterogeneous catalysts.

Herein, we report our findings on the catalytic conversion of xylose and xylan to lactic acid using a zirconium dioxide (ZrO_2) catalyst in pH-neutral high-temperature water without adding base or co-solvent. A possible bi-functional acid/base reaction mechanism is proposed to explain why the performance of ZrO_2 was superior to MgO , a solid base catalyst, towards the production of lactic acid from xylose.

4.2 Materials and methods

4.2.1 Materials

D-(+)-xylose (99%), xylan from beechwood (>90%), Glacial acetic acid (99.7%), Bis(trimethylsilyl) trifluoroacetamide (BSTFA) + trimethylchlorosilane (TMCS) (99:1), D-(+)-glyceraldehyde (98%), glycolaldehyde dimer, glycolic acid, L-(+)- lactic acid (98%), oxalic acid (99.0%), 2-hydroxybutyric acid (97%), propionic Acid (99.5%), acrylic acid (99%), pyridine anhydrous (99.8%), pyruvaldehyde (40wt% solution in water), furfural (99%), 5-(Hydroxymethyl) furfural (99%), sulfuric acid (98%), and magnesium nitrate hexahydrate (99%) were purchased from Sigma Aldrich (St. Louis, MO). Formic acid (98%) was purchased from Fluka (St. Louis, MO). Sodium hydroxide (ACS reagent) was purchased from Mallinckrodt Chemicals (St. Louis, Missouri). Zirconium oxide catalyst was purchased from Alfa Aesar (Ward Hill, Massachusetts) and calcined at 250 °C for 2 h before use. Magnesium oxide catalyst was attained by calcining magnesium nitrate hexahydrate at 550 °C in air for 3 h.

4.2.2 Catalytic reactions

All reactions were carried out in a 100 mL stirred Parr microreactor. In a typical run, solid catalyst and xylose/xylan were added into 20 mL deionized water in a glass liner

placed in the reactor. The Parr reactor was then sealed, purged with high purity nitrogen (99.99%), and then charged with reactive gases to the set pressure. The reactor was heated at a ramp rate of 10 °C/min until the desired temperature was reached. During the reaction, mixing was achieved through an internal propeller operating at 800 RPM. Once the set temperature was attained, the reactor was held for the set reaction time, and then quenched quickly in an ice bath to stop the reaction. The reactor was cooled until approximately 25 °C, and then vented after the gas pressure was recorded. The reactor was immediately broken down and the solid residue remaining in the reactor was recovered and dried for the calculation of solid residue yields. The aqueous and solid fractions were separated using a centrifuge. The weights of liquid portion and dried solid residues were recorded.

The SR yield (solid residue yield), the product yield, and the TOC yield (total organic carbon yield) are calculated using the following equations:

$$\text{SR Yield} = \frac{\text{Weight of total dried solid residue} - \text{Weight of solid catalyst}}{\text{Weight of hemicellulosic biomass feedstock}}$$

$$\text{Product Yield} = \frac{\text{Mole of aqueous phase product}}{\text{Mole of hemicellulosic biomass feedstock}}$$

$$\text{TOC Yield} = \frac{\text{Carbon weight of all aqueous phase products}}{\text{Carbon weight of hemicellulosic biomass feedstock}}$$

For the catalyst stability tests, the spent catalyst were collected and dried overnight in an oven at 105 °C, and then were reused under the same reaction conditions. Due to the collection loss, the actual weight of the catalyst was slightly lower than the initial weight and the corresponding biomass loading was reduced to keep the constant weight ratio of catalyst to biomass.

4.2.3 Product analysis

The liquid product of each reaction was characterized by a Shimadzu high performance liquid chromatography (HPLC), an Agilent gas chromatography/mass spectrometry (GC/MS), a Shimadzu total organic carbon analyzer (TOC), a Waters electron spray ionization mass spectrometry (ESI/MS), and a Bruker nuclear magnetic resonance spectrometry (NMR).

The aqueous solution after reaction was filtered through a 0.45 micron syringe filter and then diluted 15 times with ultra-pure water. HPLC analysis was performed using a Shimadzu (Kyoto, KYT) HPLC system equipped a UV-VIS Detector (Shimadzu SPD 10-AV) and Refractive Index Detector (Shimadzu RID-6A). For analysis of organic acids and reaction intermediates, the samples were separated in an Aminex 87-H column from Bio-Rad, using 5 mM H₂SO₄ as the mobile phase, 0.7 mL/min flow, at a column temperature of 55 °C. For quantitative identification and results, the UV-VIS detector was utilized at 208 nm and 290 nm. However, the peaks of lactic acid and glycolic acid overlapped under the UV-VIS detector. Thus, the refractive index detector was used to quantify the yields of lactic acid and glycolic acid.

Derivatization of the polar components was performed in order to perform qualitative GC/MS analysis and identification of unknown components in the aqueous phase. For a silylation derivatization, 125 µL liquid were lyophilized overnight in deactivated 1.5 mL vials. To the dried solids, 100 µL of acetonitrile was added and mixed to allow the solids to dissolve, and then 50 µL of pyridine and 100 µL of BSFTA with TMCS (99:1) were added. The capped vials were placed in a water bath maintained at 65 °C for 2 h to allow complete silylation. After silylation, the samples were cooled and a 100 µL mixture was

taken to be diluted with 1.4 mL of dichloromethane. The sample were injected in Agilent 6890 series GC/MS equipped with an Agilent DB5-MS column (30 m x 0.25 mm ID, 0.25 um film thickness) and Agilent 5973 Mass Selective Detector. The column temperature was maintained at 100 °C.

After the reaction, the resultant aqueous phase product samples were also prepared for total organic carbon analysis (TOC). For TOC analysis, the aqueous phase after reaction was filtered through a 0.45 micron syringe filter then diluted 200 times with ultra-pure water. TOC was measured by a Shimadzu Total Organic Carbon Analyzer (model TOC-VCSH). The TC (Total Carbon) standard was prepared by reagent grade potassium hydrogen phthalate; the IC (Inorganic Carbon) standard was prepared by reagent grade sodium bicarbonate and sodium carbonate. The carbon concentration of the standard solution corresponds to 1000 mg C/L. The standard stock solution was diluted with ultra-pure water to 100 ppm C.

All samples were detected by NMR chromatogram with a Varian model number NMR V500 (Palo Alto, CA) using DMSO (Dimethyl sulfoxide) as solvent. Before the test, all samples were dried in the freeze dry system in order to remove water in the samples.

For ESI/MS measurement, all samples were diluted by base solution and tested by ESI on Water e2695 (Milford, MA) operated on a negative mode. The base solution was prepared by adding 1 g triethylamine into 1 L ultra-pure water. Then the sample solution was diluted with the base solution to 100 ppm. The source and desolvation temperature were 130 °C and 250 °C, respectively. The pump flow rate was 10 µL/min.

4.2.4 Catalyst characterisation

Temperature-programmed desorption (TPD) of adsorbed CO or CO₂ on catalysts was carried out using a Micromeritics AutoChem II 2920 Chemisorption Analyzer (Norcross, GA). Each experiment was initiated by pre-treating the catalyst sample in pure O₂ flowing at 100 cm³/min for 2 h at 873 K. The sample was then flushed in helium and cooled to the desired adsorption temperatures, 523 K and 273 K for CO and CO₂, respectively. CO was adsorbed on the catalysts by flowing a 4% CO in helium stream for a total time of 20 min, while CO₂ was adsorbed on the catalysts by flowing a 10% CO₂ blended in helium stream for a total time of 40 min. The sample was then cooled to room temperature and flushed with helium for 30 min. Temperature-programmed desorption was carried out in flowing He (100 cm³/min) with a heating rate of 25 K/min and 10 K/min for CO and CO₂, respectively, from 300K to 700K.

The infrared (IR) spectroscopy by the Attenuated Total Reflectance (ATR) was used to characterize surface functional groups on the ZrO₂ catalyst before and after the xylose conversion reactions. The ATR-FTIR spectroscopy was recorded on the Thermo Scientific Nicolet 6700 FT-IR (Waltham, Massachusetts) with 16 scans. The background spectrum was recorded first to remove the air effect before the sample test.

4.3 Results and discussion

4.3.1 Conversion of xylose to lactic acid

Figure 4.1 compares the yields of major products by reacting xylose at different reaction temperatures while other operating conditions were kept identical. The inset in Figure 4.1 shows the solid residue yields (SR) and the total organic carbon (TOC) yields

in aqueous phase. The pronounced effect of temperature on converting xylose to lactic acid was obvious: the lactic acid yield consistently increased with the increase of temperature. However, the lactic acid yields varied little at temperatures above 200 °C, although the maximum lactic acid yield was achieved at 240 °C. In contrast, as shown in [Figure 4.2](#), the lactic acid yields decreased as the oxygen partial pressure increased and the maximum yield of lactic acid was obtained with 0% O₂. Lactic acid can be further degraded to formic acid, acetic acid, or CO₂ by oxidation. As seen in [Figure 4.2](#), the yield of formic acid significantly increased as the O₂ partial pressure increased from 0% to 100%. With increasing O₂ partial pressure from 0% to 20%, the yield of furfural decreased rapidly. When the O₂ partial pressure was larger than 20%, furfural was almost completely decomposed. In contrast, there were negligible changes in lactic acid yields in the operation range of the O₂ partial pressures from 0% to 10%. The catalyst loading effect on xylose conversion was shown in [Figure 4.3](#). Without adding the ZrO₂ catalyst, the main product was furfural through the dehydration of xylose in high-temperature water. The lactic acid yield rapidly increased to 18% when adding 0.5 g ZrO₂ (i.e., at the catalyst to xylose ratio of 0.5). The highest lactic acid yield of 25.5% was achieved when the ratio of ZrO₂ to xylose was 2:1. However, the lactic acid yield varied little as the catalyst loading was above 1 g. Other carboxylic acids such as glycolic acid and formic acid followed the same trend as lactic acid. In contrast, the furfural yield consistently decreased with increasing the ZrO₂ loading amount. To confirm the identification of the major aqueous-phase compounds, electron spray ionization mass spectrometry (ESI-MS), nuclear magnetic resonance (NMR), and gas chromatography coupled with mass spectrometry (GC/MS) were used. [Figure 4.4](#) displayed an ESI-MS total ion

chromatogram in the regions of m/z 30-160 and the signals of lactic acid, glycolic acid, formic acid, and acetic acid were observed. As shown in Figure 4.5, the ^{13}C NMR spectra of lactic acid in the reaction products matched well with the standards. The GC/MS spectra also confirm the major aqueous phase products, as shown in Figure 4.6. Overall, a relatively high yield of lactic acid from xylose can be achieved under mild reaction conditions when using a ZrO_2 as the heterogeneous catalyst.

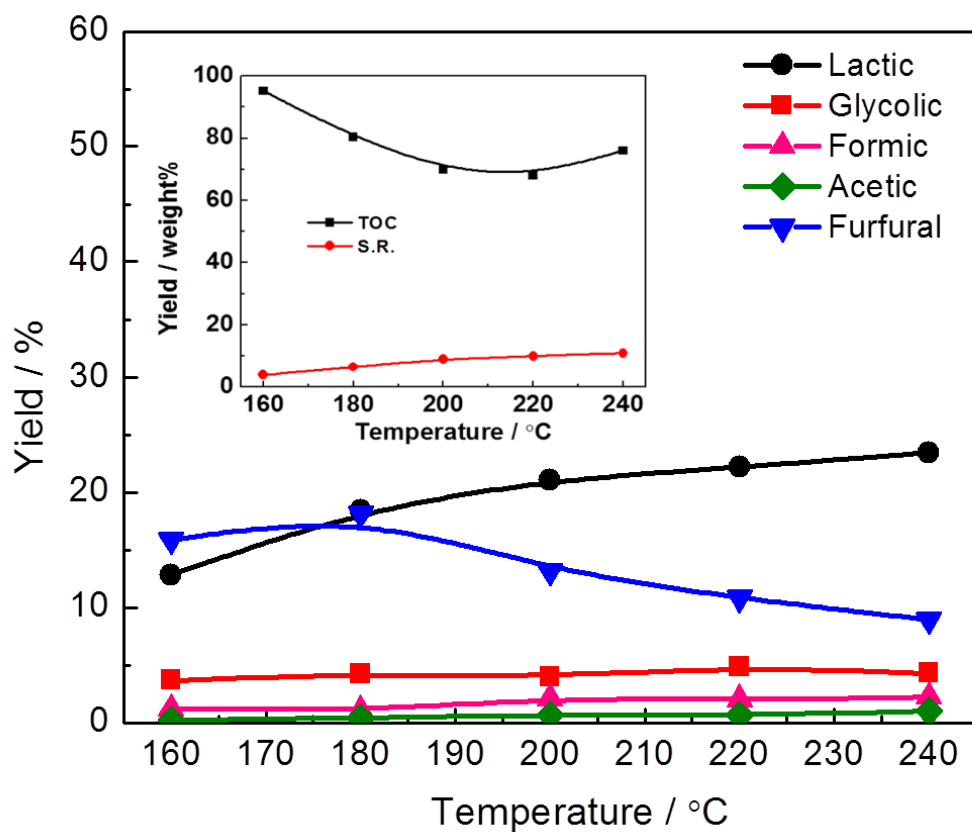


Figure 4.1 Temperature effect on the carbon yields aqueous-phase products of xylose conversion with the ZrO_2 catalyst in pH neutral aqueous solution. The inset figure shows the temperature effect on the solid residue yields and the TOC yields in the same reaction. Reaction conditions: 40 min, 2.4 MPa N_2 , 0% O_2 , 5 wt% xylose loading, and 0.8:1 mass ratio of catalyst to xylose.

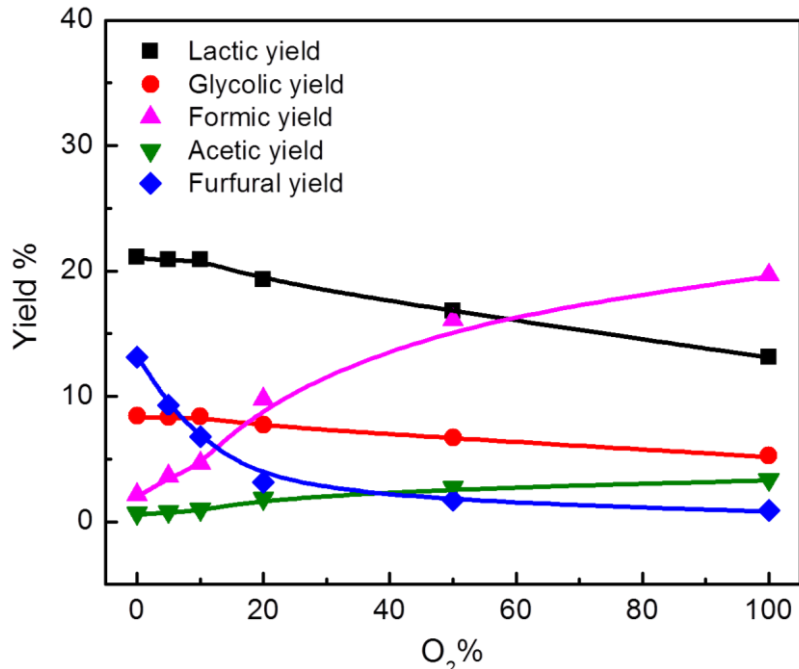


Figure 4.2 Effect of O_2 partial pressure on the yields of the aqueous-phase products by the conversion of xylose with the ZrO_2 catalyst in pH neutral aqueous solutions. Reaction conditions: 200 °C, 40 min, 2.4 MPa N_2+O_2 , 5 wt% xylose loading, and 0.8:1 mass ratio of catalyst to xylose.

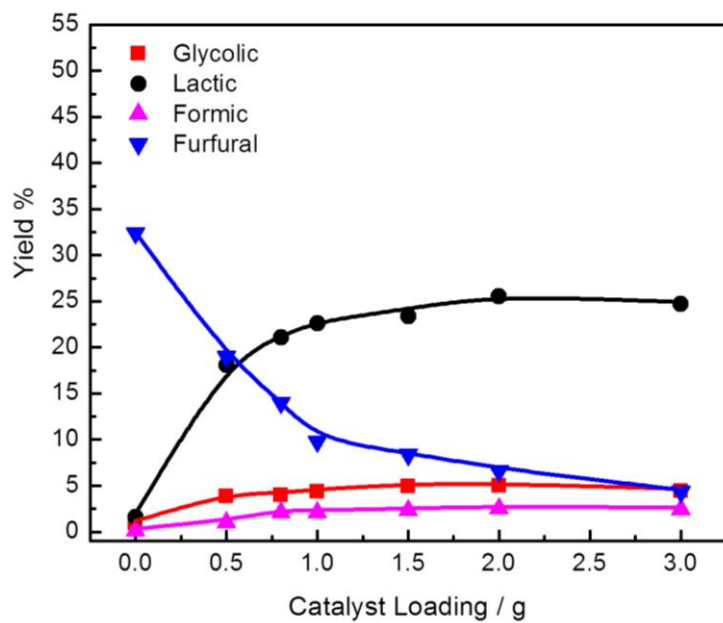


Figure 4.3 Effect of catalyst loading on the yields of the aqueous-phase products by the conversion of xylose with the ZrO_2 catalyst in pH neutral aqueous solutions. Reaction conditions: 200 °C, 40 min, 2.4 MPa N_2 , 0% O_2 , 5 wt% xylose loading, and 0.8:1 mass ratio of catalyst to xylose.

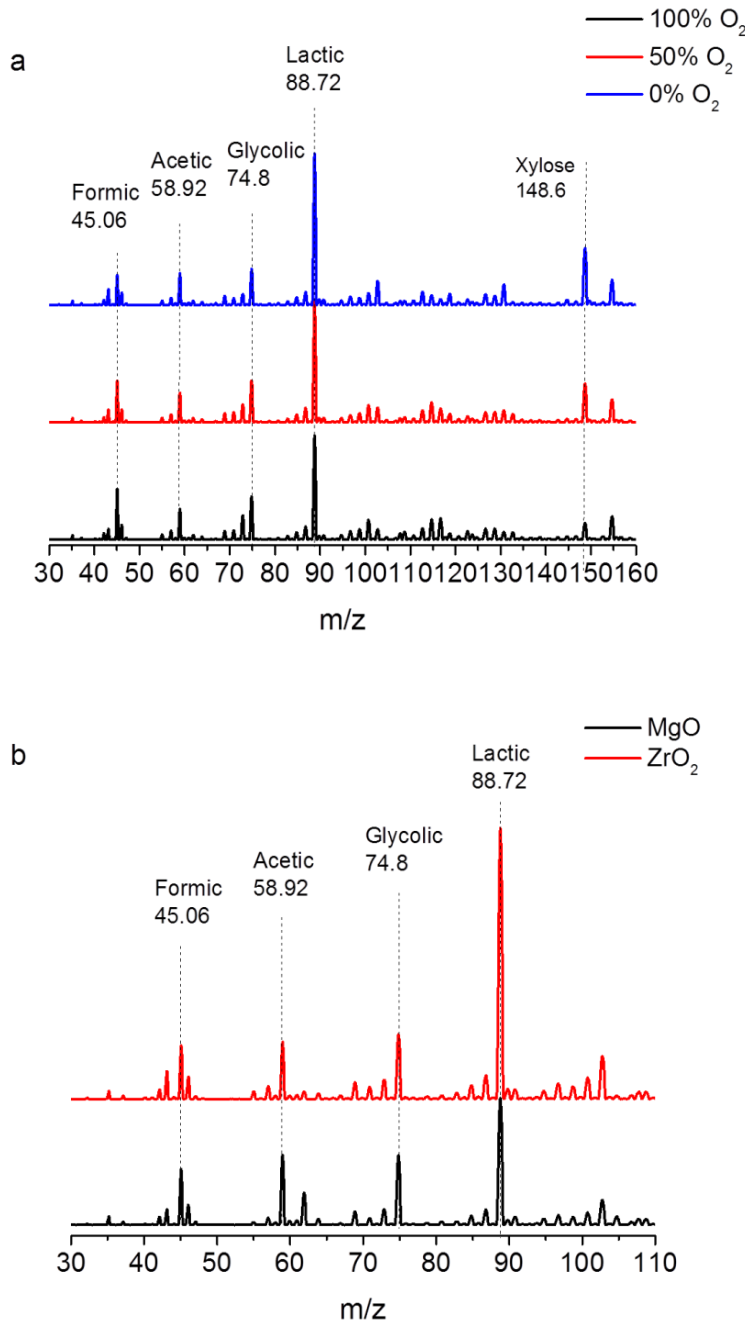


Figure 4.4 ESI-MS spectra of aqueous-phase products using xylose as the biomass feedstock. (a) Effect of O_2 partial pressure. Reaction condition: 200 °C, 40 minutes, 0.8 g ZrO_2 , 5 wt% xylose loading, 0.8:1 mass ratio of catalyst to xylose, and 2.4 MPa N_2 . (b) Comparison of ZrO_2 and MgO catalyst. Reaction condition: 200 °C, 40 min, 0.8 g catalyst, 5 wt% xylose loading, 0.8:1 mass ratio of catalyst to xylose, and 2.4 MPa N_2 .

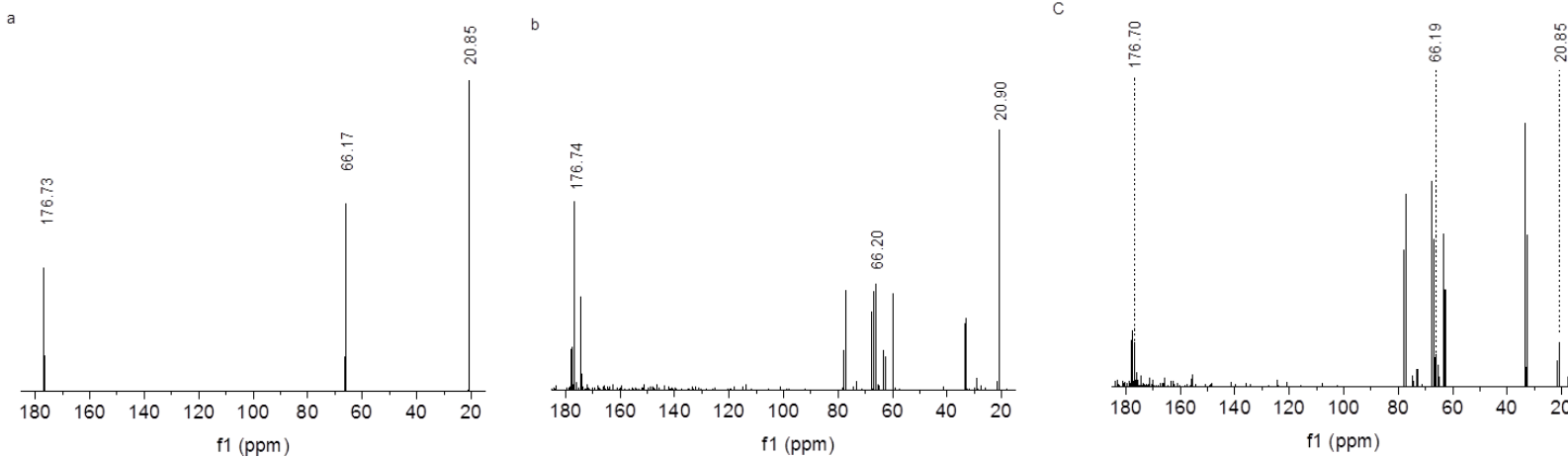


Figure 4.5 Comparison of ¹³C NMR spectra: (a) Pure lactic acid; (b) Aqueous-phase products with xylose as the feedstock. Reaction conditions: 200 °C, 40 min, 5 %O₂, 0.8 g ZrO₂, 1 g xylose, 20 g water, and 2.4 MPa N₂+O₂; (c) Aqueous-phase products with xylose as the feedstock. Reaction conditions: 200 °C, 40 min, 0 %O₂, and 0.8 g ZrO₂, 1 g xylose, 20 g water, and 2.4 MPa N₂.

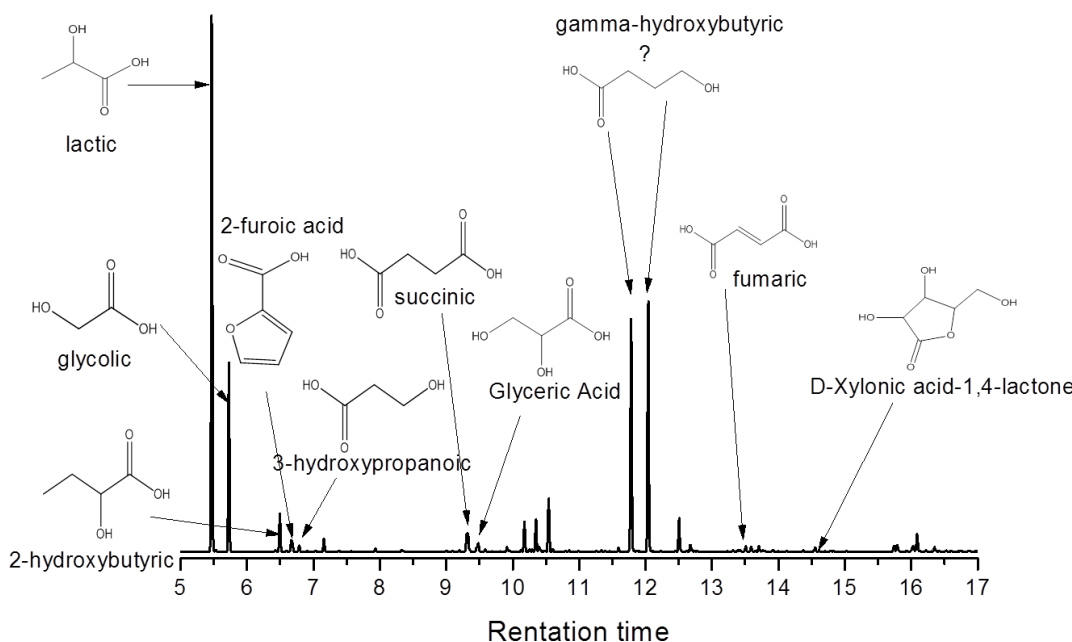


Figure 4.6 GC/MS spectra of aqueous-phase products with xylose as the feedstock. Reaction conditions: 200 °C, 40 min, 2.4 MPa N₂, 0% O₂, 0.8 g ZrO₂, 1 g xylose, 20 g water.

To further investigate the catalytic effect of ZrO₂, a mono-functional solid base catalyst, MgO, was chosen to compare with ZrO₂. Different pH values were deliberately adjusted at the beginning of the reaction. The yields of major aqueous-phase products were compared with and without the catalysts, as shown in Table 4.1. 32.4% of furfural but no lactic acid was formed (in the neutral aqueous solution) without the addition of acid or base catalyst (Table 4.1 Entry 13). With dilute sulfuric acid as catalyst (pH 3), 48.3% furfural was obtained (Table 4.1 Entry 12), while 44% lactic acid was formed using 1 mol/L sodium hydroxide (pH 14) as the catalyst (Table 4.1 Entry 15), which were comparable with the literature reported data [13]. Interestingly, ZrO₂ gave the higher yield of lactic acid than MgO in neutral or weakly acidic/basic aqueous solutions. An average lactic acid yield of 21.1 ± 2.5% was obtained with the ZrO₂ catalyst in the neutral aqueous solution (Table 4.1 Entry 3). In contrast, lactic acid with a lower yield, ~13.7%,

was produced over MgO ([Table 4.1 Entry 8](#)) under the same conditions. The lactic acid yields appeared to be insensitive to the pH in the range of 3 to 10, with either ZrO₂ or MgO as the catalyst. Unlike ZrO₂, the MgO catalyst yielded no furfural but a higher amount of low molecular-weight carboxylic acids including formic, acetic and glycolic acids in the pH range of 0 to 14. The formation of acetic acid may stem from a hydrolytic β-cleavage by the nucleophilic attack of the base [\[14\]](#). Alkaline earth metal oxides such as MgO are strong solid base catalysts [\[15\]](#), resembling the homogeneous base catalyst in terms of a similar product distribution, while MgO yielded lower amounts of lactic acid and glycolic acid than NaOH. The performance of homogeneous catalysts, by virtue of lower mass transfer resistance and higher accessibility of catalytic active sites, was usually found to be superior to that of solid catalysts. However, the reaction pathway using the ZrO₂ catalyst was obviously different from that using a mono-functional base catalyst like MgO. Besides yielding noticeable furfural, the ZrO₂ catalyst even yielded a higher amount of lactic acid and lower amounts of acetic acid and formic acid. The yield of lactic acid followed an opposite trend compared to that of furfural with temperature and catalyst loading amount. To determine whether or not furfural is the key intermediate to produce lactic acid, we examined furfural as the reactant under the same conditions that xylose reacted. No lactic acid was produced with furfural as feedstock ([Table 4.2](#)), suggesting that a dehydration step is unnecessary for lactic acid production over the ZrO₂. It is widely accepted that Brønsted acids catalyze the dehydration of xylose to produce furfural [\[16\]](#), while bases catalyze retro-aldol condensation leading to the formation of lactic acid from glucose or xylose [\[17\]](#). Herein, ZrO₂ is the only mono-metal oxide with all four different properties: acidic, basic, oxidative and reductive [\[18\]](#).

The co-existence of furfural and lactic acid in the final products indicated that both the acidic and basic sites on ZrO₂ function during the xylose conversion reactions. However, it was unclear whether or not the acid and base functionalities on the same ZrO₂ catalyst would affect each other and thus cause either suppression or promotion of a specific reaction to produce lactic acid from xylose.

Table 4.1 Comparison of different catalysts and pH values towards the xylose conversion in aqueous solutions.

Entry	Catalyst	pH	S.R.	Carbon yields of aqueous-phase products ^b						
				Ox.	Gly.	Lac.	FA	2-HB	AA	Furfural
1	ZrO ₂	0	23%	0.04%	3.2%	0.0%	3.2%	0.2%	0.5%	10.7%
2	ZrO ₂	3	11%	0.01%	4.2%	21.6%	1.5%	0.3%	0.8%	13.3%
3 ^a	ZrO ₂	7	9%	0.16%	4.0%	21.1%	2.1%	0.4%	0.7%	13.2%
4	ZrO ₂	10	14%	0.00%	4.0%	21.2%	1.6%	0.3%	0.6%	11.4%
5	ZrO ₂	14	17%	0.35%	11.4%	44.2%	7.9%	0.0%	3.0%	0.0%
6	MgO	0	15%	0.27%	6.7%	15.9%	3.5%	0.2%	3.5%	0.0%
7	MgO	3	12%	0.24%	6.2%	13.3%	3.2%	0.1%	4.0%	0.0%
8	MgO	7	21%	0.19%	6.0%	13.7%	3.0%	0.1%	4.3%	0.0%
9	MgO	10	23%	0.21%	6.2%	14.3%	3.1%	0.1%	4.5%	0.0%
10	MgO	14	52%	0.14%	11.6%	44.3%	8.3%	0.0%	3.2%	0.0%
11	H ₂ SO ₄	0	40%	0.02%	1.4%	0.0%	3.1%	0.0%	0.5%	9.4%
12	H ₂ SO ₄	3	13%	0.00%	0.5%	0.0%	0.0%	0.0%	0.3%	48.3%
13	No catalyst	7	15%	0.04%	0.9%	1.6%	0.1%	0.0%	0.2%	32.4%
14	NaOH	10	13%	0.00%	0.9%	1.2%	0.0%	0.0%	0.2%	33.2%
15	NaOH	14	37%	0.27%	11.5%	44.3%	7.7%	0.0%	3.2%	0.0%

^aData reported are the mean values of three replicates with $\pm 2.5\%$ error.

^bReaction conditions: 200 °C, 40 min, 2.4 MPa N₂, 0% O₂, 5 wt% xylose loading, and 0.8:1 mass ratio of catalyst to xylose. Abbreviation: Ox: Oxalic acid; Gly: Glycolic acid; Lac: Lactic acid; FA: Formic acid; 2-HB: 2-Hydroxybutyric acid; AA: Acetic acid.

Table 4.2 The yields of main products using furfural as the feedstock with and without the ZrO₂ catalyst at different temperatures.

Entry	Catalyst	Conversion	Temperature/°C	Identified Carbon Distribution ^a			
				lactic	Succinic	Formic	Acrylic
1	/	56%	190	0.0%	0.1%	2.2%	0.04%
2	ZrO ₂	40%	180	0.0%	0.3%	0.0%	0.04%
3	ZrO ₂	45%	190	0.0%	0.4%	0.3%	0.04%
4	ZrO ₂	50%	200	0.0%	0.4%	1.1%	0.04%
5	ZrO ₂	56%	210	0.0%	0.5%	2.4%	0.04%
6	ZrO ₂	61%	220	0.0%	0.5%	2.2%	0.04%

^aReaction conditions: 2.4 MPa N₂+O₂, 5% O₂, 60 min, 0.75g furfural, 0.5 g catalyst.

We speculate that the reaction pathway of converting xylose to lactic acid over the ZrO_2 catalyst starts from the retro-aldol condensation to form glycolaldehyde and glyceraldehyde. In the pH neutral hydrothermal media, we did not observe a high-yield production of lactic acid (only 1.6%) without adding the ZrO_2 catalyst, while the yield of furfural (21.1%) is instead significantly higher ([Table 4.1 Entry 13](#)). Thus, we conclude that the catalytic effects of the free hydroxyl ions from the auto-dissociation of subcritical water are negligible towards the formation of lactic acid from xylose. We tentatively ascribe the bi-functional Lewis acid/base pair on the ZrO_2 surface to catalyzing the retro-aldol condensation of xylose. As shown in [Figure 4.7](#), we propose that Zr^{4+} ions as the Lewis acid sites interact with the carbonyl group of xylose, increase the positive charge on carbonyl carbon, and facilitate the nucleophilic attack [\[19–21\]](#). At the same time, the Lewis acid sites increase the acidity of the active OH group at the position of C-3 carbon, and promote the deprotonation by the weak base (i.e. the O^{2-} cations on the ZrO_2 surface). Thereafter, the C-C bond between C-2 and C-3 carbons of xylose was cleaved leading to the formation of glyceraldehyde and glycolaldehyde. Glyceraldehyde may undergo the dehydration to form 2-hydroxypropenal, then to pyruvaldehyde through keto-enol tautomerization, and finally to lactic acid, as shown in [Figure 4.8](#). In the presence of a strong base catalyst like concentrated NaOH , α -keto aldehydes can be converted to hydroxy acids in excellent yields via an intramolecular disproportionation, i.e., Cannizzaro reaction [\[22\]](#). However, Lewis acids are also considered to be capable of catalyzing the intramolecular Cannizzaro reaction by activating the carbonyl function group of the aldehyde, allowing the nucleophilic attack by an electron donor and then an intramolecular rearrangement with a shift of the hydride [\[23,24\]](#). Hara *et al.* found that

water-tolerant Lewis acids such as $\text{Sc}(\text{OTf})_3$ and $\text{Nb}_2\text{O}_5 \text{nH}_2\text{O}$ can effectively catalyze the hydride transfer of pyruvaldehyde in water by Meerwein–Ponndorf–Verley (MPV) reduction under mild reaction conditions [25]. We thus propose that the transformation of pyruvaldehyde to lactic acid is via the intramolecular Cannizzaro reaction catalyzed by Lewis acid sites on ZrO_2 instead of a strong base, as shown in Figure 4.9. Free OH^- and H_3O^+ ions from the auto-dissociation of water are prevailing in subcritical water [26,27]. It is also reported that water can be dissociated on ZrO_2 [28,29]. We thus speculate that the cycle of intramolecular Cannizzaro reaction was closed with the aid of free or surface bound hydroxyl and hydronium ions.

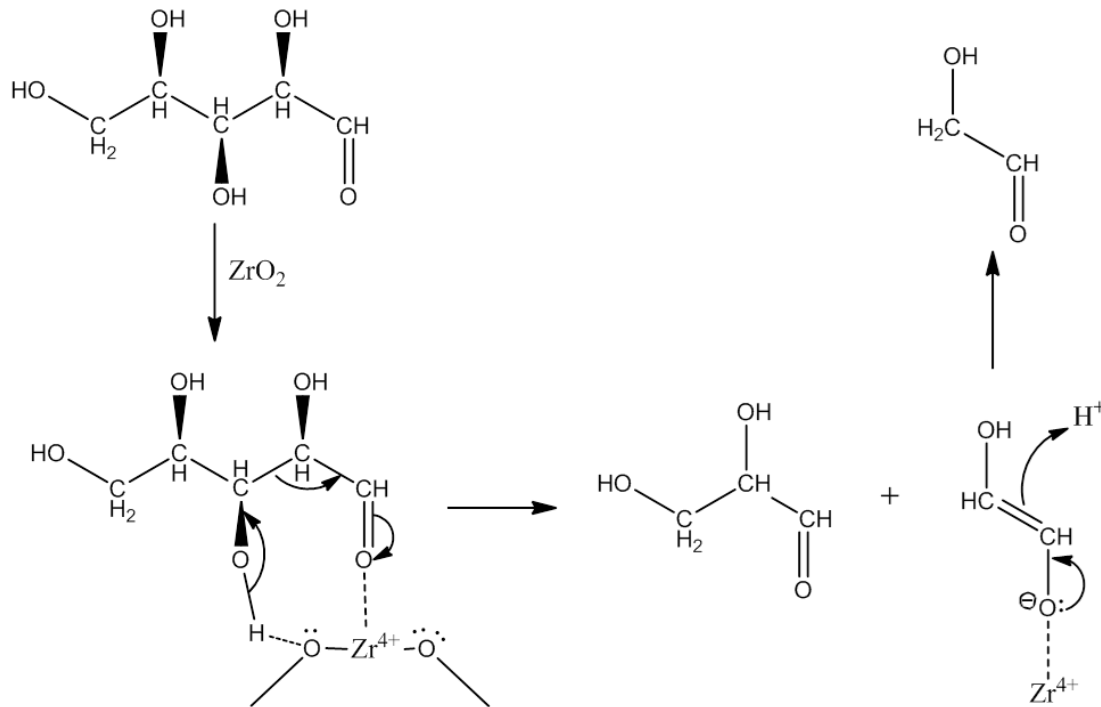


Figure 4.7 Proposed reaction mechanism of xylose retro-aldol condensation with the ZrO_2 catalyst. Xylose is converted to glyceraldehyde and glycolaldehyde via the C-C bond cleavage.

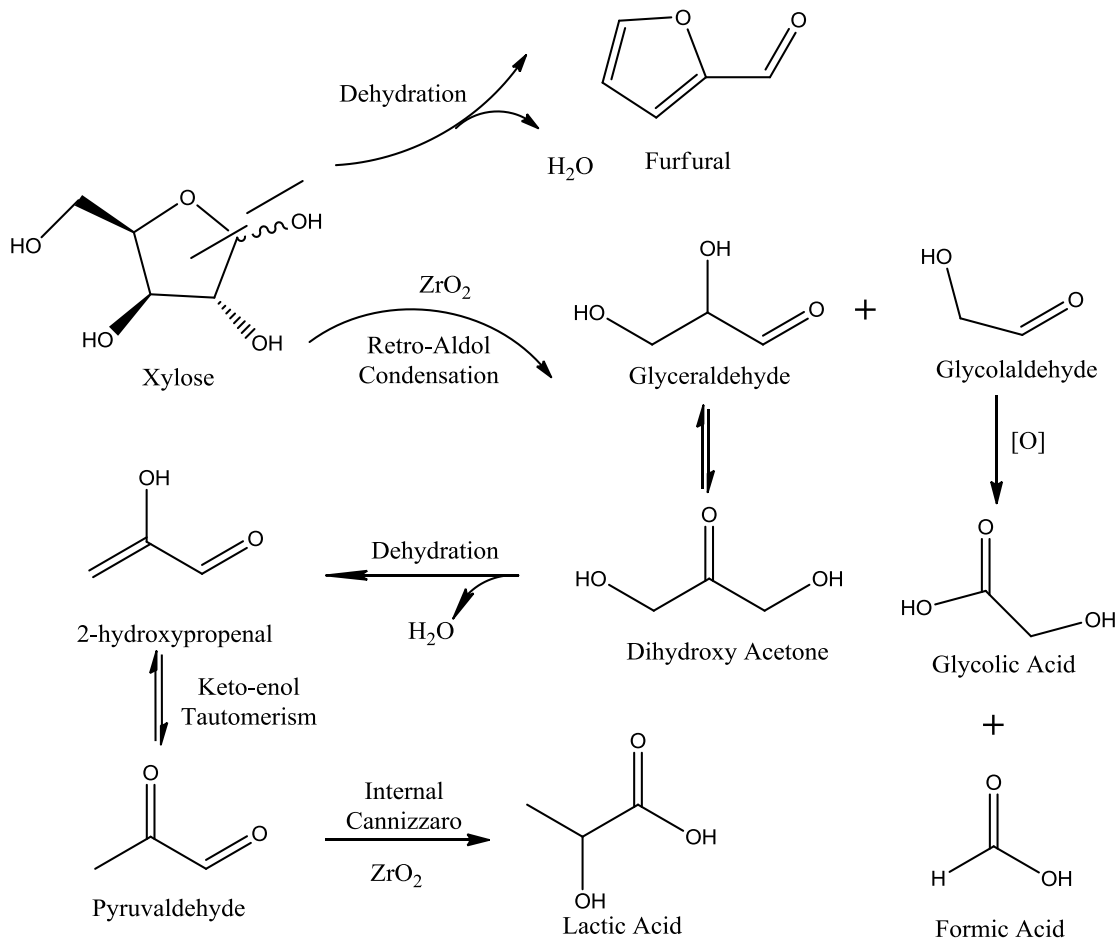


Figure 4.8 Proposed reaction mechanism for conversion of xylose to lactic acid and other intermediate and final products in subcritical water with the bi-functional ZrO_2 catalyst.

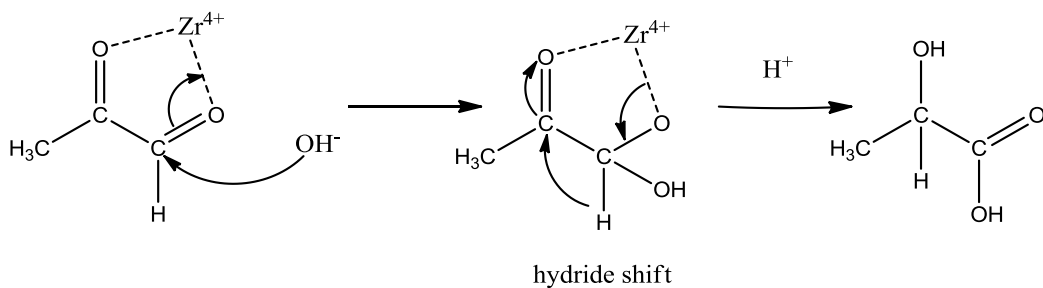


Figure 4.9 Proposed reaction mechanism of converting pyruvaldehyde to lactic acid via intramolecular Cannizzaro with the ZrO_2 catalyst. Lewis acids (Zr^{4+}) activates the carbonyl function groups of the pyruvaldehyde, following the nucleophilic attack by the electron donor (OH^-), then the intramolecular rearrangement with a shift of the hydride, and lastly the protonation to form the hydroxyl group at the C2 position.

To validate our hypothesis, the possible key intermediates from xylose (e.g. glyceraldehyde and pyruvaldehyde) were used as the probe reactants. The results shows that these possible key intermediates were readily converted to lactic acid in much higher yields: 50.5% ([Table 4.3 Entry 3](#)) and 93.3% ([Table 4.3 Entry 7](#)) from glyceraldehyde and pyruvaldehyde, respectively, than a lower yield of 40.1% ([Table 4.3 Entry 1](#)) from xylose. Yet in the absence of ZrO_2 , much lower amounts of lactic acid were produced with glyceraldehyde or pyruvaldehyde as the feedstock. In addition, using glycolaldehyde as the probe, a far less than the stoichiometric amount of glycolic acid was produced, while a large amount of formic acid was formed. Glycolaldehyde can be converted to glycolic acid, similar to the conversion of acetaldehyde to acetic acid. However, glycolic acid may be further converted into methanol and CO_2 through cleavage of the C–C bond. As shown in [Figure 4.10](#), the GC/MS spectra of the aqueous products from reacting glycolaldehyde in the presence of the ZrO_2 identified a considerable amount of higher molecular-weight compounds such as C4 hydroxyl acids, C6 aldoses, as well as C7 methyl esters. Without adding ZrO_2 , glycolic acid is the dominant product. The formation of higher molecular weight compounds from glycolaldehyde may be through aldol-condensation reactions, which likely competed against the formation of glycolic acid on the ZrO_2 surface.

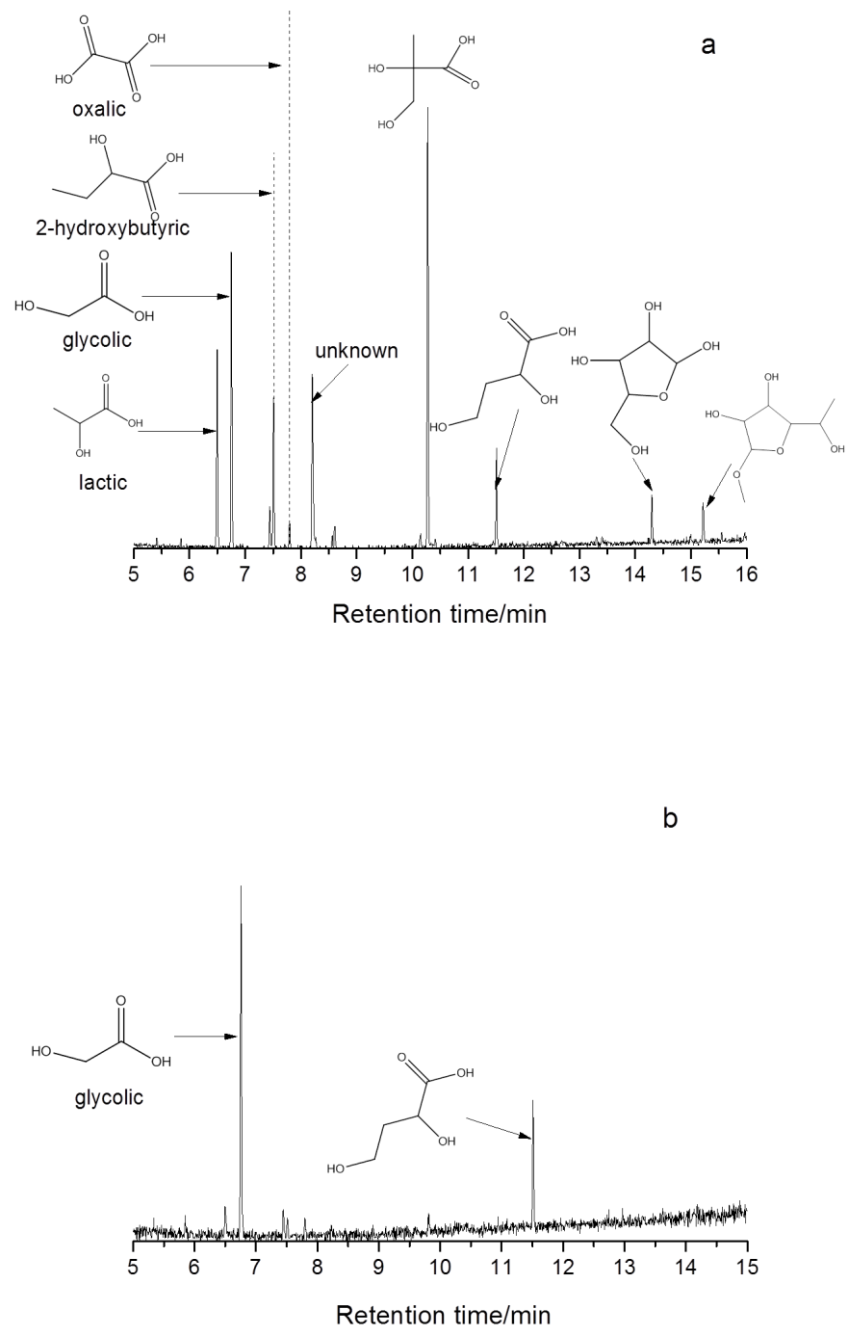


Figure 4.10 GC/MS spectra of aqueous-phase products with glycolaldehyde dimer as the feedstock. Reaction conditions: (a) 200 °C, 40 min, 0.4 g ZrO₂, 0.5 g glycolaldehyde dimer, 20 g water, and 2.4 MPa N₂; (b) 200 °C, 40 min, 0.5 g glycolaldehyde dimer, 0 g ZrO₂, 20 g water, and 2.4 MPa N₂.

Table 4.3 Comparison of different biomass derived molecules as the probe reactants which are also possible key intermediates during the catalytic conversion of xylose to lactic acid with the ZrO₂ catalyst.

Entry	Probe	Catalyst	S.R.	Conv.	Carbon yields of aqueous-phase products ^b							
					Ox.	Gly.	Lac.	FA	AA	Acrylic	Furfural	HMF
1 ^a	Xylose	ZrO ₂	3%	100%	0.02%	4.5%	24.1%	2.3%	0.3%	0.1%	15.1%	0.0%
2	Xylose	/	13%	78%	0.01%	0.0%	0.0%	0.0%	0.6%	0.07%	42.0%	0.0%
3	D-Glyceraldehyde	ZrO ₂	2%	100%	0.00%	0.0%	50.5%	1.63%	3.5%	0.01%	0.0%	0.4%
4	D-Glyceraldehyde	/	21%	100%	0.01%	0.0%	5.9%	2.10%	6.6%	0.00%	0.0%	0.03%
5	Dihydroxy acetone	ZrO ₂	8%	100%	0.2%	0.0%	48.7%	0.33%	1.5%	2.6%	0.0%	0.9%
6	Dihydroxy acetone	/	30%	100%	0.01%	0.0%	12.5%	0.93%	4.1%	0.00%	0.0%	1.4%
7	Pyruvaldehyde	ZrO ₂	4%	100%	0.00%	0.0%	93.3%	0.43%	5.0%	0.05%	0.0%	0.08%
8	Pyruvaldehyde	/	23%	100%	0.01%	0.0%	7.4%	1.57%	5.5%	0.03%	0.0%	0.3%
9	Glycolaldehyde dimer	ZrO ₂	5%	100%	0.01%	4.2%	0.0%	9.5%	0.0%	0.00%	0.0%	1.2%
10	Glycolaldehyde dimer	/	19%	100%	0.00%	6.0%	0.0%	4.0%	0.0%	0.00%	0.0%	1.2%

^aData reported are the mean values of two replicates with $\pm 1.3\%$ error.

^bReaction conditions: 200 °C, 40 min, 2.4 MPa N₂, 0% O₂, 2.5 wt% probe reactant loading, and 0.8:1 mass ratio of catalyst to probe reactant. Abbreviation: Ox: Oxalic acid; Gly: Glycolic acid; Lac: Lactic acid; FA: Formic acid; AA: Acetic acid; HMF: 5-Hydroxy methylfurfural.

To confirm the Lewis acid functionality of the ZrO₂ catalyst, the temperature-program desorption (TPD) profiles were conducted by using CO as the adsorbate molecule. The comparison of the CO TPD spectra of ZrO₂ and MgO at temperatures from 300K to 700K are shown in Figure 4.11. A large CO desorption peak at 608 K was observed on ZrO₂, while no peaks were found on MgO, indicating that the existence of much stronger Lewis acid sites on ZrO₂, although we cannot rule out the existence of very weak Lewis acid sites on MgO. We have tentatively attributed the Lewis acid functionality of the ZrO₂ catalyst to the promotion of retro-aldol condensation of xylose and the intramolecular Cannizzaro reaction of pyruvaldehyde, leading to the formation of lactic acid. There is a wealth of information in the literature on NH₃ and CO₂ TPD

characterizing the Bronsted acidity and basicity of ZrO_2 surface [30–33]. The adsorbed pyridine FTIR studies also confirmed the presence of basic sites on the surface of ZrO_2 [33,34]. In this work, the TPD of CO_2 was also carried out in the temperature range from 300 K to 800 K to compare the basicity of ZrO_2 and MgO (Figure 4.12). A large CO_2 desorption peak at 370 K and two other peaks at 530K and 590K were observed on MgO , while only one peak at 380K was found on ZrO_2 , indicating that the existence of much stronger basic sites on MgO . The results are in good agreement with the literature data. However, the sole base function cannot explain why the higher yields of lactic acid were obtained over ZrO_2 than over MgO under our test reaction conditions because MgO has a stronger basicity based on the CO_2 TPD results.

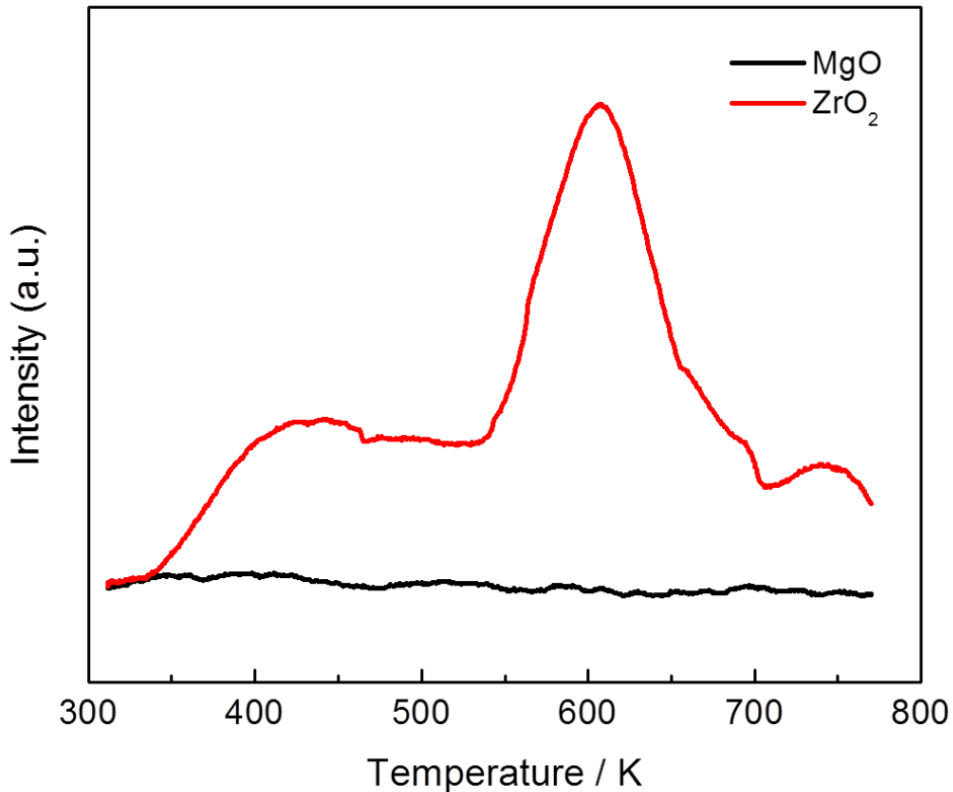


Figure 4.11 Temperature-programmed desorption profile of CO on ZrO_2 and MgO .

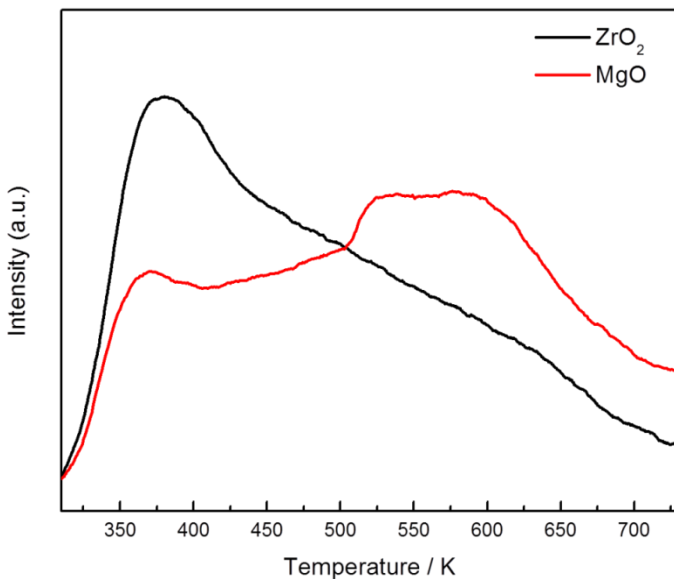


Figure 4.12 Temperature-programmed desorption profile of CO_2 on ZrO_2 and MgO .

Recyclability and reusability are of importance for heterogeneous catalysts. We thus performed a stability study on the ZrO_2 catalyst. The same catalyst without regeneration was recycled and reused for the subsequent runs under the identical reaction conditions. The yields of lactic acid and furfural from xylose using the recycled ZrO_2 catalyst are shown in Figure 4.13. Over the five consecutive runs, a slight decline in lactic acid yield, from 20.9% to 17.7%, was found with the re-used ZrO_2 catalyst. This suggests that the catalyst is relatively stable, although a regeneration process that removes the organic solid residues would be desirable for the re-use of the ZrO_2 catalyst. Interestingly, the furfural yield increased with increasing catalyst re-use cycles. It is well known that furfural can be produced through Bronsted acid catalyzed dehydration of xylose. Weak Bronsted acid sites were found on a ZrO_2 surface based on the infrared spectra of adsorbed pyridine [35]. Herein, the deposition of the xylose-derived solid residues on the spent ZrO_2 catalysts may change the surface properties and introduce a higher amount or

stronger Bronsted acid sites than the fresh ZrO_2 , thus promoting the dehydration reaction. As shown in the ATR-FTIR spectra (Figure 4.14), the spent ZrO_2 catalyst obviously shows the signal of adsorbed species: 1) the broad peak at around 3400 cm^{-1} is attributed to the stretching of the OH band; 2) the peaks at around 2980 to 2840 cm^{-1} are the stretching vibration signal of the CH band in $-\text{CH}_2-$ or $-\text{CH}_3$ groups; 3) the twin peaks located at 1750 and 1710 cm^{-1} are probably the C=O band stretching vibrations in acid anhydride molecules [36]; 4) the band at around 1380 cm^{-1} belongs to the CH_3 deformation vibrations [37,38]; and 5) the bands at 1190 and 1120 cm^{-1} may be attributed to the C-O-C band in the acid anhydride molecule [36]. Therefore, the enhanced Bronsted acidity, attributing to the increase of the furfural yields and the decrease of the lactic acid yields, may originate from the carboxylic acid anhydride groups on the surface of the spent ZrO_2 catalysts.

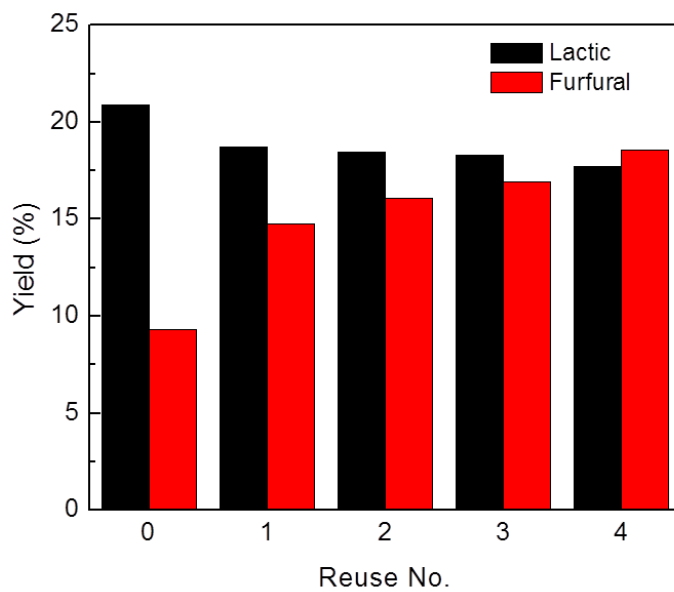


Figure 4.13 Effect of re-use of the ZrO_2 catalyst on the yields of lactic acid and furfural by the conversion of xylose in pH neutral aqueous solutions. The spent catalyst was not regenerated. Reaction conditions: $200\text{ }^\circ\text{C}$, 40 min , $2.4\text{ MPa N}_2+\text{O}_2$ pressure, $5\% \text{ O}_2$, $5\text{ wt}\%$ xylose loading, and $0.8:1$ mass ratio of catalyst to xylose.

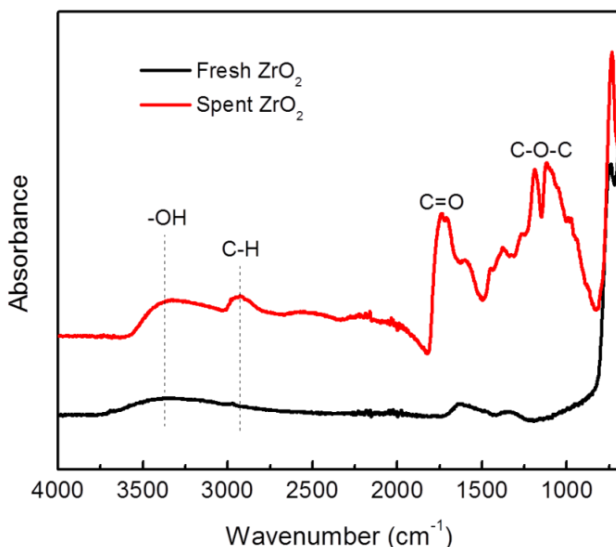


Figure 4.14 Comparison of the ATR-FTIR spectra of the fresh and spent ZrO_2 catalysts. The spent catalyst was used once and was not regenerated. Reaction conditions: 200 °C, 40 min, 2.4 MPa N_2 , 5 wt% xylose loading, and 0.8:1 mass ratio of catalyst to xylose.

4.3.2 Direct conversion of xylan to lactic acid

The conversion of xylan into lactic acid was significantly more challenging than was the transformation of water-soluble xylose due to the depolymerization of xylan requiring an intense treatment. Acid hydrolysis is widely used to depolymerize xylan and produce xylose. To further convert xylose to lactic acid, a base catalyst is commonly used. Therefore, direct conversion of xylan to lactic acid would not be realized if using a homogeneous catalyst system as acids and bases neutralize each other in aqueous solutions. However, a heterogeneous catalyst system with both the acidic and basic sites on different surface domains would catalyze the conversion of xylan to lactic acid in a one-pot process. To illuminate the effects of acid/base dual functionalities of the ZrO_2 , Beech wood xylan was selected as the model hemicellulosic biomass feedstock for further studies. A Box-Behnken design was used to investigate the influence of process conditions including temperature, reaction time, O_2 partial pressure, and catalyst loading

amount, as well as their interactions. [Table 4.4](#) displays the Box-Behnken experimental results for the yields of the aqueous products, as well as the TOC with xylan as the feedstock under various reaction conditions. And the data analysis revealed that temperature and catalyst loading amount had the greatest effects on xylan conversion. Practically, less lactic acid was formed when the catalyst amount was low even at high temperatures. Contrarily, at the high ratio of ZrO₂ to xylan, a significant amount of lactic acid was formed even at the low reaction temperature of 180 °C. Reaction time also appeared to be a variable that affects the lactic acid yield, and the longer reaction times, the higher yields. At 190 °C, the highest lactic acid yield of 18% was obtained with the ratio of 3 g ZrO₂ to 1 g xylan and under 10% O₂ partial pressure among all experimental runs. By quickly identifying the most sensitive reaction parameters on lactic acid yield, a detailed temperature and catalyst loading profiling study was performed. [Figure 4.15](#) shows that below 180 °C, lactic acid yield was negligible while a lactic acid yield of ~10.4% was obtained at 220 °C. [Figure 4.16](#) illustrates the considerable effect of the catalyst loading on the yield of lactic acid from xylan. Without a ZrO₂ catalyst, almost no lactic acid was formed while, under the identical conditions, ~16% lactic acid was produced from xylan with adding the ZrO₂ catalyst at to 4:1 ZrO₂ to xylan ratio.

The conversion of xylan is complicated, involving many competing and reversible reactions [\[39\]](#). Xylan contains as much as 0.659 acetyl groups per xylose unit and thus may be the source of acetic acid in this process. According to Garrote's study [\[40\]](#), the hydrolysis of xylan in hydrothermal media was greatly affected by the acetyl groups in xylan. Ignatchenko and coworkers [\[41,42\]](#) confirmed by DFT computation that the acetyl group can be easily adsorbed on monoclinic zirconia (-111) and (111) surfaces, which

may block the access of other reactant molecules. We tentatively relate the presence of acetyl groups in xylan to the lower lactic acid yields with xylan as the feedstock compared to those using xylose as the feed. A doping study was performed to verify the acetyl group effect on xylan. Acetic acid and ethyl acetate, as probes, were deliberately added into the xylose conversion reaction system, respectively. Table 4.5 shows that the yields of lactic acid from xylose slightly decreased from ~21.1% to ~20.2% or ~18.1% with adding ethyl acetate or acetic acid, respectively, implying that the acetyl group may only slightly affect the catalyst activity. On the other hand, under the same reaction condition, the yield of lactic acid from xylan was only ~9%. Therefore, the extent of depolymerization of xylan and the corresponding mass transfer limitations cannot be excluded that lead to a much lower lactic acid yield from xylan than that from xylose if other reaction conditions are kept identical.

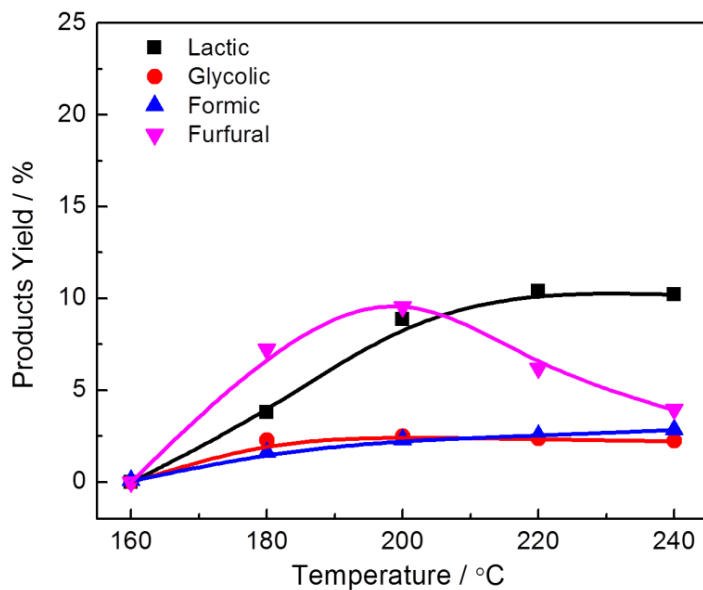


Figure 4.15 Effect of temperature on the yields of aqueous-phase products from the xylan conversion with the ZrO_2 catalyst in pH neutral aqueous solution. Reaction conditions: 60 min, 2.4 MPa N_2 , 5 wt% xylan loading, and 1:1 mass ratio of catalyst to xylan.

Table 4.4 Experimental results of the Box-Behnken design using xylan as the feedstock. All runs operated under an initial pressure of 2.4 MPa.

T/ °C	Reactio n time (min)	ZrO ₂ : xylose ratio	O ₂ mol %	TOC	S.R.	Identified Carbon Distribution ^a							
						Ox.	Gly.	Lac.	FA	2- HB	AA	Acrylic	Furfural
200	90	2	5%	61%	21%	0.00%	2.6%	14.3%	2.8%	0.0%	3.3%	0.2%	5.4%
180	90	2	5%	60%	17%	0.04%	3.0%	11.9%	1.9%	0.9%	0.4%	0.1%	13.3%
200	30	2	5%	50%	20%	0.00%	3.4%	12.3%	2.7%	0.8%	2.4%	0.2%	8.3%
180	30	2	5%	79%	20%	0.00%	0.8%	2.1%	0.9%	0.3%	0.2%	0.1%	1.5%
190	60	3	10%	49%	22%	0.04%	3.0%	18.0%	3.0%	0.9%	3.4%	0.2%	5.1%
190	60	1	10%	53%	20%	0.20%	3.5%	6.3%	3.6%	0.2%	1.6%	0.2%	12.3%
190	60	3	0%	53%	17%	0.00%	3.0%	15.2%	1.6%	1.6%	1.2%	0.1%	8.2%
190	60	1	0%	64%	15%	0.04%	2.6%	5.7%	1.5%	0.5%	1.0%	0.1%	14.2%
190	60	2	5%	53%	20%	0.04%	3.0%	14.0%	2.4%	0.8%	1.9%	0.1%	9.7%
200	60	2	10%	46%	17%	0.00%	2.3%	13.7%	4.2%	0.6%	6.5%	0.2%	5.6%
180	60	2	10%	72%	16%	0.04%	4.0%	10.8%	1.7%	0.6%	1.1%	0.1%	7.6%
200	60	2	0%	58%	26%	0.00%	2.9%	14.4%	2.0%	1.3%	1.5%	0.1%	8.0%
180	60	2	0%	71%	13%	0.12%	2.8%	9.9%	1.3%	0.9%	0.0%	0.1%	9.2%
190	90	3	5%	46%	21%	0.00%	2.9%	17.7%	2.5%	1.2%	2.5%	0.1%	5.5%
190	30	3	5%	65%	14%	0.04%	3.9%	17.0%	2.0%	1.1%	1.9%	0.1%	6.8%
190	90	1	5%	51%	16%	0.04%	3.1%	6.7%	3.4%	0.3%	1.6%	0.2%	11.1%
190	30	1	5%	79%	23%	0.04%	1.7%	3.0%	1.2%	0.2%	0.3%	0.1%	7.0%
190	60	2	5%	56%	18%	0.04%	2.9%	14.6%	2.5%	0.8%	2.0%	0.2%	10.0%
200	60	3	5%	56%	19%	0.00%	2.4%	14.9%	2.3%	1.0%	2.2%	0.1%	5.4%
180	60	3	5%	66%	12%	0.00%	2.3%	12.6%	2.2%	1.0%	2.1%	0.1%	8.6%
200	60	1	5%	58%	24%	0.00%	3.4%	8.4%	3.4%	0.3%	2.2%	0.2%	7.9%
180	60	1	5%	81%	15%	0.04%	2.3%	3.8%	13.8%	0.2%	1.2%	0.2%	7.2%
190	90	2	10%	62%	12%	0.00%	2.8%	13.4%	18.5%	0.5%	3.6%	0.2%	7.3%
190	30	2	10%	68%	15%	0.04%	3.0%	10.7%	10.7%	0.4%	0.9%	0.1%	9.5%
190	90	2	0%	60%	18%	0.00%	3.3%	12.3%	9.4%	1.4%	1.2%	0.1%	10.6%
190	30	2	0%	73%	19%	0.00%	2.8%	8.9%	5.6%	1.0%	0.0%	0.1%	7.3%
190	60	2	5%	53%	19%	0.00%	3.1%	14.4%	12.1%	0.7%	1.9%	0.1%	8.7%

^aAbbreviation: Ox: Oxalic acid; Gly: Glycolic acid; Lac: Lactic acid; FA: Formic acid; 2-HB: 2-Hydroxybutyric acid; AA: Acetic acid; TOC: total organic carbon; S.R.: solid residue yield.

Table 4.5 Effect of acetyl group in the different probe additives, ethyl acetate or acetic acid, on the catalytic conversion of xylose with the ZrO_2 catalyst.

Entry	Probe	S.R.	Carbon yields of aqueous-phase products ^a				
			Glycolic	Lactic	Formic	Acrylic	Furfural
1	/	9%	4.0%	21.1%	2.1%	0.06%	13.2%
2	Ethyl acetate	16%	3.7%	20.2%	1.6%	0.06%	12.4%
3	Acetic acid	17%	4.4%	18.1%	2.5%	0.04%	12.6%

^aReaction conditions: 40 min, 2.4 MPa N_2 , 0% O_2 , 5 wt% xylose loading, 0.1 g probe additive, and 0.8:1 mass ratio of catalyst to xylose.

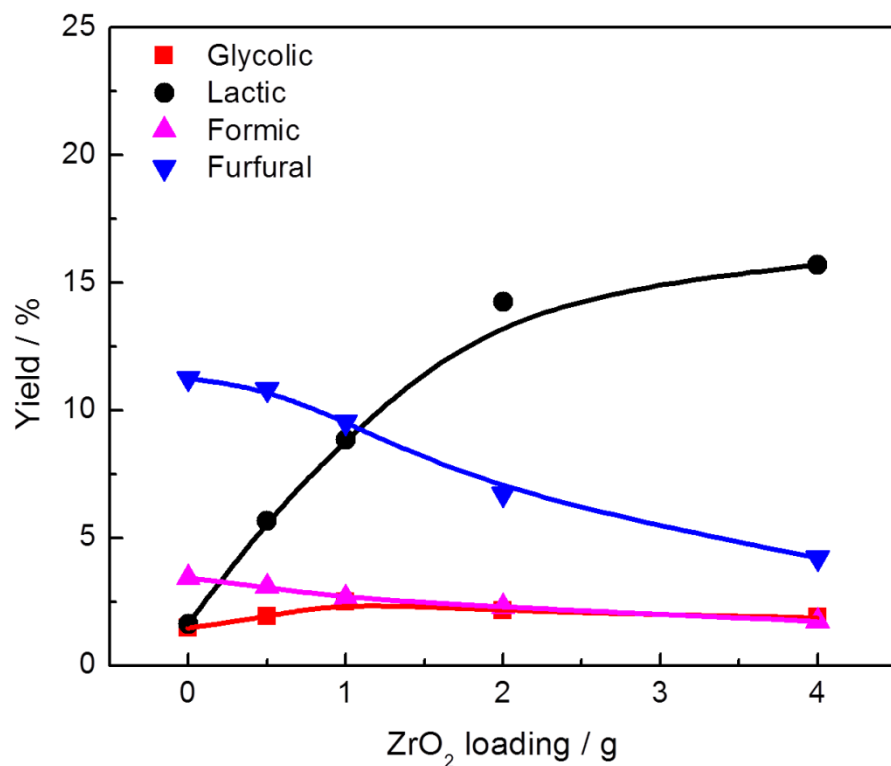


Figure 4.16 Effect of catalyst loading on the yields of aqueous-phase products from the xylan conversion with the ZrO_2 catalyst in pH neutral aqueous solution. Reaction conditions: 200 °C, 90min, 2.4 MPa N_2 , 5 wt% xylan loading.

4.4 Conclusions

In summary, we demonstrated that lactic acid was produced from xylose or xylan in the pH neutral aqueous solutions with the addition of a ZrO_2 catalyst under different reaction conditions. Under the tested conditions (e.g., 160-240 °C, 0 - 100% O_2 pressure,

and 0.5 - 4 catalyst to biomass weight ratio), the highest lactic acid yields were 25% and 18% from xylose and xylan, respectively, with the ZrO₂ catalyst, while the process without ZrO₂ only yielded negligible lactic acid production. Compared to the mono-functional base catalyst like MgO, the bi-functional ZrO₂ was superior for lactic acid synthesis from xylose. The acid/base pairs on the ZrO₂ surface likely facilitate the retro-aldol condensation of xylose, which is the initial step of the conversion of xylose to lactic acid. Through the probe reactant studies, we conclude that ZrO₂ also catalyzes the transformation of xylose-derived C3 aldehydes into lactic acid. The conversion of xylan is significantly more challenging than that of xylose and thus requires more severe process conditions such as higher temperatures, longer reaction times, and higher amounts of catalyst loading. The suppression of the catalytic activity of ZrO₂ by the acetyl groups in xylan was minimal, while the polymeric structure mainly contributed to the lower yield production of lactic acid from xylan than that from xylose. Overall, this aqueous catalytic process using the ZrO₂ catalyst appears to be a renewable and environmentally-friendly way to produce lactic acid from hemicellulosic biomass feedstocks.

4.5 References

1. (2011) "U.S. Departemnt of Energy, U.S. Billion-ton update: Biomass supply for a bioenergy and bioproducts industry" (August).
2. Mamman, A.S., Lee, J., Kim, Y., et al. (2008) Furfural: Hemicellulose/xylose- derived biochemical. *Biofuels, Bioprod. Biorefining* **2**, 438–454.
3. Dutta, S., De, S., Saha, B., and Alam, M.I. (2012) Advances in conversion of hemicellulosic biomass to furfural and upgrading to biofuels. *Catal. Sci. Technol.* **2** (10), 2025–2036.

4. Chen, Y., Dong, B., Qin, W., and Xiao, D. (2010) Xylose and cellulose fractionation from corncob with three different strategies and separate fermentation of them to bioethanol. *Bioresour. Technol.* **101** (18), 7005–7010.
5. Pordesimo, L.O., Hames, B.R., Sokhansanj, S., and Edens, W.C. (2005) Variation in corn stover composition and energy content with crop maturity. *Biomass and Bioenergy* **28** (4), 366–374.
6. Werpy, T., and Petersen, G. (2004) “U.S. Department of Energy, Top value added chemicals from biomass volume I - results of screening for potential candidates from sugars and synthesis gas.”
7. Hinman, N.D., Wright, J.D., Hogland, W., and Wyman, C.E. (1989) Xylose fermentation: An economic analysis. *Appl. Biochem. Biotechnol.* **20/21** (1), 391–401.
8. Chambon, F., Rataboul, F., Pinel, C., et al. (2011) Cellulose hydrothermal conversion promoted by heterogeneous Brønsted and Lewis acids: Remarkable efficiency of solid Lewis acids to produce lactic acid. *Appl. Catal. B Environ.* **105** (1-2), 171–181.
9. Holm, M.S., Saravanamurugan, S., and Taarning, E. (2010) Conversion of sugars to lactic acid derivatives using heterogeneous zeotype catalysts. *Science* **328** (5978), 602–605.
10. Onda, A., Ochi, T., Kajiyoshi, K., and Yanagisawa, K. (2008) Lactic acid production from glucose over activated hydrotalcites as solid base catalysts in water. *Catal. Commun.* **9** (6), 1050–1053.
11. Liu, Z., Li, W., Pan, C., et al. (2011) Conversion of biomass-derived carbohydrates to methyl lactate using solid base catalysts. *Catal. Commun.* **15** (1), 82–87.
12. Onda, A., Ochi, T., Kajiyoshi, K., and Yanagisawa, K. (2008) A new chemical process for catalytic conversion of d-glucose into lactic acid and gluconic acid. *Appl. Catal. A Gen.* **343** (1-2), 49–54.
13. Niemela, K. (1990) Conversion of xylan, starch, and chitin into carboxylic acids by treatment with alkali. *Carbohydr. Res.* **204**, 37–49.
14. Davidek, T., Robert, F., Devaud, S., et al. (2006) Sugar fragmentation in the maillard reaction cascade: formation of short-chain carboxylic acids by a new oxidative alpha-dicarbonyl cleavage pathway. *J. Agric. Food Chem.* **54** (18), 6677–6684.
15. Auroux, A., and Gervasini, A. (1990) Microcalorimetric study of the acidity and basicity of metal oxide surfaces. *J. Phys. Chem.* **94** (16), 6371–6379.

16. Antal, M.J., Leesomboon, T., Mok, W.S., and Richards, G.N. (1991) Mechanism of formation of 2-furaldehyde from d-xylose. *Carbohydr. Res.* **217**, 71–85.
17. Aida, T.M., Shiraishi, N., Kubo, M., et al. (2010) Reaction kinetics of d-xylose in sub- and supercritical water. *J. Supercrit. Fluids* **55** (1), 208–216.
18. Tanabe, K. (1985) Surface and catalytic properties of ZrO₂. *Mater. Chem. Phys.* **13**, 347–364.
19. Ma, Z.Y., Yang, C., Wei, W., et al. (2005) Surface properties and CO adsorption on zirconia polymorphs. *J. Mol. Catal. A Chem.* **227** (1-2), 119–124.
20. Bianchi, D., Chafik, T., Khalfallah, M., and Jean, S. (1993) Intermediate species on zirconia supported methanol aerogel catalysts . II . Adsorption of carbon monoxide on pure zirconia and on zirconia containing zinc oxide. *Appl. Catal. A Gen.* **105**, 223–249.
21. Tsutomu Yamaguchi, Yassuko Nakano, K.T. (1978) Infrared study of surface hydroxyl group on zirconium oxide. *Bull. Chem. Soc. Jpn.* **51** (9), 2482–2487.
22. Shen, Y., Zhang, S., Li, H., et al. (2010) Efficient synthesis of lactic acid by aerobic oxidation of glycerol on Au-Pt/TiO₂ catalysts. *Chem. Eur. J.* **16** (25), 7368–7371.
23. Kong, L., Li, G., Wang, H., et al. (2008) Hydrothermal catalytic conversion of biomass for lactic acid production. *J. Chem. Technol. Biotechnol.* **388** (August 2007), 383–388.
24. Pescarmona, P.P., Janssen, K.P.F., Delaet, C., et al. (2010) Zeolite-catalysed conversion of C3 sugars to alkyl lactates. *Green Chem.* **12** (6), 1083–1089.
25. Koito, Y., Nakajima, K., Kitano, M., and Hara, M. (2013) Efficient conversion of pyruvic aldehyde into lactic acid by Lewis acid catalyst in water. *Chem. Lett.* **42** (8), 873–875.
26. Akiya, N., and Savage, P.E. (2002) Roles of water for chemical reactions in high-temperature water. *Chem. Rev.* **102** (8), 2725–2750.
27. Yagasaki, T., Iwahashi, K., Saito, S., and Ohmine, I. (2005) A theoretical study on anomalous temperature dependence of pK_w of water. *J. Chem. Phys.* **122** (14), 144504–144509.
28. Jacob, K., Knozinger, E., and Benier, S. (1993) Adsorption sites on polymorphic zirconia. *J. Mater. Chem.* **3** (6), 651–657.
29. Hertl, W. (1989) Surface chemistry of zirconia polymorphs. *Langmuir* **5**, 96–100.
30. Bo-qing Xu, Tsutomu Yamaguchi, K.T. (1988) Acid-Base bifunctional behavior of ZrO₂ in dual adsorption of CO₂ and NH₃. *Chem. Lett.*, 1663–1666.
31. Pokrovski, K., Jung, K.T., and Bell, A.T. (2001) Investigation of CO and CO₂ adsorption on tetragonal and monoclinic zirconia. *Langmuir* **17**, 4297–4303.

32. Tomishige, K., Sakaihori, T., Ikeda, Y., and Fujimoto, K. (1999) A novel method of direct synthesis of dimethyl carbonate from methanol and carbon dioxide catalyzed by zirconia. *Catal. Letters* **58**, 225–229.
33. Tsuji, H., Okamura-Yoshida, A., Shishido, T., and Hattori, H. (2003) Dynamic behavior of carbonate species on metal oxide surface: oxygen scrambling between adsorbed carbon dioxide and oxide surface. *Langmuir* **19** (21), 8793–8800.
34. Zaki, M.I., Hasan, M.A., and Pasupulety, L. (2001) Surface reactions of acetone on Al₂O₃, TiO₂, ZrO₂, and CeO₂: IR spectroscopic assessment of impacts of the surface Acid - Base properties. *Langmuir* **17**, 768–774.
35. Zhao, Y., Li, W., Zhang, M., and Tao, K. (2002) A comparison of surface acidic features between tetragonal and monoclinic nanostructured zirconia. *Catal. Commun.* **3** (6), 239–245.
36. Ryczkowski, J. (2001) IR spectroscopy in catalysis. *Catalyst Today* **68**, 263–381.
37. Puttock, S.J., and Rochester, C.H. (1986) Infrared study of the adsorption of carbon monoxide, carbon dioxide, acetic acid and acetic anhydride on the surface of anhydrous vanadyl pyrophosphate. *J. Chem. Soc. Faraday Trans. 1* **82** (9), 3013–3018.
38. Young, R. (1969) Infrared spectroscopic studies of adsorption and catalysis. Part 3. Carboxylic acids and their derivatives adsorbed on silica. *Can. J. Chem.* **47** (12), 2237–2247.
39. Yun Yu, Xia Lou, H.W. (2008) Some recent advances in hydrolysis of biomass in hot-compressed water and its comparisons with other hydrolysis methods. *Energy & Fuels* **22** (1), 46–60.
40. G. Garrote, H. Dominguez, J.C.P. (2001) Study on the deacetylation of hemicelluloses during the hydrothermal processing of Eucalyptus wood. *Eur. J. Wood Wood Prod.* **59**, 53–59.
41. Ignatchenko, A. V. (2011) Density functional theory study of carboxylic acids adsorption and enolization on monoclinic zirconia surfaces. *J. Phys. Chem. C* **115** (32), 16012–16018.
42. Ignatchenko, A. V., and Kozliak, E.I. (2012) Distinguishing enolic and carbonyl components in the mechanism of carboxylic acid Ketonization on monoclinic zirconia. *ACS Catal.* **2** (8), 1555–1562.

Chapter 5: Catalytic conversion of holocellulose (cellulose and hemicellulose) into lactic acid derivatives via mesoporous Zr-SBA-15

To increase the lewis acid strength of catalysts, mesoporous Zr-silicates materials were developed. A variety of Zr-SBA-15 materials were synthesized with tunable structures and pore sizes that showed excellent catalytic performance for the conversion of carbohydrates to lactic acid derivatives in a “one-pot” reaction system. Biomass-derived lactic acid esters are powerful solvents that have a high boiling point and are not only biodegradable, but also non-toxic. The effects of reaction conditions, including temperature, reaction time, and catalyst loading amount, on the conversions of carbohydrates and the corresponding yields of lactate were investigated. The carbon yields of methyl lactate, up to 41 % and 44%, were produced from pentose and hexose, respectively. The key intermediates such as glyceraldehyde, glycolaldehyde and pyruvaldehyde were used as probe reactants to understand the mechanism. Furthermore, a carbon yield of up to 33% ethyl lactate was produced from cellulose with the Zr-SBA-15 catalyst. Fructose and glucose were used as intermediate reactants in order to probe the reaction mechanism. The role of the catalyst in the retro-aldol condensation of carbohydrates, as well as the catalyst stability, was discussed.

5.1: Introduction

The development of new and efficient methods to make fuels and chemicals from lignocellulosic biomass is vital if we are to reduce our dependence on fossil fuel

feedstocks [1–3]. The production of fuels and value-added chemicals from carbohydrates using non-toxic heterogeneous catalysts is an appealing environmentally benign process. Various endeavors have been made over the past few years to develop stable, recyclable, solid catalysts for the conversion of biomass into biofuels and value-added chemicals by catalytic methods [4–8]. Among the studied catalysts, microporous zeolites or zeotype materials are quite promising. Microporous zeolites are efficient catalysts in the transformation process of small molecules; however, they become unsuitable when the essential reactants involved in the catalytic process are sized comparably with the zeolite pore dimensions. A rational approach to overcoming mass-transfer limitations would be to increase the diameter of the pores, thus bringing them into the mesoporous range with a key factor here being the shape selectivity properties of these catalysts [9–14]. Shape selectivity enables excellent adjustment of catalytic transformation exclusivity, and also acts on the activity and stability of the catalyst by either protecting the acid sites from potential contaminants (in particular, coke precursors), which are contained in the feeds, or by inhibiting the formation of coke precursors in the pores. However, few reports exist on biomass conversion with mesoporous silicate materials. This scarcity of literature is because pure silica mesoporous materials possess a neutral framework, poor hydrothermal stability, low catalytic activity, and weak surface acidity, all of which limit its application as a catalyst medium [15,16]. To date, such impediments have not been completely resolved. In order to enable their application in catalysis, different structured mesoporous silicate materials have been investigated and various metal ions have been incorporated into these mesoporous materials [17–22]. Additionally, the isomorphic

substitution of silicon with transition metals has proven to be an excellent strategy to generate catalytically active sites in mesoporous silicate materials [15,23–25].

Among the mesoporous materials, the SBA-15 of 2D hexagonal-ordered structure with tunable pores in the 4-10 nm range has received great attention in the past decades due to its relatively large pore size and high hydrothermal stability in comparison with other mesoporous silica materials, such as MCM-41, its analog in the M41S family [26]. This large pore size channel network provides a distinctive open space, with easy and direct access for both guest and host species, thus facilitating inclusion and/or diffusion throughout the pore channels without pore blockage. Such properties spur their prospective utilization as catalysts and adsorbents [23,27,28]. On the other hand, zirconia-based materials have been widely applied in catalyzing various types of reactions such as oxidation, dehydration, hydrogenation, and hydroxylation [29–32]. Mesoporous materials containing zirconium have received considerable attention in heterogeneous catalysis because of their high special surface areas and potential acid properties [33]. With the incorporation of zirconium into the SBA-15 structure, the affected materials displayed dominant Lewis acidity [15]. The basic structural unit of mesoporous silicate frameworks consists of a silicon atom that is coordinated to four oxygen atoms. Zirconium atoms have a coordination number of 7 or 8. When replacing Si^{4+} with Zr^{4+} , the zirconium atom has only four coordination associations with the surrounding oxygen, resulting in empty zirconium d-orbitals, which can act as electron acceptors. Under such conditions, it is possible for a zirconium atom incorporated within the silicate framework to function as a Lewis acid site [34].

Carbohydrates constitute the largest portion of virtually all biomass, and various strategies for their efficient use as a commercial chemical feedstock are being established in the interest of converting such to value-added chemicals. The synthesis of lactate acid esters in related alcohol is a process that invokes great interest in the fields of renewable biomass conversion and green solvents in that these versatile products have numerous applications in the chemical, food, pharmaceutical, and cosmetic industries [35–39]. Various strategies to produce lactic acid esters have been established including both fermentative processes [40,41] and catalytic transformations [42,43]. Catalytic methods have many advantages over those that involve fermentation methods especially considering the latter approach's unavoidable large amounts of salt by-products, which impose a high separation cost. Studies on the conversion of carbohydrates to lactate esters over heterogeneous catalysts have emerged recently. For instance, Holm *et al.* [44,45] reported that Lewis acidic zeotype materials, such as Sn-Beta, catalyzed the conversion of mono- and disaccharides to methyl lactate in methanol at 160 °C. With sucrose as the substrate, the methyl lactate yield reached a high of 68%. When the alkali ion of K₂CO₃ was added to the solvent mixture, the methyl lactate yield was further promoted to 75% from sucrose at 170 °C in methanol with a 16-hour reaction time [44]. Carlos reported that with the Sn-MCM-41 which has an atomic ratio of Si/Sn=55, a 43% yield of methyl lactate was produced from the conversion of glucose after 20 h at 160 °C [46]. The carbon-silica composite by grafting Sn(IV) showing well-balanced Lewis/Bronsted acidity yielded 45% methyl lactate from the conversion of sucrose in methanol [47]. Sn-MWW zeolite was also demonstrated to be an effective and selective catalyst for the direct conversion of mono-and disaccharides to methyl lactate [48]. For other types of

catalysts, Dong et al reported that as high as 89.6% yield of lactic acid was obtained by using Er(OTf)₃ as the catalyst for the hydrothermal conversion of cellulose [49]. Also erbium ion-exchanged montmorillonite K10 was shown to effectively catalyze the conversion of cellulose to lactic acid with 67.6% yield by the same group, even with the erbium ion leaching during the catalyst recycling process [50]. During Wang's study, the lactic acid yield from microcrystalline cellulose and several lignocellulose-based raw biomasses was >60% at 463 K in water in the presence of dilute lead (II) ions [51]. Although many studies have been investigated to convert cellulose to lactic acid through catalyzed routes, the most catalysts used were homogenous catalysts that suffered the same problems faced in the fermentation process. Only a few reports are available on the production of lactic acid/ derivatives directly from cellulose by heterogenous catalysts. Meanwhile, the main drawbacks of tin-based heterogenous materials are the typically complex and lengthy synthesis process and the the toxicity of tin precursors, which may hamper their applications [52]. Solid base catalysts, including hydrotalcites [53] and magnesium oxide [54], and supported noble metal catalysts [42] were also used for catalyzing the formation of lactic acid or methyl lactate from glucose at rather low yields. With this in mind, the development of an environment-friendly and highly effective catalyst for converting cellulose to lactic acid/ derivatives is still highly desired. To investigate if there are other suitable catalysts for lactic acid derivatives reactions, we focused on zirconium-containing materials, which are much greenr and lower cost. In our former study, ZrO₂ was shown to be a renewable and environmentally-friendly catalyst for lactic acid prodution from hemicellulosic biomass feedstocks in aqueous catalytic process [55].

Recently, supercritical alcohols have been utilized as an alternative solvent in the liquefaction of various types of biomass, including cellulose, lignin, sewage sludge, and microalgae, due to their advantages with higher biocrude yields, better solubility of organic intermediates, hydrogen donor properties, and easy of separation due to their low boiling points [56–65]. As hydrogen donor solvent and hydroxyalkylation agents, supercritical alcohols can act not only as a solvent, but also as a reactant [66–69]. The hydrogen generated from supercritical alcohol can serve as a hydrogenolysis agent to depolymerize biomass, a deoxygenation agent to remove oxygen from biomass via H₂O formation, and a radical quenching agent to retard repolymerization and formation of char/tar [66–69]. Herein, we report our findings on the catalytic conversion of carbohydrates to lactic acid esters using a mesoporous Zr-SBA-15 catalyst in supercritical alcohol solvents, which combines the lactic acid production and esterification, into a one-pot reaction system. A possible reaction mechanism is proposed to explain the performance of the Zr-SBA-15 as a heterogeneous Lewis acid catalyst in the production of lactic acid esters from carbohydrates in alcohol solvents.

5.2: Materials and methods

5.2.1: Materials

The following reagents and products were used as received for the experiments: D-(+)-xylose (99%), D-(+)-glyceraldehyde (98%), Fructose (99%), glycolaldehyde dimer, pyruvaldehyde (40wt% solution in water), furfural (99%), 5-(hydroxymethyl) furfural (99%), hydrochloric acid (36.5-38.0%, BioReagent), triblock copolymer Pluronic P123, tetraethyl orthosilicate (>99.0%), and zirconyl chloride octahydrate (98%) were purchased from Sigma Aldrich (St. Louis, MO). Microcrystalline cellulose, average

particle size 50 μm , and cellobiose (98%) were purchased from Acros Organics. Starch (powder, certified ACS, soluble) and sucrose (crystalline, certified ACS) were purchased from Fisher Scientific (Waltham, Massachusetts). Glactose, mannose and arabinose were purchased from Carbosynth (Compton, Berkshire, UK). D(+) -Glucose (Reagent ACS Grade) were purchased from Acros Organics. Methyl lactate (97%), erythrose syrup (70% w/v), methyl levulinate (99%), methyl glycolate (98%), glycolaldehyde dimethylacetal (98%), Ethyl lactate (97%), ethyl levulinate (99%), acetaldehyde diethyl acetal (99%), glycolaldehyde diethylacetal (98%), and ethyl 3-hydroxybutanoate (98%) were purchased from Alfa Aesar (Ward Hill, Massachusetts).

5.2.2: Catalyst preparation

Zr-SBA-15 was synthesized following the procedure described by reference [26]. 2g of Pluronic P123 was added to 75 ml of 1.6 M HCl solution. The mixture was stirred at 40 $^{\circ}\text{C}$ for 3 h until all P123 was dissolved. Next, 4.25 g of TEOS and an appropriate amount of zirconyl chloride octahydrate were added into the solution and the mixture was stirred for another 24 h at 40 $^{\circ}\text{C}$. The resulting gel was placed in the Teflon-lined autoclave and heated at a range of temperatures of 80-150 $^{\circ}\text{C}$ for 24 h. The solid product was filtered with mild washing, dried at 100 $^{\circ}\text{C}$ overnight, and calcined in flowing air at 550 $^{\circ}\text{C}$ for 6 h. The x (in Zr-SBA-15-x-y $^{\circ}\text{C}$) represents the mole ratio of Si/Zr, the y represents the hydrothermal temperature. Zr-SBA-15-y $^{\circ}\text{C}$ without x means that the mole ratio of Si/Zr is 20. Zr-SBA-15-x without y means that the catalyst was synthesized at 100 $^{\circ}\text{C}$. Zr-SBA-15 without x, y means that the catalyst was synthesized at 100 $^{\circ}\text{C}$ with Si/Zr=20.

5.2.3: Catalyst characterization

Small-angle X-ray Scattering (SAXS) was performed using a sample-to-detector distance of 172.1 cm, which provided a two-theta range of approximately 0.3-2.0 degrees. Data was typically collected over 30 sec at a temperature of 20 °C. The x-ray source was Cu K α radiation with a wavelength of 1.54 Å, which was generated by a Rigaku RU-200BVH rotating anode. Measurements were made on a Siemens (Munich, Bavaria) Hi-STAR multi-wire area detector and were corrected for background and non-linearities in the detector. Integration of the 2D measurement provided a 1D plot of intensity (arbitrary units) versus the two-theta scattering angle, which was peak-fitted using Material Data Incorporated's JADE.

Transmission electron microscope (TEM) micrographs were captured using JEOL-JEM 2100F (AKISHIMA-SHI, TKY) operating at 200 kV. The samples were dispersed in 1-butanol, and a drop of the suspension was placed on lacey carbon supported on 300 mesh copper grids.

N₂ physisorption isotherms were measured on an Autosorb-iQ system (Quantachrome, Boynton Beach, Florida) at 77 K. Outgassing was done at 523 K until pressure rise in the test cell was less than 25 mTorr/min. Pore size distribution and cumulative adsorbed volume were calculated by using NLDFT (nonlocal density functional theory) adsorption model which describes N₂ adsorbed onto silica at 77 K in cylindrical pores (AsiQwin 1.02, Quantachrome). NLDFT model considers the configuration of adsorbates in pores on a molecular level and is widely used to characterize ordered porous materials with different pore geometries. With adequate fluid–fluid and fluid–solid interaction

parameters, it has been used to quantitatively predict the capillary condensation and evaporation transitions of adsorbates in novel hierarchical microporous materials.

In a typical NH₃ TPD experiment using a Micromeritics AutoChem II 2920 Chemisorption Analyzer (Norcross, GA), the catalyst was first degassed in helium at 250 °C for 1 hour, then the temperature decreased to 100 °C in helium flow. After that, 10% ammonia in helium was absorbed at this temperature for 60 min. 50 mL/min helium was then flowed over to remove ammonia gas that was physical adsorbed. Temperature programmed desorption was carried out from 100 °C to 550 °C with temperature ramp at 10 °C /min.

Drift-IR study was performed on EQUINOX 55 (Bruker, Billerica, MA) equipped with a MCT detector. The samples were degassed at 550 °C for 1 h under helium in a high temperature reaction chamber containing a Praying Mantis TM diffuse reflection attachment (Harrick). Small aliquots of pyridine were carried by helium and exposed to the sample at room temperature for 15 minutes. Prior to the characterization, the physically adsorbed pyridine was removed by flowing helium at 250 °C under helium for 1 hour. All spectra were collected at 120 °C.

5.2.4: Catalytic reactions

Reactions were carried out in a 100 mL stirred Parr micro reactor, whereby the catalyst was suspended in a solution of biomass substrate in methanol (20 ml) and the reactor was charged with 400 Psi N₂ initially and then heated at a ramp rate of 10 °C/min until the desired set temperature was reached. During the reaction, mixing was achieved through an internal propeller operating at 700 RPM. Once the set temperature was attained, the reactor was held for the set reaction time, and then quenched quickly in an

ice bath to stop the reaction. The reactor was cooled to approximately 25 °C before being vented after the gas pressure was recorded. The reactor was then immediately broken down and the solid residue remaining in the reactor was recovered and dried. The aqueous and solid fractions were separated using a centrifuge.

5.2.5: Product analysis

After the reaction, the resultant aqueous phase product samples were prepared for gas chromatography coupling with flame ionization detector (GC-FID), high performance liquid chromatography (HPLC) and gas chromatography coupling with mass spectrometer (GC/MS) analysis.

The liquid products (e.g., furfural, HMF) were quantified by HPLC analysis using a Shimadzu (Kyoto, KYT) HPLC system equipped a UV-VIS Detector (Shimadzu SPD 10-AV) and Refractive Index Detector (Shimadzu RID-6A). The liquid phase after reaction was filtered through a 0.45 micron syringe filter, and then diluted 10 times with DI water. The samples were separated in an Aminex 87-H column from Bio-Rad, using 5 mM H₂SO₄ as the mobile phase (0.7 mL/min flow rate) at a column temperature of 55 °C. The UV-VIS detector was utilized at 208 nm and 290 nm.

The liquid products identified in the methanol were qualified and quantified by GC/MS and GC-FID analysis. The liquid phase after reaction was filtered through a 0.45 micron syringe filter before being diluted 10 times with methanol. The sample were injected in an Agilent (Santa Clara, CA) 6890 series GC/MS equipped with an Agilent DB5-MS column (30 m x 0.25 mm ID, 0.25 um film thickness) and an Agilent 5973 Mass Selective Detector. The same prepared sample were also injected in a Shimadzu

GC-2010 equipped with an SHRXI-5MS column (30m x 0.25 mm ID, 0.25 um film thickness) and an FID detector.

The gaseous products were analysed by a Shimadzu GC-2014 gas chromatography equipped with a HAYESEP-N column (2.5m x 1/8in x 2.1mm. SS), a HAYESEP-D column (2.5m x 1/8in x 2.1mm. SS), a HAYESEP-S column (2m x 1/8in x 2.1mm), a HAYESEP-D column (1m x 1/8in x 2.1mm), a MOL SIEVE 5A column (3m x 1/8in x 2.1mm. SS), a Carbowax column (2m x 1/8in x 2.1mm) and a thermal conductivity detector (TCD). The gas products were injected with carrier gas (He) at the flow of 40ml/min at a column temperature of 55 °C. The injection volume was 1000ul.

A Euro EA3000 CHNS-O analyzer (Eurovector) was used for measuring the carbon content in the solid residue samples.

5.3: Results and discussion

5.3.1: Mechanistic insights into the production of methyl lactate by catalytic conversion of carbohydrates on mesoporous Zr-SBA-15

[Figure 5.1](#) shows the yields of the main products using xylose as the feedstock with and without adding catalysts. A relatively low yield of ML (~8%) was produced at 240 °C without adding a catalyst. With only the pure SBA-15, the ML yield was ~7.0%, which is close to that without catalyst. Both the as-synthesized Zr-SBA-15 and the commercial ZrO₂ resulted in noticeably higher yields of ML at 240 °C for 1 hour. The 35.9% yield of ML was achieved with the Zr-SBA-15 catalyst, which was more than twice of the 16.4% yield with the ZrO₂ catalyst. To validate the catalytic effect of Zr ion in SBA-15, Ti ions were deliberately incorporated into the SBA-15 framework so as to compare with the Zr-SBA-15 catalyst. It was found that with the Ti-SBA-15 catalyst, the

yield of ML from xylose was comparable to that with the ZrO₂ catalyst, but was still much lower than that with the Zr-SBA-15 catalyst. Notably, without a catalyst or with the Ti-SBA-15 catalyst, there were negligible amount of furfural yields, 0.7% and 0.8%, respectively. In contrast, when SBA-15, ZrO₂ and Zr-SBA-15 were employed, the furfural yields reached to 5.1%, 6.4%, and 7.9%, respectively. The mesoporous structure of the silica framework with the presence of zirconium ions confers strong Lewis acidity as well as weak Brønsted acidity [70]. Lewis acid catalysis can facilitate the retro-aldol condensation of a sugar molecule, which is the initial step in the conversion of sugars to lactic acid [71], while a Brønsted acid catalyzes the dehydration of xylose to form furfural. The co-production of ML and furfural from xylose with the Zr-SBA-15 catalyst suggest that both the Lewis and Brønsted acidic properties co-existed on the catalyst surface.

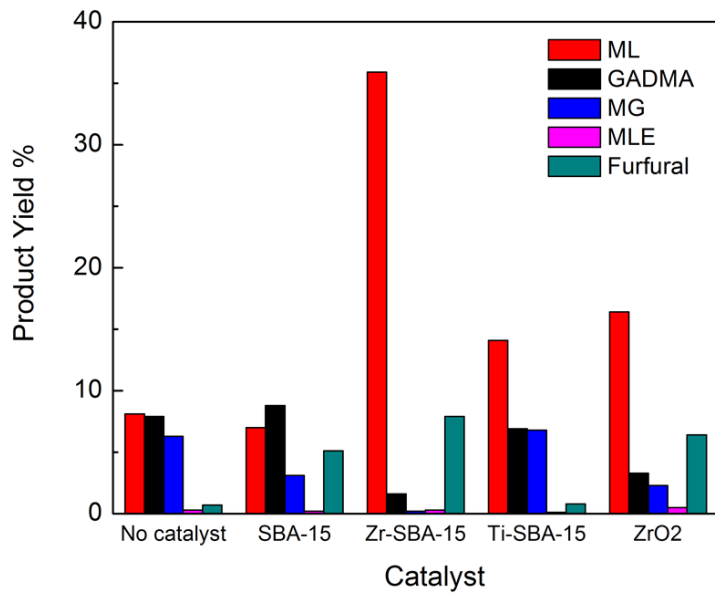


Figure 5.1 Comparison of different catalysts towards the xylose conversion in methanol solution. Reaction conditions: 240 °C, 1 h, 400psi N₂, 0.2g xylose loading, and 1:2 mass ratio of catalyst to xylose. ML: Methyl lactate, GADMA: Glycolaldehyde dimethylacetal, MG: Methyl glycolate, MLE: Methyl levulinate.

To further examine the catalytic effect of zirconium loading of the Zr-SBA-15 catalyst, the catalysts with different Si/Zr molar ratios of 100, 60, 40, 20 and 10 were prepared. As shown in [Figure 5.2](#), the total acid strength analysed by the NH₃ TPD increased with increasing the zirconium loading on the SBA-15 silicate. [Figure 5.3](#) shows the yields of the three major products, ML, glycolaldehyde dimethylacetal (GADMA), and furfural, on the Zr-SBA-15 catalysts with various Si/Zr molar ratios under otherwise identical reaction conditions. Initially, with increasing the Zr loading, the yields of increased steadily. However, as the zirconia loading further increased till the Si/Zr mole ratio of 10, the yields of all three products decreased implying the abrupt change of the catalyst properties. The maximum yield of ML was found to be in the range of the Si/Zr mole ratios of 40 to 20, e.g., with the Zr-SBA-15-40 or Zr-SBA-15-20 catalyst, approximately 19% ML and 11% GADMA were produced at 180 °C. However over-loading of Zr ions onto SBA-15 inhibited the catalyst's performance. Therefore, to confirm the structures of the Zr-SBA-15 silicate materials at different Si/Zr ratios, the small-angle X-ray scattering (SAXS) characterization was performed. As depicted in [Figure 5.4](#), the SAXS spectra exhibited the strong (1 0 0), (1 1 0), and (2 0 0) diffraction peaks at 2θ angles between 0.5° and 2° for the samples with the Si/Zr ratios from 100 to 20, which indicated the structural ordering with the symmetry of the 2D-hexagonal space group p6mm [10,15,33]. However, a further increase in Zr loading (Si/Zr = 10) drastically lowered the peak intensity suggesting that incorporating too many Zr heteroatoms was detrimental on the structure of the mesoporous SBA-15 framework, which was coincident with its low catalytic performance. From the high-resolution TEM images ([Figure 5.5](#)), highly ordered pore structure was evident for the Zr-SBA-15

materials at the Si/Zr mole ratio of 20, while the ordered mesoporous structure was destroyed when the Si/Zr mole ratio reached 10, which were consistent with the SAXS data.

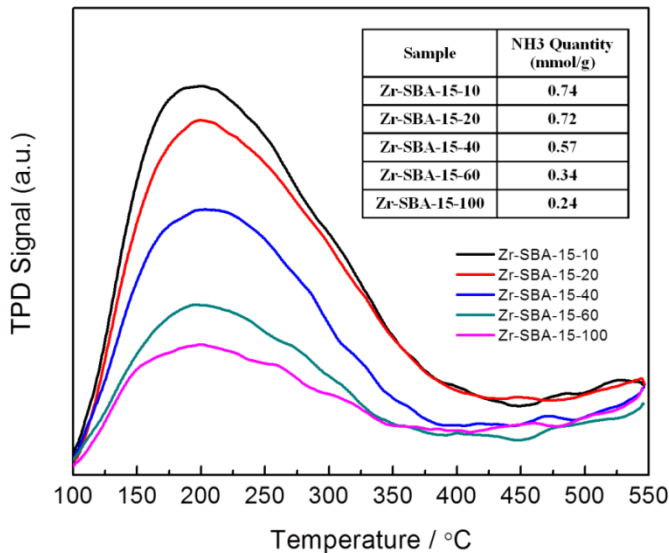


Figure 5.2 Temperature-programmed desorption of ammonia (NH₃-TPD) for Zr-SBA-15 materials with different Si/Zr molar ratios. All materials were synthesized at the hydrothermal temperature of 100°C.

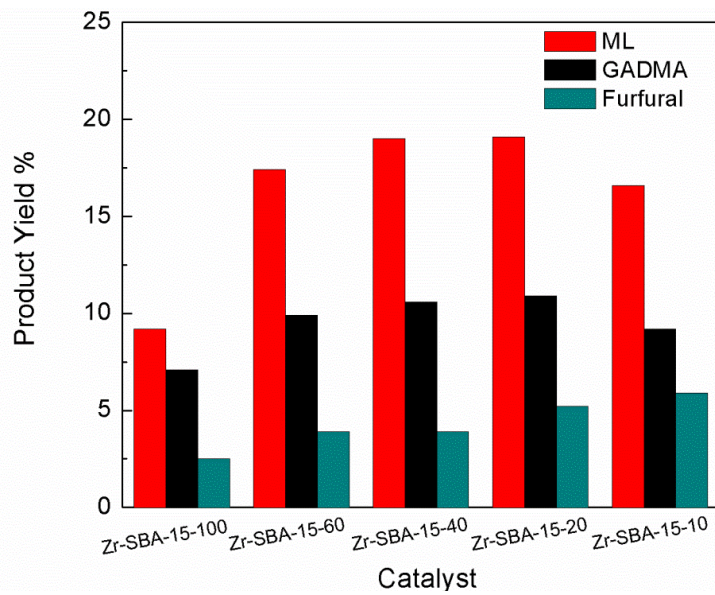


Figure 5.3 Comparison of different Zr ion loading on SBA-15 catalysts towards the xylose conversion in methanol solutions. Reaction conditions: 180 °C, 60 min, 400psi N₂, 0.2g xylose loading, and 1:2 mass ratio of catalyst to xylose. ML: Methyl lactate, GADMA: Glycolaldehyde dimethylacetal.

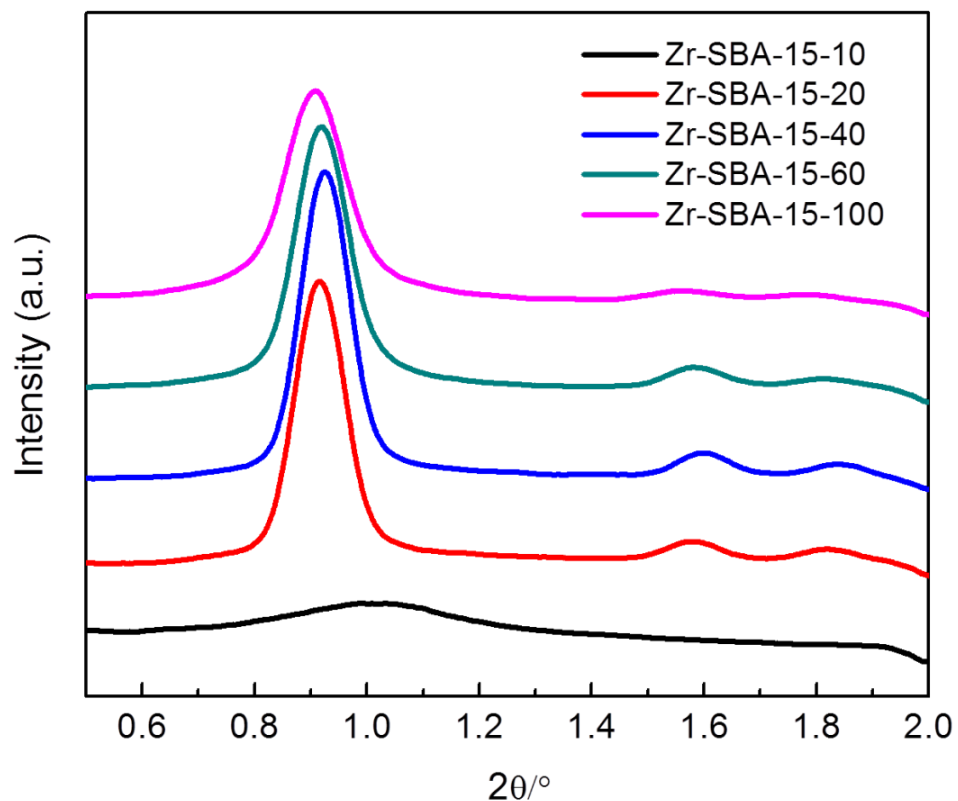


Figure 5.4 Small-angle X-ray scattering patterns of Zr-SBA-15 materials.

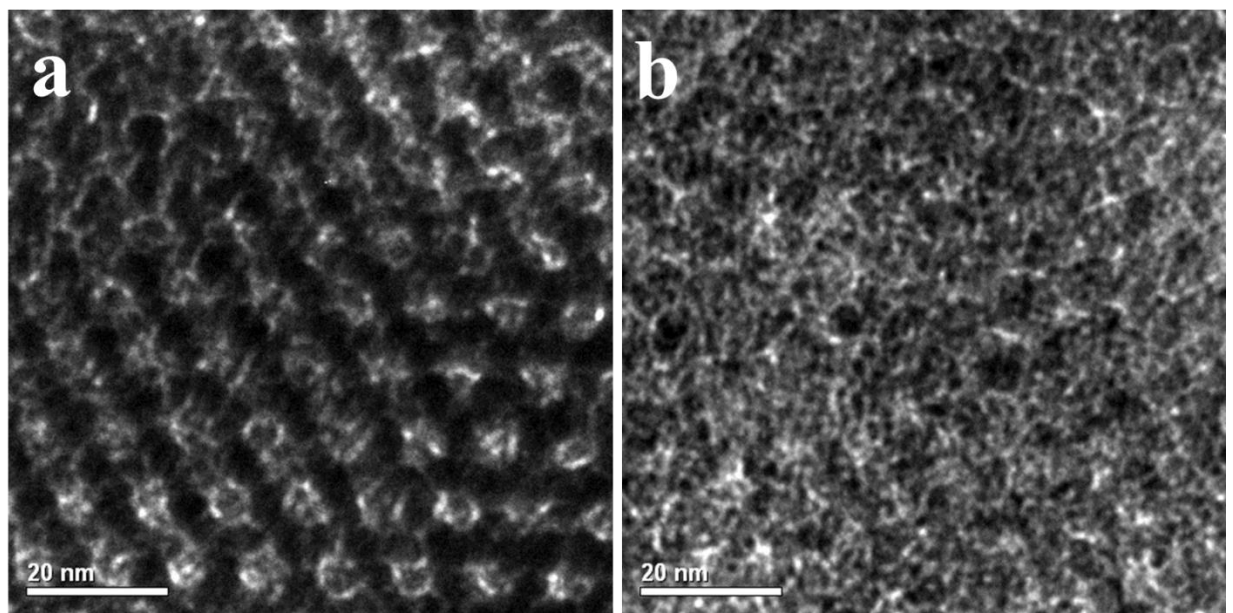


Figure 5.5 High-resolution transmission electron microscopy (HRTEM) image of Zr-SBA-15: (a) Si/Zr=20; (b) Si/Zr=10.

To maximize ML yield, process conditions were optimized for the xylose conversion reactions. As shown in [Figure 5.6](#), the varying temperature has a pronounced effect on the production of ML, yielding a steadily increasing amount of ML up to 35.9% with an increase in temperature from 160 °C to 240 °C for a 1 h reaction. The yields of other products such as furfural also increased steadily with increasing temperature. The yield of GADMA, however, decreased from 10.9% at 180 °C to 1.6% at 240 °C. The highest ML yield of 40.8% was achieved when the reaction time extended to 6 h at 240 °C as shown in [Figure 5.7](#). However, the ML yield varied little as the reaction time was longer than 3 h. Conversely, the yields of GADMA and furfural consistently decreased upon extending the reaction time. Of particular observation is the fact that GADMA almost completely vanished after 3 h at 240 °C. These results suggested that longer reaction time leads to the decomposition of GADMA and furfural. Interestingly the methyl levulinate yield increased with reaction time at 240 °C. The effects of different catalyst loading amounts on the conversion of xylose were also examined. As depicted in [Figure 5.8](#), the yields of both ML and furfural showed a similar uptrend with increasing catalyst loading, while those of GADMA and methyl glycolate decreased steadily. However, as the mass ratio of catalyst to xylose was larger than 0.2, the yield of ML was almost unchanged and reached a plateau. By substituting methanol with water as the solvent ([Table 3 entry 4](#)), the lactic acid yield was ~5.9% while the furfural yield was ~42.3% with Zr-SBA-15. In contrast, the yields of furfural and lactic acid were only 21.2% and 3.0%, respectively, without adding any catalyst. Thus the Lewis acid property of the Zr-SBA-15 catalyst appeared to vanish and be transformed to Bronsted acid in water.

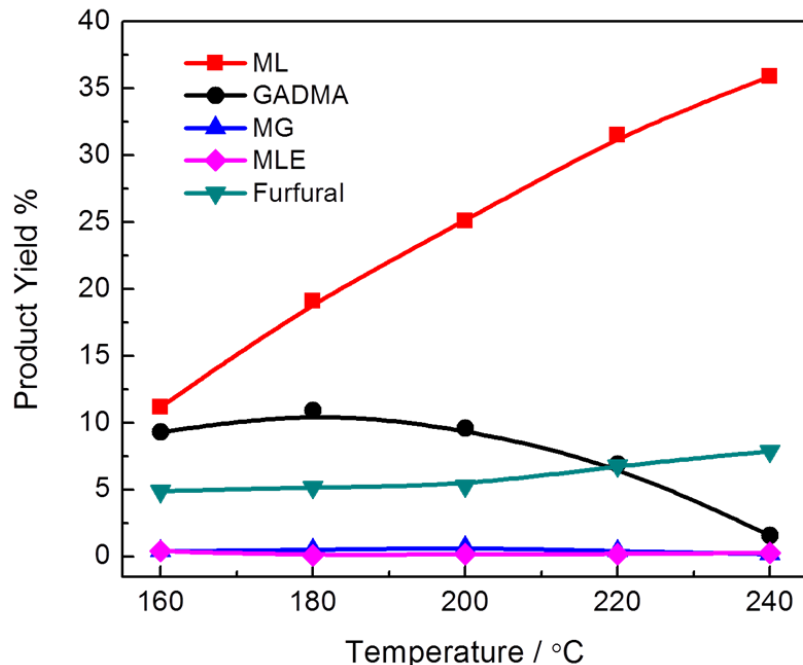


Figure 5.6 Effect of temperature on the yields liquids-phase products of xylose conversion with the Zr-SBA-15 catalyst in methanol. Reaction conditions: (a) 1 hour, 400 psi initial N₂ pressure, 0.2 g xylose, and 0.1 g catalyst.

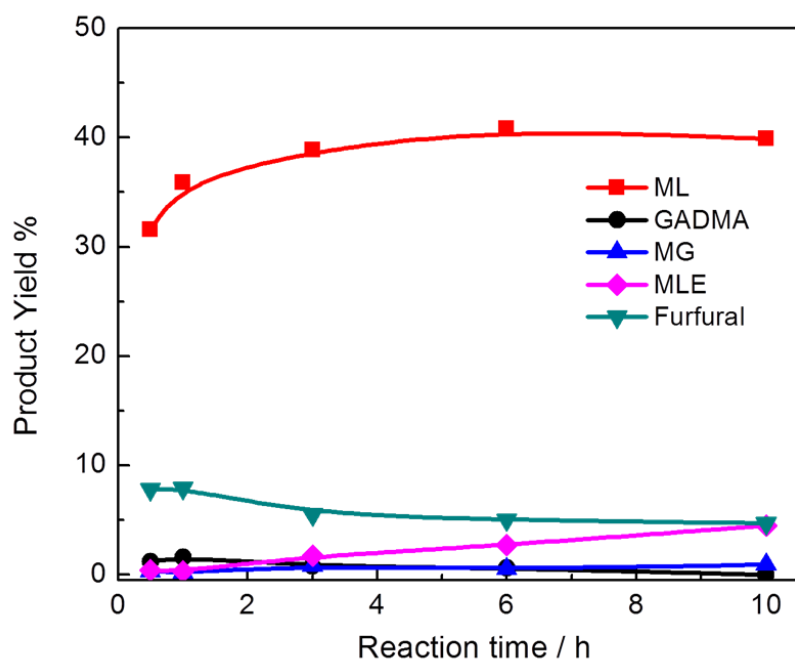


Figure 5.7 Effect of reaction time on the yields liquids-phase products of xylose conversion with the Zr-SBA-15 catalyst in methanol. Reaction conditions: 240 °C, 400 psi initial N₂ pressure, 0.2 g xylose, and 0.1 g catalyst. ML: Methyl lactate, GADMA: Glycolaldehyde dimethylacetal, MG: Methyl glycolate, MLE: Methyl levulinate.

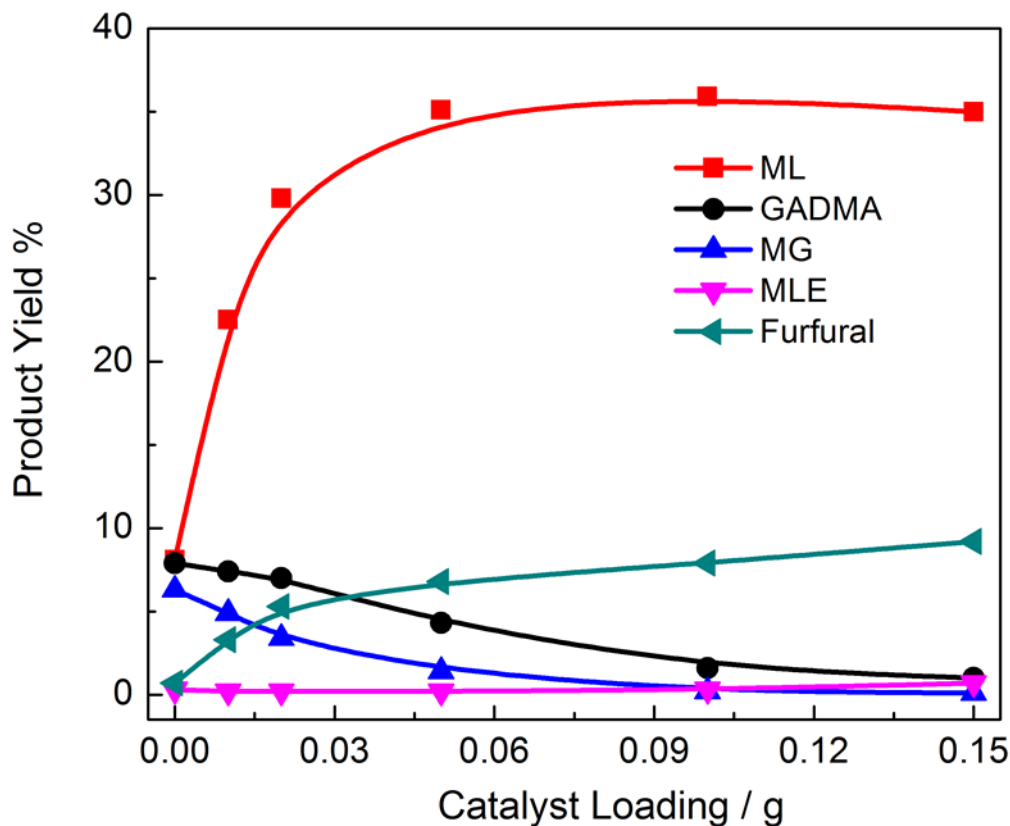


Figure 5.8. Effect of catalyst loading on the yields of liquids-phase products of xylose conversion with the Zr- SBA-15 catalyst in methanol. Reaction conditions: 240 °C, 1 h, 400 psi initial N₂ pressure, 0.2 g xylose. ML: Methyl lactate, GADMA: Glycolaldehyde dimethylacetal, MG: Methyl glycolate, MLE: Methyl levulinate.

For chemical reactions in confined channel space in mesoporous silicate materials, interesting pore size effects can be expected [72–74]. The pore size of the Zr-SBA-15 catalyst can be tuned by optimizing the hydrothermal treatment conditions during the synthesis [75]. Figure 5.9 shows the pore size distribution determined by NLDFT (NonLocal Density Functional Theory) model for the Zr-SBA-15 materials with different synthesis temperatures. The pore sizes of Zr-SBA-15-80 °C, Zr-SBA-15-100 °C, Zr-SBA-15-120 °C and Zr-SBA-15-150 °C, were 7.6, 9.1, 9.8, and 10.6 nm, respectively (Table 5.1). With increasing the hydrothermal temperature, the pore diameter of the SBA-15 materials increased while the BET (Brunauer–Emmett–Teller) surface area

decreased. The ML yield varied slightly with increasing the pore size except the catalyst synthesized at 80 °C in the smallest pore size, as shown in Table 5.2. In contrast, the furfural yield and the corresponding solid residue yield decreased significantly with increasing the pore size. Aldehyde compounds such as furfural are prone to polymerize and form humins at elevated temperatures. Apparently, large pores in a Zr-SBA-15 catalyst provide more open pore space where guest and host species can have easy access, thus facilitating the diffusion in and out the stoma channels without pore restriction. It turns out that in order to minimize the undesirable by-products such as furfural and humins, it is important to lift the pore diffusion limit of the Zr-SBA-15 catalyst for this particular ML production reaction.

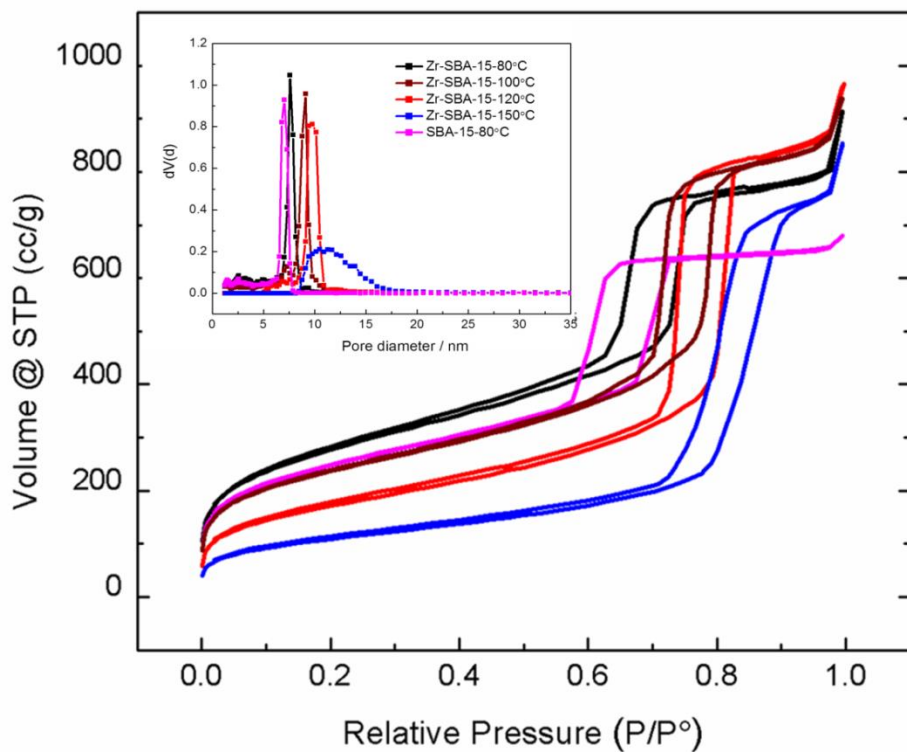


Figure 5.9 Nitrogen adsorption–desorption isotherms of the Zr-SBA-15 materials; inset is the pore size distribution determined by NLDFT model for adsorption branch for N_2 on silica at 77K (cylindrical pore model).

Table 5.1 Surface and Bulk Properties of Zr-SBA-15 silicates.

Catalyst	BET Surface area / m ² g ⁻¹	Pore volume determined by NLDFT model ^b / cm ³ g ⁻¹	Pore size determined by NLDFT model ^b / nm	Acid strength NH ₃ Quantity (mmol/g)
SBA-15-100 °C	876	0.998	7.0	0.02
Zr-SBA-15-80 °C	988	1.275	7.6	0.65
Zr-SBA-15-100 °C	841	1.357	9.1	0.72
Zr-SBA-15-120 °C	618	1.384	9.8	0.69
Zr-SBA-15-150 °C	393	1.215	10.6	0.51

^aBET surface area calculated using the BET (Bruanauer-Emmett-Teller) equation at relative pressures between 0.05 and 0.25 using the adsorption branch.

^bCylindrical pore model applied for N₂ adsorption on silica at 77K for the adsorption branch.

Table 5.2 Comparison of different pore sizes effect of Zr-SBA-15 during the catalytic conversion of xylose to methyl lactate in methanol solvent.

Entry	Feedstock	Catalyst	Conversion	Solid residue	Carbon Yield/%				
					ML	GDA	MG	MLE	Furfural
1	Xylose	Zr-SBA-15-80 °C	>99%	17.4%	30.9	1.0	0.1	0.6	9.2
2	Xylose	Zr-SBA-15-100 °C	>99%	10.8%	35.9	1.6	0.2	0.3	7.9
3	Xylose	Zr-SBA-15-120 °C	>99%	9.2%	34.1	3.0	1.0	0.2	7.3
4	Xylose	Zr-SBA-15-150 °C	>99%	6.9%	34.3	8.7	1.2	0.2	6.4

Reaction conditions: 240 °C, 1 h, 400 psi N₂ pressure, 0.2g feedstock loading, and 1:2 mass ratio of Zr-SBA-15-x catalyst to feedstock. ML: Methyl lactate, GADMA: Glycolaldehyde dimethylacetal, MG: Methyl glycolate, MLE: Methyl levulinate.

Recyclability and reusability are of importance for the heterogeneous Zr-SBA-15 catalysts. During the typical reaction, the yield of solid residue on the catalyst was relatively low, ~10.8%. However, the activity of the catalyst could decrease if solid residue continues to build up on the catalyst surface in the subsequent repeating reactions.

Figure 5.10 shows that the yield of ML from xylose only decreased slightly over five consecutive runs with the re-used catalyst without regeneration, suggesting that the Zr-SBA-15 catalyst was relatively stable, although a regeneration process to remove the solid residues would be desirable for the catalyst re-use. Interestingly the yield of solid

residue (10.7%) on the catalyst after the 5th run almost did not change compared with that after the first run (10.8%), implying that the formation of extra coke inside the pores was inhibited after the catalyst was used once. The high-resolution TEM images of the Zr-SBA-15 samples before and after reaction showed that the highly ordered pore structure maintained without any noticeable pore size shrinkage or blockage, as shown in Figure 5.11. Furthermore, ML was used as reactant to test its stability. It was found that only 3% of ML was decomposed after a 1 h reaction at 240 °C with the Zr-SBA-15 catalyst in methanol (Figure 5.12), thus indicating that ML, the final product of xylose conversion, was very stable in this reaction system.

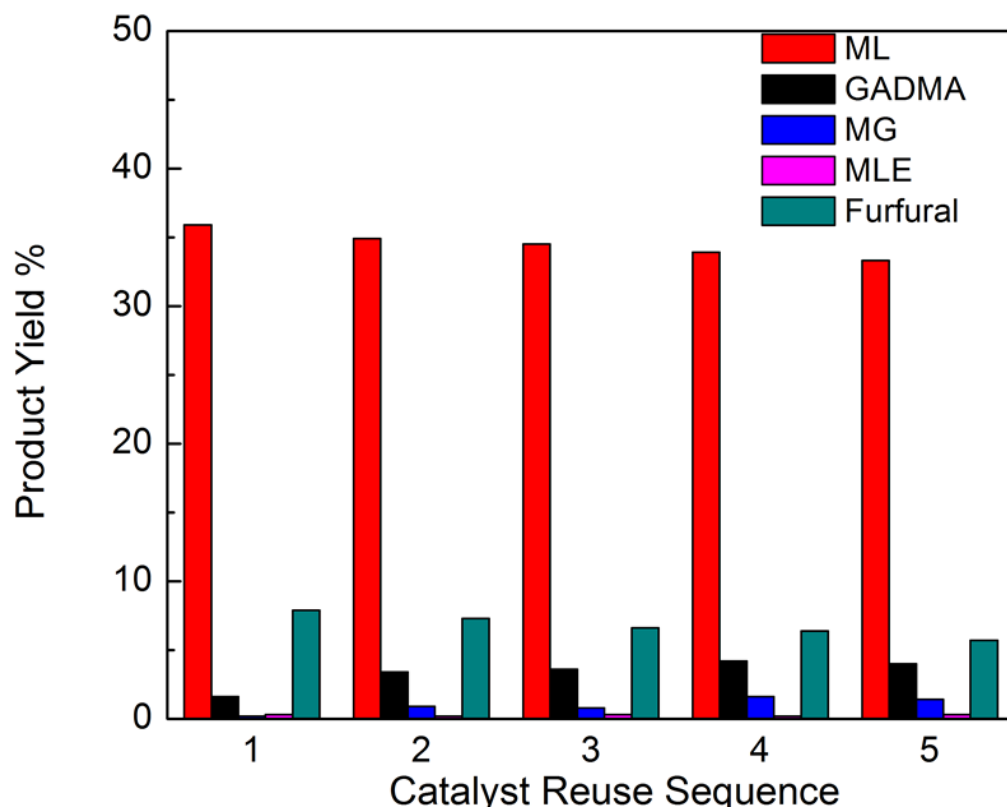


Figure 5.10 Effect of re-use of the Zr-SBA-15 catalyst on the major products by the conversion of xylose in methanol. The spent catalyst was not regenerated. Reaction conditions: 240 °C, 1 h, 400 psi N₂ pressure, 0.2g xylose loading, and 1:2 mass ratio of catalyst to xylose. ML: Methyl lactate, GADMA: Glycolaldehyde dimethylacetal, MG: Methyl glycolate, MLE: Methyl levulinate.

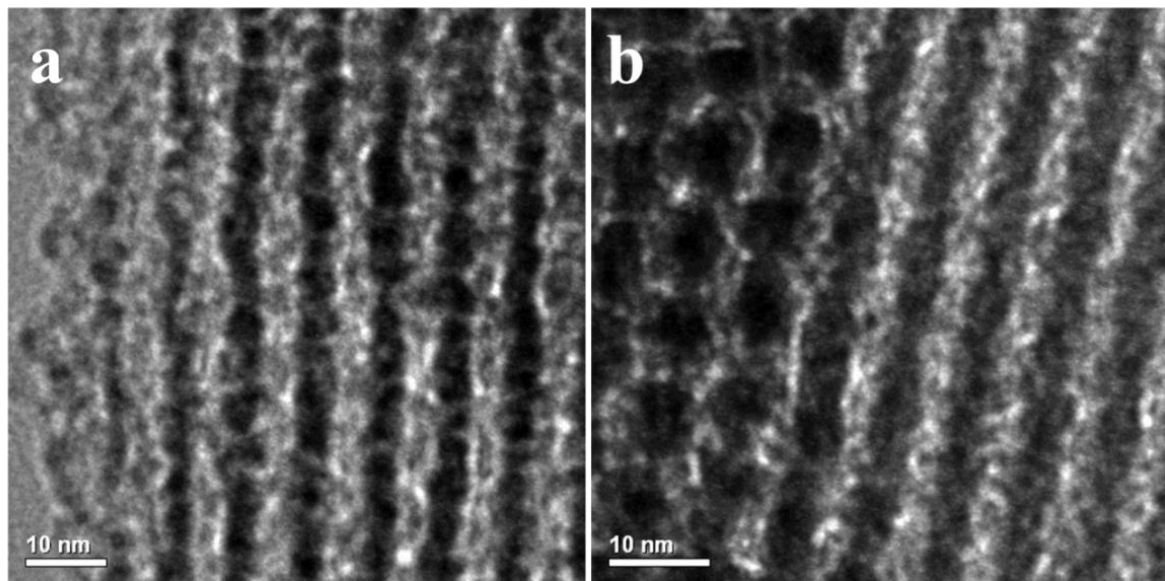


Figure 5.11 High-resolution transmission electron microscopy (HRTEM) image of Zr-SBA-15: *a*, fresh sample; *b*, after five times used.

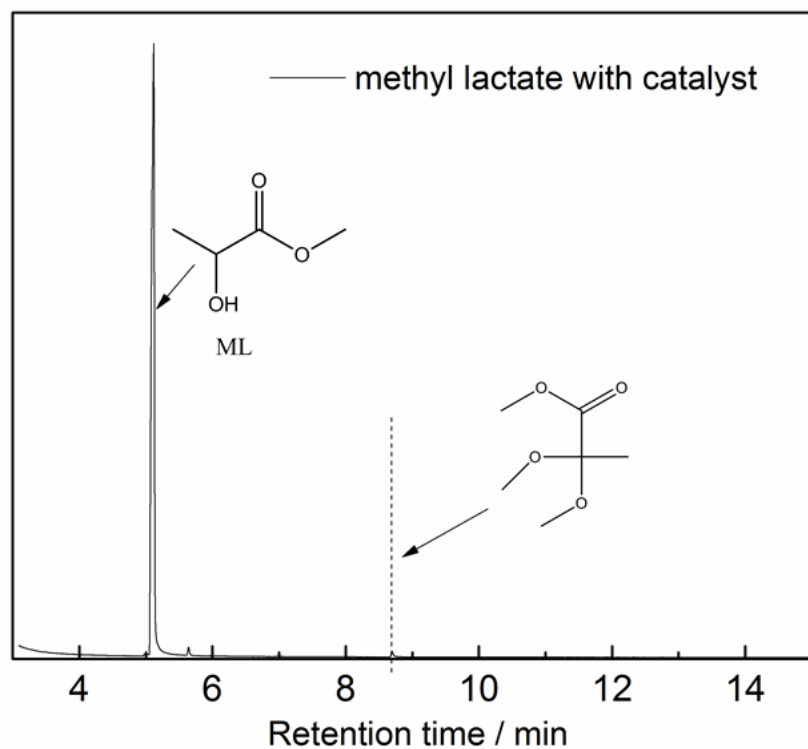


Figure 5.12 GC/MS spectra of methyl lactate stability test in methanol solvent with Zr-SBA-15 catalyst. Reaction conditions: 240 °C, 1 h, 400 psi N₂ pressure, 0.2g methyl lactate, and 1:2 mass ratio of catalyst to feedstock.

Lewis acids can promote retro-aldol condensation as the initial step in the conversion of sugars to lactic acid [71]. We thus propose that the reaction pathway of converting xylose to ML over the Zr-SBA-15 catalyst begins at the retro-aldol condensation forming glycolaldehyde and glyceraldehyde, as shown in Figure 5.13. Figure 5.14 illustrates the total acidity of the Zr-SBA-15 samples calculated from the NH₃ TPD. The pure SBA-15 silicate did not show any appreciable ammonia adsorption (only 0.02 mmol NH₃/g), while the Zr-SBA-15 samples presented high acidity of ~0.7 mmol NH₃/g. Furthermore, the FTIR spectra of pyridine adsorbed on the Zr-SBA-15 distinguished the Lewis acidic and Brønsted acidic sites, as shown in Figure 5.15. The prominent adsorption bands at 1440 and 1581 cm⁻¹ were assigned to the Lewis acid (L) sites, whereas the weak adsorption band at 1481 cm⁻¹ was attributed to a combination of Brønsted and Lewis acid (B + L) sites. A very weak band at 1541 cm⁻¹ was observed which typically corresponds to the Brønsted acid sites. The relative density of Brønsted/Lewis acid sites (B/L) was 0.117 obtained from the bands at 1541 cm⁻¹ and 1440 cm⁻¹ after normalizing the peak areas with the respective molar extinction coefficients. These results indicated that the Zr-SBA-15 sample contained predominantly strong Lewis acid sites. The Zr⁴⁺ ions in the SBA-15 silica framework as the Lewis acid sites first interacted with the carbonyl group of xylose, and then broke the C5 xylose molecule down to C3 glyceraldehyde and C2 glycolaldehyde. Glyceraldehyde underwent dehydration to form 2-hydroxypropenal, then to pyruvaldehyde via keto-enol tautomerization, and lastly to ML in methanol solvent by possible intramolecular Cannizzaro and esterification reactions. Although trioses were able to be converted to ML via Meerwein–Ponndorf–Verley reduction with methanol [76], the direct evidence of converting pyruvaldehyde to ML through intramolecular

Cannizzaro reaction was that no deuterium was incorporated into the hydrocarbon backbone of ML in the isotopic CD₃OD solvent [77]. On the other hand, the by-product, GADMA, was formed by the acetalization of glycolaldehyde with methanol.

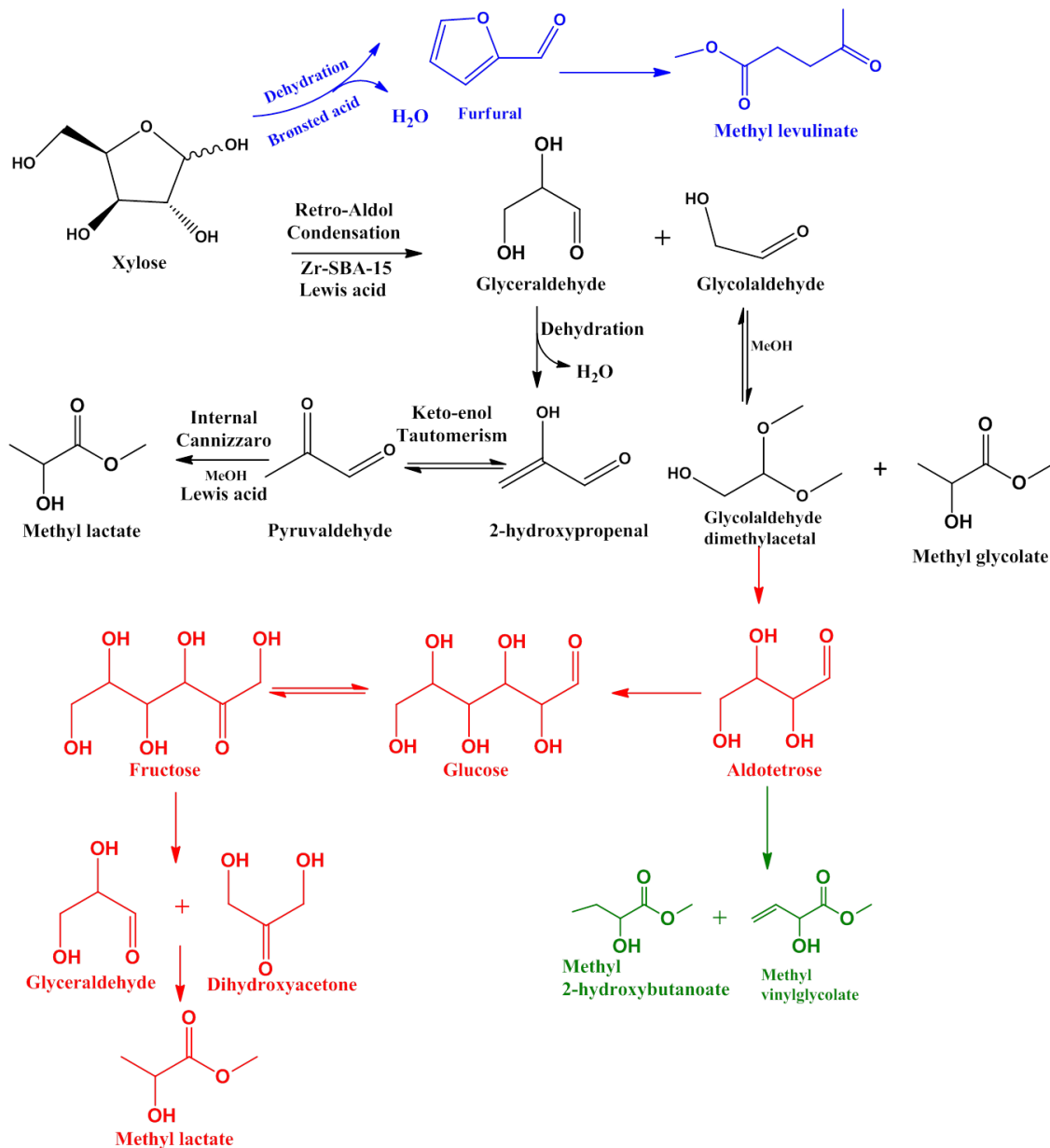


Figure 5.13 Proposed reaction mechanism for conversion of xylose to methyl lactate and other intermediate and final products in methanol solvent with Zr-SBA-15 catalyst. ML: Methyl lactate, GADMA: Glycolaldehyde dimethylacetal, MG: Methyl glycolate, MLE: Methyl levulinate, MVG: methyl vinylglycolate, MHB: methyl 2-hydroxybutanoate.

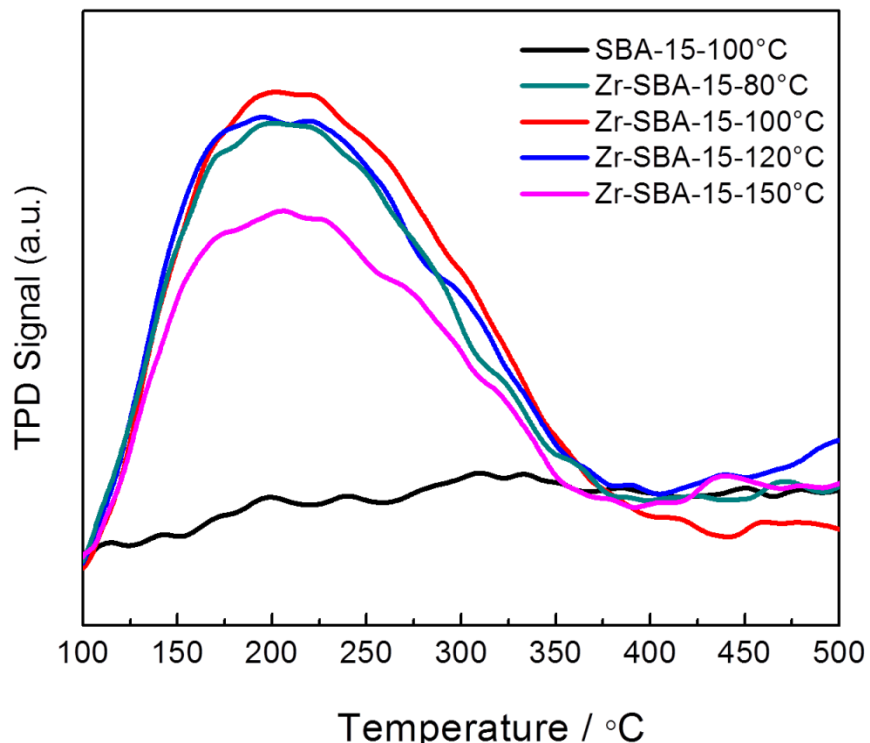


Figure 5.14 Temperature-programmed desorption of ammonia ($\text{NH}_3\text{-TPD}$) for Zr-SBA-15 materials synthesized at different hydrothermal temperature with $\text{Si/Zr} = 20$.

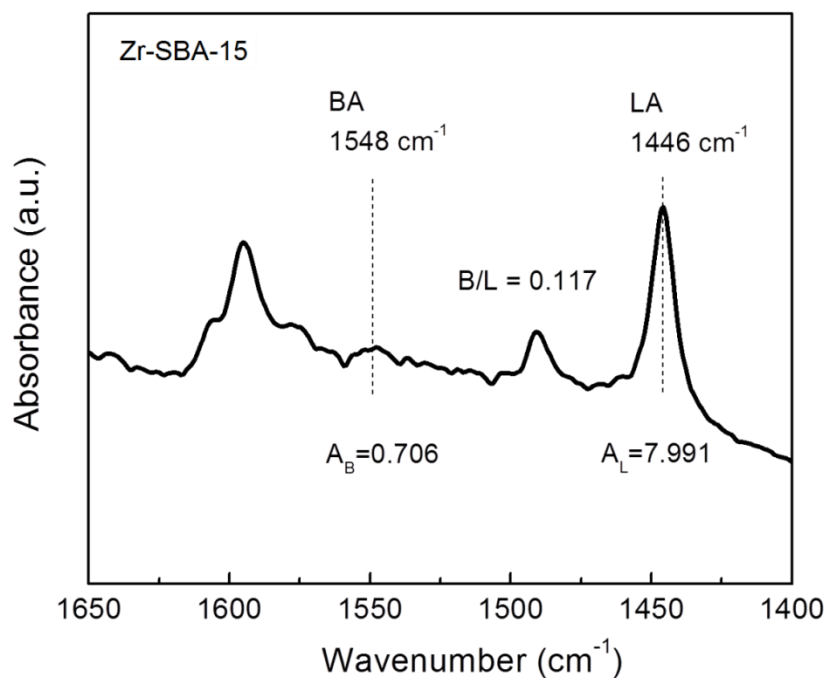


Figure 5.15 FTIR spectra of adsorbed pyridine on Zr-SBA-15.

To validate our hypothesis of the reaction pathway, the possible key intermediates, glyceraldehyde, dihydroxyacetone, pyruvaldehyde, glycolaldehyde, and GADMA were used as the probe reactants. Much higher ML yields (78.8% and 84.5%) were obtained from glyceraldehyde and dihydroxyacetone, respectively ([Table 3 Entries 6 and 8](#)), than from xylose. The yield of ML was even close to 100% from pyruvaldehyde ([Table 3 Entry 10](#)). Yet, in the absence of the Zr-SBA-15, much lower amounts of ML were produced from all three probe reactants. More interestingly, using glycolaldehyde as the probe, a high amount of GADMA was produced without catalyst, while ~ 61.3% ML was obtained with the Zr-SBA-15 catalyst. It appeared that C–C bond forming aldol condensation reactions occurred in the presence of Zr-SBA-15 in that the C4 acid ester products (e.g., methyl vinylglycolate and methyl 2-hydroxybutanoate) were also observed as the products from the C2 reactant, glycolaldehyde ([Figure 5.16](#)). Very interestingly, when using GADMA as the probe reactant, it was converted to ML in a 24% yield with the Zr-SBA-15 catalyst and the product distribution was similar to that using glycolaldehyde as the reactant: methoxyacetaldehyde dimethylacetal was another major product obtained through etherification while other products in the much lower yields were methyl vinylglycolate and methyl 2-hydroxybutanoate, as shown in [Figure 5.17](#). It revealed that GADMA and glycoaldehyde were reversibly converted to each other and the aldol-condensation reactions occurred in the presence of Zr-SBA-15 to form C4 and C6 aldehydes, while the formation of ML suggested that retro-aldol condensation reactions took place subsequently. However, it is unclear how the etherification and esterification reactions with methanol evolved in parallel to the aldo condensation and retro- aldo condensation reactions. Since most glycolaldehyde intermediates could be

further converted to ML with the Zr-SBA-15 catalyst in near critical methanol, the yields of ML from pentoses (xylose, arabinose) and hexoses (glucose, mannose) had no distinct difference, unlike the results of converting sugars to ML at 160-170 °C using the Sn-Beta catalyst reported by Taarning and co-workers [45].

Table 5.3 Comparison of different feedstocks' conversion with Zr-SBA-15 as catalyst in methanol solvent.

Entry	Feedstock	Catalyst	Time/h	Solvent	Carbon Yield/%					
					ML	GADMA	MG	MLE	Furfrual	HMF
1	Xylose	/	1h	Methanol	8.1	7.9	6.3	/	/	/
2	Xylose	Zr-SBA-15	1h	Methanol	35.9	1.6	0.2	/	/	/
3	Glyceraldehyde	/	1h	Methanol	19.9	2.3	2.9	/	/	/
4	Glyceraldehyde	Zr-SBA-15	1h	Methanol	78.8	2.5	0.8	/	/	/
5	Dihydroxy acetone	/	1h	Methanol	29.5	1.9	3.3	/	/	/
6	Dihydroxy acetone	Zr-SBA-15	1h	Methanol	84.5	1.9	0.9	/	/	/
7	Pyruvaldehyde	/	1h	Methanol	64.5	0.7	0.2	/	/	/
8	Pyruvaldehyde	Zr-SBA-15	1h	Methanol	98.7	0.8	0.2	/	/	/
9	Glycoaldehyde	/	1h	Methanol	3.9	32.6	0.7	/	/	/
10	Glycoaldehyde	Zr-SBA-15	1h	Methanol	61.3	8.4	0.6	/	/	/
11	GADMA	Zr-SBA-15	1h	Methanol	24.0	/	0.2	/	/	/
12	Glucose	Zr-SBA-15	6h	Methanol	37.3	0.6	1.0	1.3	0.9	0.2
13	Sucrose	Zr-SBA-15	6h	Methanol	39.5	0.4	0.3	2.5	1.6	2.2
14	Fructose	Zr-SBA-15	6h	Methanol	44.1	0.7	0.6	3.1	1.7	1.7
15	Glactose	Zr-SBA-15	6h	Methanol	14.8	0.8	0.1	7.2	0.9	2.1
16	Mannose	Zr-SBA-15	6h	Methanol	31.3	1.2	0.3	8.9	1.3	1.6
17	Arabinose	Zr-SBA-15	6h	Methanol	33.4	1.3	0.5	5.4	3.7	0.1
18	Cellobiose	Zr-SBA-15	10h	Methanol	24.3	0.9	0.3	4.8	1.9	2.1
19	Cellobiose	Zr-SBA-15	10h	95% Methanol	26.4	1.6	0.1	3.1	2.3	1.3
20	Cellulose	Zr-SBA-15	10h	Methanol	16.7	0.1	0.1	0.7	0.2	0.7
21	Cellulose	Zr-SBA-15	10h	95% Methanol	28.1	0.3	0.4	2.0	1.8	1.0
22	Starch	Zr-SBA-15	10h	Methanol	24.1	1.4	0.1	0.9	0.1	0.2
23	Starch	Zr-SBA-15	10h	95% Methanol	26.8	0.7	0.2	1.1	0.6	1.5
24	Erythrose	Zr-SBA-15	1h	Methanol	19.6	0.3	0.7	/	/	/

Reaction conditions: 240 °C, 400 psi N₂ pressure, 0.2g feedstock loading, and 1:2 mass ratio of Zr-SBA-15 catalyst to feedstock. ML: Methyl lactate, GADMA: Glycolaldehyde dimethylacetal, MG: Methyl glycolate, MLE: Methyl levulinate.

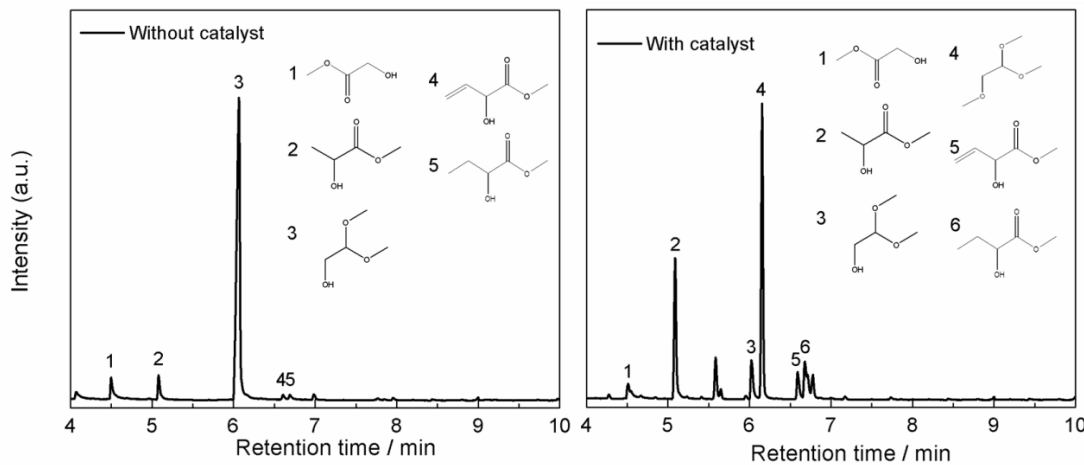


Figure 5.16 GC/MS spectra of products from glycoaldehyde conversion in methanol solvent with Zr-SBA-15 as catalyst. Reaction conditions: 240 °C, 1 h, 400 psi N₂ pressure, 0.2g glycoaldehyde loading, and 1:2 mass ratio of catalyst to feedstock.

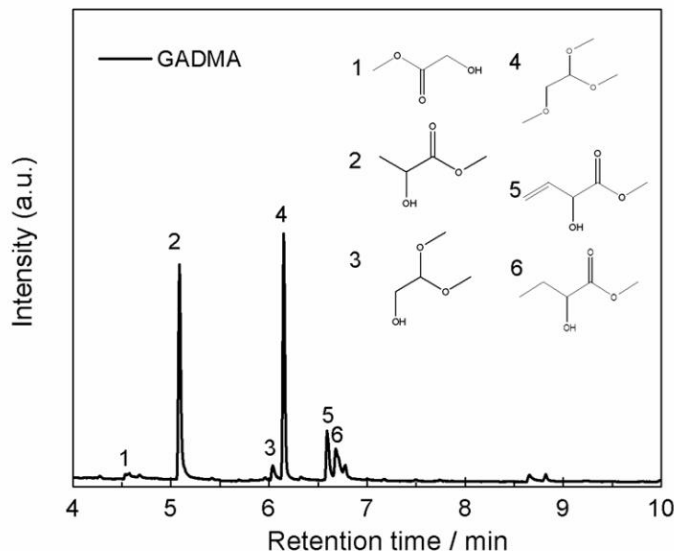


Figure 5.17 GC/MS spectra of products from glycolaldehyde dimethyl acetal conversion in methanol solvent with Zr-SBA-15 as catalyst. Reaction conditions: 240 °C, 1 h, 400 psi N₂ pressure, 0.2g glycolaldehyde dimethyl acetal loading, and 1:2 mass ratio of catalyst to feedstock.

Furfural was the undesirable by-product from the dehydration of xylose, usually catalyzed by Brønsted acid. The furfural yield decreased sharply at high temperatures or for a long reaction time, while methyl levulinate yield increased at the same time during the xylose conversion with the Zr-SBA-15 catalyst. Using furfural as the probe reactant,

the main product was methyl levulinate in the yields of 3.6% and 33.2% after reactions for 1 h and 10 h, respectively, at 240 °C, as shown in Figure 5.18. Alkyl levulinate is known to be produced from furfuryl alcohol with solid acid catalyst [78]. A hydrogenation step is needed in the conversion of furfural to methyl levulinate, while methanol was the only hydrogen source in the probe reaction. We thus contemplate that furfural was converted into furfuryl alcohol via Meerwein-Ponndorf-Verley (MPV) transfer hydrogenation with methanol as the hydrogen donor, which was probably promoted by the Lewis acid, followed by the conversion of furfuryl alcohol into methyl levulinate through ring-opening reactions with the aid of the weak Brønsted acid sites on the Zr-SBA-15 catalyst. Corma's group demonstrated the intermolecular transfer hydrogenation between alcohols and ketones in organic solvents using Sn-Beta and Zr-Beta as the solid Lewis acid catalysts [79–81].

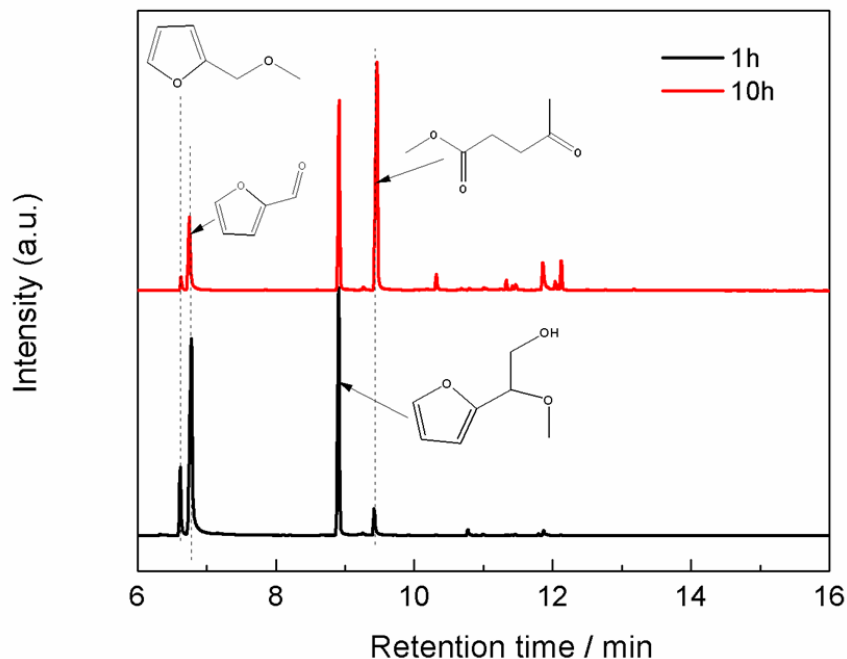


Figure 5.18 GC/MS spectra of products from furfural conversion in methanol solvent with Zr-SBA-15 as catalyst. Reaction conditions: 240 °C, 400 psi N₂ pressure, 0.2 g furfural loading, and 1:2 mass ratio of catalyst to feedstock.

The proposed reaction pathway for the conversion of xylose to ML can be generalized for the conversion of other cellulosic biomass. The retro-aldol condensation of pentoses and hexoses, however, may form different aldehyde or ketone products with solid Lewis acid catalysts [45,71]. The conversion of pentoses to ML can be divided as the following steps: retro-aldol condensation of an aldopentose leads to glyceraldehyde and glycolaldehyde, while retro-aldol condensation of a ketopentose forms dihydroxyacetone and glycolaldehyde. The outcome of both reaction pathways is the formation of a triose and a glycolaldehyde [45]. In contrast, the fragments formed from a hexose depend on the ketose or aldose form. Disintegration of an aldohexose leads to the fragments of a C4 aldotetrose and a C2 glycolaldehyde, while the ketohexose fragmentation results in two C3 fragments, dihydroxyacetone and glyceraldehyde [71]. With a Lewis acid catalyst, however, glucose and fructose can be inter-converted through isomerization before experiencing subsequent reactions [46,82]. Table 3 shows that the disparate yields of ML were produced from glucose and fructose, respectively, while the comparable yields are seen for fructose and sucrose, the dimer of glucose and fructose (products were identified by GC/MS as shown in Figure 5.19). Glucose yielded a lower amount of ML relative to fructose (37.3% versus 44.1%). The difference in the ML yields from different monosaccharides reflects the dynamic equilibrium between the isomerization, retro-aldol condensation and degradation reactions. In all cases, the conversions of both monosaccharides and disaccharides were greater than 99% after 6 h of reaction at 240 °C and the considerable yields of ML were formed using the Zr-SBA-15 catalyst (Table 3). Using disaccharides or polysaccharide including cellobiose, starch, and cellulose as the reactants, substantially lower conversions were observed (products

were identified by GC/MS as shown in [Figure 5.20](#)). Cellobiose and starch, which are soluble in methanol, reached the similar yields of ML, 24.3% and 24.1%, respectively. However, only 16.7% ML was produced from cellulose at 240 °C for a 10 h reaction, suggesting that depolymerization is the bottleneck for cellulose conversion. In order to enhance the yield of ML from cellulose, a small amount of water (5 wt%) was added into methanol to facilitate the hydrolysis of cellulose. As the result, as high as 28.1% yield of ML was obtained directly from cellulose.

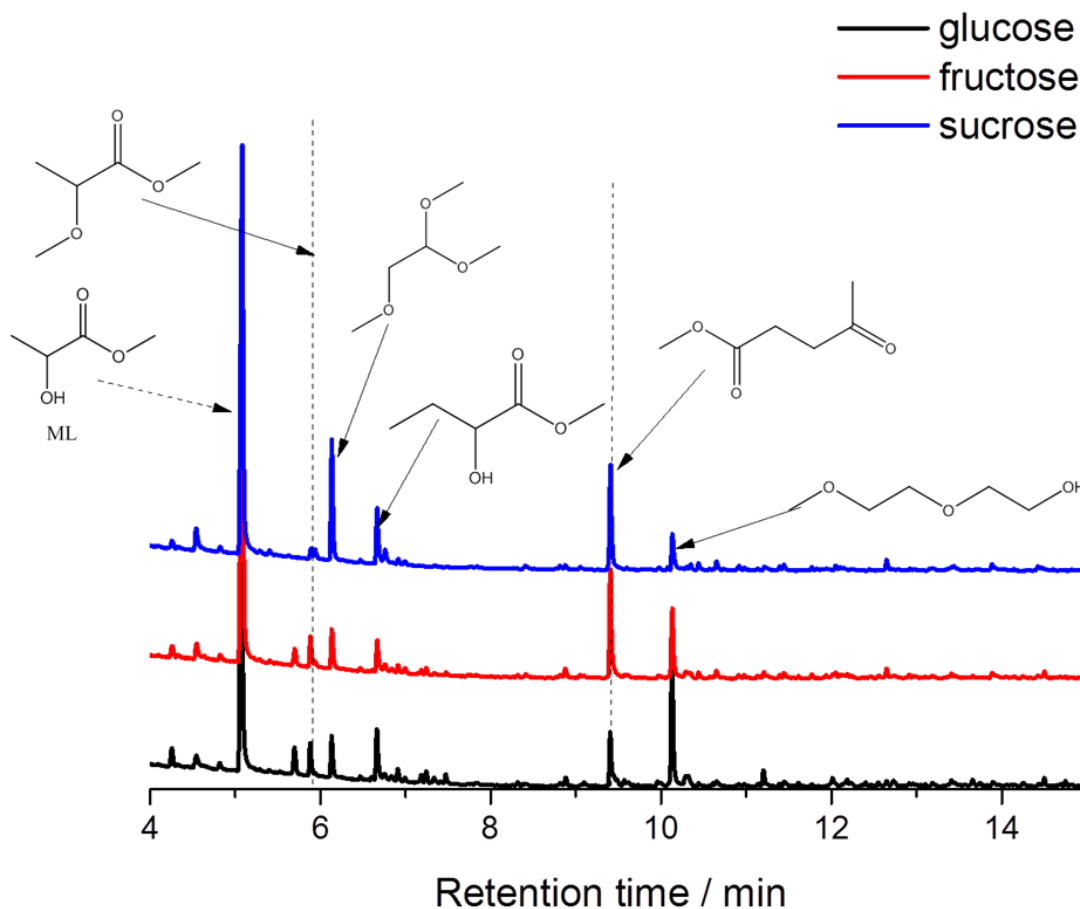


Figure 5.19 GC/MS spectra of the products from the conversion of glucose, fructose and sucrose in methanol solvent with the Zr-SBA-15 catalyst. Reaction conditions: 240 °C, 6 h, 400 psi initial N₂ pressure, 0.2 g feedstock, and 0.1 g catalyst.

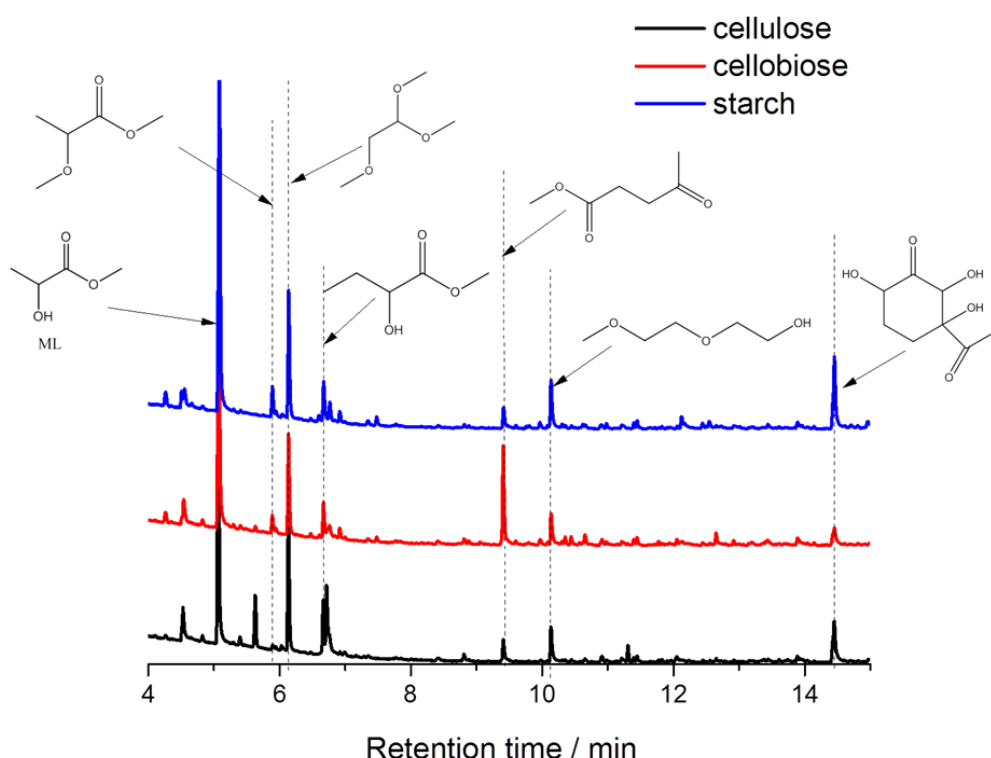


Figure 5.20 GC/MS spectra of the products from the conversion of cellulose, cellobiose and starch in methanol solvent with the Zr-SBA-15 catalyst. Reaction conditions: 240 °C, 10 h, 400 psi initial N₂ pressure, 0.2 g feedstock, and 0.1 g catalyst.

5.3.2: Directly catalytic conversion of cellulose into ethyl lactate via Zr-SBA-15

The selective conversion of cellulose, the most abundant and non-edible biomass, as the renewable carbon resource for the production of value-added chemicals is of vital importance for sustainable economy [3,83–85]. Among biobased chemicals, lactic acid and lactates have attracted much attention as platform chemical building blocks with potential to replace petroleum-based raw chemical materials [39,86–88]. Ethyl lactate (EL) is derived from lactic acid (LA) and ethanol, which are both renewable chemical materials currently made from fermentation of sugars originally from corn. As the commercialized “green” solvent, EL works in numerous chemical applications especially as a photoresist carrier solvent, edge-bead remover, and clean-up solvent for semiconductor manufacture [41,89,90].

Table 5.4 compares the yields of the main products by reacting microcrystalline cellulose with different catalysts, solvents, and feed loadings. The catalytic effect of the Zr-SBA-15 was obvious for promoting the yield of EL. Neither the commercial ZrO₂ nor the pure SBA-15 silica resulted in the high yields of EL (8.2% and 5.1%, respectively), whereas the EL yield increased to ~30% over the Zr-SBA-15 after reacting cellulose at 260 °C for 6 h in the ethanol-water solvent (95% ethanol and 5% of water). Without adding a catalyst, the EL yield of ~2.1% was obtained. Note that without catalyst or with the pure SBA-15, the noticeable amounts of HMF and furfural were yielded. The much higher yields of C4 compounds of ethyl 2-hydroxybutanoate (EHB) were obtained over the Zr-SBA-15 than over either the ZrO₂ or the SBA-15. These results suggest that maintaining the strong Lewis acidity of the Zr-SBA-15 is crucial for the conversion of cellulose to EL.

Table 5.4. The comparison of the main products yields of cellulose conversion with and without catalysts in different solvents.

Entr y	Catalyst	Solvent	Carbon Yield/%					S.R. /%
			EL	EHB	ELE	Furfura l	HMF	
1	/	95% ethanol	2.1	1.0	0.2	0.8	6.6	52.3
2	SBA-15	95% ethanol	5.1	1.8	0.3	2.2	5.7	30.8
3	ZrO ₂	95% ethanol	8.2	2.3	0.6	0.1	0.1	21.5
4	Zr-SBA-15	95% ethanol	30.1	13.5	2.2	0.3	0.1	8.6
5 ^a	Zr-SBA-15	95% ethanol	26.7	10.6	1.2	0.2	0.1	16.1
6 ^b	Zr-SBA-15	95% ethanol	24.9	6.3	0.6	0.4	0.1	33.8
7	Zr-SBA-15	Water	1.4 ^c	/	20.9 ^d	0.7	14.6	19.8

Reaction condition: 260 °C, 400 psi initial pressure of N₂, 20 g solvent (95% ethanol and 5% water), 6 h, 0.2 g cellulose, 0.1 g catalyst. EL: Ethyl lactate; EHB: Ethyl 2-hydroxybutanoate; ELE: Ethyl levulinate. ^a 1 g cellulose, 0.5 g catalyst, ^b 2 g cellulose, 1 g catalyst, ^c lactic acid, ^d levulinic acid.

In fact, one of the major barriers to cellulose conversion is the recalcitrance of cellulose to depolymerization [40]. In our “one-pot” catalytic process, several factors enable the selective conversion of cellulose to EL. Firstly, water in the supercritical ethanol-water mixture solvent ([Table 5.4 entries 1-6](#)) weakens the intra-molecular hydrogen bonds responsible for the robustness of cellulose and thus decreases the crystallinity of cellulose until dissolution. Secondly, Zr⁴⁺ metal centers with empty d orbitals in the silica framework serve as water-tolerant Lewis acid sites and the limited hydrophobic property of silica may stabilize the Zr⁴⁺ Lewis acidic sites inside the pores of the SBA-15 silica in the presence of 5 wt% water. In contrast, the loss of Lewis acidity of the Zr-SBA-15 catalyst was observed in the subcritical water: only a trace amount of lactic acid (1.4%) was produced whereas HMF (14.6%) and levulinic acid (20.9%) were the main products ([Table 5.4 entry 7](#)). The transformation of cellulose to EL was thus completed in the supercritical ethanol-water mixture at moderate temperatures and pressures which are sufficient for the depolymerization of cellulose but more compatible for stabilizing the solid Lewis acid sites of the Zr-SBA-15 catalyst. It is noted that the cellulose loading affected the yield of EL to a lesser extent. With increasing the cellulose loading from 1 wt% to 10 wt% and keeping the constant mass ratio of cellulose to catalyst, the EL yield decreased from ~30% to ~25% while those of solid residue increased from ~8.6% to ~34%. The solid residue included unreacted cellulose, and thus longer reaction time would be needed at higher loadings of cellulose.

To further understand the role of water in ethanol, anhydrous ethanol and ethanol-water mixture solutions at different water to ethanol ratios were used under super- and sub- critical conditions. The critical conditions of ethanol-water solutions, adapted from

the data reported by Barr-David and Dodge [91], were shown in Table 5.5. We found that the water content in the ethanol-water solutions has the profound effect on the yield of EL. As shown in Figure 5.21, in supercritical anhydrous ethanol, the yield of EL from cellulose was ~17% after reacting for 6 h at 260 °C, while by adding 5% water, the EL yield was almost doubled (~30%) under the otherwise identical conditions. The yield of solid residue (the indicator of unreacted cellulose here) decreased significantly from ~20% to ~8% with adding 5% water in the pure ethanol solvent, suggesting that water facilitates the deconstruction of cellulose. Kim and coworkers compared the effect of subcritical water to supercritical ethanol on the rate of liquefying lignocellulosic biomass and found that faster hydrolytic cleavage was associated with subcritical water, while slower pyrolytic cleavage was dominant in supercritical ethanol in the temperature range of 250–350 °C [56]. Therefore adding a small amount of water (5 wt%) in supercritical ethanol might enhance the hydrolytic degradation of cellulose and thus much faster depolymerization of cellulose was achieved. On the other hand, in supercritical alcohol, the repolymerization of intermediates was suppressed due to the reactions between ethanol and biomass intermediates such as aldehydes, carboxylic acids, ketones, etc. Therefore, we think that faster depolymerization of the cellulose and slower recombination of the intermediates in the ethanol-water mixture solvents (up to 15 wt% water) enhanced the yields of EL. The synergistic effects of alcohol and water on biomass liquefaction were also observed by other groups [92,93]. Yet the EL yield reached the maximum as the proportion of water was 5 wt%, further increasing the ratio of water to ethanol decreased the EL yield. Higher water proportion in the solvent may result in two consequences: deactivating the Lewis acid sites and increasing the critical

temperatures of the mixed solvent. The deactivation of Lewis acid caused by water adsorption leads to the transformation of Lewis acid to Brønsted acid [94,95]. When the water proportion is >20 wt%, the critical temperature of the ethanol-water mixture is > 260 °C. However, no distinct difference of product distribution was observed between the supercritical solvent containing 15 wt% water and the subcritical solvent with 25 wt% water. Thus the inhibitive effect of water on the Lewis acid sites, instead of the change of the ethanol-water solvent states, is the primary factor causing the decrease of the yield of EL with increasing the water content in the ethanol-water mixtures (> 5 wt% water).

Table 5.5. Critical conditions of the ethanol-water solutions at different ethanol to water ratios.

Ethanol		Water		Supercritical Pressure psi	Supercritical Temperature °C
Mole percentage%	Weight percentage%	Mole percentage%	Weight percentage%		
100	100	0	0	922	242
95	98.0	5	2.0	950	243
90	95.8	10	4.2	975	245
85	93.5	15	6.5	1000	247
80	91.1	20	8.9	1060	250
75	88.5	25	11.5	1090	253
70	85.6	30	14.4	1120	256
65	82.6	35	17.4	1190	259
60	79.3	40	20.7	1250	263
55	75.8	45	24.3	1300	268
50	71.9	50	28.1	1370	274

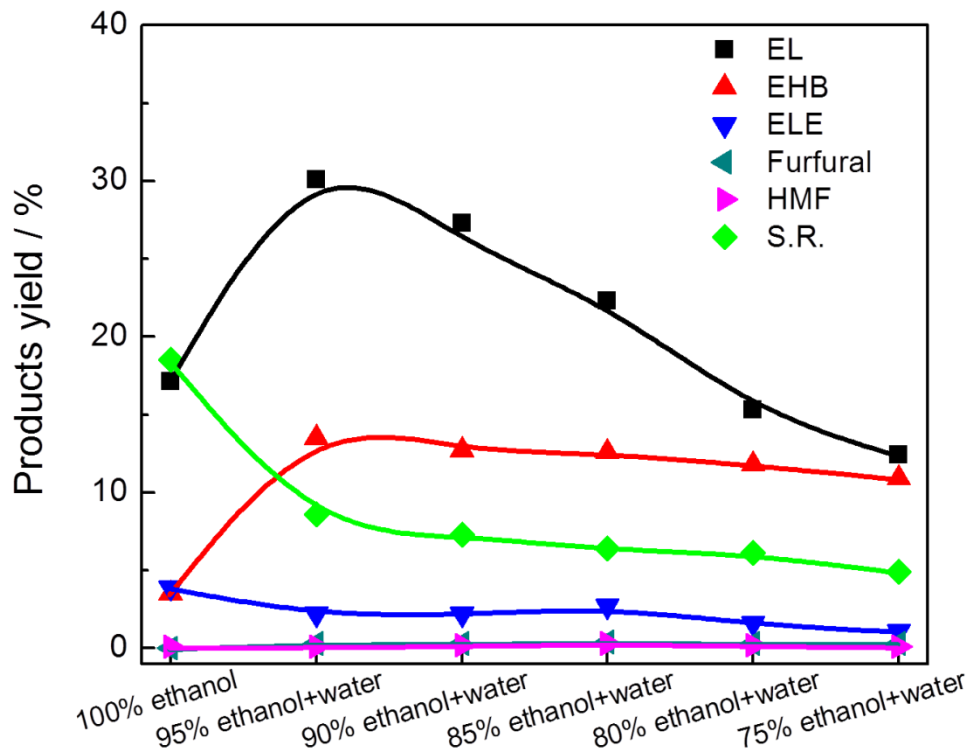


Figure 5.21. Solvent effect on the yields of liquid-phase products from the cellulose conversion with the Zr-SBA-15 catalyst. Reaction conditions: 260 °C, 6 h, 400 psi initial pressure of N₂, 0.2 g cellulose, 0.1g catalyst. EL: Ethyl lactate; EHB: Ethyl 2-hydroxybutanoate; ELE: Ethyl levulinate.

To optimize the yield of EL, cellulose was converted at different process conditions. As shown in Figure 5.22 and Figure 5.23(c), varying temperatures has a pronounced effect on the production yield of EL. Below 200 °C, cellulose did not show an appreciable conversion. At 240 °C (subcritical condition), the highest yield of 25.4% was achieved after a 10 h reaction. A steadily increasing amount of EL till ~30% was produced at 250 °C (near-critical condition) yet it took 6 h to reach the plateau. While at 260 °C (supercritical condition), after 2 h, the yield of EL varied little and reached the maximum yield of 30.3%. Similarly, the yields of EHB and ethyl levulinate (ELE) consistently increased when the reaction time was extended. Conversely, the HMF and

furfural yields consistently decreased with extended reaction times. Brønsted acids can hydrolyze cellulose to glucose, followed by the dehydration of glucose to HMF [96,97]; thus, the co-existence of furfural, HMF and EL in the final products indicates that the Lewis acid and Brønsted acid sites co-existed on the Zr-SBA-15 catalyst, which was also confirmed by the pyridine-FTIR characterization ([Figure 5.15](#)). Of particular note is the fact that HMF and furfural were almost completely vanished after 4 h at 260 °C. Higher temperatures led to the transformation of HMF and furfural to ELE through a Bronsted acid catalyzed rehydration and a transfer hydrogenation reaction promoted by Lewis acid [98], respectively. Notably, the solid residue decreased steadily with reaction time indicating the conversion of cellulose increased. The effect of different catalyst loading amounts on the conversion of cellulose was depicted in [Figure 5.24](#). The yield of EL showed the steady uptrend as the catalyst loading increased, reaching ~33% as the mass ratio of catalyst to cellulose was 1:1. The yield of ELE also increased steadily with increasing the catalyst loading but was much lower than that of EL. While the EHB increased first with increasing the catalyst loading and then decreased as the catalyst-to-cellulose ratio was higher than 0.5. Contrarily, the yields of HMF and furfural consistently decreased as the catalyst loading increased.

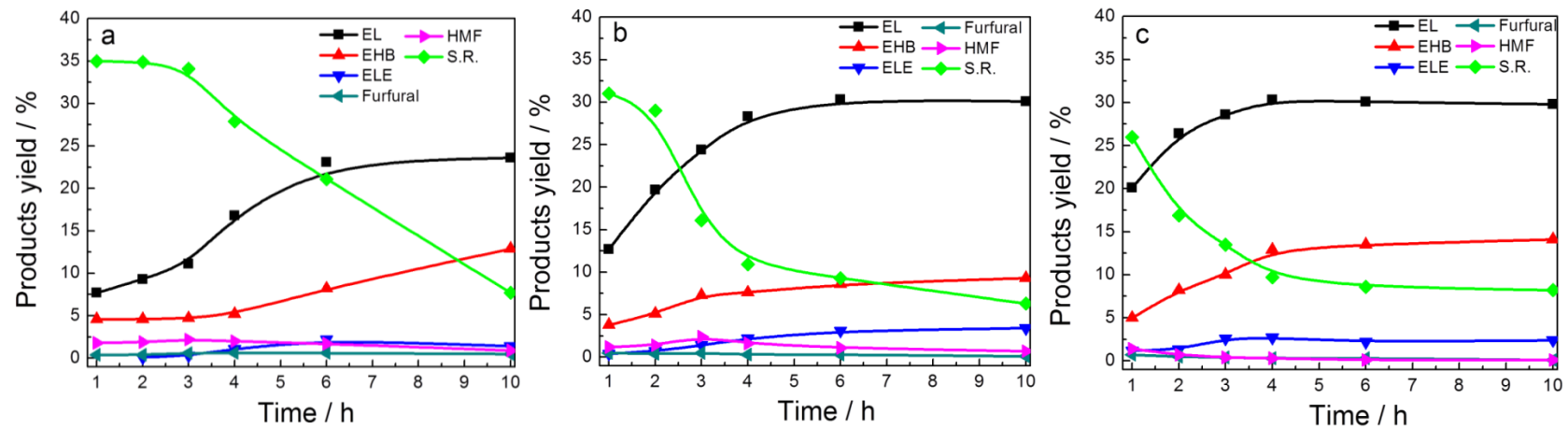


Figure 5.22 Effects of temperature and reaction time on the yields of the products from the conversion of cellulose with the Zr-SBA-15 catalyst in ethanol-water mixture solution (95 wt% ethanol and 5 wt% water). Reaction conditions: 20 g solvent, 400 psi initial pressure of N_2 , 0.2 g cellulose, 0.1 g catalyst, and (a) 240 °C; (b) 250 °C; (c) 260 °C. EL: Ethyl lactate; EHB: Ethyl 2-hydroxybutanoate; ELE: Ethyl levulinate.

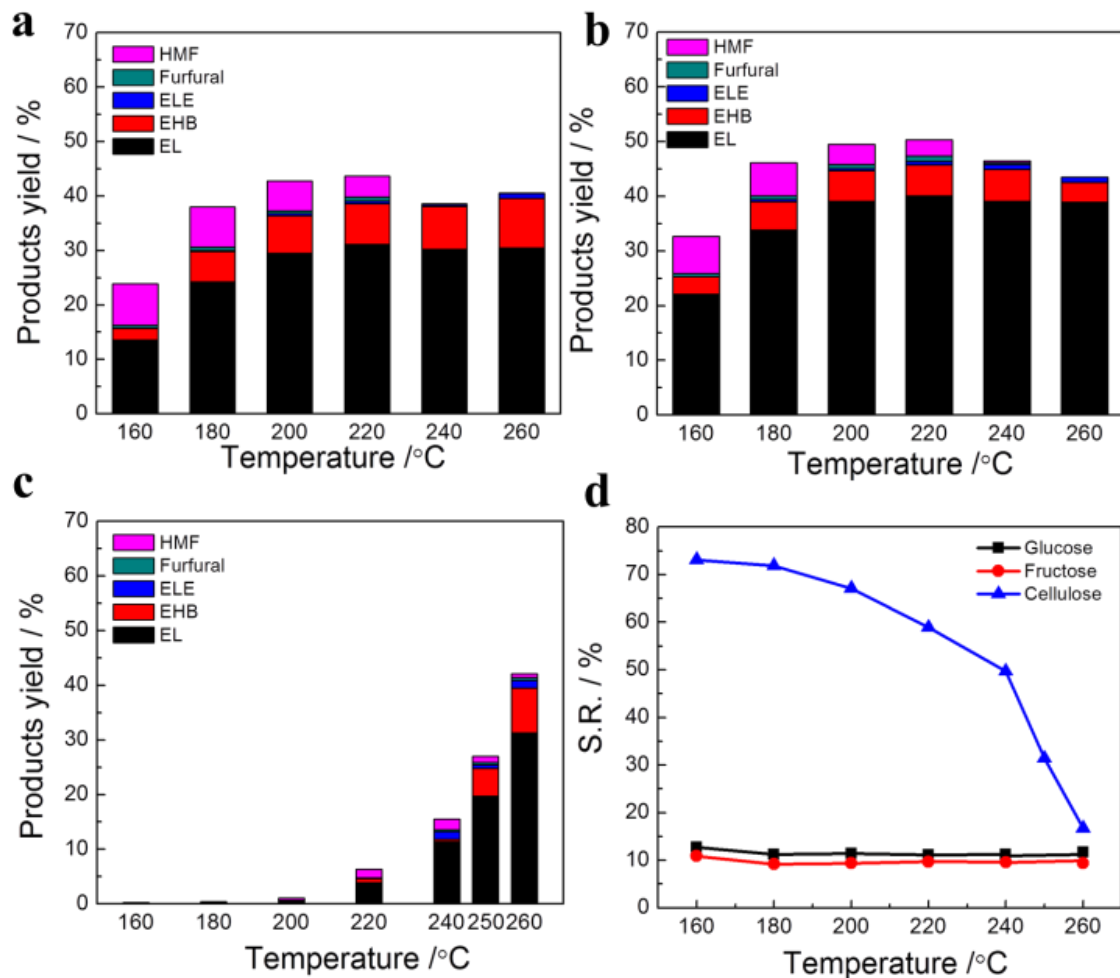


Figure 5.23 Different feedstocks conversion at different reaction temperatures with the Zr-SBA-15 catalyst. (a) Glucose conversion; (b) fructose conversion; (c) cellulose conversion; (d) solid residue (S.R.) after the conversion of the different feedstocks. Reaction conditions: 2 h, 400 psi initial pressure of N_2 , 20 g solvent (95% ethanol and 5% water), 0.2 g biomass substrate, and 0.15 g catalyst. EL: Ethyl lactate; EHB: Ethyl 2-hydroxybutanoate; ELE: Ethyl levulinate.

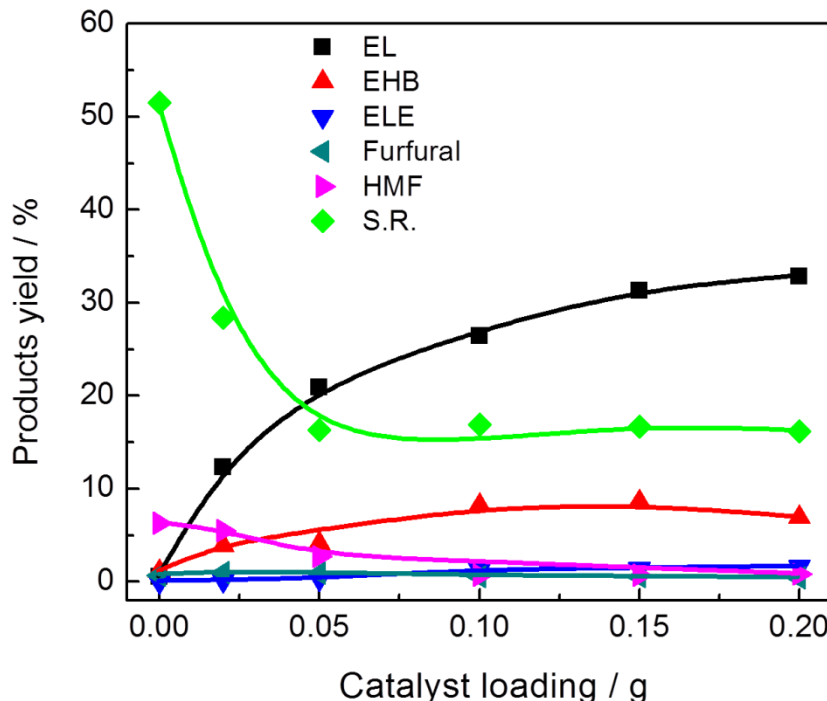


Figure 5.24 Effect of catalyst loading on the yields of the products from the conversion of cellulose with the Zr-SBA-15 catalyst in ethanol-water mixture solution (95 wt% ethanol and 5 wt% water). Reaction conditions: 260 °C, 2 h, 400 psi initial pressure of N₂, 0.2 g cellulose, 20 g solvent. EL: Ethyl lactate; EHB: Ethyl 2-hydroxybutanoate; ELE: Ethyl levulinate.

We propose that the reaction pathway of converting cellulose to EL over the Zr-SBA-15 catalyst begins at the hydrolytic / pyrolytic deconstruction of cellulose, as shown in Figure 5.25. Cellulose decomposed to glucose which was then isomerized to fructose. The Zr⁴⁺ ions as the Lewis acid sites interacted with the carbonyl group of fructose, breaking it down to glyceraldehyde and dihydroxyacetone via retro-aldol condensation. Glyceraldehyde underwent the dehydration to form 2-hydroxypropenal, then to pyruvaldehyde through keto-enol tautomerization, and finally to EL in ethanol solvent. Glucose might also lead to one C4 fragment of aldo-tetrose and another C2 piece of glycolaldehyde, which are the precursors of C4 and C2 acid ester products. To validate our hypothesis of the reaction pathway, glucose and fructose were used as the probe reactants (Figure 5.23a and b). The glucose was readily converted to EL in a ~30% yield

at a low temperature of 200 °C. Yet, the yield of EL reached as high as ~40% from fructose. The position of the C-C bond cleavage via retro-aldol condensation of ketohexose and aldohexose led to the different yields of alkyl lactates, respectively and thus the higher yield of EL from fructose is due to the preferred disintegration of the carbon bond between the C3 and C4 position [45,48,71]. Figure 5.23d clearly showed that at subcritical conditions (bond °C), the conversion of cellulose was low, which was corresponding to the high solid residue yield of 50%-70%, while the solid residue yield decreased sharply at near-critical (250 °C) and supercritical (260 °C) conditions. Thus the depolymerization of cellulose was likely the rate-limiting step of converting cellulose to EL with the Zr-SBA-15 catalyst.

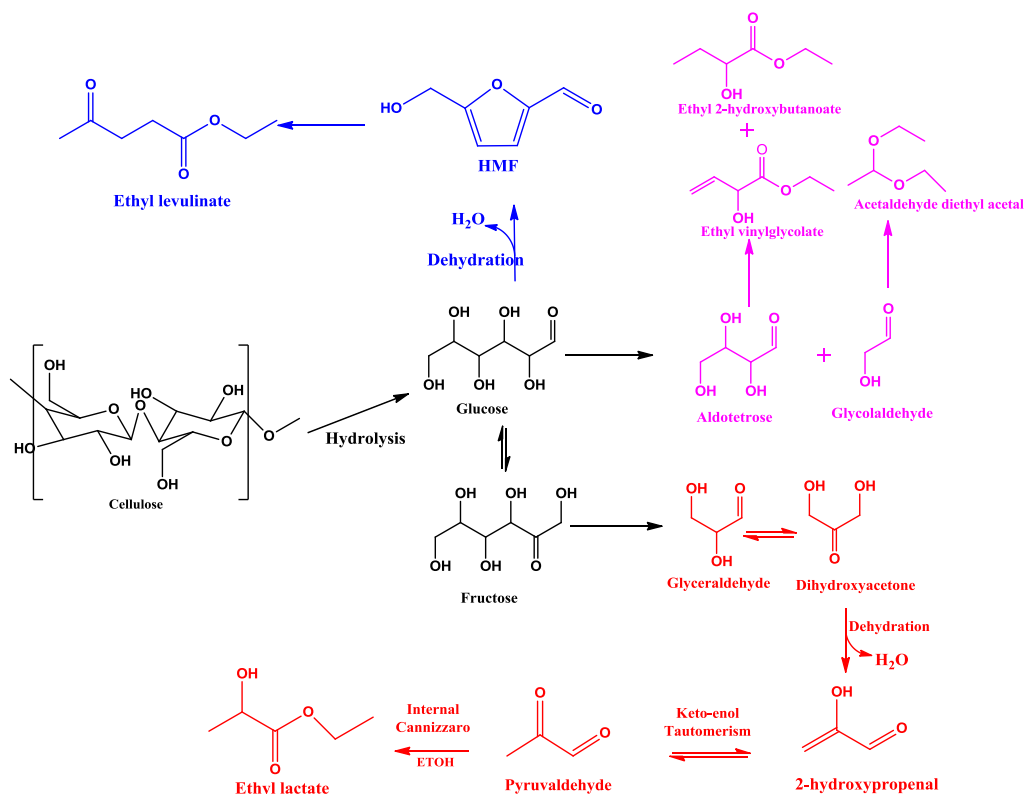


Figure 5.25. Proposed reaction mechanism for the conversion of cellulose to ethyl lactate in ethanol solvent with the Zr-SBA-15 catalyst.

The stability of the Zr-SBA-15 catalyst is of importance in the supercritical ethanol-water solvents. Over the three consecutive runs at 260 °C, the yield of EL from cellulose steadily decreased with the re-used catalyst without regeneration ([Figure 5.26](#)), which implied that the re-polymerized humins might inhibit the catalyst's activity. The yields of furfural and HMF increased with increasing the re-use cycles of the catalyst. Since only the weak Brønsted acid sites on the fresh Zr-SBA-15 catalyst were identified, the deposition of the cellulose-derived solid residues on the spent Zr-SBA-15 catalyst apparently changed the surface properties. As shown in [Figure 5.27](#), the ATR-FTIR spectra of the spent Zr-SBA-15 catalyst exhibited a broad peak at ~ 3380 cm⁻¹ which is attributed to the stretching -OH band; the peaks at 2960 to 2840 cm⁻¹ are the stretching vibration signal of the CH band in -CH₂- or -CH₃ groups; the peaks located at 1730 cm⁻¹ is probably the stretching vibrations of C=O bands in carboxylic acids and the bands at 1460 and 1360 cm⁻¹ belong to the -CH₂- and -CH₃ deformation vibrations [[99–101](#)]. Therefore, carboxylic acid groups were identified on the spent catalyst surface which enhanced the Brønsted acidity and led to the higher yields of HMF and furfural. The organic solid residues on the spent catalysts can be easily removed by calcination in air flow. According to the FTIR characterization, the regenerated catalyst showed the similar spectra with the fresh catalyst. Correspondingly, after the regeneration, the yield of EL was much steady in the consecutive runs ([Figure 5.28](#)). The TEM images ([Figure 5.29](#)) also showed that the structure of the regenerated catalyst was still highly ordered and the average pore size was unchanged compared to the fresh sample.

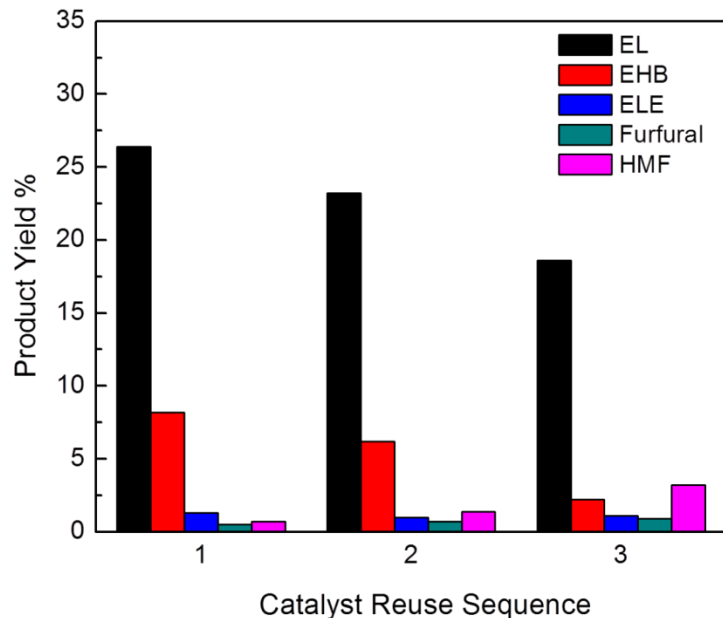


Figure 5.26 Re-use of the spent Zr-SBA-15 catalyst for the conversion of cellulose in ethanol-water solvent. The spent catalyst was not regenerated. Reaction conditions: 260 °C, 2 h, 400 psi initial pressure of N₂, 20 g ethanol-water mixture solvent (95 wt % ethanol and 5 wt% water), 0.2 g cellulose, and 0.1 g catalyst. EL: Ethyl lactate; EHB: ethyl vinylglycolate and ethyl 2-hydroxybutanoate; ELE: Ethyl levulinate.

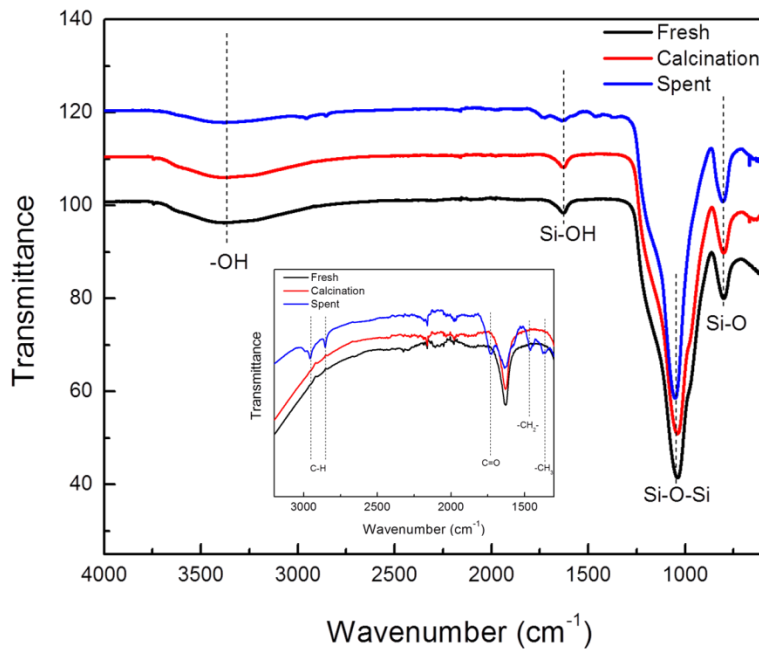


Figure 5.27 Comparison of the ATR-FTIR spectra of the fresh, spent, and regenerated Zr-SBA-15 catalysts. The spent catalyst was used once and was not regenerated. The regenerated Zr-SBA-15 was used five times and then regenerated by calcination. Reaction conditions: 260 °C, 2 h, 400 psi initial pressure of N₂, 20 g ethanol-water mixture solvent (95 wt % ethanol and 5 wt% water), 0.2 g cellulose, and 0.1 g catalyst.

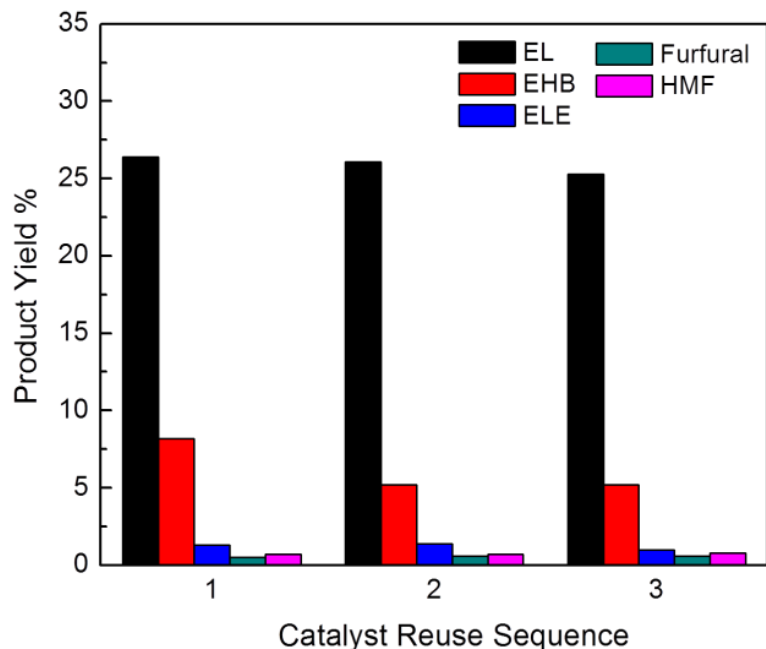


Figure 5.28 Effect of re-use of the Zr-SBA-15 catalyst on the yields of the main products from the conversion of cellulose in the ethanol-water mixture solvent containing 5 wt% water. The spent catalyst was regenerated by the calcination in air at 550 °C for 5 h. Reaction conditions: 260 °C, 2 h, 400 psi initial pressure of N₂, 0.2 g cellulose, 0.1 g catalyst. EL: Ethyl lactate; EHB: ethyl 2-hydroxybutanoate; ELE: Ethyl levulinate.

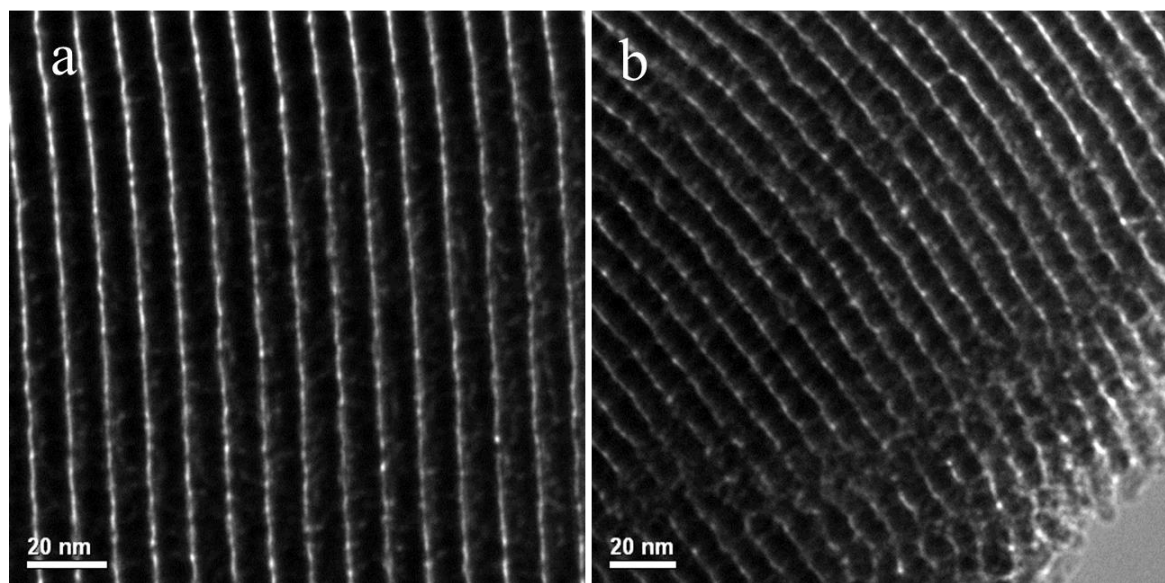


Figure 5.29 High-resolution transmission electron microscopy (HRTEM) images of Zr-SBA-15: (a) fresh sample; (b) spent sample after three time use and regenerated in flowing air at 550 °C for 6 h.

The stability of the ethanol solvent itself is also important from the perspective of process intensification since the recyclability of the solvent may impact the overall process economics. In the presence of the solid Lewis catalyst and at the supercritical condition, ethanol may undergo reactions such as gasification, dehydration, dehydrogenation, etc. However, to our surprise, ethanol was very stable and no gaseous products (e.g., H₂, CO, CO₂, C₂H₄) were detected ([Figure 5.30](#)), while the only liquid-phase product was acetaldehyde diethyl acetal (ADA) in the control reaction without adding any biomass feedstock in the supercritical ethanol-water mixture solvent with the Zr-SBA15 catalyst ([Figure 5.31](#)). Yet the yield of ADA was nearly negligible, ~0.04% (carbon percent yield from ethanol), after 6 h. We assumed that acetaldehyde could be produced from the dehydrogenation of ethanol [\[102\]](#) which was the potential hydrogen donor for transfer hydrogenation reactions. And ADA was produced by reacting acetaldehyde with ethanol as follows: 2EtOH + CH₃CHO → ADA + H₂O [\[103\]](#). The formation of ADA from ethanol was a reversible reaction as the ADA yield decreased sharply with increasing the water content in ethanol indicating that water inhibited the ADA production ([Figure 5.32](#)). However, a much higher amount of ADA, ~0.69% or ~26.7% carbon yields based on ethanol and cellulose, respectively, was detected during the conversion of cellulose under the otherwise identical conditions. Thus, ADA could be one of the main by-products yielded from the possible C2 intermediate, glycolaldehyde, during the cellulose conversion. We found that approximately 21.8% ADA was produced with glycolaldehyde as the feedstock; meanwhile, considerable amounts of EL and EHB were also yielded ([Figure 5.33](#)). The formation of the C3 and C4 acid esters from the C2 aldehyde indicates that the C-C bond forming aldol condensation occurred on the Lewis

acidic Zr-SBA-15 catalyst and then the retro-aldol condensation reactions took place thereafter. However, it is unclear whether or not the cellulose derived intermediates and products promoted or inhibited the dehydrogenation of ethanol to form ADA.

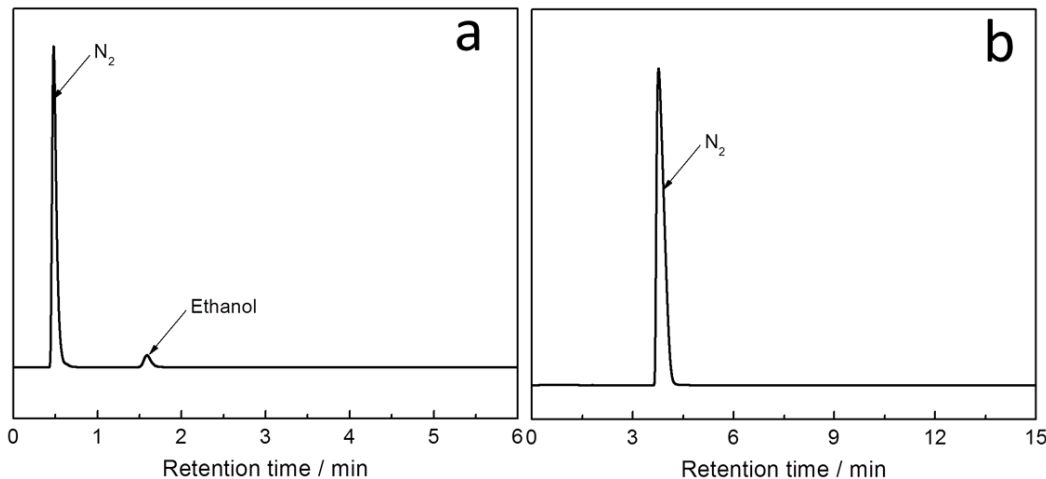


Figure 5.30 GC spectra of the gas-phase products from the ethanol-water solvent stability test. Reaction conditions: 260 °C, 6 h, 400 psi initial pressure of N₂, 20 g solvent (95 wt% ethanol and 5 w% water), no biomass feedstock, 0.1 g Zr-SBA-15 catalyst. a) The gas products were separated in Carbowax column; and b) the gas products were separated in other columns (listed in section 1.4).

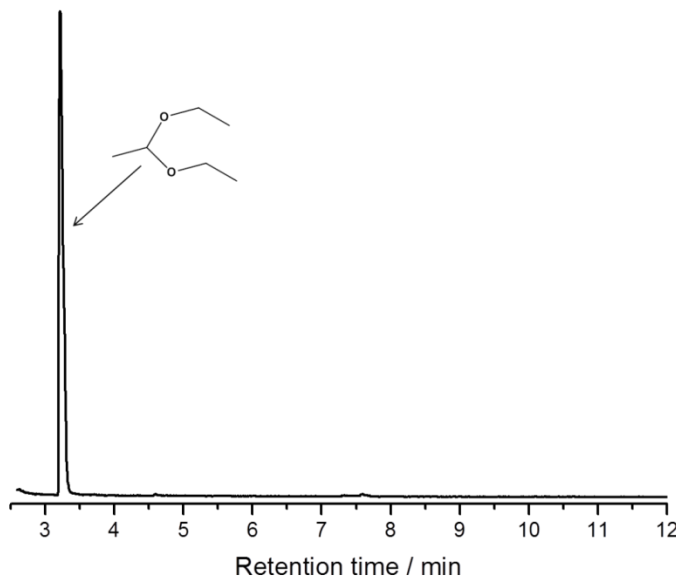


Figure 5.31 GC/MS spectra of the liquid-phase products from the ethanol-water solvent stability test. Reaction conditions: 260 °C, 6 h, 400 psi initial pressure of N₂, 20 g solvent (95 wt% ethanol and 5 w% water), no biomass feedstock, 0.1 g Zr-SBA-15 catalyst.

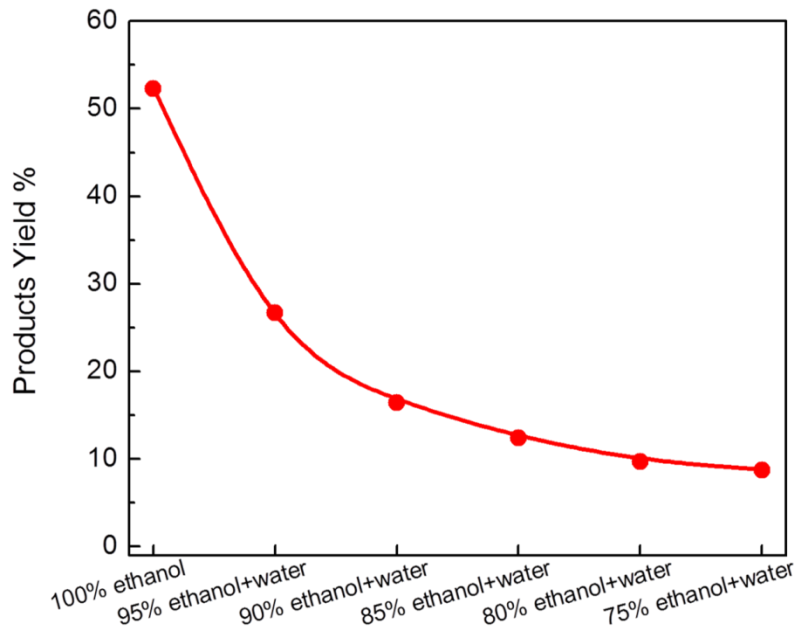


Figure 5.32 Solvent effects on the yield of ADA from the cellulose conversion with the Zr-SBA-15 catalyst. Reaction conditions: 260 °C, 6 h, 400 psi initial pressure of N₂, 0.2 g cellulose, 0.1 g catalyst.

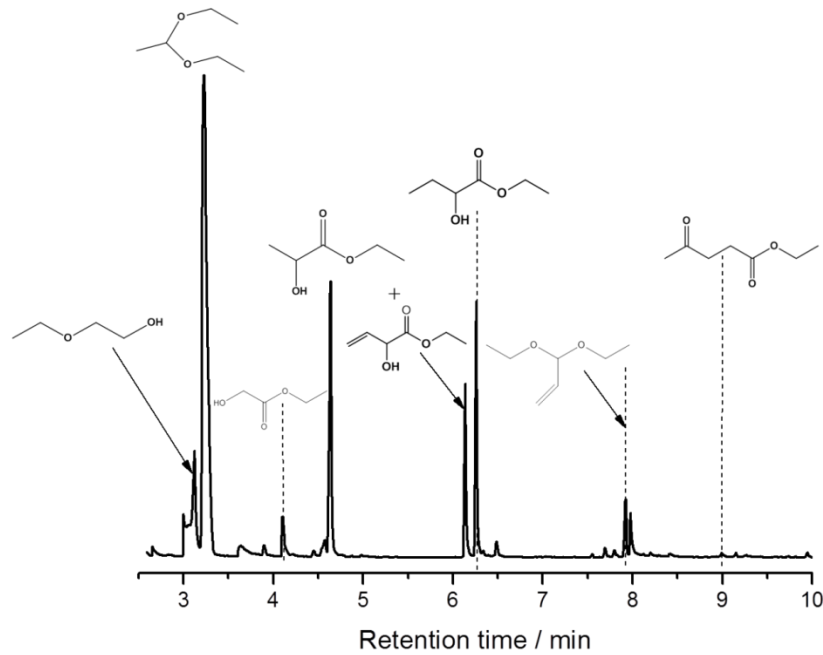


Figure 5.33 GC/MS spectra of the liquid-phase products from the conversion of glycolaldehyde dimer in the ethanol-water mixture solvent (95 wt% ethanol and 5 w% water) with the Zr-SBA-15 catalyst. Reaction conditions: 260 °C, 6 h, 400 psi initial pressure of N₂, 0.2 g glycolaldehyde dimer and 0.1 g catalyst.

5.4: Conclusions

In summary, we demonstrated that methyl lactate was generated from various carbohydrates in methanol solution with the Zr-SBA-15 catalysts under different reaction conditions. Under the optimum conditions, the highest methyl lactate yields were 42% and 44% from xylose and fructose, respectively, with the Zr-SBA-15 catalyst. The Zr-SBA-15 catalyst was relatively stable after five consecutive catalytic cycles without regeneration to produce methyl lactate from xylose. We proposed that the Lewis acid sites on the Zr-SBA-15 facilitated the retro-aldol condensation of carbohydrates, which is the initial step of the conversion of carbohydrates to methyl lactate. Through the probe reaction studies, we conclude that Zr-SBA-15 also catalyzed aldol condensation of C2 aldehydes to form C4 and C6 compounds, followed by subsequent retro-aldol condensation, and finally to produce methyl lactate. Under the tested conditions, the highest ethyl lactate yield was ~33% at 260 °C in the supercritical 95:5 (w/w) ethanol/water mixture solvent. After regeneration, the Zr-SBA-15 catalyst exhibited excellent stability after three consecutive catalytic reaction cycles for ethyl lactate production. The addition of appropriate amount of water (5 wt% in this study) in ethanol, as well as the weak Bronsted acid sites on Zr-SBA-15, facilitated the hydrolysis of cellulose. The water-tolerant Lewis acidity of the Zr-SBA-15 catalyst was crucial to produce ethyl lactate from saccharified cellulose through a series of isomerization, retro-aldol condensation, Cannizzaro, and esterification reactions. The 95:5 (w/w) ethanol/water mixture solvent was relatively stable under the test conditions. Overall, this one-pot process using the Zr-SBA-15 catalyst is efficient and environmentally-friendly to produce lactic acid esters from cellulosic biomass feedstocks.

5.5: References

1. Braden, D.J., Henao, C.A., Heltzel, J., et al. (2011) Production of liquid hydrocarbon fuels by catalytic conversion of biomass-derived levulinic acid. *Green Chem.* **13** (7), 1755–1765.
2. Girisuta, B. (2007) “Levulinic acid from lignocellulosic biomass.”
3. Geboers, J.A., Van de Vyver, S., Ooms, R., et al. (2011) Chemocatalytic conversion of cellulose: opportunities, advances and pitfalls. *Catal. Sci. Technol.* **1** (5), 714–726.
4. Deng, H., Lin, L., and Liu, S. (2010) Catalysis of cu-doped co-based perovskite-type oxide in wet oxidation of lignin to produce aromatic aldehydes. *Energy & Fuels* **24** (13), 4797–4802.
5. Deng, W., Wang, Y., Zhang, Q., and Wang, Y. (2012) Development of bifunctional catalysts for the conversions of cellulose or cellobiose into polyols and organic acids in water. *Catal. Surv. from Asia* **16** (2), 91–105.
6. Hegner, J., Pereira, K.C., DeBoef, B., and Lucht, B.L. (2010) Conversion of cellulose to glucose and levulinic acid via solid-supported acid catalysis. *Tetrahedron Lett.* **51** (17), 2356–2358.
7. Jow, J., Rorrer, G.L., Hawley, M.C., and Lamport, D.T.A. (1987) Dehydration of d-fructose to levulinic acid over LZY zeolite catalyst. *Biomass* **14** (3), 185–194.
8. Karski, S., and Paryjczak, T. (2003) Selective oxidation of glucose to gluconic acid over bimetallic Pd – Me catalysts (Me = Bi , Tl , Sn , Co). *Kinet. Catal.* **44** (5), 618–622.
9. Mellaerts, R., Aerts, C.A., Van Humbeeck, J., et al. (2007) Enhanced release of itraconazole from ordered mesoporous SBA-15 silica materials. *Chem. Commun.* (13), 1375–1377.
10. Katiyar, A., Yadav, S., Smirniotis, P.G., and Pinto, N.G. (2006) Synthesis of ordered large pore SBA-15 spherical particles for adsorption of biomolecules. *J. Chromatogr. A* **1122** (1-2), 13–20.
11. Valle-vigón, P., Sevilla, M., and Fuertes, A.B. (2012) Sulfonated mesoporous silica – carbon composites and their use as solid acid catalysts. *Appl. Surf. Sci.* **261**, 574–583.
12. Koster, R., Linden, B. Van Der, Poels, E., and Bliek, A. (2001) The mechanism of the gas-phase esterification of acetic acid and ethanol over MCM-41. *J. Catal.* **204** (2), 333–338.

13. Agirrezabal-Telleria, I., Requies, J., Güemez, M.B., and Arias, P.L. (2014) Dehydration of d-xylose to furfural using selective and hydrothermally stable arenesulfonic SBA-15 catalysts. *Appl. Catal. B Environ.* **145**, 34–42.
14. Marcilly, C.R. (2000) Where and how shape selectivity of molecular sieves operates in refining and petrochemistry catalytic processes. *Top. Catal.* **13**, 357–366.
15. Chen, S.-Y., Lee, J.-F., and Cheng, S. (2010) Pinacol-type rearrangement catalyzed by Zr-incorporated SBA-15. *J. Catal.* **270** (1), 196–205.
16. Jiang, T.S., Zhou, X.P., Li, Y.H., et al. (2011) Characterization of Zr-based MCM-41 mesoporous molecular sieves obtained by microwave irradiation or hydrothermal method. *Inorg. Mater.* **47** (3), 296–302.
17. Zhu, J., Gao, Q., and Chen, Z. (2008) Preparation of mesoporous copper cerium bimetal oxides with high performance for catalytic oxidation of carbon monoxide. *Appl. Catal. B Environ.* **81** (3-4), 236–243.
18. Lima, S., Antunes, M.M., Fernandes, A., et al. (2010) Acid-catalysed conversion of saccharides into furanic aldehydes in the presence of three-dimensional mesoporous Al-TUD-1. *Molecules* **15** (6), 3863–3877.
19. Morey, M.S., Brien, S.O., Schwarz, S., and Stucky, G.D. (2000) Hydrothermal and postsynthesis surface modification of cubic, MCM-48, and ultralarge pore SBA-15 mesoporous silica with titanium. *Chem. Mater.* **12** (4), 898–911.
20. Kumaresan, L., Prabhu, A., Palanichamy, M., and Murugesan, V. (2010) Mesoporous Ti-KIT-6 molecular sieves: Their catalytic activity in the epoxidation of cyclohexene. *J. Taiwan Inst. Chem. Eng.* **41** (6), 670–675.
21. Pan, Q. (2013) “Intrinsic kinetics of lower alcohols: C₂, C₃ dehydration over Lewis acidic ordered mesoporous silicate: Zr-KIT-6.”
22. Kim, T., Kleitz, F., Paul, B., and Ryoo, R. (2005) MCM-48-like large mesoporous silicas with tailored pore structure : facile synthesis domain in a ternary triblock copolymer - butanol - water system. *J. Am. Chem. Soc.* (2), 7601–7610.
23. Pan, Q., Ramanathan, A., Snavely, W.K., et al. (2013) Synthesis and dehydration activity of novel Lewis Acidic ordered mesoporous silicate: Zr-KIT-6. *Ind. Eng. Chem. Res.* **52** (44), 15481–15487.
24. Bérubé, F., Nohair, B., Kleitz, F., and Kaliaguine, S. (2010) Controlled postgrafting of titanium chelates for improved synthesis of Ti-SBA-15 epoxidation catalysts. *Chem. Mater.* **22** (6), 1988–2000.

25. Tsoncheva, T., Ivanova, L., Rosenholm, J., and Linden, M. (2009) Cobalt oxide species supported on SBA-15, KIT-5 and KIT-6 mesoporous silicas for ethyl acetate total oxidation. *Appl. Catal. B Environ.* **89** (3-4), 365–374.
26. Chen, S., Jang, L., and Cheng, S. (2004) Synthesis of Zr-incorporated SBA-15 mesoporous materials in a self-generated acidic environment. *Chem. Mater.* (14), 4174–4180.
27. Prabhu, A., Kumaresan, L., Palanichamy, M., and Murugesan, V. (2009) Synthesis and characterization of aluminium incorporated mesoporous KIT-6: efficient catalyst for acylation of phenol. *Appl. Catal. A Gen.* **360** (1), 59–65.
28. Vinu, A., Gokulakrishnan, N., Balasubramanian, V. V., et al. (2008) Three-dimensional ultralarge-pore ia3d mesoporous silica with various pore diameters and their application in biomolecule immobilization. *Chem. A Eur. J.* **14** (36), 11529–11538.
29. Yang, L., Su, J., Carl, S., et al. (2015) Catalytic conversion of hemicellulosic biomass to lactic acid in pH neutral aqueous phase media. *Appl. Catal. B Environ.* **162**, 149–157.
30. Zhu, Y., Jaenicke, S., and Chuah, G.K. (2003) Supported zirconium propoxide - a versatile heterogeneous catalyst for the Meerwein- Ponndorf -Verley reduction. *J. Catal.* **218**, 396–404.
31. Lin, H., Strull, J., Liu, Y., et al. (2012) High yield production of levulinic acid by catalytic partial oxidation of cellulose in aqueous media. *Energy Environ. Sci.* **5**(12) (12), 9773–9777.
32. Zhu, Y., Liu, S., Jaenicke, S., and Chuah, G. (2004) Zirconia catalysts in Meerwein-Ponndorf-Verley reduction of citral. *Catal. Today* **97** (4), 249–255.
33. Fuxiang, L., Feng, Y., Yongli, L., et al. (2007) Direct synthesis of Zr-SBA-15 mesoporous molecular sieves with high zirconium loading: characterization and catalytic performance after sulfated. *Microporous Mesoporous Mater.* **101** (1-2), 250–255.
34. Rodriguez-Castellón, E., Jiménez-López, A., Maireles-Torres, P., et al. (2003) Textural and structural properties and surface acidity characterization of mesoporous silica-zirconia molecular sieves. *J. Solid State Chem.* **175** (2), 159–169.
35. Kishida, H., Jin, F., Yan, X., et al. (2006) Formation of lactic acid from glycolaldehyde by alkaline hydrothermal reaction. *Carbohydr. Res.* **341** (15), 2619–2623.
36. Maas, R.H.W., Bakker, R.R., Eggink, G., and Weusthuis, R.A. (2006) Lactic acid production from xylose by the fungus Rhizopus oryzae. *Appl. Microbiol. Biotechnol.* **72** (5), 861–868.

37. Wang, L., Zhao, B., Liu, B., et al. (2010) Efficient production of l-lactic acid from corncob molasses, a waste by-product in xylitol production, by a newly isolated xylose utilizing *Bacillus* sp. strain. *Bioresour. Technol.* **101**, 7908–7915.
38. Yan, X., Jin, F., Tohji, K., et al. (2010) Hydrothermal conversion of carbohydrate biomass to lactic acid. *AIChE J.* **56** (10), 2727–2733.
39. Fan, Y., Zhou, C., and Zhu, X. (2009) Selective catalysis of lactic acid to produce commodity chemicals. *Catal. Rev.* **51** (3), 293–324.
40. Himmel, M.E., Ding, S., Johnson, D.K., et al. (2007) Biomass recalcitrance: engineering plants and enzymes for biofuels production. *Science* **315** (5813), 804–807.
41. Aparicio, S., and Alcalde, R. (2009) The green solvent ethyl lactate: an experimental and theoretical characterization. *Green Chem.* **11** (1), 65–78.
42. Onda, A., Ochi, T., Kajiyoshi, K., and Yanagisawa, K. (2008) A new chemical process for catalytic conversion of d-glucose into lactic acid and gluconic acid. *Appl. Catal. A Gen.* **343** (1-2), 49–54.
43. Kong, L., Li, G., Wang, H., et al. (2008) Hydrothermal catalytic conversion of biomass for lactic acid production. *J. Chem. Technol. Biotechnol.* **388** (August 2007), 383–388.
44. Tolborg, S., S álaba, I., Osmundsen, C.M., et al. (2015) Tin-containing silicates: alkali salts improve methyl lactate yield from sugars. *ChemSusChem* **8** (4), 613–617.
45. Holm, M.S., Pag án-Torres, Y.J., Saravanamurugan, S., et al. (2012) Sn-Beta catalysed conversion of hemicellulosic sugars. *Green Chem.* **14** (3), 702–706.
46. Murillo, B., S ánchez, A., Sebasti án, V., et al. (2014) Conversion of glucose to lactic acid derivatives with mesoporous Sn-MCM-41 and microporous titanosilicates. *J. Chem. Technol. Biotechnol.* **89** (9), 1344–1350.
47. De Clippel, F., Dusselier, M., Van Rompaey, R., et al. (2012) Fast and selective sugar conversion to alkyl lactate and lactic acid with bifunctional carbon-silica catalysts. *J. Am. Chem. Soc.* **134** (24), 10089–10101.
48. Guo, Q., Fan, F., Pidko, E.A., et al. (2013) Highly active and recyclable Sn-MWW zeolite catalyst for sugar conversion to methyl lactate and lactic acid. *ChemSusChem* **6**, 1352–1356.
49. Wang, F.-F., Liu, C.-L., and Dong, W.-S. (2013) Highly efficient production of lactic acid from cellulose using lanthanide triflate catalysts. *Green Chem.* **15** (8), 2091–2095.
50. Wang, F.-F., Liu, J., Li, H., et al. (2015) Conversion of cellulose to lactic acid catalyzed by erbium-exchanged montmorillonite K10. *Green Chem.* **17**, 2455–2463.

51. Wang, Y., Deng, W., Wang, B., et al. (2013) Chemical synthesis of lactic acid from cellulose catalysed by lead(II) ions in water. *Nat. Commun.* **4**, 2141.
52. Dapsens, P.Y., Mondelli, C., and Pérez-Ramírez, J. (2013) Highly selective Lewis acid sites in desilicated MFI zeolites for dihydroxyacetone isomerization to lactic acid. *ChemSusChem* **6** (5), 831–839.
53. Onda, A., Ochi, T., Kajiyoshi, K., and Yanagisawa, K. (2008) Lactic acid production from glucose over activated hydrotalcites as solid base catalysts in water. *Catal. Commun.* **9** (6), 1050–1053.
54. Liu, Z., Li, W., Pan, C., et al. (2011) Conversion of biomass-derived carbohydrates to methyl lactate using solid base catalysts. *Catal. Commun.* **15** (1), 82–87.
55. Yang, L., Su, J., Carl, S., et al. Catalytic conversion of hemicellulosic biomass to lactic acid in pH neutral aqueous phase media. *Appl. Catal. B Environ. 2015 Jan;* **162**, 149–157.
56. Brand, S., Hardi, F., Kim, J., and Suh, D.J. (2014) Effect of heating rate on biomass liquefaction: Differences between subcritical water and supercritical ethanol. *Energy* **68**, 420–427.
57. Lalanne, P., Andanson, J.M., Soetens, J.-C., et al. (2004) Hydrogen bonding in supercritical ethanol assessed by infrared and raman spectroscopies. *J. Phys. Chem. A* **108** (18), 3902–3909.
58. Peng, J., Chen, P., Lou, H., and Zheng, X. (2008) Upgrading of Bio-oil over aluminum silicate in supercritical ethanol. *Energy & Fuels* **22** (1), 3489–3492.
59. Jin, B., Duan, P., Xu, Y., et al. (2014) Lewis acid-catalyzed in situ transesterification/esterification of microalgae in supercritical ethanol. *Bioresour. Technol.* **162**, 341–349.
60. Brand, S., and Kim, J. (2015) Liquefaction of major lignocellulosic biomass constituents in supercritical ethanol. *Energy* **80**, 64–74.
61. Chen, W., Luo, Z., Yu, C., et al. (2014) Upgrading of bio-oil in supercritical ethanol: Catalysts screening, solvent recovery and catalyst stability study. *J. Supercrit. Fluids* **95**, 387–393.
62. Tang, C., Tao, H., Zhan, X., and Xie, X. (2014) Mechanism of esters formation during cellulose liquefaction in sub- and supercritical ethanol. *BioResources* **9**, 4946–4957.
63. Huang, X., Korányi, T.I., Boot, M.D., and Hensen, E.J.M. (2014) Catalytic depolymerization of lignin in supercritical ethanol. *ChemSusChem* **7** (8), 2276–2288.

64. Mukai, S., Koyama, T., Tsujii, K., and Deguchi, S. (2014) Anomalous long-range repulsion between silica surfaces induced by density inhomogeneities in supercritical ethanol. *Soft Matter* **10** (35), 6645–6650.
65. Zhang, Q., Xu, Y., Li, Y., et al. (2015) Investigation on the esterification by using supercritical ethanol for bio-oil upgrading. *Appl. Energy*, In Press.
66. Brand, S., Susanti, R.F., Kim, S.K., et al. (2013) Supercritical ethanol as an enhanced medium for lignocellulosic biomass liquefaction: Influence of physical process parameters. *Energy* **59**, 173–182.
67. Vasilakos, N.P., and Austgen, D.M. (1985) Hydrogen-donor solvents in biomass liquefaction. *Ind. Eng. Chem. Process Des. Dev.* **24** (1976), 304–311.
68. Nakagawa, T., Ozaki, H., Kamitanaka, T., et al. (2003) Reactions of supercritical alcohols with unsaturated hydrocarbons. *J. Supercrit. Fluids* **27** (3), 255–261.
69. Yuan, Z., Cheng, S., Leitch, M., and Xu, C. (Charles) (2010) Hydrolytic degradation of alkaline lignin in hot-compressed water and ethanol. *Bioresour. Technol.* **101** (23), 9308–9313.
70. Do, D.M., Jaenicke, S., and Chuah, G.K. (2012) Mesoporous Zr-SBA-15 as a green solid acid catalyst for the Prins reaction. *Catal. Sci. Technol.* **2** (7), 1417–1424.
71. Holm, M.S., Saravanamurugan, S., and Taarning, E. (2010) Conversion of sugars to lactic acid derivatives using heterogeneous zeotype catalysts. *Science* **328** (5978), 602–605.
72. Konishi, Y., Okazaki, M., Toriyama, K., and Kasai, T. (2001) Nanotube effect on a liquid-phase photoreaction in mesoporous silica. *J. Phys. Chem. B* **105** (38), 9101–9106.
73. Wei, D., Chueh, W. Te, and Haller, G.L. (1999) Catalytic behavior of vanadium substituted mesoporous molecular sieves. *Catal. Today* **51** (3-4), 501–511.
74. Hu, X., Foo, M.L., Chuah, G.K., and Jaenicke, S. (2000) Pore size engineering on MCM-41: selectivity tuning of heterogenized AlCl₃ for the synthesis of linear alkyl benzenes. *J. Catal.* **195** (2), 412–415.
75. Pirez, C., Caderon, J., Dacquin, J., et al. (2012) Tunable KIT-6 mesoporous sulfonic acid catalysts for fatty acid esterification. *ACS Catal.* **2**, 1607–1614.
76. Wang, J., Masui, Y., and Onaka, M. (2011) Conversion of triose sugars with alcohols to alkyl lactates catalyzed by Brønsted acid tin ion-exchanged montmorillonite. *Appl. Catal. B Environ.* **107** (1-2), 135–139.

77. Pescarmona, P.P., Janssen, K.P.F., Delaet, C., et al. (2010) Zeolite-catalysed conversion of C3 sugars to alkyl lactates. *Green Chem.* **12** (6), 1083–1089.
78. Lange, J.P., van de Graaf, W.D., and Haan, R.J. (2009) Conversion of furfuryl alcohol into ethyl levulinate using solid acid catalysts. *ChemSusChem* **2** (5), 437–441.
79. Boronat, M., Corma, A., and Renz, M. (2006) Mechanism of the Meerwein - Ponndorf - Verley - Oppenauer (MPVO) redox equilibrium on Sn - and Zr - Beta zeolite catalysts. *J. Phys. Chem. B* **110** (42), 21168–21174.
80. Corma, A., Domine, M.E., Nemeth, L., and Valencia, S. (2002) Al-Free Sn-Beta Zeolite as a catalyst for the selective reduction of carbonyl compounds (Meerwein - Ponndorf - Verley Reaction). *J. Am. Chem. Soc.* **124**, 3194–3195.
81. Corma, A., Domine, M.E., and Valencia, S. (2003) Water-resistant solid Lewis acid catalysts: Meerwein–Ponndorf–Verley and oppenauer reactions catalyzed by tin-beta zeolite. *J. Catal.* **215** (2), 294–304.
82. Li, G., Pidko, E.A., and Hensen, E.J.M. (2014) Synergy between Lewis acid sites and hydroxyl groups for the isomerization of glucose to fructose over Sn-containing zeolites: a theoretical perspective. *Catal. Sci. Technol.* **4** (8), 2241–2250.
83. Serrano-Ruiz, J.C., and Dumesic, J.A. (2011) Catalytic routes for the conversion of biomass into liquid hydrocarbon transportation fuels. *Energy Environ. Sci.* **4** (1), 83–89.
84. Kobayashi, H., Ohta, H., and Fukuoka, A. (2012) Conversion of lignocellulose into renewable chemicals by heterogeneous catalysis. *Catal. Sci. Technol.* **2** (5), 869–883.
85. Corma, A., Iborra, S., and Velty, A. (2007) Chemical routes for the transformation of biomass into chemicals. *Chem. Rev.* **107** (6), 2411–2502.
86. Dusselier, M., and Sels, B.F. (2014) Selective Catalysis for cellulose conversion to lactic acid and other α -Hydroxy acids, in *Selective catalysis for renewable feedstocks and chemicals* (eds.Nicholas, K.M.), Springer-Verlag, pp. 85–125.
87. Datta, R., and Henry, M. (2006) Lactic acid : recent advances in products , processes and technologies – a review. *J. Chem. Technol. Biotechnol.* **1129** (August 2005), 1119–1129.
88. Carlos Serrano-Ruiz, J., and Dumesic, J.A. (2009) Catalytic upgrading of lactic acid to fuels and chemicals by dehydration/hydrogenation and C–C coupling reactions. *Green Chem.* **11** (8), 1069–1272.
89. Pereira, C.S.M., Silva, V.M.T.M., and Rodrigues, A.E. (2011) Ethyl lactate as a solvent: Properties, applications and production processes – a review. *Green Chem.* **13** (10), 2658–2671.

90. Dapsens, P.Y., Menart, M.J., Mondelli, C., and Pérez-Ramírez, J. (2014) Production of bio-derived ethyl lactate on GaUSY zeolites prepared by post-synthetic galliation. *Green Chem.* **16** (2), 589–593.
91. Barr-David, F., and Dodge, B.F. (1959) Vapor-Liquid equilibrium at high pressures: The systems ethanol - water and 2-propanol - water. *J. Chem. Eng. Data* **4** (2), 107–121.
92. Cheng, S., D'cruz, I., Wang, M., et al. (2010) Highly efficient liquefaction of woody biomass in hot-compressed alcohol–water co-solvents. *Energy & Fuels* **24** (9), 4659–4667.
93. Cheng, S., Wilks, C., Yuan, Z., et al. (2012) Hydrothermal degradation of alkali lignin to bio-phenolic compounds in sub/supercritical ethanol and water–ethanol co-solvent. *Polym. Degrad. Stab.* **97** (6), 839–848.
94. Gounder, R. (2014) Hydrophobic microporous and mesoporous oxides as Bronsted and Lewis acid catalyst for biomass conversion in liquid water. *Catal. Sci. Technol.* **4**, 2877–2886.
95. Duke, M.C., da Costa, J.C.D., Do, D.D., et al. (2006) Hydrothermally robust molecular sieve silica for wet gas separation. *Adv. Funct. Mater.* **16** (9), 1215–1220.
96. Qi, X., Watanabe, M., Aida, T.M., and Smith, R.L. (2011) Catalytic conversion of cellulose into 5-hydroxymethylfurfural in high yields via a two-step process. *Cellulose* **18** (5), 1327–1333.
97. Su, Y., Brown, H.M., Huang, X., et al. (2009) Single-step conversion of cellulose to 5-hydroxymethylfurfural (HMF), a versatile platform chemical. *Appl. Catal. A Gen.* **361** (1–2), 117–122.
98. Bui, L., Luo, H., Gunther, W.R., and Román-Leshkov, Y. (2013) Domino reaction catalyzed by zeolites with Brønsted and Lewis acid sites for the production of γ -valerolactone from furfural. *Angew. Chemie Int. Ed.* **52** (31), 8022–8025.
99. Ryczkowski, J. (2001) IR spectroscopy in catalysis. *Catalyst Today* **68**, 263–381.
100. Puttock, S.J., and Rochester, C.H. (1986) Infrared study of the adsorption of carbon monoxide, carbon dioxide, acetic acid and acetic anhydride on the surface of anhydrous vanadyl pyrophosphate. *J. Chem. Soc. Faraday Trans. 1* **82** (9), 3013–3018.
101. Young, R. (1969) Infrared spectroscopic studies of adsorption and catalysis. Part 3. Carboxylic acids and their derivatives adsorbed on silica. *Can. J. Chem.* **47** (12), 2237–2247.

102. Dewilde, J.F., Czopinski, C.J., and Bhan, A. (2014) Ethanol dehydration and dehydrogenation on γ -Al₂O₃: mechanism of acetaldehyde formation. *ACS Catal.* **4**, 4425–4433.
103. Silva, V.M.T.M., and Rodrigues, A.E. (2005) Novel process for diethylacetal synthesis. *AICHE J.* **51** (10), 2752–2768.

Chapter 6 Conclusions and recommendation for future research

6.1 Conclusions

The potential for chemical and polymer production from biomass is substantial. Carboxylic acids (e.g., lactic, levulinic acid, maleic acid, etc.) are among the wide-spread “platform-molecule”, which may be further converted into possibly derivable high-value-added chemicals. On the other hand, chemical catalysis often presents improved process design options, resulting in higher productivity and lower costs. Heterogeneous catalysts were studied in this work and proven to be efficient for converting numerous low-cost products from lignocellulosic biomass. Also, the whole roadmap for lignocellulosic biomass conversion was given in this work.

First, the arid-land adapted, highly water-use efficient CAM species *A. tequilana* and *O. ficus-indica*, which are unique biomass species compared to other C₃ and C₄ plants, were characterized by series of standard biomass analytical procedures. Both *Agave* and *Opuntia* contained a high amount of water at 84.9% and 93.9%, respectively, which might make them especially attractive for aqueous phase processes. In addition, carboxylic acids and simple sugars were found to be the major constituents of freshly expelled juice. *A. tequilana* and *O. ficus-indica* dry bagasses possessed structural carbohydrate mass fractions of 43.8% and 36.3%, respectively, with low relative lignin mass fractions of 13.1% and 12.3%, respectively. Moreover, the amorphous and para-crystalline cellulose fractions accounted for over 80% of the total cellulose in both

species indicating that bagasse from both *Agave* and *Opuntia* might be more readily deconstructed into fermentable sugars than biomass from traditional herbaceous or woody feedstocks.

The catalytic conversion of model compound from lignin, guaiacol, was investigated at low temperatures with aqueous-phase H₂O₂ over heterogeneous TS-1 catalysts producing maleic acid with the maximum yield of ~28%. The synergetic effect of the Bronsted base and the TS-1 with H₂O₂ as the oxidant leads to the aromatic-ring opening reactions of guaiacol, a key step to selectively produce maleic acid. The proposed guaiacol oxidation reaction mechanism indicates that the oligomerization of guaiacol and its derivatives is the undesired side reactions for maleic acid production. Further research will be carried out toward in-depth investigations of how to inhibit oligomerization and further enhance the yield of maleic acid.

For the holocellulose conversion, zirconia was chosen as catalyst because it showed high catalytic performance and stability among different kinds of solid catalysts. The acid/base pairs on the ZrO₂ surface were demonstrated to effectively facilitate the retro-aldol condensation of xylose, which is the initial step of the conversion of xylose to lactic acid in the aqueous phase. Under the tested conditions (160-240 °C, 0 - 100% O₂ partial pressure, and 0.5 - 4 catalyst to biomass weight ratio), the highest lactic acid yields were 25% and 18% from xylose and xylan, respectively. Compared to the mono-functional base catalyst like MgO, the bi-functional ZrO₂ was superior in lactic acid synthesis from xylose.

Furthermore, the mesoporous Zr-silicates catalysts, which were synthesized with tunable structures and pore sizes, showed excellent catalytic performance for the

conversion of carbohydrates to lactic acid derivatives in a “one-pot” reaction system. The mesoporous structure of the silica framework together with the presence of zirconium confers strong Lewis acidity as well as weak Brønsted acidic sites. The effects of reaction conditions, including temperature, reaction time, and catalyst loading amount, on the conversions of carbohydrates and the corresponding yields of lactate were investigated. The carbon yields of methyl lactate, up to 41 % and 44%, were produced from pentose and hexose, respectively using Zr-SBA-15 catalyst. The key intermediates such as glyceraldehyde, glycolaldehyde, and pyruvaldehyde were used as probe reactants to understand the mechanism. Furthermore, the carbon yield of ethyl lactate, up to 33% was produced from cellulose with the Zr-SBA-15 catalyst. Fructose and glucose were also used as intermediate reactants in order to probe the reaction mechanism. The role of the catalyst in the retro-aldol condensation of carbohydrates, as well as the catalyst stability, was discussed. The difference in the lactic acid derivatives yields from different carbohydrates reflects the dynamic equilibrium between the isomerization, retro-aldol condensation and degradation reactions.

Overall, various heterogeneous catalysts were investigated in this work and demonstrated “green” alternative approaches to selectively convert lignocellulosic biomass components to value-added carboxylic acids and derivatives.

6.2 Recommendations for Future Work

In this study, supercritical ethanol solvent has been proved to be an efficient solution for cellulose conversion. The advantages of biomass conversion in supercritical alcohols include: better solubility of reaction intermediates and products; less corrosion of reactors, easier product separation procedures; and unique hydrogen donation ability of alcohols at

the liquefaction condition. Additionally, the water that is naturally present in biomass feedstocks does not need to be evaporated firstly which is more energy efficient for feedstocks with high water content such as *Agave* and *Opunita* species. However, a grasp of the process parameters, e.g., the behavior of single biomass constituents (cellulose, hemicellulose, and lignin) during the liquefaction, needs to be understood in order to gain insight into the liquefaction mechanism so that an optimized liquefaction process can be designed for raw bioamss. When the raw biomass sample is used as feedstock, it would be extremely difficult to understand reaction pathways due to the complexity of their chemical structures and the presence of various types of polymers. For the future work, an investigation into the influence of physical process parameters for the liquefaction of other biomass constitutes (xylan, and lignin) in supercritical ethanol solvent regarding conversion, product distribution, and gas formation will be procceded to illuminate the interactive effects between cellulose, hemicelluloses, and lignin. The parameters are to include reaction temperatures, initial pressures, reaction times, and biomass-to-solvent ratios. We will characterize solid, liquid, and gaseous products using various analytical methods to understand their chemical composition, properties and value as for biofuels and biochemicals.

In the future, more flexible, robust and multi-functions catalysts for raw biomass conversion will be developed. The use of heterogeneous Lewis acid catalysts with liquid water is often fraught with issues related to structural instability and active site inhibition caused by deactivation mechanisms [1]. For porous silica-based catalysts, one strategy to address these issues is to design or functionalize their surfaces with hydrophobic moieties or domains. Surface hydrophobicity enhancement is a commonly employed technique to

improve the hydrothermal stability in silica-based materials [2]. Grafting organosilane compounds onto mesoporous silicate is one of the methods to increased their hydrophobicity and reactivity. The surface nature of the silicates can be modified by silanization with silane coupling agents. Stabilization of the hydrophobic nature is important to utilize the silica material for adsorption in the presence of water. Trimethylsilylation can effectively remove the surface silanols to greatly enhance the hydrophobicity [3]. For the trimethylsilylation of silanol groups, various reagents can be used such as hexamethyldisilazane (HMDZ), trimethylchlorosilane (TMCS), N-methyl-N- (trimethylsilyl)trifluoroacetamide (MSTFA), trimethylsilylimidazole, and hexamethyldisiloxane (HMDS) with/without a solvent [4]. The degree of trimethylsilylation is affected by various factors such as dose and reactivity of silylating agent and reaction temperature.

6.3 References

1. Gounder, R. (2014) Hydrophobic microporous and mesoporous oxides as Bronsted and Lewis acid catalyst for biomass conversion in liquid water. *Catal. Sci. Technol.* **4**, 2877–2886.
2. Duke, M.C., da Costa, J.C.D., Do, D.D., et al. (2006) Hydrothermally Robust Molecular Sieve Silica for Wet Gas Separation. *Adv. Funct. Mater.* **16** (9), 1215–1220.
3. Wu, P., and Tatsumi, T. (2002) Properties in Alkene Epoxidation of Hydrothermally Stable Mesoporous Ti-SBA-15. (11), 1657–1664.
4. Igarashi, N., Hashimoto, K., and Tatsumi, T. (2007) Catalytical studies on trimethylsilylated Ti-MCM-41 and Ti-MCM-48 materials. *Microporous Mesoporous Mater.* **104** (1-3), 269–280.